UNIVERSITY OF SOUTHAMPTON

FACULTY OF PHYSICAL SCIENCES AND ENGINEERING
ELECTRONICS AND COMPUTER SCIENCE

An Investigation into Separation Enhancement Methods for Miniaturised Planar Capillary Electrophoresis Devices

by Adam Paul Lewis

Supervisors: Dr Nick R. Harris,
Dr Andy Cranny,
Dr Nicolas G. Green.

Thesis for the degree of Doctor of Philosophy

September, 2013

UNIVERSITY OF SOUTHAMPTON

ABSTRACT

FACULTY OF PHYSICAL AND APPLIED SCIENCES
ELECTRONICS AND COMPUTER SCIENCE

Thesis for the degree of Doctor of Philosophy

AN INVESTIGATION INTO SEPARATION ENHANCEMENT METHODS FOR MINIATURISED PLANAR CAPILLARY ELECTROPHORESIS DEVICES

by Adam Paul Lewis

The analytical capability of field-portable instruments and in-situ devices is often limited due to cost, complexity and spatial restrictions. With powerful analytical methods incorporated onto miniaturised sensor platforms, in-depth sample and environmental examinations become feasible. There has been significant research reported in the literature for improving miniaturised capillary electrophoresis systems alongside lab-on-a-chip applications. The work presented in this thesis discusses the development of novel methods to improve the separation resolution of capillary electrophoresis on microfluidic devices without compromising device size. Further to this, complex chemical buffering systems have been avoided since they tend to make the end device highly application specific.

The separation resolution of capillary electrophoresis can be enhanced by dynamic control of the electroosmotic flow. This is achieved through control of the zeta-potential, which can be modified by applying a potential to an electrode close to the surface of the separation channel. The separation enhancement methods increase the effective channel length and therefore can be used to aid the incorporation of capillary electrophoresis into both portable field instruments and for in-situ systems.

Computational models have been developed for an in-depth investigation into the proposed separation enhancement routines. Where possible, these models have been experimentally verified. The operation limits of the enhancement methods have been investigated, and related to the composition of the sample to infer design criteria.

Table of Contents

Acknowledgements i
Nomenclature ix
Abbreviations xiii
Chapter 1 Introduction 1
1.1. Aims and Motivation of this Research 1
1.2. Novel Contributions 2
1.3. Structure of the Thesis 4
Chapter 2 Project Description and Methods for Enhancing Separation 7
2.1. Project Description 7
2.1.1. Contribution of the Ph.D to the Project 12
2.2. Capillary Electrophoresis: Theoretical Operation 14
2.3. Electroosmotic Flow 17
2.4. Separation Enhancement Methods 20
2.4.1. EOF Manipulation through Control of the Zeta-potential 20
2.4.2. Matching EOF to Electrophoretic Flow 22
2.4.3. Switching EOF Direction to Cycle Ions Along the Channel 23
2.4.4. Practical Considerations 25
2.5. Control Systems 30
2.5.1. Open-loop System 30
2.5.2. Closed-loop System 31
2.5.3. Mixing Open- and Closed-loop Systems 32
2.6. Conclusions 33
Chapter 3 Literature Review 35

3.1. Reasons and Motivations for Miniaturising CE 36
3.2. Design Considerations and Challenges for Miniaturised CE Systems 38
3.3. The Ideal Portable CE system 42
3.3.1. Typical Chip-based CE Microfluidic Devices 43
3.3.2. Considerations for In-situ CE Systems 44
3.4. A Brief History of CE 45
3.5. Standard CE Systems 46
3.5.1. Variations on CE 46
3.6. Truly Portable CE Systems 52
3.6.1. Chip-based CE Systems 53
3.6.2. Non-chip-based CE Systems 57
3.6.3. In-situ CE Systems 62
3.6.4. Summary on Truly Portable CE Systems 63
3.7. Energy Requirements for CE Separations 64
3.8. High Voltage Power Supply Considerations 65
3.9. Sample Injection Schemes 69
3.10. Dynamic Zeta-potential Modification Techniques 71
3.11. Conclusions 79
Chapter 4 Computational Modelling 81
4.1. Background Showing Evolution of Double Layer Models 81
4.1.1. Helmholtz Model 82
4.1.2. Gouy-Chapman Model 82
4.1.3. Gouy-Chapman-Stern Model 84
4.1.4. Debye-Hückel Approximation 85
4.1.5. Grahame Model 87
4.1.6. Bockris, Devanathan and Müller Model 88
4.1.7. Summary of EDL Models 88
4.2. Modelling the Electrical Double Layer 89

4.3. Theory for Fluidic Modelling 94
4.3.1. Nernst-Planck Model 94
4.3.2. Modelling Diffusion 94
4.4. Microfluidic Modelling using Finite Element Method Analysis 96
4.4.1. Modelling the Fluid Flow in a Microfluidic Channel 96
4.4.2. Modelling CE with Uniform EOF 101
4.4.3. Modelling CE with Non-uniform EOF 108
4.4.4. Dispersion Induced by Difference in EOF 110
4.5. Conclusions 115
Chapter 5 Detection System 117
5.1. Background on Detectors for Miniaturised CE Systems 117
5.1.1. Optical Detection 119
5.1.2. Electrochemical Detectors 120
5.1.3. Detector Placement 121
5.1.4. Detector Design 124
5.2. Development of the CCD Electrical Model 127
5.2.1. Simulating the CCD Circuitry 132
5.3. Conclusions 139
Chapter 6 Experimental Work and Device Fabrication 141
6.1. Introduction 141
6.2. Discussion on Material Considerations for Microfluidic CE Devices 142
6.3. Typical Fabrication Methods for Microfluidic CE Devices 144
6.3.1. Moulding 145
6.3.2. Micromachining 148
6.3.3. Milling 150
6.3.4. Screen-printing 151
6.3.5. Powder-blasting 151
6.3.6. Channel Formers 152
6.3.7. Conclusions on Fabrication Methods 152

6.4. Overview of Proposed Device and Prototypes for Design Optimisation 153

6.5. Experiment 1: Characterisation of the Electrophoretic Dyes 156

6.5.1. Aims of Experiment 1 156

6.5.2. Experiment 1: Verification of the Apparent Mobilities of the Fluorescent Dyes 157

6.5.3. Outcomes from Experiment 1 158

6.6. Experiment 2: Confirm Control of Ionic Species in a Microfluidic Device 159

6.6.1. Aims of Experiment 2 159

6.6.2. Fabrication of Device 1 159

6.6.3. Refinement of Device 1 161

6.6.4. Experiment 2: Ionic Species Migration along Channel Subjected to Electric-Field 162

6.6.5. Outcomes from Experiment 2 166

6.7. Experiment 3: Setup and Test of Experimental Control Systems 167

6.7.1. Aims of Experiment 3 167

6.7.2. Fabrication of Device 2 168

6.7.3. Experiment 3: Suitability of Micro-pump for Sample Injection and Flushing of Buffer 171

6.7.4. Experiment 3: Integration and Testing of Detection System and HVPS into the Test Platform 173

6.7.5. Experiment 3: Investigating Effect of ZPM Electrode on Migration Time 178

6.7.6. Outcomes from Experiment 3 179

6.8. Experiment 4: Characterise Ability to Modify the EOF with a Planar ZPM Electrode 181

6.8.1. Aims of Experiment 4 181

6.8.2. Fabrication of Device 3 181

6.8.3. Experiment 4: Modification of EOF using Planar ZPM Electrode 188

6.8.4. Outcomes from Experiment 4 191

6.9. Experiment 5: Evaluate Performance of Detection System 192

6.9.1. Aims of Experiment 5 192
6.9.2. Experiment 5: Measuring the Limits of Detection for the Detection System 192
6.9.3. Outcomes from Experiment 5 197
6.10. Experiment 6: Demonstrate Separation and Detection of Low Concentration of a Metal Ion Sample 197
6.10.1. Aims of Experiment 6 197
6.10.2. Experiment 6: Separation and Detection of $CuCl_2$ 197
6.10.3. Outcomes from Experiment 6 201
6.11. Experiment 7 201
6.11.1. Aims of Experiment 7 201
6.11.2. Fabrication of Device 4 202
6.11.3. Reliability Issues with Device 4 206
6.11.4. Outcomes from Experiment 7 213
6.12. Conclusions 214
Chapter 7 Conclusions and Future Work 219
7.1. Summary of Work 219
7.1.1. Main Contributions 222
7.1.2. Publications 224
7.2. Recommendations for Future Work 224
7.2.1. Short-term Future Work 224
7.2.2. Addressing the Corrosion Monitoring Application 228
7.2.3. Further Applications and Additional Work 228
7.2.4. Conclusion 229
Appendix A Conference and Workshop Attendance 231
Appendix B Publications 233
Appendix C COMSOL Multiphysics Modules 237
Appendix D LabView Program 239
Appendix E Novel Fabrication Method 243
Appendix F Recipe for Bonding PDMS to SU-8 247

References 249

Academic Thesis: Declaration Of Authorship

I, Adam Paul Lewis declare that this thesis and the work presented in it are my own and has been generated by me as the result of my own original research.

An Investigation into Separation Enhancement Methods for Miniaturised Planar Capillary Electrophoresis Devices

I confirm that:

1. This work was done wholly or mainly while in candidature for a research degree at this University;

2. Where any part of this thesis has previously been submitted for a degree or any other qualification at this University or any other institution, this has been clearly stated;

3. Where I have consulted the published work of others, this is always clearly attributed;

4. Where I have quoted from the work of others, the source is always given. With the exception of such quotations, this thesis is entirely my own work;

5. I have acknowledged all main sources of help;

6. Where the thesis is based on work done by myself jointly with others, I have made clear exactly what was done by others and what I have contributed myself;

7. Either none of this work has been published before submission, or parts of this work have been published as listed in Appendix B

Signed: ……..…….

Date: ……..…….

Acknowledgements

There are a large number of people who have helped and supported me throughout the course of the Ph.D. Firstly, I would like to thank my supervisors Andy Cranny, Nic Green and Nick Harris, and I would also like to thank, my technical advisors from the National Centre for Advanced Tribology Southampton (nCATS) Julian Wharton, Keith Stokes and Robert Wood, for without their guidance I'd have certainly gotten lost along the garden path. In particular, I shall miss the regular conversations with Andy and Nick from our Monday meetings, during which many new garden paths were explored.

I would like to thank Geoff for all his advice and for inspiring me to do a Ph.D, his friendship and support has helped me maintain my usual level of 'sanity', for the most part. I would also like to thank Alex who helped me find my feet at the start and kept me amused to the end.

There are too many to mention them all individually (and therefore too great a risk of missing someone out), but thank you to all my friends, you know who you are, you have kept me company on what would have otherwise been a lonely journey.

Thank you the Engineering and Physical Sciences Research Council UK and Defence Science and Technology Laboratory for their financial support under grant number EP/F004362/1.

And last but by no means least I would like to thank all my family whom have always been there for me. Mum and dad, your continuous support has made it impossible for me to feel truly stressed.

Thank you!

Nomenclature

a	amplitude of Gaussian peak	
A	area	m^2
b	position of Gaussian peak	
c	concentration of species	M
C	capacitance	F
c_0	initial concentration	M
c^∞	bulk concentration	M
C_{cu2_start}	initial concentration of Cu^{2+} ions	M
C_d	capacitance of diffuse layer	F
C_{fe2_start}	initial concentration of Fe^{2+} ions	M
C_{fe3_start}	initial concentration of Fe^{3+} ions	M
c_i	concentration of ion *i*	M
c_i^∞	bulk concentration of ion *i*	M
C_{SOL}	solution capacitance	F
c_w	width of Gaussian peak	
C_{wall}	capacitance of channel wall	F
d	gap between electrodes	m
D_{cu2}	diffusion coefficient of Cu^{2+} ions	$m^2\ s^{-1}$
D_{fe2}	diffusion coefficient of Fe^{2+} ions	$m^2\ s^{-1}$
D_{fe3}	diffusion coefficient of Fe^{3+} ions	$m^2\ s^{-1}$
D_i	diffusion coefficient	$m^2\ s^{-1}$
e	elementary charge	C
E	electric-field	$V\ m^{-1}$
E_L	electric-field strength in leading electrolyte zone	$V\ m^{-1}$
E_S	electric-field strength in sample zone	$V\ m^{-1}$
E_{S1}, E_{S2}, …, E_{Sn}	electric-field strength in zone containing analyte 1, 2, …, n	$V\ m^{-1}$
E_T	electric-field strength in terminating electrolyte zone	$V\ m^{-1}$
f	frequency	Hz
F_{drag}	Stokes' drag force	N
F_{el}	electrophoretic force	N

G	gain	
h	channel height	m
I	current	A
k	Boltzmann's constant	$J\ K^{-1}$
K	cell constant	m^{-1}
L	length	m
p	pressure	$kg\ m^{-1}\ s^{-2}$
Q	flow rate	$m^3\ s^{-1}$
r	hydrated radius of particle	m
r_a	circular cross-section	m^2
$R_{feedback}$	resistance of feedback resistor	Ω
R_{ground}	resistance of ground resistor	Ω
R_{hyd}	hydraulic resistance	$kg\ m^{-4}\ s^{-1}$
R_{SOL}	solution resistance	Ω
T	temperature	K
t	time	s
u_a	velocity of species a	$m\ s^{-1}$
u_b	velocity of species b	$m\ s^{-1}$
u_{cu2}	electrophoretic velocity of Cu^{2+} ions	$m\ s^{-1}$
u_{eff}	effective velocity	$m\ s^{-1}$
u_{eof}	electroosmotic velocity	$m\ s^{-1}$
u_{EOF_bottom}	EOF velocity at bottom of channel	$m\ s^{-1}$
u_{EOF_top}	EOF velocity at top of channel	$m\ s^{-1}$
u_{ep}	electrophoretic velocity	$m\ s^{-1}$
u_{fe3}	electrophoretic velocity of Fe^{3+} ions	$m\ s^{-1}$
u_{fluid}	fluid velocity	$m\ s^{-1}$
u_{ion}	velocity of ion	$m\ s^{-1}$
u_{sep}	separation velocity	$m\ s^{-1}$
V	voltage	V
V_{sol}	potential in solution	V
V_{ZPM}	potential on ZPM electrode	V
w	channel width	m
x	distance	m
x_a	distance travelled by species a	m
x_b	distance travelled by species b	m
x_b	broadening distance	m
$x_{\Delta EOF}$	broadening distance caused by variation in EOF velocity	m
y	distance	m

z	distance	m
Z_C	impedance	Ω
z_i	valence number of ion *i*	
ε_0	permittivity of free space	F m^{-1}
ε_r	relative permittivity	
ε_{sol}	relative permittivity of the buffer solution	
ζ	zeta-potential	V
η	fluid viscosity	Pa s
κ	conductivity	S
λ_D	Debye length	m
μ_{eof}	electroosmotic mobility	m^2 V^{-1} s^{-1}
μ_{ep}	electrophoretic mobility	m^2 V^{-1} s^{-1}
μ_{ion}	electrophoretic mobility of ion	m^2 V^{-1} s^{-1}
μ_L	electrophoretic mobility of leading electrolyte	m^2 V^{-1} s^{-1}
μ_S	electrophoretic mobility of sample	m^2 V^{-1} s^{-1}
μ_{S1}, μ_{S2}, …, μ_{Sn}	electrophoretic mobility of analyte 1, 2, …, n in sample	m^2 V^{-1} s^{-1}
μ_T	electrophoretic mobility of terminating electrolyte	m^2 V^{-1} s^{-1}
ν	packing parameter	
ρ	charge density	C m^{-1}, C m^{-2}, C m^{-3}
ρ_{fluid}	fluid density	kg m^{-3}
ρ_{SOL}	solution resistivity	Ω m
τ	charging time	s
ϕ	potential	V
ψ_0	surface potential	V

Abbreviations

APTES	amino-propyl-triethoxysilane
AMD	amperometric detection
BBD	boron doped diamond
CCD	contactless conductivity detection
CD	conductivity detection
CE	capillary electrophoresis
CEC	capillary (electro)-chromatography
CGE	capillary gel electrophoresis
CIEF	capillary isoelectric focussing
CITP	capillary isotachophoresis
COC	cyclic olefin copolymer
COP	cyclic olefin polymer
CTAH	cetyltrimethylammonium hydroxide
ECD	electrochemical detection
EDL	electrical double layer
EK	electrokinetic
EOF	electroosmotic flow
EWOD	Electrowetting on dielectric

FEM	finite element method
FET	field effect transistor
FIA	flow injection analysis
FI-CE	flow injection-capillary electrophoresis
HPLC	high pressure (or performance) liquid chromatography
HVPS	high voltage power supply
HY	hydrodynamic
HYCS	hydrodynamic cross-sampler
IC	integrated circuit
IHP	inner Helmholtz plane
ITP	isotachophoresis
LIF	laser-induced fluorescence
MECC, MEKC	micellar electrokinetic capillary chromatography
NAB	nickel aluminium bronze
OHP	outer Helmholtz plane
PAD	pulsed amperometric detection
PB	Poisson Boltzmann
PCB	printed circuit board
PDMS	polydimethylsiloxane
PECVD	plasma enhanced chemical vapour deposition
PMD	potentiometric detection
PMMA	poly (methyl methacrylate)
PR	pressure

PTFE	polytetrafluoroethylene
RTFS	real-time fluorescence spectroscopic analysis.
SHE	standard hydrogen electrode
TMAH	tetramethylammonium hydroxide
μ-TAS	micro-total analysis system
ZPM	zeta-potential modification

Chapter 1

Introduction

1.1. Aims and Motivation of this Research

The aims of this work are to improve the applicability of capillary electrophoresis (CE) into portable and in-situ devices. The requirement of long lengths of capillaries (or channels) limits the ability to miniaturise CE systems. To address this issue, novel separation enhancement methods have been developed. In standard CE the sample migrates in a single direction along the capillary or channel subjected to an electric-field. As the sample migrates, it becomes separated; the channel length plays an important part in the amount of separation attained. In this work, the dynamic control of a secondary fluid flow, termed the electroosmotic flow (EOF), to increase the effective channel length is investigated. Increasing the effective channel length should enable greater separations within a given length of channel. CE is a powerful separation technique and its applications are widespread. Furthering the applicability of CE into portable or in-situ systems improves the feasibility of performing a highly detailed analysis on-site. The project, of which this research is a part of, is interested in using portable and in-situ CE analysis to detect and monitor corrosion. The supporting project is described in greater detail in Chapter 2.

The primary application considered in this research is the separation of metal ions such as those typically found in metal crevices undergoing corrosion. In the context of this project, a crevice is defined as a confined space within a metal part where a fluid is able to ingress. For example: gaskets are often used to fill the space between multiple components being joined together; if there is a gap between the gasket and the component, this gap is a crevice. The

crevice needs to be wide enough such that liquid can enter it, however for crevice corrosion to occur, the crevice solution needs to be depleted of oxygen [1]. Therefore the crevice solution should be stagnant and the diffusion of oxygen into the crevice solution should be slower than its consumption within the crevice solution [1]. Three metal systems were encompassed within the scope of the project, these were: nickel aluminium bronze (NAB), stainless steel 316 and duplex stainless steel. These metals are of particular interest to structures used within marine environments since they exhibit high corrosion resistance [2]. During the corrosion process metal ions are released into the crevice; later in Section 2.2, Table 1 provides a list of the metal ions of interest to the project. Some of the metal ions (for example Cu^{2+} and Fe^{2+}) have very similar mobilities and consequently are difficult to separate. To address this difficulty, separation enhancement methods were developed in this research. To investigate the separation enhancement methods a computational model was created. This model has been used to describe the effect that the separation enhancement methods have on separation. With one eye on fabrication, the limitations that this places on the design have been considered in the model. The result being, a computational model which serves as a design tool for miniaturised CE systems. Where possible, aspects of the model have been verified either using experimental results from fabricated prototype devices, or by using results published in the literature.

1.2. Novel Contributions

A number of novel contributions have been made during the course of this research, these are summarised below:

- Novel methods to improve the amount of separation attainable in CE analysis for a given channel length have been devised and modelled. To describe the separation of charged species, a model based on the Nernst-Planck equations was developed and modified. Further to this the limitations of the separation enhancement methods have been explored. From this a method to infer design criteria depending on the sample composition has been discussed.
- Practical methods for the implementation of the separation enhancement techniques on planar devices have been created, developed and modelled. The use of a closed-loop control system to overcome the anticipated issues with the high-precision control required is considered. This has the further advantage of making the design resilient to unpredictable experimental variability.

- A model incorporating classical electrical double layer (EDL) models has been developed to describe the effect of the separation enhancement methods in the presence of a solution potential along the fluidic channel.
- Using a prototype device, an ionic species was sent back and forth along a microfluidic channel designed for CE analysis using a single zeta-potential modification (ZPM) electrode. To the author's knowledge this is the first time that this has been demonstrated, on a planar device, using the method described here.
- Finally, during the course of device fabrication, a novel fabrication method which enables the rapid fabrication of sealed microfluidic channels was devised and developed.

Through a range of events and publications (complete list given in Appendix A and Appendix B) the novel contributions have been disseminated to the wider research community.

1: Introduction	*Introduce aims and motivation for work along with contributions and structure of thesis.*
2: Project Background	*Background on the funding project and the role of the Ph.D within it.* *Brief explanation of the principle of operation of CE and EOF.* *Details on the separation enhancement routines and the role of the control systems.*
3: Literature Review	*Describe history of CE and the advances its miniaturisation.* *Discuss a range of portable and in-situ CE systems presented in the literature.* *Describe published work and applications regarding the use of dynamic modification of the EOF.*
4: Computational Modelling	*Background on evolution of computation models for describing the EDL.* *Discussion on models for describing behaviour of ionic species in a fluid in the presence of an electric field.* *Description of developed models with discussion on simulation results and limits placed on device fabrication.*
5: Detection System	*Background on types and placement of detection systems.* *Discussion on development of detection system presented with simulation results for a range of parameters mimicking the fabricated prototype devices.*
6: Device Fabrication and Experimental Work	*Description of typical fabrication methods and materials for chip-based CE devices.* *For each prototype device, details on the fabrication, the aims of the device and observations of the results are presented.* *Discussion on reflections of prototype devices, which combined with modelling informed the re-designs.*
7: Summary and Future Work	*Summary of the thesis, concluding the main points of the work presented and highlighting the key contributions.* *A discussion on the direction of the research and future work.*

Figure 1: Chart describing the content and structure of thesis.

1.3. Structure of the Thesis

A chart describing the content and structure of the thesis is given in Figure 1. It can be seen that following this chapter, the supporting project and how this work fits within the project is described. Further to this, in Chapter 2 an explanation of CE and EOF are given, since knowledge on their operation is crucial for understanding the separation enhancement routines. In Chapter 2 the difficulties in separation of the metal ions of interest to the project are discussed, following which the separation enhancement methods to address this problem are described. A discussion on the control systems required for the separation enhancement routines is also provided.

In Chapter 3 a discussion of the published literature is presented. The history of CE and recent improvements are presented to show how the CE method has been developed. The challenges specific to miniaturised CE systems are discussed and presented with the concept of the ideal device. This ideal device gives a metric with which portable and in-situ CE systems can be compared. A number of truly portable CE systems have been created where a holistic approach to design has been employed. These along with the few in-situ CE systems are discussed in detail. A typical design for chip-based CE systems is discussed alongside considerations regarding the ancillary hardware. The literature has been analysed with consideration given to the project requirements; these being: separation and detection of certain metal ions in a self-powered portable device. The power requirements of this system have been identified and compared with reports in the literature where a range of approaches have been employed. Since the separation enhancement methods required dynamic modification of the EOF, a range of published works on dynamic modification of EOF for various applications are also discussed in Chapter 3.

In Chapter 4, the development of the computational model to both predict the performance of the fabricated device and to inform fabrication decisions is discussed. A discussion on the background regarding modelling work presented by other researchers in the literature is given. Results and observations of the results are discussed with a view to development of a device using planar fabrication technology since the end device will be planar.

Following a review on the background of typical detection systems and schemes for miniaturised CE systems, the design of a detection system for the prototype devices is given in Chapter 5. The modelling of this detection system was conducted for a range of conditions representative of the prototype devices. The limits of detection are discussed with consideration of metal ion concentrations typical of those found in a crevice. This

demonstrates their suitability for their implementation into selected fabricated devices. These simulation results are discussed with a consideration of their predicted performance against the required specification.

A discussion on typical fabrication methods followed by details on the fabrication of four prototype devices is presented in Chapter 6. For each device a discussion of the aims, experiments performed and reflection on the results is given. A detailed description and evaluation of the methods employed for the fabrication of the prototype devices is provided. The results from one prototype device informed on the redesign of subsequent prototype devices. Where possible, results from the prototype devices have been compared with the computational model discussed in Chapter 4.

The final chapter in the thesis is Chapter 7 which concludes the work presented and gives a discussion on the research direction and outlook to future work.

Chapter 2

Project Description and Methods for Enhancing Separation

2.1. Project Description

The research described here was an integral part of a larger project entitled 'Microfluidic Devices for Structural Health Monitoring and Integrity'. The project encompasses work conducted by researchers undertaken jointly in the Faculty of Physical and Applied Sciences and the Faculty of Engineering and the Environment with funding from the Engineering and Physical Sciences Research Council (EPSRC) and the Defence Science and Technology Laboratory; EPSRC reference: EP/F004362/1.

This project addresses difficulties regarding corrosion monitoring, particularly within aerospace and marine environments. There are a variety of reasons why it is important to monitor and measure corrosion. Understanding the evolution of corrosion enables both an accurate prediction of material lifetime and cost effective scheduling of maintenance. The latter issue is further aided by autonomous in-situ monitoring. Further to this, an in-situ corrosion monitoring system would be able to detect and notify a user to a potentially dangerous failure.

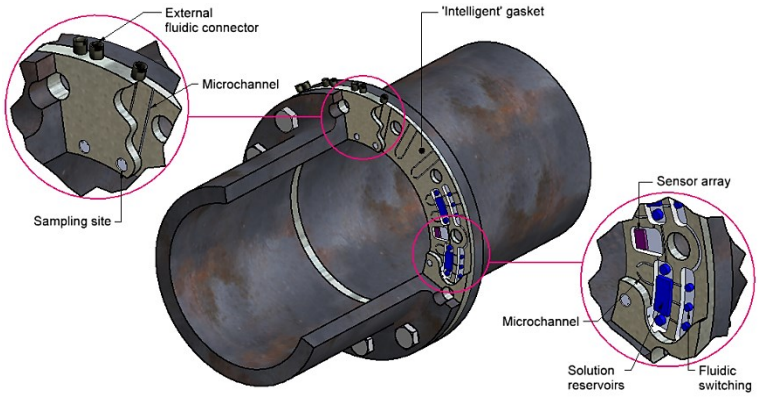

Figure 2: Intelligent gasket concept illustration (image courtesy of Dr Andy Cranny).

There are a large variety of devices and methods for monitoring corrosion in situ. Usually these either tend to require a user to evaluate the extent of the corrosion or are simple pass/fail type devices [1, 3, 4]. Incorporating CE into a corrosion monitoring system enables a more detailed analysis of the corrosion sample solution, identifying all the sample constituents. Different metal systems can undergo several different stages (phases) of corrosion at which certain metal ions are released. Detailed monitoring of the sample solution over time could therefore enable the identification of the corrosion phase which in turn could indicate of the extent of the corrosion. Later in this chapter the difficulties of using CE analysis for this application are discussed and new separation enhancement techniques are proposed as solutions to these difficulties. The separation enhancement routines described and investigated in this thesis will aid the development of a corrosion monitoring system which combined with a sensor system and knowledge database can indicate to the user the state and progression of corrosion. As well as informing on the monitored structures' health, the system will be a useful tool for characterising corrosion profiles. Results from the device could be used to evaluate the performance of a structural material within a particular environment which in turn would aid future material choices and inform design decisions.

Two concepts were described in the project proposal. The first concept was that of the 'intelligent gasket' which is able to detect and monitor corrosion within certain structures (e.g. at the interface between two sections of a pipe as shown in Figure 2). As can be seen from Figure 2, the sensor array and associated microfluidic components are positioned in the gasket and are able to report on the structural health and give advanced notification of structural faults. The system would only be able to report locally on the heath within the vicinity of the monitoring system. These results however would be indicative of the state of

the rest of the component. Furthermore, it was envisaged that the system would not only be able to detect corrosion but to inhibit it by the timely introduction of corrosion inhibitors, thereby prolonging the structural lifetime.

The second idea presented was for attaching a corrosion monitor to the structure, as opposed to embedding it, as suggested in the 'intelligent gasket' concept. This system would be of a portable format and could either be taken to a site, where corrosion monitoring is of interest and then attached for in-situ measurements or used to make 'handheld' measurements. A design schematic for this instrument is presented in Figure 3. The second concept can be considered as a step towards the 'intelligent gasket' concept and so it was decided that the focus would be to develop a portable corrosion monitoring device prior to the 'intelligent gasket'.

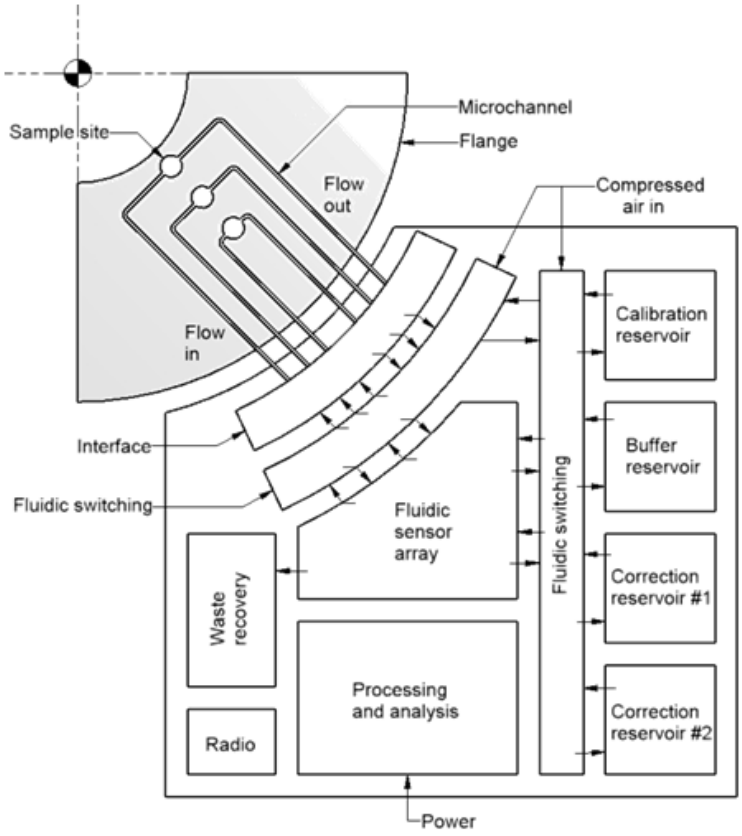

Figure 3: Schematic of the in-situ corrosion detection/monitoring instrument presented in the project proposal (image courtesy of Dr Andy Cranny).

The project sponsors expressed an interest in monitoring crevice corrosion, particularly in marine environments. As the name suggests this is corrosion which occurs within a small gap or crevice. The chemistry within these environments is complex; it depends on the composition of the material being corroded and the corrosive environment. Further to this,

the corrosive process itself varies with the evolution of the composition of the crevice environment over time [5]. During the different stages of corrosion the solution within the crevice varies in metal ion concentration which has a direct effect on the crevice pH. The corrosion rate is often accelerated once corrosion has been initiated [2].

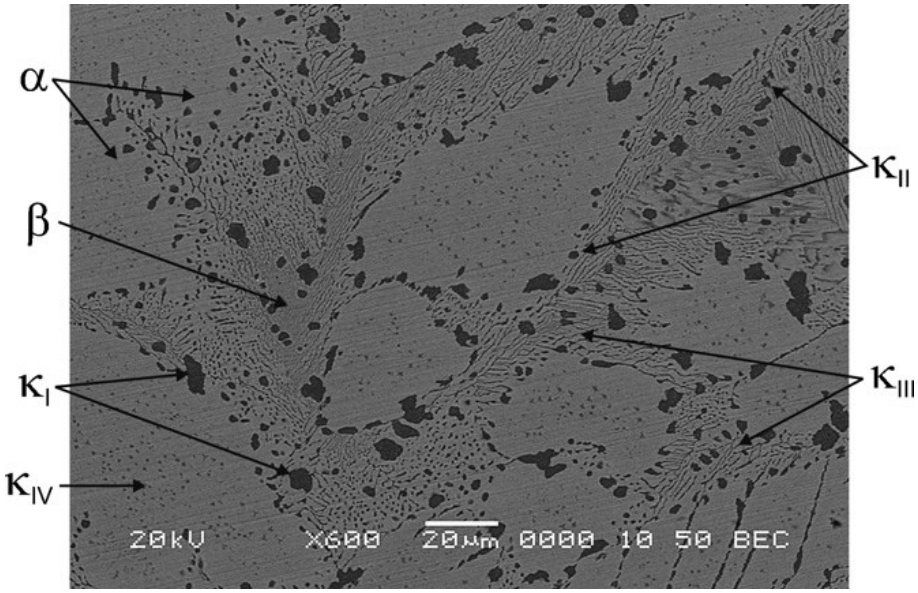

Figure 4: Scanning electron microscopy image of cast NAB with phases identified, taken from [2].

Since the crevice corrosion process is material dependent, a detailed description of the evolution process for NAB is given here. A scanning electron microscopy image of the NAB surface shown in Figure 4 highlights the various phases of corrosion. The table in Figure 5 shows the different elemental compositions of the various phases. Wharton *et al.* discuss how the κ-phases can exist as a range of elemental compositions and are distinguishable by a combination of their morphology, location and distribution in the microstructure [2].

Phase	Al	Mn	Fe	Ni	Cu
α	8.3 ± 1.7	1.4 ± 0.1	2.7 ± 2.0	2.5 ± 1.4	85.4 ± 4.0
Retained β	8.7	1.0	1.6	3.5	85.2
κ_I	13.0 ± 5.0	2.0 ± 0.4	55.0 ± 7.0	15.0 ± 3.0	15.0 ± 5.0
κ_{II}	19.0 ± 3.0	2.2 ± 0.6	32.0 ± 3.0	27.0 ± 4.0	21.0 ± 5.0
κ_{III}	18.0 ± 6.0	2.0 ± 0.3	22.0 ± 0.7	32.0 ± 2.0	26.0 ± 4.0
κ_{IV}	20.0 ± 3.0	1.5 ± 0.3	62.0 ± 4.0	4.0 ± 1.0	13.0 ± 1.0

Figure 5: Elemental composition of the NAB phases, taken from [2], originally cited in [6].

In the case of NAB, initially the copper rich α-phase is preferentially attacked over the iron rich κ_{III}-phase; however as the pH changes from slightly alkaline to highly acidic, the κ_{III}-phase begins corroding [2]. The evolution of the chemical composition in the crevice

was measured by Wharton *et al.* [7]. It was shown that once corrosion had initiated, the concentration of chloride ions increased to 98,000 ppm (2.8 M) over a period of 2 weeks; this can be seen in left graph of Figure 6. In this same time, the concentration of cupric ions increased to approximately 5000 ppm (0.079 M). 10 days following the initiation of the corrosion, the ferric ion concentration increased to about 1200 ppm (0.021 M).

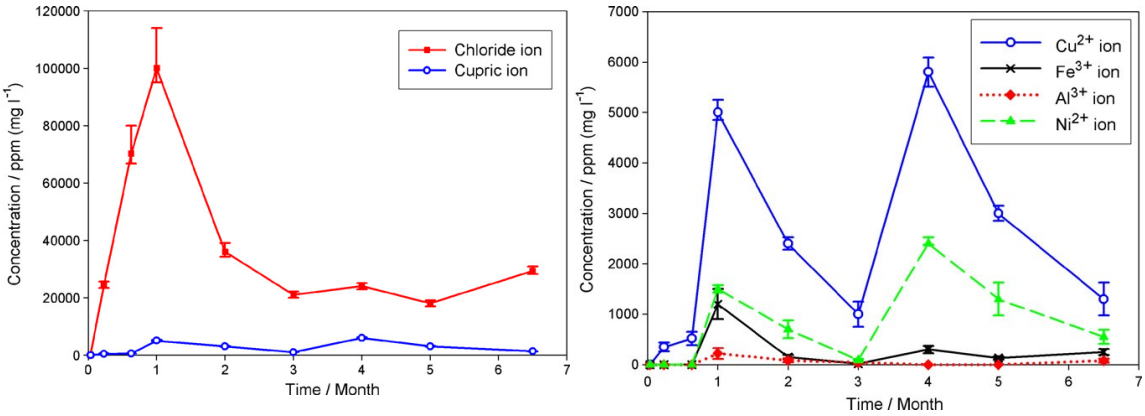

Figure 6: Graph showing change in concentration of chloride and cupric ions (left) and metal ions (right) in crevice solution with time, taken from [7].

An understanding of the complex chemistry within the crevice environment and the evolution of metal ion products over time would inform on the failure mechanism. It is also possible to generate corrosion signatures for different metal systems; these would aid the monitoring of metal structures. Combining the history of the solution composition within the crevice with the current solution chemistry could then be used to predict device failure [8, 9].

At the start of the project it was discovered that electrochemical detectors alone would not be suitable for the detection and analysis of corrosion processes. Work by Cranny *et al.* using methods such as cyclic voltammetry, whilst able to detect one or two ionic species, were often unable to distinguish between multiple ions in a mixed sample [10]. For this reason it was decided that in order to perform electrochemical analysis it would be necessary to separate the constituent analytes in the sample. Separation of the analytes can be achieved using CE. Nie *et al.* have successfully used a laboratory-based CE instrument to separate a mixed sample of metal ions taken from a corrosion site [11, 12]. This work was conducted early on in the project and identified those ionic species which would need to be separated in the corrosion monitoring system. Further to this it also provided information about the corrosion evolution over time and showed that CE is an effective method for separation of corrosion samples.

There are a variety of areas covered by this project including the design and development of an electrochemical detection (ECD) system, investigations to further the understanding of corrosion processes (particularly within crevices), and the development of a microfluidic device capable of separating ionic species within a sample of corrosion analytes. The research presented in this thesis focuses on the development and improvement of separation resolution for miniaturised, portable CE systems.

2.1.1. Contribution of the Ph.D to the Project

The primary aim of the work towards a Ph.D was the development and in-depth investigation of novel methods to separate charged chemical species, these being metal ions released during corrosion in the case of the project. The metal ions of interest to the project were: Al^{3+}, Cr^{3+}, Cu^{2+}, Fe^{2+}, Fe^{3+}, Mn^{2+} and Ni^{2+}. The primary application considered for the metals under test is for structures in marine environments. Therefore initially, the crevice solution will typically be sea water, which contains ~3.5 % NaCl (0.6 M) [13]. Following corrosion, metal ions will elute into the crevice, the concentration of the metal ions is strongly dictated by the metal being corroded and the stage of corrosion, as discussed in Section 2.1. Following separation, metal ions are to be identified and quantified by electrochemical methods. The requirement for the system to be portable (and later in-situ) places numerous restraints on the design. One of the main restrictions was that the separation needs to be obtained within a short channel length. There are a variety of challenges to be addressed brought about by miniaturising the CE analysis technique and these are discussed in Section 3.2.

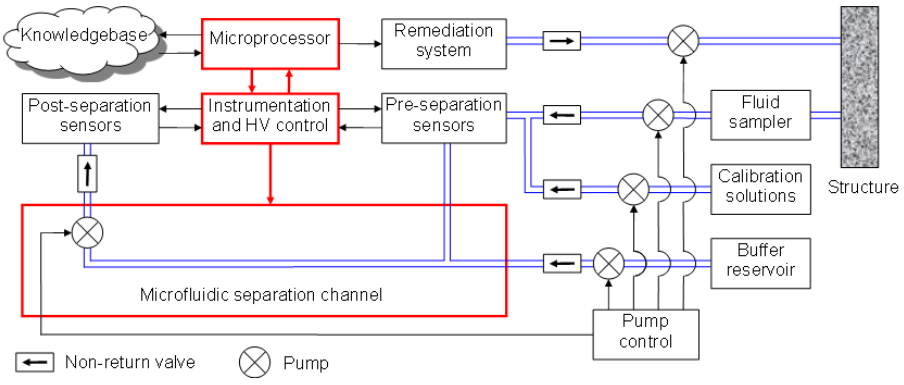

Figure 7: System overview of the device for the project. The sections highlighted in red are those that are important to the Ph.D side of the project since they are concerned primarily with the separation (image courtesy of Dr Andy Cranny).

In the literature, it is clear that there has already been significant research effort into the miniaturisation of CE systems and these are discussed later in Chapter 3. The approach presented in this thesis is different in that it avoids the use of complex chemical buffering systems. The separation enhancement is achieved through exploitation of the ability to control the EOF. The theory behind EOF and controlling it is described later in this chapter and this is explored in further detail in Chapter 4, which discusses computational modelling of the system. To describe the separation enhancement methods and investigate their limits or the window of operation, a detailed model has been developed to bring together all parts of the system. For the model to be a useful design tool for the miniaturised CE system, it is important that consideration is given to the fabrication of the device and to material specification. Where possible, the model has been experimentally validated, this is discussed in Chapter 6.

The expected outcome of the project was a miniaturised device capable of separating analytes of corrosion samples using novel techniques. An overview of how it was thought that the system would look is shown in Figure 7. This highlights where this research fits into the overall project, the focus being an investigation into the separation enhancement methods. Alongside this was the building of a microfluidic device to prove the methods. Aside from the fabrication of a microfluidic device, this encompasses a range of tasks including the development of a: high voltage power supply (HVPS), control system, and detection system.

A more detailed illustration on the microfluidic device to be built during the course of the Ph.D is shown in Figure 8. Here, a control system controls the HVPS system, the fluidic pumping system and the detection system. The detection system feeds into the control system which enables the control system to monitor the condition of the microfluidic CE device. Control of the fluidic pumping system refers to acquiring samples, and channel flushing and cleaning. The control of the HVPS system enables control of the sample injection and the separation.

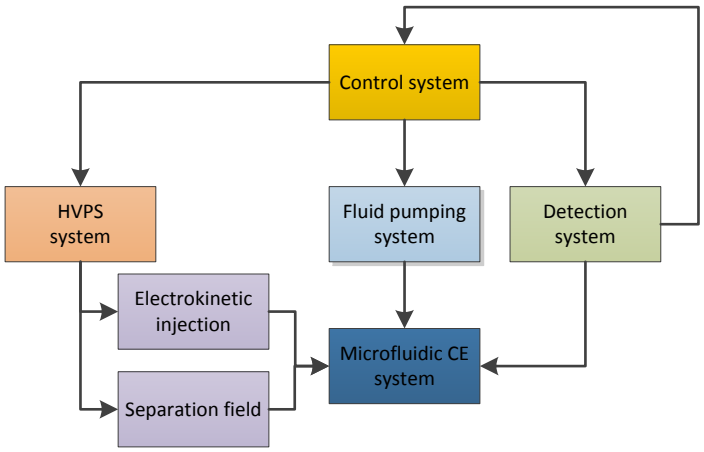

Figure 8: Illustration of the links between the various components of the microfluidic CE system.

Whilst this project requires the device to separate metal ions released from corroding materials, there is a much larger range of applications for this system. For example, Al is a known neurotoxin to organisms and has been linked to Alzheimer's disease [14, 15]. In 1989, the World Health Organisation (WHO) identified Al as a food pollution source; the limit of Al in drinking water was set to 7.41 μM [16]. Conventional methods for monitoring Al are typically based on atomic absorption or emission spectroscopy which requires expensive instrumentation [16]. Copper is required for physiological processes such as bone formation, cellular respiration and bone connective tissue development, a deficiency can lead to anaemia or pancytopenia [17]. However, excessive amounts of copper have been linked to eczema and may result in kidney disease, damage to the central nervous system and Alzheimer's and Wilson diseases [17-19]. For drinking water, the WHO set the maximum allowable level of Cu at 30 μM [20]. The detection of Cr is of importance for environmental chemistry, ecotoxicology and clinical toxicology as well as in the food industry [21]. Urbanek *et al.* discuss their interest in the detection of Fe, Co and Ni metal ions for monitoring heat exchanger fluids of nuclear power plants to monitor corrosion [22]. Other more general example applications of a miniaturised CE instrument include: drug development and quality control; proteomics and DNA analysis [23-27].

2.2. Capillary Electrophoresis: Theoretical Operation

In the case of crevice corrosion there is a solution which can be analysed to inform on the development of the corrosion. Depending on the metal system corroding, this solution contains a mix of metal ions from the bulk metal. These metal ions vary in size and charge and so exhibit differences in diffusivity and mobility. The metal systems of interest to the

project were primarily for marine environments and contained the metal ions shown in Table 1. As described in Section 2.1, Cu^{2+} and Fe^{3+} ions are of particular interest for monitoring NAB structures, since their presence in the crevice solution is indicative of corrosion [2, 7]. Later in Chapter 4, computational modelling of the separation of samples of Cu^{2+}, Fe^{2+} and Fe^{3+} ions using the separation enhancement methods is described. As can be seen in Table 1, the mobility of Cu^{2+} and Fe^{2+} are similar; this makes them difficult to separate within a small channel length. Demonstrating the ability of the techniques to separate metal ions with such similar mobilities clearly emphasises their significance for miniaturised CE systems. The values in the table for conductivity and diffusivity were taken from [28]. From the values of diffusivity D_{ion} it is possible to calculate corresponding values for mobility μ_{ion} using Einstein's relation, shown in Equation (1) [29].

$$\mu_{ion} = \frac{D_{ion} \cdot z_i \cdot e}{k \cdot T} \tag{1}$$

As can be seen from Equation (1) the value of mobility is inversely dependent on temperature, T. Here z_i, e and k denote the ion valence, elementary charge and Boltzmann's constant respectively. It should be noted that the value of diffusivity is exponentially dependent on temperature. The calculation for the values of mobility given in Table 1 assumed a temperature of 298.15 K (25 ˚C) since the values for diffusivity were given at 25 ˚C [28].

Table 1: Values for conductivity, diffusivity and derived mobility of metal ion of interest to the project [28].

Ion	Conductivity ($\times 10^{-4}$ m^2 S mol^{-1})	Diffusivity, D_{ion} ($\times 10^{-9}$ m^2 s^{-1})	Mobility, μ_{ion} ($\times 10^{-8}$ m^2 V^{-1} s^{-1})
Al^{3+}	61	0.541	6.32
Cr^{3+}	67	0.595	6.95
Cu^{2+}	53.6	0.714	5.56
Fe^{2+}	54	0.719	5.60
Fe^{3+}	68	0.604	7.05
Mn^{2+}	53.5	0.712	5.54
Ni^{2+}	49.6	0.661	5.15

An electrophoretic driving force acts on the metal ions when they are subjected to an electric-field. Due to the fluid mechanics there is also an opposing force known as Stokes' drag force which is dependent on the viscosity η, of the supporting buffer medium [30]. The electrophoretic driving force $\boldsymbol{F_{el}}$ is given by the product of the valence, z_i, elementary charge, and electric-field strength, $\boldsymbol{E}$, as shown in Equation (2).

$$\boldsymbol{F}_{el} = z_i e \boldsymbol{E} \tag{2}$$

The Stokes' drag force ($\boldsymbol{F}_{drag}$) acting on a particle, with a hydrated radius *r*, moving through a fluid at a steady state velocity is given by Equation (3).

$$\boldsymbol{F}_{drag} = -6\pi\eta r\boldsymbol{u}_{ep} \tag{3}$$

Figure 9 illustrates how both of the forces act on the charged species to accelerate it in a direction and at a rate dependant on their individual magnitudes and direction. These two forces are balanced (i.e. $\boldsymbol{F}_{el} + \boldsymbol{F}_{drag} = 0$) within a few microseconds resulting in no net force acting on the species, thus they move at a constant velocity, referred to as the electrophoretic migration velocity, shown in Equation (4).

$$\boldsymbol{u}_{ep} = \frac{z_i e\boldsymbol{E}}{6\pi\eta r} \tag{4}$$

The electrophoretic migration velocity of an analyte in an electric-field is given by the product of the mobility and electric-field strength. Using Equation (4) an expression for the electrophoretic mobility can be obtained, see Equation (5).

$$\mu_{ion} = \frac{ze}{6\pi\eta r} \tag{5}$$

From Equation (5) it can be seen that the electrophoretic mobility, and therefore the electrophoretic velocity, is proportional to the ionic charge of a sample and inversely proportional to those parameters which increase the drag within the buffer solution. These drag components increase with viscosity and the hydrated radius. Ions in aqueous solutions tend to be surrounded by a tightly bound atomic layer of water molecules; this increases the effective radius of the ions, hence the use of the hydrated radius as opposed to the ionic radius.

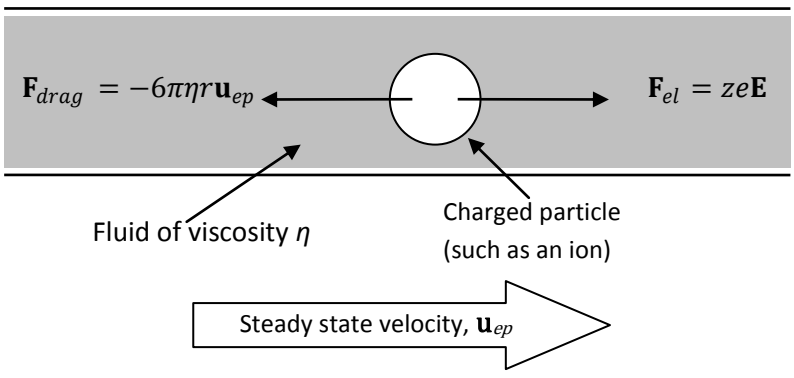

Figure 9: Forces acting on a charged particle with hydrated radius r, as it moves through a fluid under the influence of an electric-field (image derived from [30]).

When two or more ionic species, with different electrophoretic mobilities, are subjected to an electric-field within a solution, they migrate through the solution at different velocities proportional to their mobility. This difference in velocity means that over time they separate.

CE uses this principle by injecting the sample of mixed ions into a buffer filled capillary, along which an electric-field is established. Further to understanding the movement of the charged species in an electric-field due to their mobilities, it is important to understand that when using a capillary or channel, there is another flow, the EOF, which needs to be considered.

2.3. Electroosmotic Flow

Electroosmotic flow (also termed electroendosmotic flow) describes the movement of the entire buffer solution in a capillary (or channel) when subjected to an electric-field. The reason EOF occurs is due to the presence of surface charge along the walls of the capillary or channel and their interaction with an electrolyte (the buffer solution) [31]. In the case of a fused-silica capillary (commonly used with laboratory-based CE machines) which is filled with a buffer solution, the surface silanol (Si-OH) groups become ionised to negatively charged silanoate ($Si–O^-$) groups [32]. The silanoate groups are catalysed by the OH- ions in the solution [32]. A method of enhancing the ionisation process in fused-silica capillaries is to flush a basic/alkali solution such as KOH or NaOH through the channel [33]; this replenishes the capillary wall. The cations in the buffer will be attracted to the negatively charged capillary walls and move towards them to form an inner layer (called the fixed or Stern layer). Since the density of cations at the inner layer will not be large enough to neutralise all the negative charges on the capillary surface, an outer layer that extends further into the centre of the capillary is also formed (known as the mobile layer) [33]. As a result a double diffuse layer is formed by the two layers of cations. The resultant potential between these two layers is referred to as the zeta-potential [34]. An in-depth discussion on models for predicting the EDL is presented in Chapter 4. Figure 10 shows a representation of the position of the charges and layers in EOF.

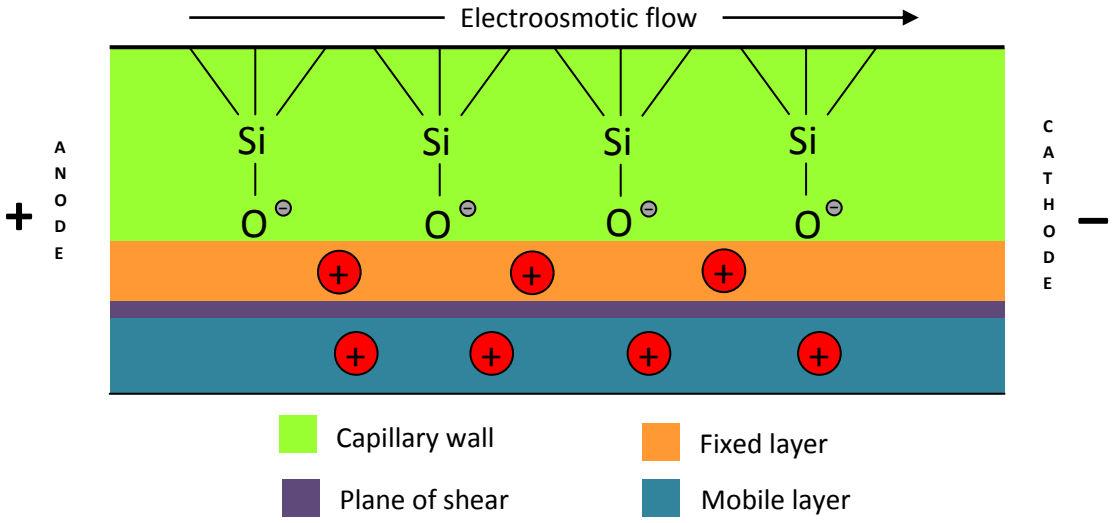

Figure 10: Representation of EOF in a fused silica capillary (imaged derived from [33]).

The rate of the EOF depends on the field strength and the zeta-potential which is related to the charge density of the capillary/channel wall. For example, changing the pH alters the charge density and therefore affects the EOF rate, the limit being when the ionic groups (silanol groups in the case of a fused silica capillary) along the wall of the capillary/channel become fully ionised [35].

The velocity of the electroosmotic flow, $\boldsymbol{u}_{eof}$ shown in Equation (6) can be written in a similar form as the electrophoretic velocity seen earlier [30].

$$\boldsymbol{u}_{eof} = \mu_{eof}\boldsymbol{E} \tag{6}$$

The electroosmotic mobility (μ_{eof}) is defined by the Smoluchowski equation [36] shown in Equation (7).

$$\mu_{eof} = \frac{\varepsilon_r \varepsilon_0 \zeta}{\eta} \tag{7}$$

Experimentally, the electroosmotic mobility can be determined by measuring the retention time of a neutral analyte in a channel subjected to an electric-field. The neutral analyte will migrate along the capillary due solely to the EOF, there being no electrophoretic force on the analyte [37].

Combining Equations (6) and (7) shows that the EOF flow velocity can be described by the Helmholtz-Smoluchowski equation [38] shown in Equation (8).

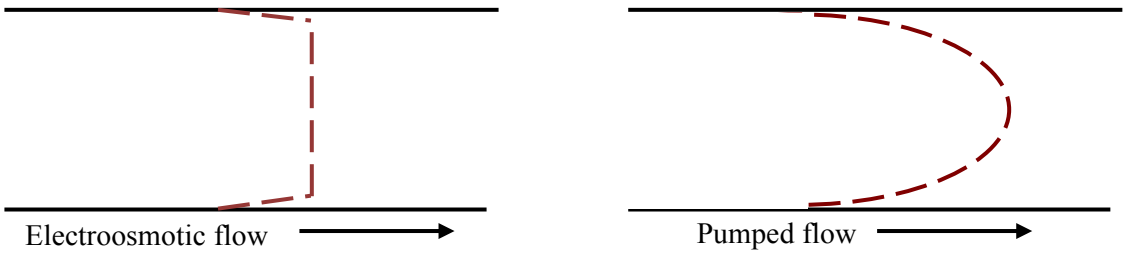

Figure 11: Velocity profiles for electroosmotic (left) and pumped flow (right) (image derived from [33]).

$$\boldsymbol{u}_{EOF} = \frac{\varepsilon_0 \varepsilon_r \zeta}{\eta} \boldsymbol{E} \tag{8}$$

Equation (9) shows the effective velocity ($\boldsymbol{u}_{eff}$) of an analyte in an electric-field due to electrophoretic migration and EOF.

$$\boldsymbol{u}_{eff} = \boldsymbol{u}_{ep} + \boldsymbol{u}_{eof} = (\mu_{ep} + \mu_{eof})\boldsymbol{E} \tag{9}$$

A property of the EOF flow profile compared with pumped (Poiseuille) flow is that it is flat, and for analysis purposes this is an advantage since there is less variation in the velocity profile across the width of the capillary or channel. For comparison with a pumped flow fluid profile see Figure 11. The flat flow profile caused by EOF is highly beneficial for separation systems in favour of a pumped flow profile, where the variable velocity along the channel cross-section contributes to band-broadening; for this reason all pressure differences during the separation must be minimised [39, 40]. Band-broadening also known as sample dispersion is where the sample travels at different speeds depending on its position in relation to the channel wall. This causes the sample to spread as it travels along the capillary or channel [39].

If separation of anions and cations is required together, then this can be achieved by making the EOF of the buffer greater than the mobilities of the negatively charged ions (assuming normal operation where the buffer flows towards the negative electrode). Without the EOF the negatively charged ions would simply migrate down the capillary or channel toward the anode and away from the detection system [33].

When separating a sample of analytes of mixed or zero charge the EOF moves the sample plug through the capillary/channel; anions will try and move against the EOF and move back towards the anode, cations will move with the aid of the EOF towards the cathode, whereas the neutral ions will have no electrophoretic velocity to contribute to their overall velocity and will move at the EOF velocity. Provided the EOF velocity is greater than the

electrophoretic velocity of the anions, all the ions in the sample will move along the capillary and will separate in a manner as illustrated in Figure 12.

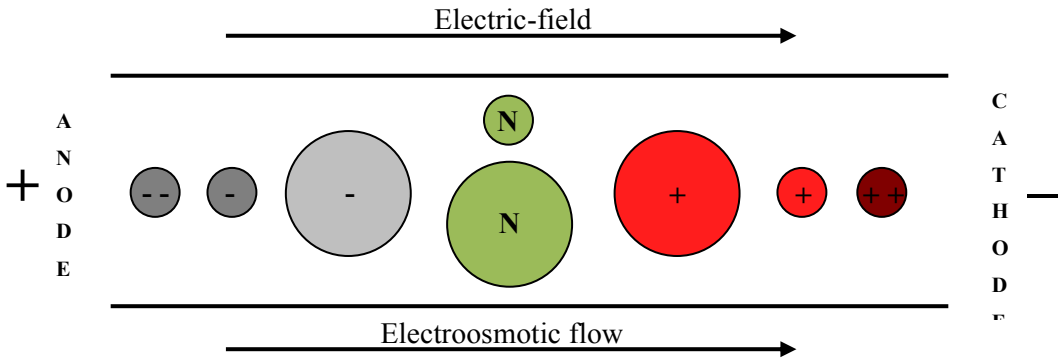

Figure 12: The order of separation of charged and neutral analytes according to their physical size and electrical charge; N denotes an ion of neutral charge (image derived from [33]).

2.4. Separation Enhancement Methods

Novel separation enhancement methods are discussed in this section. These are a primary part of this research and have undergone significant investigation, the details of which are discussed analytically and numerically in Chapter 4 and experimentally in Chapter 6. Here an explanation of the methods is provided to describe the aims of this work.

2.4.1. EOF Manipulation through Control of the Zeta-potential

As shown earlier in Section 2.2 the velocity at which ions move is directly related to the electric-field strength, thus control of the electric-field implies control of ion speed and direction along a capillary or channel. With a standard capillary or channel in CE there are two electrodes, one at each end, and the electric-field is established between the electrodes. The electric-field causes the ions to move because of electrophoretic forces and EOF. As explained earlier with Equation (8) the EOF is caused by a double layer on the surface of the channel walls; the velocity associated with the EOF is a function of solution permittivity, zeta-potential and viscosity. Wouden *et al.* [41] have demonstrated the ability to control EOF in microfluidic channels through the incorporation of insulated electrodes near the channel walls. This electrode could alter the surface charge by attracting/repelling ions thus increasing/decreasing the zeta-potential. Using this ability to dramatically alter the EOF,

Wouden *et al.* stated that they were able to stop and even control the direction of the EOF. It is therefore possible to improve separation, which is of increased interest especially for devices with shorter channels. More detail on work by Wouden *et al.* and other researchers in the area of zeta-potential modification is given in Section 3.10. With control of the EOF it becomes possible to achieve better separation of the sample. Schützner *et al.* discussed two methods to modify the EOF by altering the zeta-potential of capillary walls; these were by varying the buffer pH and through the addition of organic solvents to the buffer solution [42]. For the separation enhancement routines described later in Sections 2.4.2 and 2.4.3, dynamic control of the EOF is required throughout the experimental run. Modification of the buffer solution during an experimental run would not be possible without first removing the sample from the separation channel before flushing the channel with the new (modified) buffer solution. Doherty *et al.* reviewed the use of micro-channel wall coatings to tune the EOF [43]. These methods would be useful for initially setting the EOF to a desired value before using the ZPM electrodes to dynamically alter the zeta-potential.

2.4.1.1. Zeta-potential Modification in Microfluidic Devices

Work on the dynamic modification of the zeta-potential using externally applied electric-fields and the effect on the EOF has been investigated in both chip- and non-chip-based devices [44, 45]. Later in Section 3.10, work by numerous researchers is explored in detail; here a brief overview of the considerations is provided to give context when discussing the separation enhancement methods described in the following Sections (2.4.2 and 2.4.3).

Where a capillary is used, the whole of the capillary can be coated in a conductive paint so that the zeta-potential is modified uniformly radially around the capillary [46-48]. It is difficult to fabricate a microfluidic channel with an electrode in close proximity to all the supporting walls. Interestingly, the EOF can be modified by the use of just one electrode near the channel wall [49]. Work in the literature focuses primarily on using this method for modifying the EOF solely for electrokinetic transport and its use for improving the separation in CE systems has not been addressed [38, 50-52]. The effect of modifying the EOF using a single channel wall, rather than all of them, on the separation of charged species warranted further investigation. The effect will depend on a number of parameters, including channel dimensions, buffer composition and proximity of ZPM electrode to channel wall [53, 54]. An understanding of the effect on all the parameters will give insight into the design constraints.

For planar systems, where the zeta-potential modification is enabled using one electrode next to a single channel wall, rather than along all of the channel surface, results in peak broadening due to a cross-channel variation in the EOF flow profile [39, 55]. In contrast to partially covered channels, Wu *et al.* confirmed that in their system which was based on a capillary where EOF modification occurred radially around the capillary, there was no measurable additional broadening induced by direct control of the EOF [56]. Peak broadening is highly undesirable for a separation system. The broadening of a peak can cause it to overlap with nearby peaks, hence making separation more difficult. Further to this, the spreading of the sample, reduces the peak concentration and therefore makes detection more challenging. The effect of partial channel coverage on the peak broadening is explored theoretically with the aid of modelling, to deduce the window of operation for a given set of parameters in Chapter 4.

2.4.2. Matching EOF to Electrophoretic Flow

With an electric-field applied across the channel in CE, the mixed sample of ions migrates along the channel. As stated in Section 2.2, the charged species in the sample will migrate at different velocities dependent on their individual values of electrophoretic mobility and the EOF. For the project, the sample to be separated will primarily consist of the ions of interest (listed in Table 1, Section 2.2), these are all cations and therefore are attracted to the cathode. In this case if the EOF also flows towards the cathode then this can make attaining a good separation more difficult. The sample will migrate along the channel in a short time because both the EOF and electrophoretic flow are acting in the same direction, however, only the electrophoretic force acts to separate the sample. The longer the sample is in the electric-field the larger the separation, assuming the diffusion is limited, which is a reasonably valid assumption for most microfluidic devices. Some researchers, for example Doherty *et al.* try to eliminate EOF by modifying the channel walls prior to performing the separation [43]. Other researchers report work where they modify buffer solutions to get the EOF to a value which aids separation [57]. If the EOF is against the flow of ions down the channel, such that it reduces the speed of the ions, then the ions spend more time in the electric-field and so become more separated as they approach the end of the channel. This research investigates the ability to control the EOF and thus affect the separation by placing an electrode, the ZPM electrode, close to the channel surface.

In the case of a sample of two ionic species, species S_A and S_B, if S_A has a higher electrophoretic mobility than S_B, then after some time travelling along a channel subjected to

an electric-field, S_A will move ahead of S_B and the sample will become separated. This assumes that the channel is long enough for the difference in the values of mobility of the ions to produce this separation. By comparison when the two ions have similar electrophoretic mobilities they will not have undergone significant separation by the time they reach the end of the channel. The concept of matching the EOF to the electrophoretic flow relies on knowing how the potential applied to the ZPM electrode affects the EOF. It also requires knowledge of the values of electrophoretic mobility of the sample analytes being separated. For the case of the mixed sample of species S_A and S_B, if a potential is applied to the ZPM electrode to make the EOF equal and opposite to the velocity of species S_B, then the net force acting on B will be zero and so it will not migrate down the channel. On the other hand, S_A, which has the slightly higher mobility, will be able to travel along the channel, albeit it relatively slowly. With an understanding of the theory of CE operation described in Section 2.2 it is possible to calculate the time taken for species S_A to separate from S_B. For samples where there are more than two ionic species to be separated the problem becomes more complicated. In many cases matching the EOF to be equal in magnitude and opposite in direction to the mean velocity of the ensemble of ionic species will improve the separation. The composition of every sample is different and so the optimum value to set the EOF will vary. In the next section, the switching concept is described, whereby finding the optimum value for the EOF is deemed less important.

2.4.3. Switching EOF Direction to Cycle Ions Along the Channel

For samples composed of species with similar values of electrophoretic mobility, all the sample constituents migrate along the channel with similar velocities. If the ionic species are not modified, a long channel length is required to attain a good separation. In miniaturised CE systems, channel lengths tend to be short, and so it is difficult to attain separation of the sample. As discussed earlier in Section 2.4.1.1, using the ZPM electrode it is possible to reverse the EOF [49, 51, 52]. The EOF affects the velocity of all the species simultaneously, therefore the sample can be made to migrate from the injection point to the channel end (but not leaving the channel) and then by reversing the EOF significantly, the sample can be made to migrate back to the start of the channel. Upon reaching the start of the channel, the EOF can be reset back to its natural value enabling the sample to migrate toward the channel end once again.

This work on separation enhancement methods was accepted for presentation at the fifteenth symposium on field and flow-based separations (FFF 2011); an international peer-reviewed

conference. Figure 13 shows an illustration presented at FFF 2011 to demonstrate the switching routine [58]. In this illustration it can be seen that when the sample reaches the end of the channel, there is some separation but not enough to clearly distinguish the analytes. The sample is moved back to the start of the channel by reversing the EOF, which

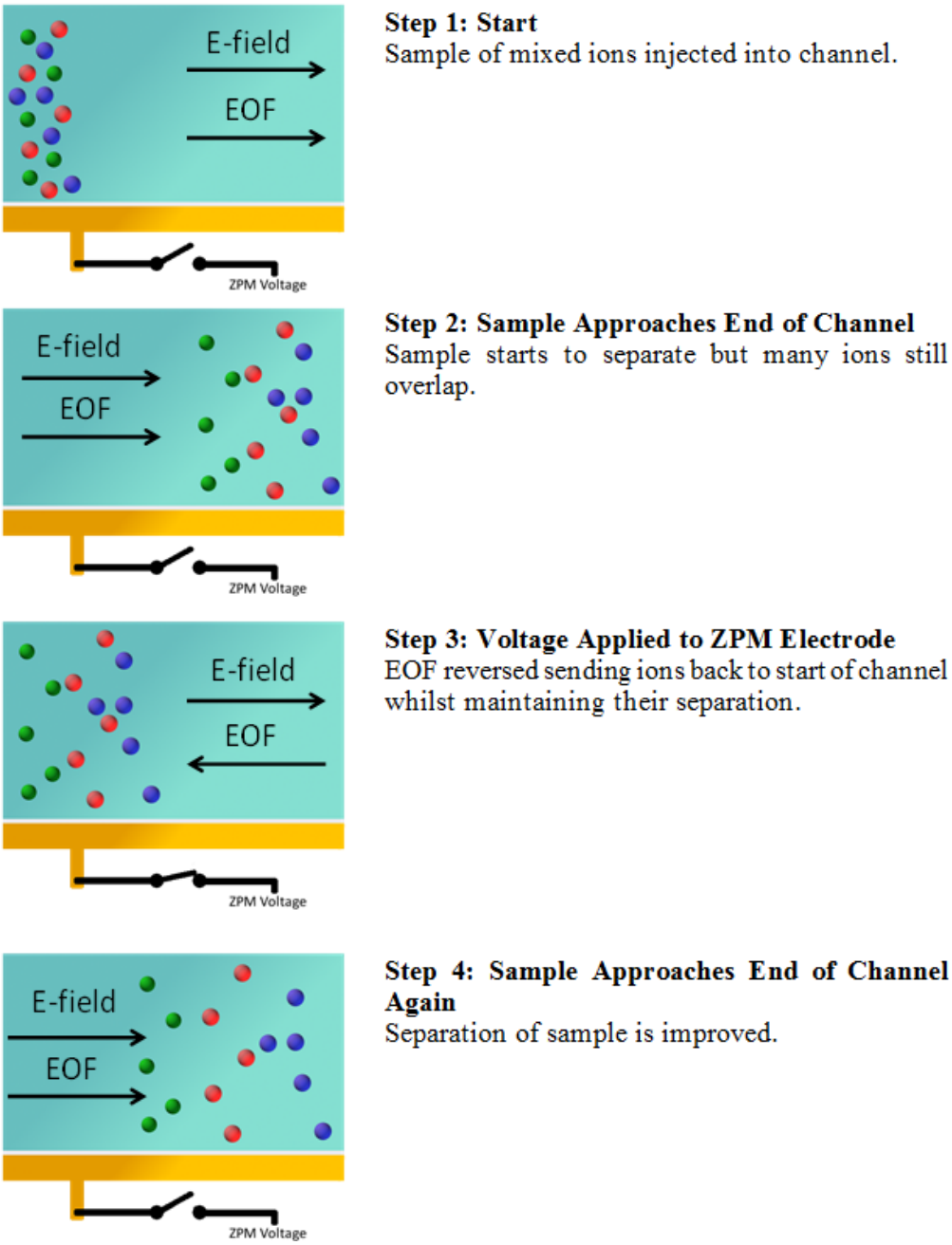

Figure 13: Illustration of switching EOF separation enhancement method taken from presentation given at FFF 2011 conference [58]. The blue ions have the highest mobility, followed by the red, with the green ions having the lowest mobility.

does not affect the separation thus far achieved. The sample then starts to migrate along the channel again, and as it reaches the end of the channel for a second time, it has become further separated.

The reason for cycling the sample along the channel length is that it increases the effective length along which the sample travels. Upon each migration along the channel length the sample becomes further separated. This process can be repeated until the ions are separated enough such that different groups of ions can be detected individually. The retention time of the ions in the electric-field is greatly increased without compromising the physical channel length. The separation of two species is given by Equation (10); for a given difference in velocity, the amount of separation is proportional to the time spent in the electric-field.

$$\boldsymbol{x}_a - \boldsymbol{x}_b = (\boldsymbol{u}_a - \boldsymbol{u}_b) \cdot t \tag{10}$$

The time spent in the electric-field depends on the velocity of the species and the effective channel length. Theoretically the EOF could be reversed any number of times, thus increasing the channel length to however long is required. The main limiting factor will be the diffusion of the sample; later in Section 4.3.2, modelling of diffusion is discussed and it is incorporated into the computational model.

2.4.4. Practical Considerations

The EOF is a complex process which is strongly dominated by the zeta-potential. Precise control over the zeta-potential is difficult, since it is sensitive to variations in temperature, buffer pH, channel contamination, etc. [53]. A rapid switching technique to overcome the anticipated difficulties of accurately matching the EOF to the sample velocity has been described in the previous section. This method uses a closed-loop control system to monitor the position of the sample within a small area. Two detectors are placed close together in the microfluidic channel; these inform the control system when the sample has arrived into their respective detection areas. At this point, the control system switches the EOF direction. Shortly afterwards, the sample moves into the detection window of the other detector. This sends a signal to the control system indicating that the EOF direction should be switched again. Using this method, the sample is made to travel between the two detectors which are located close to each other for numerous iterations. The numerous EOF switching events overtime has the effect of emulating the mean velocity of the sample analytes. The effect of this is that the average EOF is matched to the average sample velocity. As a closed-loop

system it has the further advantage that it is resilient to unwanted experimental variations. Such variations could arise due to a number of reasons such as: temperature changes, pressure differences and sample composition. It should be noted that if the constraint on time for identification is removed then an additional constraint is placed on the detection method, in that it would need to identify the separated species.

Work by Nie *et al.* [11, 12] has demonstrated that different ions, of interest to this project, can be separated out using a variety of buffering systems and that in some buffer solutions the separation of one group of ions is greatly improved over that of others. For example, it was determined that the surfactant cetyltrimethylammonium hydroxide (CTAH) efficiently isolates and separates Cu^{2+} and Ni^{2+} ions from a mixture of metal cations, whilst the surfactant tetramethylammonium hydroxide (TMAH) will separate Mn^{2+} ions with no effect on Cu^{2+} and Ni^{2+} [11]. A similar approach of using complex buffering systems for the portable system is undesirable since it would limit its applications. The buffers are designed for the analysis of a specific type of sample. The research focus is on a more generic method of enhancing the separation resolution of CE systems which can be applied to a large range of sample types.

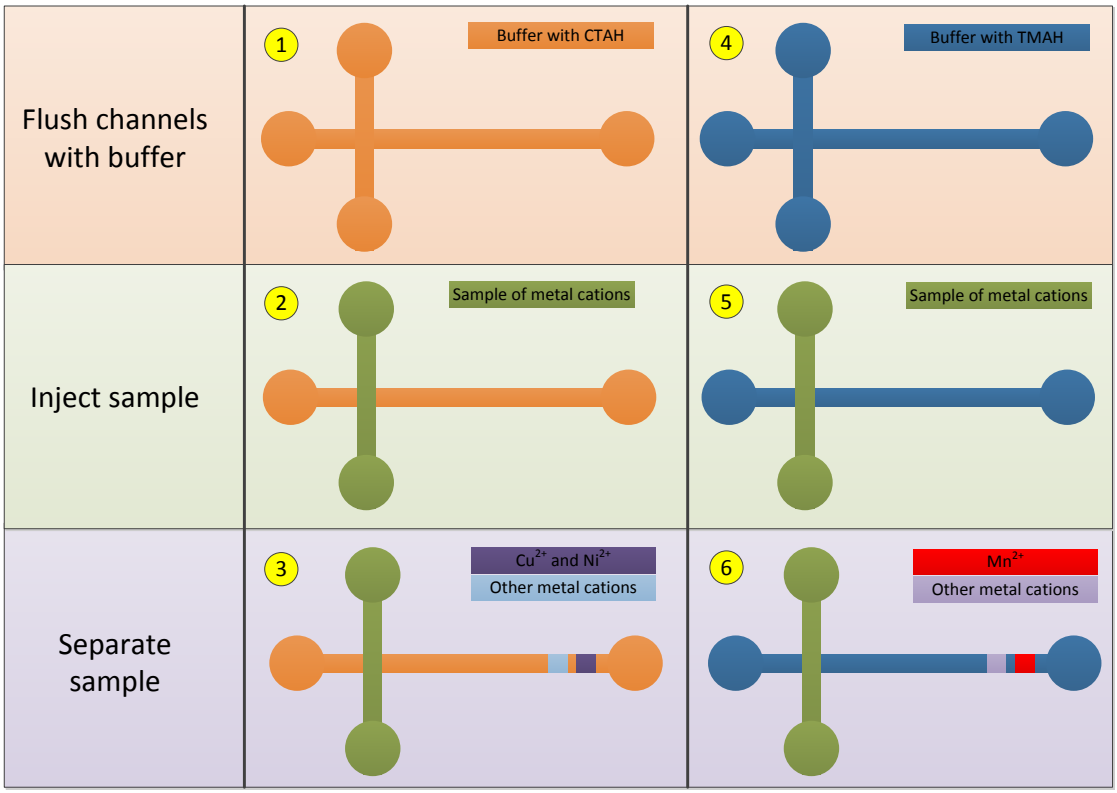

Figure 14: Separation scheme where the separation is enabled by the use of multiple buffer solutions.

Further to limiting the applicability of the system, there are numerous practicality issues with using complex buffering systems. For the samples the project is concerned with, which contain a variety of metal ions, there would be the requirement for multiple buffering systems. In a portable CE system, and even more-so in an in-situ CE system, this would introduce the requirement for a complex fluidic network control. Figure 14 illustrates the case where two buffer systems would be required, such as those described by Nie *et al.* [11, 12]. In the first run, with the first buffer selected (buffer modified with CTAH), Cu^{2+} and Ni^{2+} can be separated from the rest of the sample. The sample is injected and then separates as it travels along the channel. Once these species have been separated, the channel must then be flushed out and the next buffer flushed through the channel. Following this, a small amount of sample is injected into the channel. The new buffer is designed to separate a different species from the sample, for example, the buffer modified with TMAH aids the separation of Mn^{2+} ions from the other metal cations. Combining the results, from the numerous runs with different buffers, enables the identification of the sample composition.

2.4.4.1. Combining Separation with Electrochemical Detection Methods

Earlier in Section 2.1 it was stated that ECD methods, such as cyclic voltammetry, were not suitable to detect all the ions of interest of the project. This is because the electrochemical potentials at which redox reactions occur are too close together. In turn this informed the decision to separate the metal ions prior to analysing them electrochemically. A table of the standard electrode potentials versus the standard hydrogen electrode (SHE) are given in Table 2. These values show the redox potentials of the ionic species; the word redox is a portmanteau of reduction and oxidation. Reduction reactions involve the gain of electrons, whereas oxidation is the loss of electrons.

Table 2: Values of standard electrode potential for ions of interest to this project. Potentials given for aqueous solutions at 25 ˚C and versus SHE.

Half-reaction	Standard electrode potential (V)	Ref.
$Al^{3+}(aq) + 3e^- \leftrightarrows Al\ (s)$	-1.676	[59]
$Mn^{2+}(aq) + 2e^- \leftrightarrows Mn\ (s)$	-1.19	[60]
$2H_2O\ (aq) + 2e^- \leftrightarrows H^2\ (g) + 2OH^-(aq)$	-0.84	[60]
$Cr^{3+}\ (aq) + 3e^- \leftrightarrows Cr\ (s)$	-0.74	[61]
$Fe^{2+}\ (aq) + 2e^- \leftrightarrows Fe\ (s)$	-0.44	[59]
$Ni^{2+}\ (aq) + 2e^- \leftrightarrows Ni\ (s)$	-0.26	[59]
$Fe^{3+}\ (aq) + 3e^- \leftrightarrows Fe\ (s)$	-0.04	[62]
$Cu^{2+}\ (aq) + 2e^- \leftrightarrows Cu\ (s)$	0.34	[59]
$O^2\ (g) + 4H+\ (aq) + 4e^- \leftrightarrows 2H_2O\ (aq)$	1.23	[59]

Whilst the metal ions cannot all be identified in a single voltammogram, certain metal ion reactions occur at potentials far enough apart that they can be independently identified within a voltammogram. This advantage of ECD methods means that some ions can be detected and quantified in the presence of other ions and so the sample does not need to be completely separated. An example of this would be for the analysis of a sample of Cu^{2+}, Fe^{2+} and Fe^{3+} ions. Cranny *et al.* designed and developed thick-film platinum electrodes, a photograph showing a selection of these can be seen in Figure 15 [10, 13].

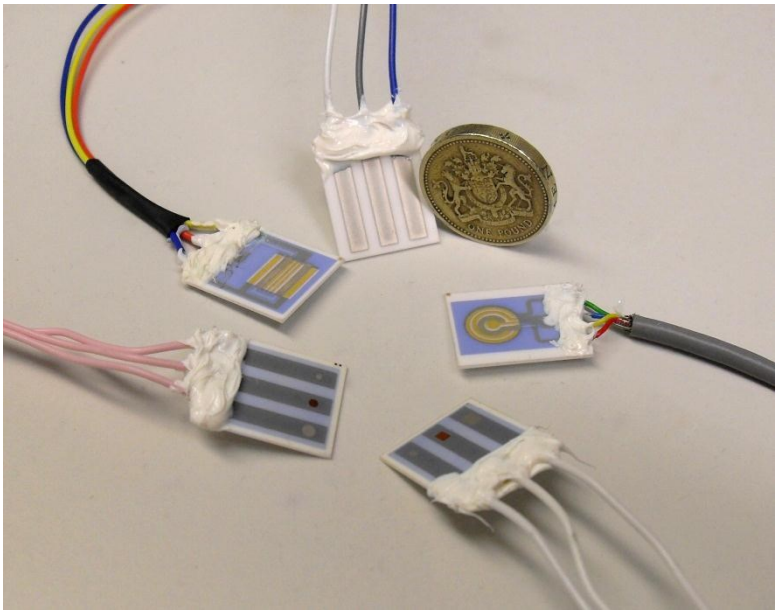

Figure 15: Photograph showing a variety of the thick-film electrochemical detectors designed by Cranny et al.

Using the thick-film electrodes it is possible to perform voltammetric sweeps, an example of results for a range of runs where the sample concentration is varied can be seen in Figure 16. This voltammogram shows the detection of Cu^{2+}, Fe^{2+} and Fe^{3+}; the various peaks correspond to the oxidation of the species. Numerous electroanalytical methods have been explored Cranny *et al.*, such as differential pulse voltammetry, square-wave voltammetry and linear sweep voltammetry [13]. Each method has its own advantages and disadvantages. They are not explained here in detail because they fall outside the scope of this thesis. An understanding of the ability of the detectors to detect mixtures of ions is of importance since it identifies the groups of ions which need to be separated. Furthermore it is important to understand the composition of the metal systems of interest to this project, and the metal ions which shall be released during corrosion, when deciding which electrochemical detector(s) and method(s) to use.

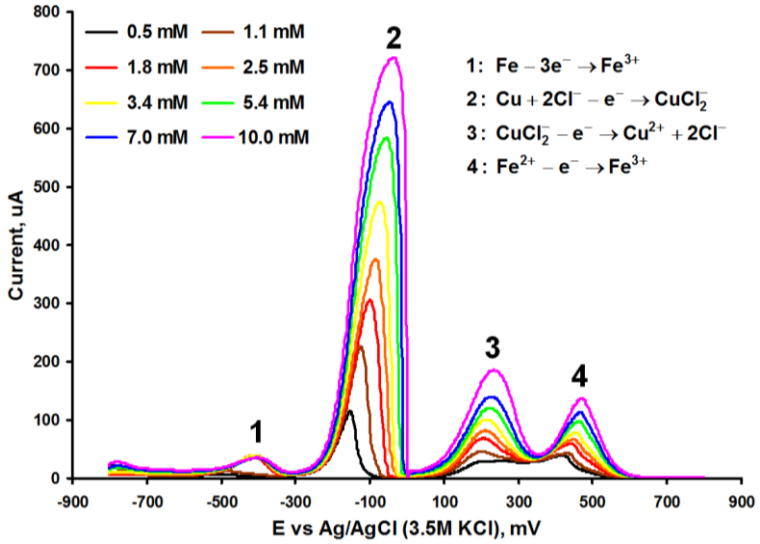

Figure 16: Voltammogram showing oxidation of equal concentrations of Cu^{2+} and Fe^{3+} using a platinum screen-printed electrode in 3.5 % NaCl, achieved using differential pulsed voltammetry (images courtesy of Cranny et al. [10]).

The fact that cupric (Cu^{2+}) and ferrous (Fe^{2+}) ions can be detected in the presence of one another using voltammetric methods was particularly useful for this project because these two ionic species have very similar values of mobility. These values differ by only $4x10^{-10}$ m^2 V^{-1} s^{-1} which makes them difficult to separate using electrophoresis. For example, after travelling a length of 0.5 m metre along a capillary in an electric-field, if the effect of EOF and diffusion are neglected for simplicity, the separation distance between the cupric and ferrous ions as they arrive at the capillary end is approximately $3.5x10^{-3}$ m.

It was decided that an electrochemical sensing system would be fabricated into the microfluidic device. This would be required to identify the ions following the electrophoretic separation process. The use of this detection method was selected to improve the accuracy and reliability, which is of particular interest for the corrosion application, since the sample could be contaminated with unknown ionic species.

The use of electrochemical sensors alleviates the requirement to fully separate cupric and ferrous ions from one another. If the cupric and ferrous ions are separated from the rest of the sample, then they can be analysed electrochemically together. This saves time, since the smaller the difference in mobility, the longer the separation time.

Neodo *et al.* developed ECD methods with boron doped diamond (BDD) electrodes [63, 64]. The hydrolysis of water is one of the limiting factors for the ECD. There are three main contributors to mass transport which influence the electrolysis reaction, these are: diffusion, convection and migration [59, 65]. At the potential at which the hydrolysis of water occurs

hydrogen and oxygen are evolved at the cathode and anode respectively, and consequently a large Faradaic current is produced [59]. Further to this, the process creates a change in the pH. Therefore it is not possible to make any measurements at or beyond this potential. For BBD electrodes this hydrolysis potential is larger than for the thick-film platinum electrodes and so analysis can be performed over a wider range of potentials. In unpublished work, Cranny *et al.* demonstrated that it was not possible to detect nickel ions with the thick-film platinum electrodes; however detection of nickel ions is possible with the BDD electrodes. Depending on the environment to be monitored, either just one, or a combination of, thick-film platinum electrodes and BBD electrodes will be required. An advantage of the thick-film platinum electrodes is that they are significantly cheaper than the BDD electrodes.

2.5. Control Systems

The separation enhancement methods require precise control of the electric-field, in terms of the magnitude, polarity and timing. There is the option of using either: an open-loop control system, a closed-loop control system or possibly a mixture of the two. Following a discussion on the control systems, a summary of the main attributes is given in Table 3.

2.5.1. Open-loop System

With an open-loop system, there is no feedback and therefore the operation of the device would require empirical knowledge about how the sample is expected to behave throughout the entire analysis. If the time taken for each ion to travel to specific parts of the device, for a given set of conditions, is known then the control signals can be time based. From other studies conducted within the project, the ions of interest with regard to corrosion and the metal-systems under test have been identified. It is therefore theoretically possible to set up a control system which aims at separating out the ions based on this knowledge.

For example if the matched EOF system, as described in Section 2.4.2, was to be controlled by an open-loop system it would require the knowledge of the sample velocity. Further to this the effect of the ZPM potential on the EOF would need to be repeatable, reliable and precise.

For the switching scheme, as described in Section 2.4.3, to be controlled by an open-loop control system, the migration times for the species along the channel, the time to perform the

EOF switching and the number of switching events required to attain the separation between analytes would need to be known.

Generally, the knowledge required by open-loop control systems severely limits their ability to adapt to unpredictable variations during the analysis. For example, in the case of the EOF switching method, the EOF needs to be switched when the ions reach a precise location along the channel. A change in temperature during an experimental run would change the species migration velocity and therefore the species would be at a different location to that required by the control system at the point at which the EOF is switched. For an open-loop system to be practical, the system must operate in a well-defined environment, or conduct calibration and adjust accordingly to account for the environmental changes.

2.5.2. Closed-loop System

Since the control system needs to know when sample species have reached certain points in the channel, a closed-loop system has the advantage that it can feedback signals from detectors positioned along the capillary length, reporting on the progression of the sample. The system can then be designed to account for variation between sample behaviour due to a number of factors, be they experimental or environmental. This kind of variation would severely compromise an open-loop system. Further to this, the fabrication method will introduce manufacturing tolerances. It is desirable for the system to be able to operate without the requirement for individual calibration.

As an example, one method to implement a closed-loop control system for the switching EOF concept would be to place a detector located near both ends of the channel. As the sample passes the detector, if it is not adequately separated the EOF can be modified to send the sample back towards the other detector. The EOF will remain modified until this other detector informs the control system that a sample has arrived; after which the EOF will be set to send the sample back towards the first detector. As it arrives at the “first” detector for a second time the degree of separation needs to be evaluated. If the control system deems that the sample is not separated then it repeats the EOF modification process to send the sample between the detectors. This process can be repeated until the required separation is achieved.

An advantage of the closed-loop system is that where a sample does not contain every ion of interest, the controller will not initiate a needless routine to find them. For example, with the open-loop timed system, the routine for detection of the ions in the sample is the same for

any sample composition; with the closed-loop system however, the routine becomes dependent on the sample composition. The closed-loop control system is more complex than the open-loop system since it needs to be capable of evaluating whether or not a sample is separated.

2.5.3. Mixing Open- and Closed-loop Systems

Technically, the mixing of an open- and closed-loop system is an extension to a closed-loop system. The combination of known data patterns with feedback can simplify the controller and improve separation, detection and analysis. For example, for the switching EOF technique, the controller could be operated in a closed-loop manner; it could have a detector at either end of the channel. However, if this system knows the electrophoretic mobility of the ions to be expected then it would be capable of anticipating the arrival of ionic species. When a sample is detected, the closed-loop control system is then able to identify the ionic species based its migration time. If it is know that ion *i,* takes *t* seconds to arrive at the detector then a reading by the detector at that time would imply that it was caused by ion *i*. This could then be verified using the electro-analytical methods described earlier in Section 2.1. If the system is well characterised and knows the mobility of the ionic species in the sample (and which species to expect) then it would be possible for it to perform a self-calibration. For example, if the system knows that the sample will definitely contain some Fe^{3+} ions and that they will be the first to arrive then by monitoring the time taken for the ions to arrive, the migration time can be measured and compared to the expected migration time. Any difference between the values would be attributed to experimental variation. By combining knowledge of the monitored environment with the feedback, the complexity of the control system can be reduced. In a well understood and controlled environment it would be possible to operate without the ECD system. Further information on detection schemes for miniaturised CE systems is given in Chapter 5.

Table 3: Summary of properties of open- and closed-loop control systems.

Property of control system	Open-loop	Closed-loop	Mixed
Required knowledge	Mobilities of all analytes to be separated. EOF rate.	Number of ionic species to separate	Mobilities of all analytes to be separated
Robustness to experimental variability	Poor	Good	Good
Complexity of implementation	Low	High	Medium
Requires qualitative detection system	No	Yes	No

2.6. Conclusions

In this chapter, the supported project and its aims have been described. Within this the contribution of this research to the project were specified. The novel separation enhancement methods and their importance for miniaturised CE systems have been discussed. Practical design considerations have been addressed to aid the fabrication of a system for demonstration of the separation enhancement methods. The issues related to modifying the zeta-potential on a single channel wall have been raised and are investigated later. To investigate the methods and their limits it is important to develop a realistic computational model of all aspects of the system. This includes modelling the effect of the ZPM potential on the EOF. This then needs to be combined with a model for the transport of charged species in a microfluidic device. The models will require validation which can be achieved by comparison with empirical results.

Chapter 3

Literature Review

The work presented in this chapter formed the basis of a publication: the review paper entitled "Review on the Development of Truly Portable and In-situ Capillary Electrophoresis Systems" [66].

CE has undergone numerous improvements since its discovery. The various requirements, such as: a HVPS, detection systems and complex fluid control systems, have hindered its progress into portable instruments and even more-so as in-situ devices. In the literature there have been a wide variety of attempts at making portable CE yet only a few at in-situ systems. Technological developments in the last decade or so have made it feasible to fabricate these miniaturised CE systems with increasingly smaller dimensions. The research has digressed into numerous streams related to the miniaturisation of CE. For example, there are a large number of papers on novel fabrication methods for microfluidic platforms. Another area which has attracted significant attention is detection systems. It is clear that for the successful development of portable and in-situ systems that a holistic approach is required. All aspects of the system need to be made portable or suited to in-situ monitoring. This chapter will discuss the advances in CE, focussing on miniaturised CE, and the design of sample injection schemes and HVPSs. A number of successful truly portable and in-situ CE systems will be critiqued. Here, "truly portable" is used to mean that the research produced a miniaturised CE device, integrated with all the necessary supporting hardware, which had also been developed into a portable format. This hardware typically consists of battery powered HVPSs and detection systems, combined with a fluidic channel and an integrated fluidic pumping system.

In the literature there are numerous reports on attempts to integrate CE analysis into sensor systems. The work tends to be application driven and as a consequence the aim is usually to address very specific problems, rather than a more generic solution. With the requirements stated at such an early stage, the versatility of the end device becomes severely limited. Unfortunately whilst there have been many different novel concepts explored during the course of the research, a single device suitable for a multitude of applications has yet to be developed. One of many limiting factors is the requirement for buffering systems, the composition of which are often tailored for specific applications. To avoid non-linear electric-field drops across the buffer solution and sample, the conductivity of the buffer solution should be matched to that of the sample [67]. Many researchers make the sample conductivity at least 10 times lower than the buffer solution to generate a higher electric-field across the sample; a technique known as field-amplified sample stacking [68]. A further requirement of the buffer, aside from maintaining the pH, is that it is a good solvent.

The separation enhancement schemes described in Chapter 2 require modification of the zeta-potential to control the EOF. A discussion on applications which have used dynamic control of the EOF is presented.

3.1. Reasons and Motivations for Miniaturising CE

In order to monitor and gain a detailed understanding of various environments it is often necessary to take a sample from the environment for analysis. This sample is commonly a mixture of numerous components, and this makes it difficult to perform in-depth analysis of the sample as a whole. Provided the environment under test is already somewhat understood, one method for analysis is using an array of sensors, where the sensors are tailored to detect the individual components (such as an array of different ion selective electrodes, salinity/chloride sensors or conductivity probes). Whilst this approach has many advantages, the bespoke nature of these systems tends to limit their use to specific applications. A second method is to separate the sample into its individual components for analysis using CE. Depending on the sample composition, methodology and mode of operation used, it may be possible to analyse the sample in a single run using a detector to identify both positively and negatively charged species in the sample. An example of this analysis is capillary zone electrophoresis, whereby both anionic and cationic species in the sample are separated due to differences in their electrophoretic mobility [33]. There is a large range of variations in the methodology used for CE analysis; a discussion on these is included later in Section 3.5.1.

With an increasing demand to perform in-depth monitoring out in the field, it is no surprise that there have been a large number of attempts at incorporating separation technologies into portable instruments. Generally there are two commonly exploited routes for fabricating portable CE systems. One of which, uses a shortened capillary (such as a fused-silica capillary) and builds the miniaturised hardware around it [69]. The other method is to fabricate a microfluidic channel using microfabrication techniques [69-74]. The first method shall be referred to as non-chip-based CE systems, and the second as chip-based CE systems. The majority of the reported work relates to field-portable or point-of-care devices, though there has been some but not much research into the development of autonomous in-situ CE systems [75, 76].

Numerous authors have reported on the advantages which can be gained from the miniaturisation of fluidic systems [77]. The use of microfluidic systems for sensing and analysis in various environments is becoming increasingly popular. Commonly quoted advantages of miniaturised CE systems are:

- portability,
- stepping stone towards in-situ monitoring,
- reduced cost,
- disposability,
- reduction in required sample volume,
- faster analysis times,
- simplification regarding generation of large electric-fields.

Miniaturisation of CE can significantly reduce the cost and analysis time [57]. As an example application, in drug development and analysis, moving to the micro- and nano-scale has two significant advantages. Firstly a smaller device requires less of the drug to test. Secondly, a smaller sample volume reduces the material cost and analysis time, which in turn means that more tests can be conducted and more samples can be evaluated in a shorter period of time.

As well as saving on labour, cost, time and laboratory space, to perform the analysis, the ability to perform a complex analysis, such as CE, in the field gives credence to the possibility of intelligent remote sensors for a comprehensive range of monitoring applications. Throughout this chapter, the wide range of applications for CE will become apparent. This not only enables laboratory level analysis to be done in the field, but enables sensors and detection systems to respond to a much wider range of stimuli, producing useful and informative data. Before research into the miniaturisation of CE commenced, CE analysis was limited to the laboratory. There is still however, more research required to

further improve the integration of CE into intelligent sensor systems. It is hoped that the work in this thesis goes some way to helping this process.

3.2. Design Considerations and Challenges for Miniaturised CE Systems

In the literature there are numerous reports on the miniaturisation of CE systems. The focus can often be split into one of these three categories: novel fabrication methods, material choice, or detection methods. CE system design requires consideration of the following aspects:

- channel dimensions,
- device material,
- shape of the channel path,
- sample injection,
- detector method and placement,
- electric-field generation.

The channel dimensions, device material and shape of channel are considerations for chip-based CE. For non-chip-based CE, a cylindrical fused-silica capillary is most commonly used, though thought needs to be given to the diameter selected.

A small volume of sample needs to be injected into the capillary or channel for analysis. This sample injection needs to be repeatable. In the case of microfluidic chips, the sample is usually injected using a sample injection channel which crosses the separation channel. The area of overlap denotes the injection point. Electrokinetic or hydrodynamic methods may be used to inject a sample. For injection into capillaries, there are a few schemes employed. For example, the use of capillary forces, exploited by the lifting of sample vials, has been used to successfully inject samples. More information on sample injection schemes is discussed later in Section 3.9.

In many ways, CE seems suited to miniaturisation. The principle is relatively straight-forward, it requires a fluidic channel or capillary, a HVPS and a detection system. The largest challenge is due to the reduced channel length. With shorter channel lengths, it becomes difficult to attain sample separation before the sample migrates to the end of the channel. This is particularly a problem when the sample constituents exhibit similar values of electrophoretic mobility and therefore arrive at the detector window at similar or indistinguishable times.

Although CE requires large electric-fields, it does not require large amounts of electrical current flow and actually benefits from smaller current flow through the capillary or channel [78]. Small electrical current flow is important to avoid Joule heating. Further to this, in the case of portable CE systems, smaller current means smaller power consumption and hence longer operational lifetime. To keep the current flow small, narrow channels or capillaries are used in conjunction with low conductivity buffer solutions. Large current flow leads to Joule heating which is detrimental on the performance of CE [79]. Joule heating occurs when a current flows through a conductive liquid. As well as causing temperature increase, it can also create a temperature gradient. Both of these effects have an impact on the EOF and CE separation, which can cause strong sample dispersion and reduce the analysis resolution [80]. Joule heating can also cause the formation of gas bubbles which can block fluid flow through the channel.

Another cause of the formation of bubbles is electrolysis. This occurs at the high voltage electrodes. A consequence of electrolysis is that it changes the solution pH. This is particularly a problem for miniaturised CE systems due to the low volume buffer reservoirs, where the electrolysis occurs. Oki *et al.* investigated the relationship between reservoir volume and resilience to electrolysis induced pH changes [81]. They confirmed that smaller volume reservoirs are more prone to large variations in pH induced by electrolysis. The consequence of which is a variation in the EOF [82].

In miniaturised CE systems, channels with small cross-sectional areas are used because they have higher electrical resistances. This means that for a given potential difference along the channel, less current will pass through the channel and therefore the amount of Joule heating is reduced. A consequence of small channel cross-sectional areas, especially for long channels, is that difficulties can be experienced in priming and pumping fluid through the channel. If the fluid flow is subjected to a constant pressure drop Δp, the flow rate, Q, will also be constant; this can be seen in the Hagen-Poiseuille equation, shown in Equation (11) [30].

$$\Delta p = R_{hyd} \cdot Q \tag{11}$$

Where R_{hyd}, the hydraulic resistance, is a proportionality factor and is the inverse of the hydraulic conductance [30]. For different shaped capillaries or channels the value of R_{hyd} is different, for example in a capillary of circular cross-section it is calculated by using Equation (12).

$$R_{hyd} = \frac{8}{\pi}\eta L \frac{1}{{r_a}^4} \tag{12}$$

Where r_a is the radius of the circular cross-section; decreasing r_a has a significant effect on the hydraulic resistance. Equation (13) gives the expression for R_{hyd} for a capillary or channel with a rectangular cross-section of height h, and width w.

$$R_{hyd} = \frac{12}{1 - 0.63\left(\frac{h}{w}\right)}\eta L \frac{1}{h^3 w} \tag{13}$$

As well as reducing the electrical current flow, reducing the channel cross-sectional area can cause issues with the filling of the channels. As the geometries are scaled down, the surface tension force becomes increasing important [30]. Depending on the wettability of the surface, capillary forces alone may pull a fluid along a channel a certain amount but may not be capable of completely filling the channel. There are three cases to be considered when filling a microfluidic channel [83].

1. At the start, before the channel is filled with solution (i.e. it is filled with air).
2. As the channel becomes partially filled, the proportion of air to buffer solution reduces.
3. At the end once the channel is completely filled with buffer solution.

The second case, describes the situation during filling where the surface tension needs consideration. Here, the surface tension at the channel walls causes the formation of a meniscus. During the filling the momentum change is balanced by this surface tension force, the pressure difference and the viscous force [83]. Using fluids which have low values of surface tension, for example, solvents such as methanol or ethanol result in a low contact angle which reduces the surface tension force [30]. Once a channel is filled, the surface tension force no longer dominates, therefore one method to fill a channel with buffer solution is to first fill the channel with a fluid which has a low surface tension and then flush with the buffer solution. There are a variety of methods to fill the channel such as using pressure to force the fluid along the channels [84], or submerging the device in the fluid and lowering the surrounding pressure, for example by using a desiccator [85].

Even with low current operation, the high electric-field means that a large potential difference is required, and as such the power usage is not negligible. Depending on the power requirements and battery system employed, reports on the operational time show values which vary from 2 hours up to 15 hours [86, 87].

The generation of high electric-field strengths in shorter length channels requires smaller potential differences. The shorter channel lengths however are one of the primary challenges for miniaturised CE. As discussed earlier, the separation of analytes obtained using CE requires a certain amount of capillary or channel length. Shortened channel lengths have led to research into coatings, sample complexation and buffer solution development in order to achieve separation within the available channel lengths [88].

Material choice is another important factor to be considered. For in-situ monitoring in particular, usually the material will need to be robust to ensure a good device lifetime. Portable instruments are not so constrained; robustness is desirable, however it may be traded against cost or convenience. For example, there is the option to develop a replaceable fluidic-chip, rather than a robust fluidic-chip which may require an anti-fouling surface and a reliable cleaning system to have a long lifetime. A detailed discussion on material choices is included later in Section 6.2.

Increasingly, microfluidic systems incorporate electrokinetic methods, i.e. EOF, for moving samples and buffers around microfluidic chips. Smaller channel lengths mean that smaller voltages can be used to generate the high electric-fields required for EOF. This method of fluid flow control can be easily designed in miniaturised CE systems, since a HVPS will is available given that the operating principle relies on electric-fields.

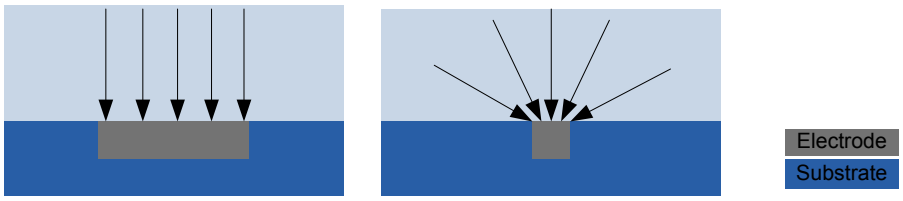

Figure 17: Flux density increases as the size of the electrode decreases.

As research has progressed, the fabrication of narrow/shallow channels has become more routine and more reliable. With this scaling down on the device size, there are negative impacts on other parts of the system. For example, if an optical detection system is used, then its sensitivity can become compromised [89]. For amperometric detection techniques however, the sensitivity is greater due to enhanced flux towards the surface [89]. Figure 17 illustrates how the flux density increases as the electrode size decreases. There has been a significant amount of research reported on detection systems for CE applications; a detailed discussion on these is given later in Chapter 5. Specifically, a discussion on optical and electrochemical detections systems is given in Sections 5.1.1 and 5.1.2 respectively. A brief summary of the respective merits of the detection systems is shown in Table 4. It can be seen

that unlike optical detection methods, electrochemical detection methods require decoupling from the HVPS [74]; considerations for the electrical decoupling of electrochemical detection systems are discussed in Section 5.1.3. A disadvantage of optical detection methods is that they usually require sample complexation to enhance the extinction coefficient of the sample at the detection wavelength [90].

Table 4: Summary of optical and electrochemical detection systems.

Detection method	Requires decoupling from HVPS	Requires sample preparation (e.g. complexation)	Scalability	Qualitative analysis	Typical limits of detection [90] (mol L^{-1})
Optical	No	Usually	Low	Yes	$10^{-4} – 10^{-8}$ [b] $10^{-5} – 10^{-9}$ [c]
Electrochemical					
Amperometric	Yes	No	High	Yes	$10^{-5} – 10^{-11}$
Conductometric	Yes [a]	No	High	No [d]	$10^{-4} – 10^{-8}$
Potentiometric	Yes	No	High	Yes	$10^{-3} – 10^{-8}$

[a] if the conductometric detection method is contactless then it is inherently decoupled.
[b] value for indirect UV absorption.
[c] for fluorescence detection.
[d] species identification can be inferred from migration time.

Earlier in Section 2.1 it was shown that the concentration of an ionic species of interest (from a sample taken from a corroding NAB crevice) would typically be >20 mM. As can be seen from Table 4 this value is significantly larger than the typical limits of detection for both ECD and optical detection methods [90]. Therefore the species concentration with regards to the corrosion monitoring application, addressed in this work, do not pose a significant challenge for the detection system. However, in Section 2.4.4.1 the issues associated with the electrochemical detection of one ionic species in the presence of another were discussed. A focus of this work was to enable the separation of the ionic species such that they can be detected individually by the ECD system developed by Cranny *et al.* [10, 13].

3.3. The Ideal Portable CE system

To give a metric by which to quantify the success of a truly portable CE system, a number of required characteristics are shown in Figure 18. Many of the characteristics are important for the portability of the device, others for the CE analysis aspect. Some aspects are important to both.

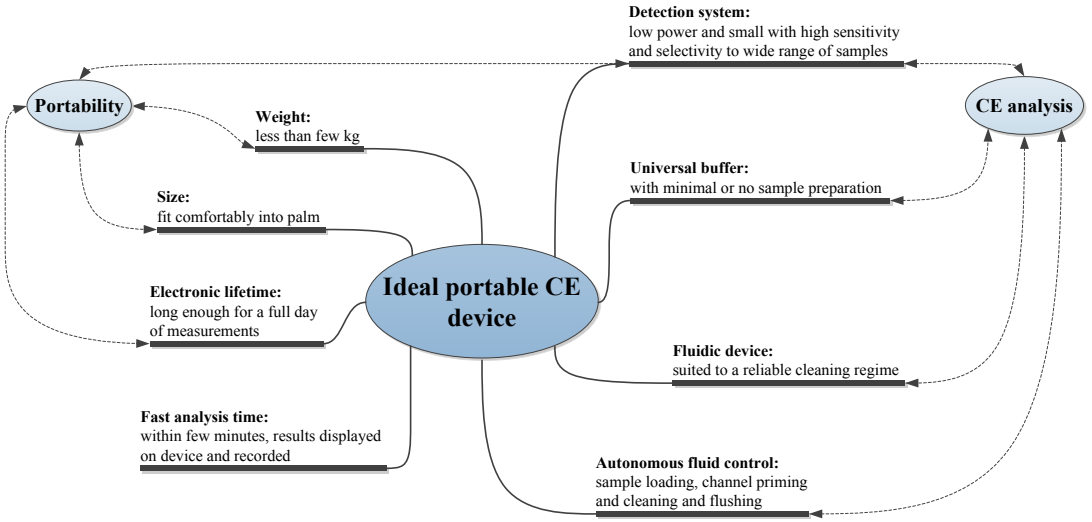

Figure 18: Schematic showing aspects required for an ideal portable CE device.

The ideal device here is defined as being a portable system capable of performing CE analysis for any appropriate application. This is clearly unfeasible but it is a useful concept to help map and guide research and design. It is also useful to refer to the ideal device when developing a practical design idea for lab-on-a-chip and portable CE systems. An understanding of how all the components fit together and their importance enables the designer to evaluate all the advantages and disadvantages of the design decisions. With the specification of the end users' requirements in mind, a comparison with the concept of the ideal device gives a useful insight into the extent of the compromises and the consequence on the resulting device.

There are numerous trade-offs between some of the criteria for portable CE systems. For example, portability requires the device to be small (handheld) and lightweight (less than a few kg), but it also requires a self-contained power source. The obvious power source is batteries, however these can be large and heavy. Further to this, the amount of energy stored in a battery is finite and therefore the electrical lifetime is limited. Since analysis times tend to be short, the real issue becomes the number of analyses which can be performed within the battery lifetime. For the ideal device, with field measurements in mind, here it is stated that it is desirable to have an electrical lifetime that enables a full day of measurements.

3.3.1. Typical Chip-based CE Microfluidic Devices

A common layout for channels in miniaturised CE devices is to have two channels crossing each other as shown in Figure 19. The open channel is created in one substrate and then

sealed by bonding the channel substrate to a flat substrate. Prior the bonding, the reservoirs are usually established by drilling or punching holes through the channel substrate. Often the two substrates are the same material. It is not uncommon however, for a device to have a channel created in one material, for example, a polymer (such as polydimethylsiloxane (PDMS)) sealed to a flat glass substrate [49].

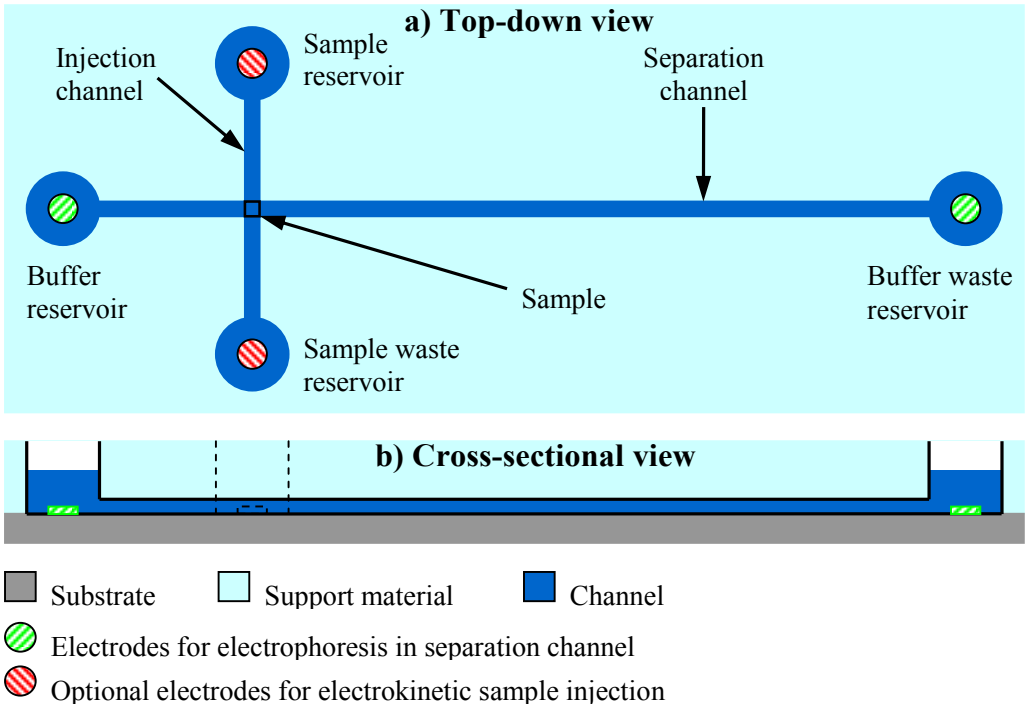

Figure 19: Top-down view (a) and cross-sectional view (b) of a typical layout for miniaturised CE device.

3.3.2. Considerations for In-situ CE Systems

There are different interpretations of exactly what in-situ means. Some researchers consider an in-situ system as one that is embedded into an environment, whereas others, and as is described here, consider in-situ to mean a system that sits within an environment and performs analyses autonomously. Since many of the major challenges that face portable CE also face in-situ CE, it is easy to consider in-situ CE as an extension of portable CE. For example, if you take a portable CE system and modify the control system such that it automatically initiates an analysis when required, then provided the fluid control system is capable of acquiring a sample, the system could be considered in-situ.

On the other hand however, it should be noted that an in-situ system does not necessarily need to be portable. For example, in a water quality monitoring plant, the system could be

large, heavy and mains powered, thus removing a number of the constraints pertaining to portability.

In-situ implies complete autonomy, therefore the system must acquire samples from the environment without a user. It must prepare and clean the microfluidic channels automatically and operate without maintenance for significantly long periods of time. If powered by a limited power source, such has batteries then the lifetime needs to enable an adequate number of analyses. Reading the literature regarding the electronic lifetime, stating the electronic lifetime as a time may be misleading, given that the lifetime depends strongly on the system usage. Authors are keen to report long lifetimes usually where they have conducted continuous analysis. This is useful for portable systems, where the researcher in field wishes to perform multiple CE runs in a single field-trip. Many in-situ applications however, would not require continuous monitoring, but periodic monitoring. By considering the lifetime in terms of the number of CE runs it becomes clear that the battery systems for portable CE systems would often also suitable for in-situ CE systems. Whilst their electrical lifetime is typically a few hours, the analysis time is only minutes, and so an in-situ device could function for many weeks, depending on the number of CE runs performed per day.

3.4. A Brief History of CE

In 1937, Arne Wilhelm Kaurin Tiselius developed moving boundary electrophoresis and was awarded the Noble Prize for Chemistry in 1948 for his efforts in advancing useful scientific methods in biochemistry [91]. Under the supervision of Tiselius, Stellan Hjertén of Uppsala University (Sweden) received his Ph.D in 1967, with the development of the first fully autonomous CE machine. In 1981 James Jorgenson of the University of North Carolina developed the first modern CE machines utilising 75 μm inner diameter capillaries [92]. Over the last few decades the focus of CE research has spread over numerous areas, such as buffer solution optimisation, capillary fabrication/material development and various modifications to the methods/modes of operation. Since the first fully automated CE machine there have been significant advances in making the system smaller. For example Figure 20 shows how the size of CE instruments has decreased significantly since the first system. The middle photograph shows a typical laboratory based desktop CE instrument. The photograph on the right shows a commercial portable CE system developed by CE Resources Pte Ltd.

Figure 20: Photograph of Stellan Hjertén next to the first fully automatic CE machine, 1967 (left) [93]. Typical modern commercial laboratory-based desktop CE system: PrinCE-C 700 series instrument developed by Prince Technologies (middle) [94]. Commercial portable CE system (CE-P2) developed by CE Resources Pte Ltd (right) [95].

3.5. Standard CE Systems

There have been a wide range of novel methods reported in the literature to improve CE in terms of: separation efficiency and resolution; overall device size; fabrication methods; detection systems, and analysis time. The widespread applicability of CE analysis combined with the detailed information it provides has led to it becoming a popular research tool for the analysis of a vast range of sample types. Sample types commonly reported in the literature include: amino acids and proteins [96, 97], organic acids [98], DNA [99] and enzymes [100]. There have also been numerous reports on development of the technology to aid the separation and detection of substances found in explosive media and nerve agent degradation products, such as those used by terrorists [101-106]. Other biological and chemical species such as uric acid, ascorbic acid, carbohydrates and glucose etc. have also attracted attention [107-111]. Further to this, research has led to CE analysis of individual cationic and anionic species [22, 90, 112-116]. Whilst there are some discussions, it appears that the use of CE for corrosion monitoring has not been explored in great depth [117]. Nie *et al.* has published in this area, on his method to separate the ions of interest to this project using specific sample pre-treatments and designed buffering systems [8, 9, 11, 12].

3.5.1. Variations on CE

As with many techniques, there are a variety of methods in which CE can be applied [33]. The more common of these variations are described briefly below and their suitability to miniaturisation is considered. Each method has its advantages and disadvantages specific to the range of applicable uses. The majority of the literature focuses on miniaturisation of

standard CE rather than its variants. In recent years, portable CE technology has reached such a level of maturity that the research will start expanding into development to make a greater range CE techniques portable.

3.5.1.1. Capillary Gel Electrophoresis (CGE)

A common variation of electrophoresis is gel electrophoresis. Here a gel is used in place of the liquid buffer solution. It does not necessarily require a capillary, a slab of gel may be used instead. When a capillary is used it is referred to as CGE and the capillary is filled with a gel. Commonly, polyacrylamide or agarose gels are used. The gel in the capillary contains pores which allow analytes to pass through at different rates depending on their size. Smaller molecules are able to pass through the gel more easily and therefore arrive at the end of the capillary first, whereas larger molecules take longer and arrive later. The gel used in CGE systems suppress the heating induced by the electric-field and strongly retard the movement of analytes. To prevent or reduce the gel from eluting out of the capillary when subjected to an electric-field, the capillary walls are usually treated to eliminate EOF. Due to the nature of CGE in that it separates out samples based on the molecule size, it is not suitable for use where there is a variation in the size-to-charge ratio of the analytes [33].

A miniaturised gel electrophoresis system was demonstrated by Demianova *et al.* [118]. Fabricated from poly (methyl methacrylate) (PMMA), the chip measured ~30 mm x 25 mm x 10.4 mm. The analysis focused on the separation of proteins which typically took between 10 – 60 minutes with an applied voltage of 100 V. Whilst the PMMA chip itself was small, the ancillary hardware required to perform the analysis had not been made portable. Their work is therefore an example of a chip-in-a-lab rather than a portable system. It is however useful to analyse work on miniaturised gel systems to determine their suitability to portability. It is beyond the scope of this thesis to investigate all the variations of gel electrophoresis but a common feature they share are quite long analysis times. For example, in the case of pulsed field gel electrophoresis, Li *et al.* [119] state that analysis times could take 10 – 15 hours. The analysis time for one run of the work by Li *et al.* with a miniaturised gel slab apparatus was much lower at 60 – 90 minutes. One of their main interests, enabled by the use of a miniaturised device, was the ability to continuously monitor the entire system in real time with a high resolution camera. With this setup they were able to see the DNA fragments separate over time as they travelled along the slab.

3.5.1.2. Capillary Isoelectric Focussing (CIEF)

This method of CE separates amphoteric solutes based on differences in their isoelectric points [33]. The capillary is filled with a solution containing ampholytes and the sample (usually proteins). An amphoteric solution behaves differently depending on the pH; the isoelectric point of an ampholyte is defined as the pH at which the ampholyte charge is neutral. A pH gradient is set-up along the channel and the solutes migrate to a zone where their net charge is zero. There are a variety of methods to set-up a pH gradient, one of which is use a tapered channel, which will have an electric-field which changes magnitude along the length of the channel. The variable electric-field strength along the channel length will cause a progressive amount of Joule heating and therefore a temperature gradient. This temperature gradient can have a direct effect on the pH of some electrolytes. For example, the acid dissociation constant (pK_a) and therefore the pH of a tris-based buffer is temperature sensitive. Different proteins have different pIs and so move into different zones. Once all the solutes have moved to their zones, the zones are moved en masse past a detector. The composition of the buffer solution is usually adjusted to eliminate EOF so that only ionic solutes move through the capillary. It has been reported that this technique is not capable of separating both anions and cations in the same run [33].

Raisi *et al.* [120] discuss their system which consisted of a 60 mm long channel. Analysis of peptides was achieved within 5 minutes. One area where CIEF is useful is in the study of protein-protein interactions. Tan *et al.* [121] described their work on a miniaturised CIEF system for this purpose. Their work focussed on demonstrating CIEF on a miniaturised microfluidic device which if later designed with a holistic approach could be implemented into a portable system. A more in-depth review of work on miniaturised CIEF systems has been presented by Dolnik *et al*. [122].

3.5.1.3. Micellar Electrokinetic Capillary Chromatography (MECC or MEKC)

MEKC combines electrophoretic separation and EOF with a chromatographic separation mechanism for separating solutes within a sample [78]. A major advantage of MEKC is its ability to separate electrically neutral molecules. In MEKC the buffer solution is modified by adding surfactants which form micelles. A micelle is a collection of surfactant molecules evenly distributed within a liquid. The separation occurs due to differences in the hydrophobicity of the sample-micelles and buffer solution. An important property of the micelles is that they have a hydrophilic head and a hydrophobic tail region; which means

that when there are many in a solution they tend to form spheres with a hydrophilic outer surface and hydrophobic inner.

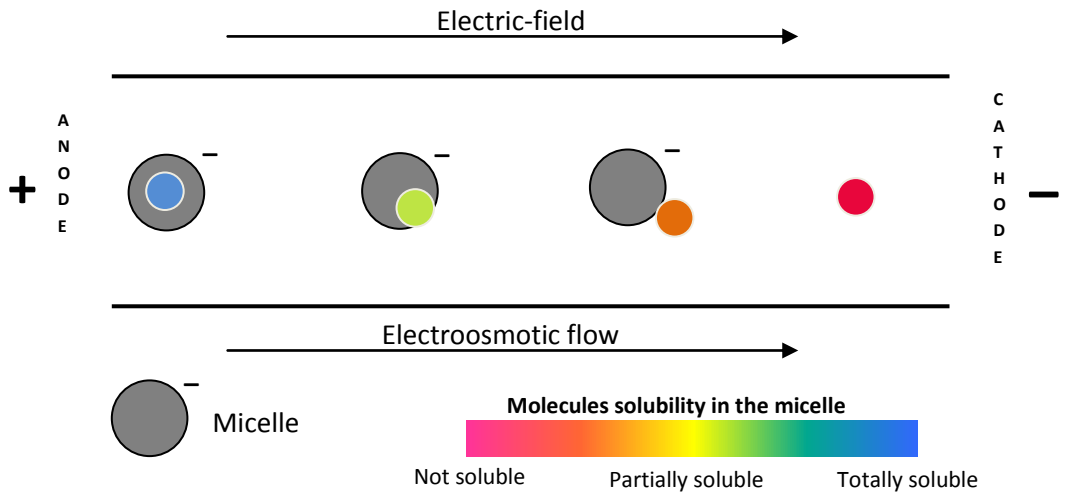

Figure 21: Representation of MEKC. Non-soluble molecules do not enter the micelle and so move through the capillary at the rate of EOF. The highly soluble molecules spend more time in the micelles and thus they move towards the capillary at a rate less than the EOF; the reduction owing to the pull from the anode on the negatively charged micelle.

The technique relies on the fact that components of the buffer solutions and sample have different hydrophobicities and therefore present different solubilities to the micelles. Highly hydrophobic molecules are highly soluble to the micelles and therefore spend most of their time travelling along the capillary within the micelles. The less soluble molecules spend less time in the micelle and so their progress along the capillary is less hindered. Since the non-soluble molecules do not enter the micelle they emerge from the capillary or channel first, at the rate of EOF if neutral, as illustrated in Figure 21.

Pumera [123] compared microchip MEKC against conventional CE for the analysis of a wide variety of explosive compounds. For example, microchip MEKC was used for the successful separation of neutral nitroaromatic explosives in a portable analysis system for counter terrorism measures. Wakida *et al.* [124] discussed their work towards a portable analyser for performing MEKC analysis of phenolic chemicals which are of interest in many environmental monitoring applications.

3.5.1.4. Capillary Electrochromatography (CEC)

This method of separation is a combination of high-performance liquid chromatography and CE, where instead of using a hydraulic pump to move the mobile phase through the

capillary, an electric-field is applied, generating an EOF [125, 126]. Strictly, CEC is not a variation on CE but a variation on chromatography, the separation of analytes is not based on differences in the electrophoretic mobility. It is discussed here because it bears significant similarities and requirements to CE. Further to this, unlike CE systems, CEC is able to separate out neutral solutes. Szekely *et al.* [82] discuss the difficulty of maintaining a stable EOF due to pH changes, a consequence of electrolysis in the small buffer reservoirs inherent of microfluidic systems. They measured moderate changes in the pH of buffered solutions following the application of a high voltage to the reservoirs. Further to this it was noted that as system dimensions decrease the application of high pressures becomes more difficult thus making the EOF a more attractive option. Ladner *et al.* discuss the production of monoliths in cyclic olefin copolymer (COC) microchips for portable CEC analysis [127]. The microchips were prepared by injecting by syringe a polymerization mixture. Further details are presented in their publication.

3.5.1.5.Isotachophoresis (ITP)

There is a large overlap in both the fabrication and operation of devices employing ITP methods for separation [128-131]. ITP and capillary ITP (CITP) are often considered a variation on CE. In ITP, instead of having just a single buffer solution to support the separation, there is a leading electrolyte and a terminating electrolyte enclosing the sample solution. The leading electrolyte has the highest mobility and the terminating electrolyte has the lowest.

The constituents of the sample are restricted to those that have values of mobility that lie within the range defined by the leading and terminating electrolytes. By introducing the sample between the two electrolytes and applying a potential across the channel, an electric-field is established with a lower strength over those components with the higher mobilities. Equation (14) shows the separation velocity, $\boldsymbol{u_{sep}}$, this is the velocity with which the sample plug travels.

$$\boldsymbol{u_{sep}} = \mu_L \boldsymbol{E}_L = \mu_S \boldsymbol{E}_S = \mu_T \boldsymbol{E}_T \tag{14}$$

Where μ denotes mobility and $\boldsymbol{E}$ denotes the electric-field. The subscripts L, S and T, represent the leading electrolyte, sample and terminating electrolyte respectively. This shows how the electric-field is distributed across the electrolyte zones. The sample electrolyte itself

will be composed of numerous analytes which each have their own individual values of mobility and therefore could be represented as shown in Equation (15).

$$\mu_S \boldsymbol{E_S} = \mu_{S1}\boldsymbol{E_{S1}} + \mu_{S2}\boldsymbol{E_{S2}} + \cdots + \mu_{Sn}\boldsymbol{E_{Sn}} \tag{15}$$

Here the subscript *n* denotes the number of analytes in the sample to be separated. From this it can be seen that the magnitude of the electric-field over the different sections will be inversely proportional to the mobility of that section. Separation of the analytes in the sample occurs as the sample migrates along the channel. The separation is further assisted by the self-sharpening effect. Consider the case where a sample has three components (analytes 1 to 3), then at all boundaries, even between the leading and terminating electrolytes, there is likely to be some diffusion, see Figure 22. Since each component of the fluid moving along the channel is now arranged in order of electrophoretic mobility, the electric-field is arranged the opposite way. If, for example, an individual analyte from analyte 3 were to diffuse into the analyte 2 region, it would experience a higher electric-field than it did in the analyte 3 region, and since it has a higher mobility than the other analytes in the analyte 2 region, it would move faster and return to the analyte 3 region. The opposite is true for analytes diffusing into regions of higher mobility. A disadvantage that ITP has is its inability to separate a sample containing both anions and cations in a single run. To overcome this, some work has been done by researchers such as Prest *et al*. [128] and Hirokawa *et al*. [132] on bi-directional ITP. Here, the researchers moved the ions in two directions along the channel using different methods. Prest's group injected the mixture into the middle of a channel along which an electric-field was applied. The anions migrated towards the cathode and the cations to the anode. ITP requires the sample to be loaded between two electrolytes, this is difficult to achieve in bidirectional ITP. Due to the low Reynold's number two streams could be flowed parallel to each other with almost no mixing. This meant that with a

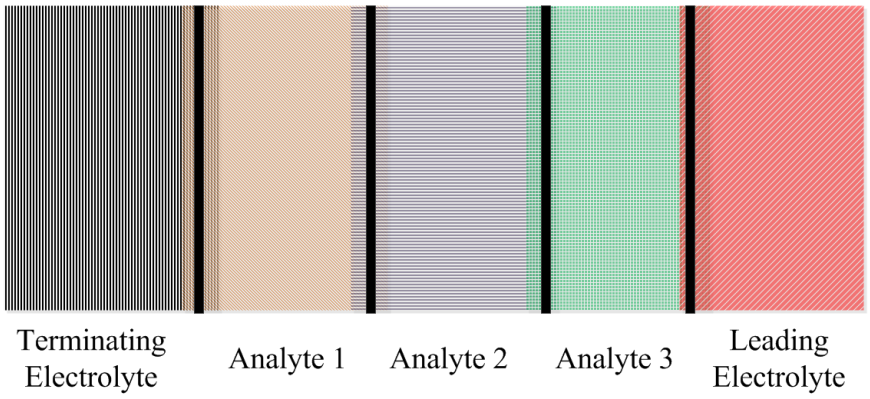

Figure 22: The self-sharpening effect in ITP due to the isotachophoretic (Kohlrausch) boundaries.

hydrodynamic injection scheme it was possible to setup the sample as required for bidirectional ITP. More in-depth details of the separation conditions for bidirectional ITP are given in their paper [128]. More recently the group's work on miniaturised ITP systems has focussed on analysis of explosive residues [129]. Hirokawa and co-workers used ethylenediaminetetraacetic acid as a chelating agent to modify a variety of different metal cations and then began separation. The advantage of using bidirectional ITP is that it can save on analysis time and enables the simultaneous separation of anions and cations. There is however, the requirement for two detectors at each end of the capillary/channel.

More recently, Prof Santiago of Stanford University has spearheaded research into microchip ITP; his group has published 22 papers to date on the topic since 2006, for example [133-135]. The focus of his group is primarily on developing microchip ITP though a portable handheld ITP instrument has been produced [136]. It had dimensions 76 mm by 57 mm by 38 mm, the detection system used a laser diode with a photodiode. An image of the instrument is shown in Figure 23.

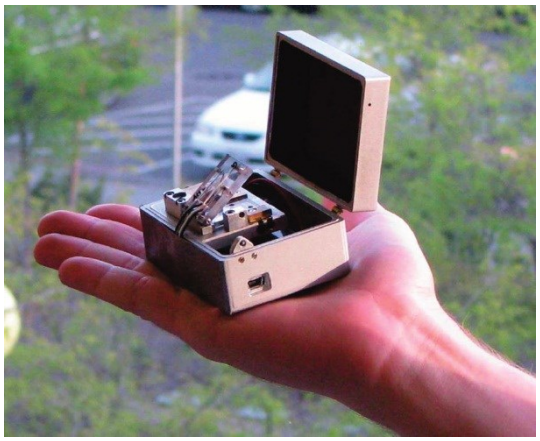

Figure 23: Photograph of handheld ITP instrument produced by Bercovici et al. (taken from [136]).

3.6. Truly Portable CE Systems

Whilst there is some overlap there is a clear distinction between miniaturising CE systems and the development of portable CE systems. The unique requirements of portability necessitate stringent and careful system design. Often the work on miniaturised CE results in a chip-in-a-lab rather than a lab-on-a-chip. This is often the case where the portability issues of the ancillary hardware, which are crucial to the operation of the device, have been neglected. It is important to design the system with a holistic approach.

There are two distinct branches of research regarding portable CE, the first, chip-based CE incorporates elements of the fabrication methods as described later in Section 6.3 . The second, non-chip CE, skips much of the complexities regarding the fabrication of microfluidic channels by using a ready-made capillary, such as a fused silica capillary [69]. The CE device is then built around the capillary, to aid portability the capillary is usually cut shorter.

3.6.1. Chip-based CE Systems

In the literature, two main reasons for the miniaturisation of CE systems become apparent, firstly for improving the portability of CE, and secondly for point-of-care and lab-on-a-chip devices. The aims of both are to increase the availability and usability of CE analysis. The focus here will remain on miniaturised CE devices where a holistic approach was implemented to achieve true portability, akin to the earlier described ideal device. Where appropriate, the challenges pertaining to the portability of CE, which have been overcome in the literature, even where the primary focus is not portability, will of course be included. Unlike non-chip-based CE systems, the devices are often fabricated using new and emerging materials. The channel surface is important and needs to resist contamination. As discussed earlier it plays an important role in the generation of the EOF. The use of these new and emerging materials introduces the problem of unpredictability. This is exacerbated by the fact that different fabrication methods affect the channel surface in a variety of ways [137, 138]. Further to this, whereas a capillary has just one material for the channel wall, many of the fabrication methods use two or more materials. This results in a channel with non-uniform EOF characteristics [139].

At Pittcon 2001, Jackson *et al.* first reported on an instrument they had developed, focussing primarily on the compact battery powered HVPS and its use in microchip CE [140, 141]. This instrument was combined with a microchip CE device, which highlighted its applicability as a step towards a portable CE system [141, 142]. Later amperometric detection circuitry alongside the HVPS was integrated into the instrument. The dimensions for this instrument were approximately 102 mm x 152 mm x 25 mm, with a weight of 0.35 kg. This accompanied a microchip CE device to render the main parts of a portable CE system [86]. This system weighed over 20 times less and is significantly smaller than the non-chip-based system by Kappes and Hauser, described later. It may therefore be deemed more portable. The primary reduction in weight was enabled by the use of AA batteries to power the HVPS module and a 9 V battery for the ECD system as opposed to the lead acid

batteries. The HVPS system by Jackson *et al.* was capable of producing a dual output of ±1 kV. The use of microchip CE rather than capillary based CE, resulted in short channel lengths and this meant that separation was possible with lower voltages. Jackson *et al.* [86] achieved 15 hours of continuous operation with 4 AA rechargeable 1300 mAH NiMH batteries, where continuous operation was defined as time the separation voltage could be kept active. The ECD circuitry was powered by a 9 V battery and could operate continuously for 40 h [86]. The work specifically on the HVPS, developed by Jackson *et al.,* is discussed later in Section 3.7.

Figure 24: Photograph of the µChemLab handheld CE system (taken from [143]).

A handheld CE system named µChemLab was discussed by Renzi *et al*. [143] from the Sandia National Laboratories, CA in 2005, though the concept of µChemLab was first discussed by Lindner in 2001 [144]. It is an example of where a holistic approach has resulted in a truly portable CE system. This system contained a HVPS capable of providing ±5000 V for currents up to 100 µA. Unlike most other portable CE systems which tend to use electrochemical based detection methods, the µChemLab system uses laser induced fluorescence (LIF). Figure 24 shows the µChemLab is housed in an ergonomic case (115 mm x 115 mm x 190 mm) which weighed less than 2 kg. It is clearly a convenient size and weight. The device consumes 4.5 W of power and is able to run for several hours on batteries. The microfluidic chips were designed for repeated use and the authors stated that the chips had well-characterized electrokinetic surfaces, which could be cleaned and were

suited to surface property modification. The sample passes an in-line filter before entering the microfluidic channels to help protect the channels.

In a publication by Zhang *et al.* [145], the main components required for a portable CE system are discussed. Their fluidic system was fabricated in glass with a channel of width, depth and length of 100 μm, 28 μm and 60 mm, respectively. Their detection scheme was composed of integrated platinum electrodes which served as part of a simplified conductivity detection system. To generate the high voltages required for CE, Zhang *et al.* used piezoelectric transformers because they offer a high transformation ratio whilst being smaller and cheaper than magnetic transformers [145]. Piezoelectric transformers operate by using two pieces of piezoelectric material. The first converts the applied electric potential into a mechanical force which in turn actuates a second piezoelectric material and produces an electric potential [146]. Further to this, piezoelectric transformers have higher efficiency, smaller size and lower electromagnetic noise than magnetic transformers [146]. Zhang e*t al.* stated that their HVPS was capable of producing an output of 14 kV with a ripple of less than 0.2 % [145]. The paper showed promising simulation results but no experimental data or any performance data, such as operational time, power consumption, etc. was given.

In 2008 there was a publication by Mühlberger and Hoffmann *et al.* who collaborated with Becker *et al.* to produce a report on their collaborative work. The project was a collaboration between three Germany institutions: Forschungszentrum Karlsruhe (Institute for Microstructure Technology), microfluidic ChipShop GmbH, and CLEMENS GmbH. The technical report by Becker *et al.* [147] discusses the details of the finalised device whereas the other publication [148] focuses on the development of the microfluidic device and investigates various materials discussing their properties. Figure 25 shows the device developed by Becker *et al.* the design is similar, though slightly larger, to that presented by Mühlberger *et al.*, also shown in Figure 25 [148]. The overall size of Becker's instrument was 190 mm x 120 mm x 80 mm whereas MinCE (Mühlberger's instrument) was 170 mm x 100 mm x 70 mm. The polymer substrates investigated were PMMA, polycarbonate, polypropylene, COC and polyether ether ketone (PEEK). The micro-channels were fabricated using a hot embossing method where processing parameters such as temperature and pressure profiles were varied for the different polymer substrates. The channels were thermally sealed to a thin foil, the thickness of which varied from 15 to 80 μm. The channels had square cross section with a height and width of 50 μm. Further fabrication details are described in the paper [148].

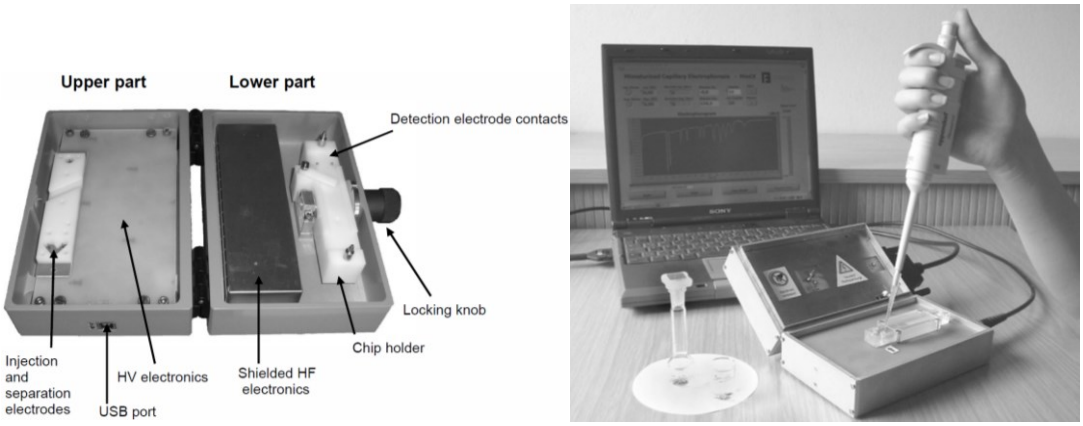

Figure 25: Left: Portable CE instrument developed by Becker et al. (taken from [147]). Right: MinCE prototype developed by Mühlberger et al. (taken from [148]).

Becker *et al*. state that for their system the HVPS system was composed of two commercial miniature unipolar power supply modules (each capable of 4 kV) coupled together to provide a bipolar driving power supply. This was required to enable the separation of anions and cations [147].

Fernández-la-Villa *et al.* [149] developed a portable CE system which incorporates amperometric detection. They used a mini-HVPS-PT001 purchased from MicruX Fluidic, which used 1 W and a maximum output current of 0.34 mA. The system was controlled by a laptop or PC, which added to the cost and reduced its feasibility as an in-situ device. As the author notes however, it helps pave the way towards in-situ analysis. Whilst a lifetime in terms of hours was not specified, they stated that on one charge the device would last for a day of experiments. The power was supplied by a Li-ion polymer battery rated at 3300 mAh. They also purchased the Pyrex chip from MicruX Fluidic; a downside of ordering standard components has been that it limited their ability to miniaturise the system. Here the size of the system is strongly limited by the size of the HVPS which was 150 mm x 165 mm x 70 mm. A summary of literature on portable and in-situ chip-based CE systems is given in Table 5.

Table 5: Summary of portable and in-situ chip-based CE systems.

Size (mm x mm x mm)	Weight (kg)	HV range (kV)	Channel material	Channel length (mm)	Power source	Detection method	Ref.
HVPS and detection circuitry[a] 102x152x25	0.35	± 1	Glass	20	AA (x4) 9V (x1)	PMD, AMD	[86, 140]
-	-	14	Glass	60	-	CD	[145]
170x100x70	-	-	Various polymers	~75-85	-	CCD	[148]
190x120x80	-	4	PMMA	75	-	CCD	[147]
Lab-on-a-robot	-	1.2	PDMS	-	9V (x1) 12V (x1)	PAD	[75]
HVPS: 150x165x70	2	± 2.5	Pyrex	40-50	Li-ion polymer	AMD	[149]
324x127x310	-	-15	-	215	-	RTFS	[76]

PMD: **potentiometric; AMD: amperometric; CD: conductivity detection; CCD: contactless conductivity detection; PAD: pulsed amperometric detection; and RTFS: real-time fluorescence spectroscopic analysis. [a] excluding microchip.**

3.6.2. Non-chip-based CE Systems

Here, by non-chip-based CE the reference is to miniaturised CE systems whereby the fluidic channel is not embedded in a substrate but is a capillary [69]. This has many differences over chip-based CE where micromachining techniques are used for a variety of lab-on-a-chip devices. One of the major advantages of using a capillary is that it has been well characterised due to many years of investigations by numerous researchers. This enables reasonably accurate predictions of the device performance to be made. Further to this, cleaning and preparation protocols have been established and the channel wall material is a single material. Fused-silica capillaries are known to be rugged and well characterized. Further to this, the cylindrical nature of the capillary presents maximum volume-to-surface ratio [69]. The other obvious advantage for non-chip CE is that both the financial and labour costs of fabrication are reduced or avoided. One of the major challenges for miniaturised non-chip-based CE systems is attaining reliable, accurate and repeatable sample injections. Sample injection methods are discussed in detail later in Section 3.9.

One of the first reports of a non-chip-based portable CE instrument was published in 1998 by Kappes and Hauser [150]. The capillary used had a length of 72 cm or 90 cm depending on the sample being analysed. This instrument consisted of a fused-silica capillary, a HVPS module, detection electronics and a data acquisition board which interfaced with a palmtop

PC. Excluding the PC, all the equipment was housed together in a PVC case of dimensions 340 mm x 175 mm x 175 mm, along with compartments and supports to align and secure the components in place. An illustration of the instrument can be seen in Figure 26, which highlights many similarities that the instrument bears to commercial CE machines. The total weight of the instrument was 7.5 kg. The main contributor being the two 12 V DC lead acid batteries, though this size and weight can be considered portable. The use of narrow capillaries (25 μm inner diameter) restricted the electrophoretic current flow, this meant that the lead acid batteries could last for 5 hours on a single charge.

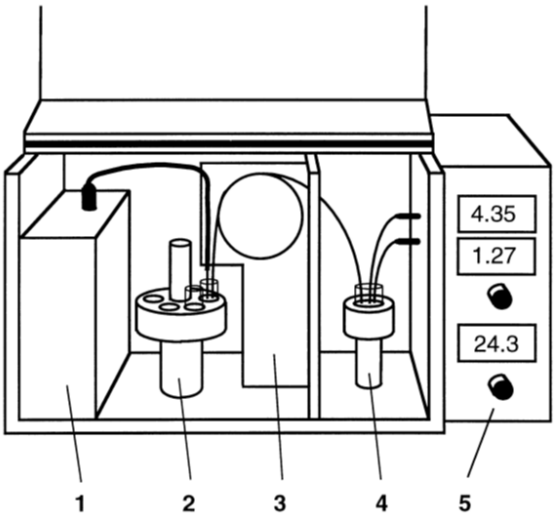

Figure 26: Illustration of the instrument developed by Kappes et al., (1): HVPS; (2): carousel for sample vials; (3): capillary holder; (4): detector compartment; (5): detection electronics (taken from [151]).

Their first field-portable CE instrument incorporated only potentiometric detection. This instrument formed the basis for much research into a variety of detection schemes which were incorporated into the instrument. In 1999 the authors reported on a similar device where they integrated both potentiometric and amperometric detection methods [152]. Further details on the specifics of their amperometric detection method can be found in [153]. In 2001 conductometric detection capabilities were added to the instrument [151]. The use of three different yet complementary ECD methods made the instrument versatile in the range of analytes that it could separate [151]. The authors showed results demonstrating the ability of the device to separate a range of inorganic anions and cations, as well as numerous organic species. Unlike bench-top-based CE instruments, which use integrated pumps for flushing the capillaries, here the capillary was flushed manually using a syringe. The use of a syringe negated the need for pumps which would have reduced the portability by increasing the weight and power consumption. Injection of the sample was achieved electrokinetically.

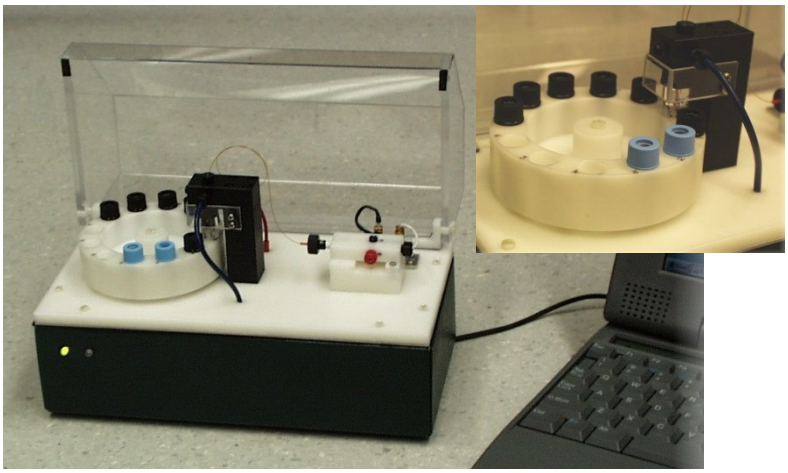

Figure 27: Miniaturised CE system developed by Gerhardt. It featured an automated sample carousel, which would lift to inject a sample (image provided courtesy of Dr Geoff Gerhardt).

Gerhardt created an elegant miniaturised non-chip-based CE system; however his interest was focussed on the development of a robust detection method [154]. This system incorporated a 30 cm long capillary, over which a high voltage up to 10 kV could be applied. Further to this the system was made completely autonomous; in that each sample vial could be moved by a stepper-motor and lifted for analysis as well as for capillary cleaning and preparation. Whilst it was not mentioned in the report [155] the HVPS module, from Spellman (model: MM10PN) was one of the larger features; the datasheet for the HVPS module states a case size of 42 mm x 76 mm x 101 mm [156]. Further to this, it was not made clear where the HVPS module or the motors, pumps and control system got their power.

Kubáň and Hauser further extended the work by Kappes and Hauser [151] to incorporate dual opposite end injection [157]. This enabled the separation of anions and cations in a single run by injecting the sample at opposite ends of the separation capillary. The analytes migrated towards the centre of the capillary where a CCD was placed [21, 157]. An interesting aspect of their work was their approach to sample injection where, they used a flow injection-capillary electrophoresis (FI-CE) system. A sample capillary was connected to the separation capillary via a valve composed of ceramic and polymeric parts [157]. There is generally no problem with high voltages damaging the flow injection analysis (FIA) equipment at the end of the capillary where the injection is commonly situated, since the potential here tends to be close to electrical ground. For the dual opposite end injection scheme however, there will always be one injection point at a high voltage and so the

insulating properties of the valve components were important in protecting the FIA equipment.

From the schematic given by Kubáň *et al.* [158], the layout of the portable CE device was similar to that by Kappes *et al.* [151], though the dimensions were slightly different: 310 mm x 220 mm x 260 mm. This meant that the volume was 1.7 times greater than that of the work by Kappes *et al*. Further to this, the control electronics to operate the portable CE system were housed in a separate aluminium box of dimensions 70 mm x 205 mm x 160 mm. The device developed by Kubáň *et al.* did not require the HVPS modules to be swapped depending on the polarity desired, unlike that of Kappes *et al.* This is probably one of the contributing factors to the size increase. The HVPS modules were powered by 12 V lead acid batteries. In the device by Kubáň *et al.* a further two 12 V lead acid batteries were used to give a ±12 V supply for the electronics. With this large power supply, the detector and data acquisition system, which used separate batteries, could operate continuously for 9 hours. This length of time could be considered adequate for a day's worth of in-field or on-site testing.

In more recent work by Kubáň and Seiman *et al.* [159, 160] the authors used milled PMMA and polyimide pieces to facilitate the sample injection. This system is a kind of hybrid of chip and non-chip CE; sample injection in chip CE tends to consist of a sample intersecting across a separation channel and adds little extra work in the processing. This method benefits from simple manufacturing techniques, as well as a well-defined and characterised separation capillary surface. Unlike in chip-based CE where the channel surface is important, the milling of the polymer cross-samplers was not critical because the separation 'channel' is a fused-silica capillary. An image of the PMMA cross-sampler is shown in Figure 28. The system designed by Seiman *et al.* fitted into a box of dimensions: 330 mm x 180 mm x 130 mm, weighed less than 4 kg and was powered by 10 AA batteries. In 2011, from a collaboration between Kubáň and Seiman *et al.* they published details on their portable CE system with dimensions of 300 mm x 300 mm x 150 mm and weighing approximately 5 kg [160].

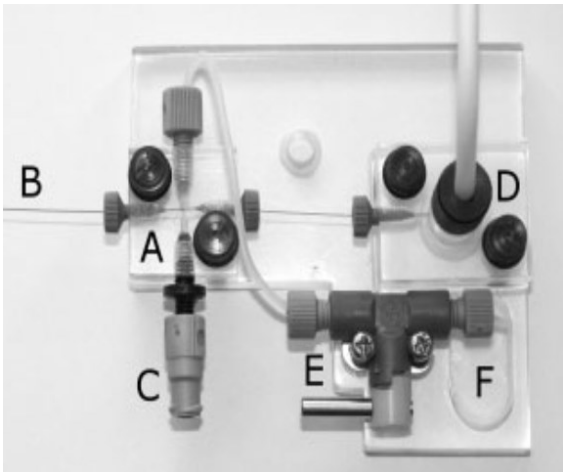

Figure 28: Image of a PMMA cross-sampler used to enable easy injection into the capillary, A: cross-sampler; B: capillary, C: socket for syringe; D: buffer vessel with electrode lead; E: shut-off valve and F: waste reservoir (taken from [159]).

A portable non-chip-based CE system designed by Xu *et al.* had dimensions 320 mm x 230 mm x 150 mm and weighed less than 2 kg [87]. They developed a CCD cell through which they threaded a capillary. The CCD cell operated with an input signal of 240 V_{pp} at 125 kHz. The whole system was powered by an internal battery and could operate for 2 hours. The system was heavily based on the CE-P2 system, a commercially available portable CE system (shown earlier in Figure 20). By using a pre-built portable CE system, they had little control over design compromises which limited the degree to which they could further miniaturise their system. It should be noted that the aim of their work however, was focussed on the detection of a specific sample for their application, rather than the portability of a CE system.

Wang *et al.* fabricated a hybrid chip-non-chip CE device with a capillary length of 55 mm supported in PDMS [161]. Whilst the height of the microfluidic device size was not given, the system fitted on top of a glass slide of size 20 mm x 70 mm x 1 mm, excluding ancillary hardware. This microfluidic device is essentially a capillary with detection electrodes built-in and bares many similarities to the chip-based approach to miniaturising CE.

It is clear from a survey of the literature on non-chip-based CE that there are not many groups whom have explored this technique with a view to portability. The review by Ryvolová *et al.* [69] discussed work by various research groups but overlooked the collaboration between many of them, a consequence of which is that it makes the area of non-chip CE appear larger than it actually is. A summary of the portable non-chip-based CE systems is given in Table 6. With regard to detection strategies, due to its convenience, the preferred method of detection is CCD, usually using two electrodes. A downside of CCD is

that the capillary thickness is typically a few microns and therefore large electrode areas are required, or operation at high frequencies, to overcome the resulting small wall capacitances.

Table 6: Summary of portable non-chip-based CE systems.

Size (mm x mm x mm)	Weight (kg)	HV range (kV)	Capillary length (cm)	Injection method	Electrical lifetime (h)	Power source	Detection method	Ref.
340x175x175	7.5	± 30	40, 72, 90, 104	EK	5	12 V lead acid (x2)	PMD, AMD, CCD	[151-153]
254x127x203	-	10	30	HY	-	NiCd	PMD	[154, 155]
-	-	1.5	5.5	FIA	-	-	CCD	[161]
310x220x260 + 70x205x160	-	± 15	62, 75	EK/HY	9	12 V lead acid (x3)	CCD	[158]
320x230x150	< 2	- 25	60	EK	2	-	CCD	[87]
330x180x130	< 4	25	48	HYCS	> 4	AA (x10)	CCD	[159]

EK: electrokinetic; HY: hydrodynamic; and HYCS; hydrodynamic cross-sampler.

3.6.3. In-situ CE Systems

The concept of lab-on-a-robot was discussed by Berg *et al.* [75]. Their system was a wireless enabled mobile unit, fitted with a global positioning system, capable of navigating to a location, acquiring a gaseous sample, performing CE and sending the data to a remote station. The gaseous sample was pumped into the sample reservoir, which initially contains buffer solution, using a micro-pump. After a few minutes of pumping a CE analysis is run. This system contains components which are important for portable CE systems and helps to bridge the gap towards in-situ devices. The HVPS on the system, capable of providing a voltage up to 1200 V, was based on the commonly used HV-DC-to-DC converters manufactured by EMCO High Voltage Corporation [162].

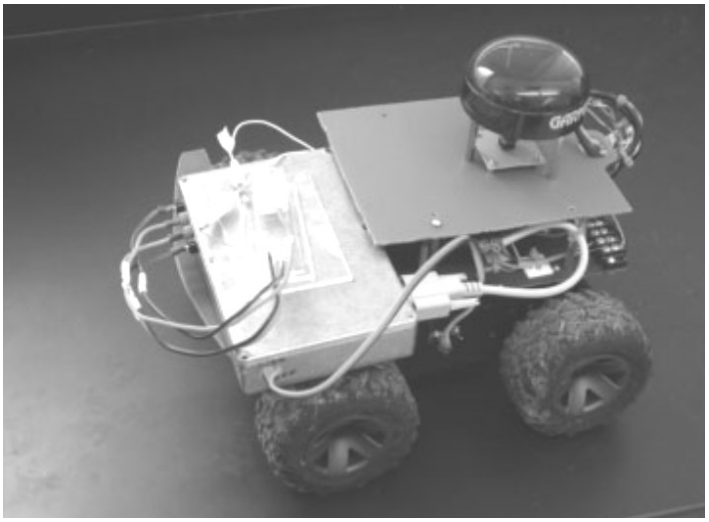

Figure 29: Photograph of the lab-on-a-robot system (taken from [75]).

An in-situ CE system which used a four-layer chip and contained eight CE systems has been designed by Benhabib *et al.* [76]. The system included a completely autonomous fluidic control system and was demonstrated by analysing a variety of organic compounds. The aim of their project was the development of an instrument to perform analysis in places where humans cannot go, an example being Mars, hence the requirement for complete user independence. It contained three HVPS and was capable of producing voltages to –15 kV though no details were provided on the battery system used. The channel cleaning routine consisted of filling the reservoirs with buffer solution and using EOF to flush the buffer solution through the channels.

3.6.4. Summary on Truly Portable CE Systems

In the majority of the work reviewed, the difference in electrophoretic mobility of the species in the samples was usually large enough that separation in a short capillary or channel was possible provided the EOF was kept low. Further to this, the capillaries used in many of the non-chip-based CE systems were typically longer than the channels in the chip-based CE systems. Many of the non-chip-based CE systems used capillaries with lengths comparable to those used in laboratory CE instruments. In some of the earlier work the use of 12 V lead acid batteries added to both the size and weight of the system. The use of smaller high-capacity batteries clearly lends itself to portability. In all of the devices, CE separation was performed in a single direction along the capillaries or channels. Most of the systems reviewed incorporated some form of ECD systems, with CCD being highly popular amongst both chip- and non-chip-based CE systems. Whilst there has not been a significant amount of work on in-situ CE systems, the work that has been done shows promise.

3.7. Energy Requirements for CE Separations

Whilst large electric-fields are required for CE analysis, it is desirable to maintain a low current to avoid Joule heating. Methods to achieve low current flow were discussed earlier in Section 3.2. During separation the current through the capillary or channel is typically of the order of μA [36, 163]. Electric-field strengths are usually quoted in the range from 5 kV m^{-1} to 40 kV m^{-1} [164]. Therefore it is possible to deduce that the power consumption of a single electrophoretic separation is in the region of 0.1 to 1 W, this is in agreement with Jiang *et al.* who calculated that their system used 0.6 W during separation [165]. Assuming a typical separation run takes 5 minutes, then with a power consumption of 0.6 W, each run will consume 180 J. Table 7 summarises the energy storage capability of typical battery systems from which an energy storage value has been derived; based on a value of 180 J per separation, an estimated number of separations for each battery system is also stated.

Table 7: Table summarising typical energy storage capabilities of various battery systems [166].

Battery System	Typical Energy Storage (mAh)	Nominal Voltage (V)	Derived Energy Storage (J)	Estimated number of separations
Carbon-zinc (AAA)	300	1.5	1620	9
Carbon-zinc (AA)	400-1700	1.5	2160-9180	12-51
Alkaline (AAA)	800-1200	1.5	4320--6480	24-36
Alkaline (AA)	1800-2800	1.5	9720-15120	54-84
Lithium (AAA)	1200	1.5	6480	36
Lithium (AA)	2500-3400	1.5	13500-18360	75-102
Nickel-cadmium (AAA)	300-500	1.2	1296-2160	7-12
Nickel-cadmium (AA)	600-1000	1.2	2592-4320	14-24
Nickel-metal hydride (AAA)	600-1250	1.2	2592-5400	14-30
Nickel-metal hydride (AA)	800-2700	1.2	3456-11664	19-65

Estimated number of separations assumed 180 J per separation.

It should be noted that the power consumption of the detection system has been neglected in the calculation of the estimated number of separations for each of the battery systems. Kappes *et al.* reported that the detection current used by their amperometric detection system was in the nA-range [153]. A conductivity detection system produced by Prest *et al.* was reported to use a detection current in the range of 1-10 μA [167]. Detection systems operate at voltages significantly lower than the separation voltage and therefore their power consumption compared with the HVPS can be considered negligible.

There is a significant variation in the range of estimated number of separations for the battery systems as shown in Table 7. Comparing the AA size batteries, at the lower end, the nickel-cadmium AA batteries would enable just 14 to 24 separations per battery, whereas a lithium AA battery would support between 75 to 102 separations. For a portable device, the presence of a user means that any of the battery systems would be suitable since the user is able to change the batteries as and when required. To reduce this inconvenience, there would be a clear advantage to opt for using the batteries with high capacity, e.g. the lithium, nickel-metal hydride or alkaline. For powering an in-situ device, where battery replacement is undesirable, the use of high-capacity batteries is of greater importance. However, for the application of corrosion monitoring, the inherently slow nature of corrosion means that one separation per every few days would suitable to capture the necessary information. Earlier in Section 2.1 the time scale of the corrosion was in the order of months; the data was captured at most twice a month over a period of 6 months. Therefore if CE analysis is performed every 7 days, this would be suitable for monitoring the corrosion of NAB. Over a 6 month monitoring period approximately 26 separations would be performed. Comparing this value with those estimated in Table 7, it can be see that there is a range of battery options which would be suitable for powering the separation HVPS and detection system.

3.8. High Voltage Power Supply Considerations

In many of the earliest attempts at designing portable CE systems the use of commercial HVPS tended to be one of the larger components limiting size, weight and lifetime [114, 152]. Cases where the researchers designed and built their own power supplies yielded more portable systems. This is because power supplies designed for commercial use are not restricted in terms of power consumption or size. Further to this, the commercial power supplies will be designed for good performance and will contain circuits to significantly reduce non-critical factors, such as ripple, etc., which could be considered unnecessary for portable CE systems. Whilst high performance power supplies are desirable, there needs to be a compromise between size, power consumption and performance, and this will depend strongly on the application. Commercial HV DC-to-DC converters are an attractive method to generate high voltages for portable and in-situ CE systems. The requirement for a high voltage does of course raise safety considerations. The safety of the user is of the utmost importance and so any device needs to be designed such that it is impossible for the user to accidentally access any connection to the high voltage. A common safety precaution used by

many researchers is to incorporate trip switches into the instrument case which cut off the high voltage the moment the case is opened [151].

Jackson *et al.* [86] developed a small HVPS combined with the detector circuitry in a single box, shown in Figure 30. The HVPS module was powered by 4 AA batteries and could operate for 15 hours. The dual-source HVPS was enabled using a commercial HV DC-to-DC converter module which operated at 0.5 W. The HV DC-to-DC converter chips used by Jackson *et al.* are developed by EMCO High Voltage Corporation [162]. These printed circuit board (PCB) mountable chips are not particularly low power (~0.5 – 1.25 W) when considering battery use, but they have reasonably small dimensions of only 12.7 mm x 12.7 mm x 12.7 mm and weight just over 4 g [162]. With separation times in the range of a few minutes, this enables a reasonable number of separations to be performed before battery replacement is required, as discussed earlier in Section 3.7. There are a large range of HV DC-to-DC converter chip devices available, capable of providing up to 10 kV for a 5 V input [162]. Since portable and in-situ CE systems tend to have relatively short channel lengths, a power supply providing up to 10 kV will yield a suitably high electric-field strength for separation.

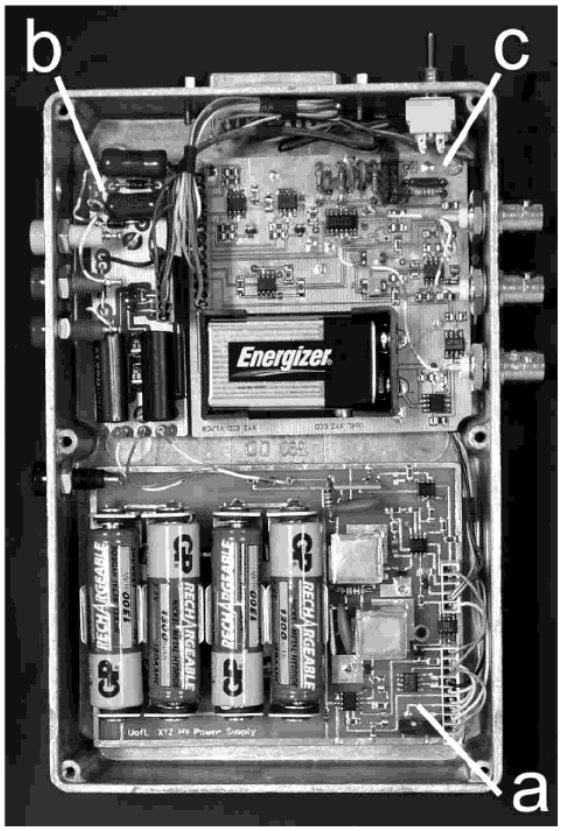

Figure 30: Photograph of instrument developed by Jackson et al. (a) portable HVPS (b) interface circuitry and (c) amperometric detection circuitry (taken from [86]).

Using two types of commercial HV DC-to-DC converters from UltraVolt Inc. one positive polarity, the other negative, García *et al.* [168] were able to generate potentials up to ± 4000 V. The power consumption of their HVPS was up to 30 W, implying that it could support an electrophoretic current up to 7.5 mA. During their separations they used their HVPS up to 1200 V, enabling the generation of electric-fields with a magnitude of over 20 kV m^{-1}, highlighting an advantage of shorter channels for portable/in-situ CE systems.

A HVPS system designed to be used with PDMS-based microfluidic systems by Erickson *et al.* [169, 170] also used the EMCO DC-to-DC converter. Their complete integrated system fabricated primarily in PMMA, onto which PDMS devices were placed, measured 21 mm x 25 mm x 100 mm, and voltages up to 700 V could be generated by the system. Interestingly, the authors detailed the power usage of the system components which used the most energy. They found that the HVPS used 55 % and the control circuitry used a further 37 %. Their system was powered by a coin cell to aid miniaturisation, and although coin cells tend to have lower energy storage than many other types of battery, they were still able to perform 40 runs. The power use varied from 145 mW to 71 mW, depending on the number of cycles and hence the charge-state of the power source.

In 2007 Jiang *et al.* [165] described their USB-powered mini-HVPS, which had dimensions of 47 x 56 x 25 mm. They used the commercial HV DC-to-DC converter from EMCO and performed separations with voltages in the range of 400 to 1500 V. One focus of their work which has not been widely considered elsewhere was on reducing the power wasted by the HVPS. One way in which they achieved this was by decreasing the number of components wherever possible. They highlighted that in many systems which use electrokinetic injection, the power consumption could be decreased by using a single HVPS and a system of relays instead of two HVPS and switching between the two. This is not an option if pinched sample injection is desired. They measured power consumption for three periods: during injection (1.9 W), separation (0.6 W) and idling (0.2 W) [165].

Recently Behnam *et al.* [171] developed an integrated circuit (IC) for use in portable and in-situ CE devices. The IC was less than 5 mm x 5 mm and had a power consumption of 28 mW. It could provide a voltage up to 300 V, further details solely on the HV part of the IC are described in an earlier paper [172]. The HV CMOS chip was mounted on a 70 x 70 mm PCB, to test, though this could be shrunk further with careful consideration of component placement. The HV chip was further modified to include LIF detection. This is interesting since miniaturised CE systems, especially those designed for portability have moved away from LIF, which was once the most widely used detection method in CE. One of the reasons

for the shift from LIF to other detection systems, such as ECD methods, including conductivity detection (especially contactless), was because electro-chemical methods are suited to miniaturisation. Many benefit from smaller dimensions due to enhanced flux at the electrode surface [89]. The same is not true of LIF whereby the resolution is related to the detection area. Further to this, the addition of electrodes on a chip (in the case of chip-CE) is considerable simpler than the implementation of a LIF detection system. The other disadvantage of LIF is that it is limited in terms of the samples it can analyse since not all analytes fluoresce [173]. In many cases pre-treatment of the sample is required to make its components fluoresce, thus adding greater complexity to the system [173].

The smallest, lowest power and most flexible solutions discussed here were for the cases where the HVPS was designed by using a HV DC-to-DC converter, rather than employing commercial systems. There are a range of methods available to generate high voltages. The Cockcroft-Walton multiplier is a relatively simple method, which can be designed using a ladder network of capacitors and diodes. Compared with transformers, which tend to be larger, a Cockcroft-Walton implementation lends itself to being cheaper and lighter [174]. By implementing a switched capacitor into a DC-to-DC conversion circuit, Abutbul *et al*. were able to get high voltage ratios without requiring transformers; this resulted in a high conversion efficiency of 91–95 % [175]. Careful design of high voltage transformers and the DC-to-DC converter is required to ensure high conversion efficiencies; losses caused by parasitic capacitances, leakage inductances, etc. must be minimised [176]. Using a transformer based approach for a DC-to-DC converter, Nymand *et al.* reported an efficiency of between 96.8 and 98 % [177]. Recent developments and reports on the use of HV DC-to-DC converters has meant that high efficiencies are possible with careful design, and therefore HVPS are no longer an issue for portable or in-situ CE systems.

Given the high voltage nature of CE, there will always need to be a reasonable amount of power usage and so the lifetime is limited by the capacity of batteries. The advantage of chip-based CE systems is that the channels tend to be quite short, and therefore an electric-field can established in the channel with the application of a lower voltage. Furthermore separations can be attained quicker and so more runs can be performed in a short amount of time. In this section reports from a range of authors have been discussed. Often where the electrical lifetime of the devices is discussed, the value is given in units of time rather than number of separations. In Section 3.7, a typical value for the power consumption during by the HVPS during a separation was given (0.6 W). Whilst some work in this section (for example that by Behnam *et al.* [171, 172]) had lower values of power consumption, the

voltage and current capabilities have also varied which is directly related to the power consumption.

3.9. Sample Injection Schemes

This is an area where chip-based CE systems clearly hold an advantage over non-chip-based approaches. Non-chip-based CE systems require sample injections into capillaries, which introduces design complexities. This problem has been addressed however, and there are various simple solutions [154, 159]. Sample injection methods for chip-based CE systems tend to consist of a sample channel crossing the separation channel. In terms of fabrication this usually adds little or no further complexity. To inject a sample into the channel, the user flows a sample from the sample reservoir to the sample waste reservoir. The cross-section is a defined volume which is filled with sample. This is a simple and repeatable method for sample injection. The point at which the channels intersect is where the sample is injected into the channel. In some cases the sample injection channel is offset as shown earlier in Figure 19, in other cases it cuts directly across the separation channel as shown in Figure 31. The former design is used where a larger sample volume is desired.

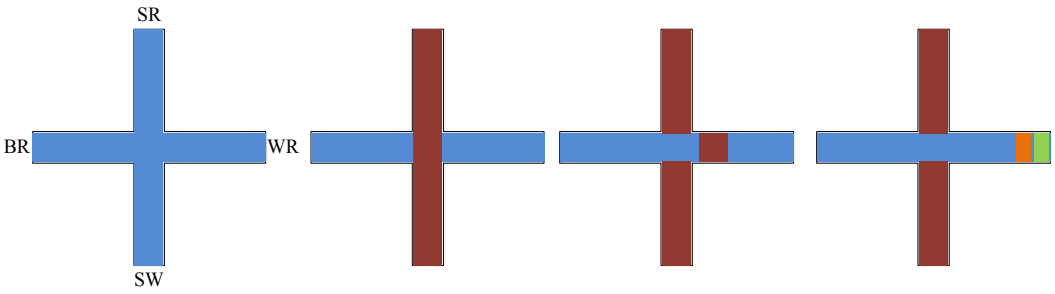

Figure 31: Sample injection scheme for planar microfluidic devices. BR: buffer reservoir, SR: sample reservoir, WR: buffer waste reservoir and SW sample waste reservoir.

A typical sample injection process is shown in Figure 31 and explained in the following four steps:

1. Fill and flush the separation and injection channels with buffer solution.
2. Inject sample from sample reservoir to sample waste reservoir.
3. Apply electric-field along separation channel. Here a small volume of sample enters separation channel at the cross-section.
4. Sample migrates along the separation channel and undergoes electrophoretic separation.

If the sample flow through the sample injection channel is caused by the use of pressure, for example using a pump or syringe, then this is referred to as hydrodynamic injection. One of the downsides of manual injection is that it is difficult to attain highly reproducible injections [178]. Whilst the importance of reproducibility in portable/in-situ devices may not be as critical as in laboratory based analytical chemistry, it is clearly desirable to ensure that the volume of injected sample varies as little as possible.

Often researchers will use electrokinetic injection to drive the sample across the separation channel. To achieve this, an electric-field is established between the sample and sample waste reservoirs. The advantage of electrokinetic injection is that there is no requirement for fluidic pumps to create pressure differences. This saves space and reduces power consumption. One downside of electrokinetic injection is that it can lead to sample biasing during injection, due to the differences in mobility of the sample constituents. Furthermore, the presence of a potential on an electrode in the sample reservoir could induce a pH change, if electrolysis occurs [81]. This may alter analyte behaviour due to processes such as complexation [179].

Where electrokinetic injection is used, there is the additional option of using a pinched injection scheme. This is where the electric-field is controlled to cause the fluid to flow towards the sample waste reservoir in a manner which pinches the flow where the separation channel crosses the sample injection channel. Usually a potential is applied to all four reservoirs (buffer, buffer waste, sample and sample waste) to control flow for the pinched injection. The use of a pinched injection scheme enables accurate and well-defined sample volumes which in turn lead to repeatable, high separation efficiencies [179].

Another method discussed in the literature is FIA, where a sample is injected into the separation channel whilst the fluid is flowing along the channel [157, 161]. Using this method it is possible to attain numerous separations sequentially by repeated injections. FIA requires precise fluidic control which can be difficult to attain in a portable device. For priming the channels, flushing buffer solutions and setting up the device, a pump is required. Due to the small capillary or channel cross-sectional areas typical in CE systems, there are usually large hydraulic resistances which need to be overcome by the pump. This means that the pump will need to be able to flow fluid at a reasonable pressure and therefore it will consume a non-negligible level of power. Since the volumes of fluid concerned tend to be relatively small there is the possibility for the use of micro-pumps, designed specifically for moving small amounts of fluid. An example of a commercial micro-pump is the MP-6 from Bartels Mikrotechnik [180]. Due to the typically high values of hydraulic resistance, most

micro-pumps will struggle to achieve high flow rates but this becomes a compromise for size, weight, power consumption, and simplicity.

For flushing capillaries or channels, a simple, cheap and low power method, discussed by Kappes *et al.* [152] was the use of a syringe. They used a syringe for capillary flushing but performed sample injection electrokinetically. Making the user push or pull a syringe to create positive negative pressures at a reservoir is a technique that can be used to flush the channels with a reasonable flow rate. Through appropriate choice of valves it is also possible to use this flow to provide sample injection. Alternatively, given that high voltages are required for the separation and so in principle are already available, electrokinetic injection is a useful sample injection technique since it does not require any additional pumps. On the downside there does however, need to be either a physical switch or circuitry to control the high voltages.

There is a clear trade-off which needs to be considered regarding electrokinetic versus hydrodynamic injection, and this will depend strongly on the application. For example, if the device is portable this implies that there is a user present and so the option of using a syringe, or similar manual pump is a viable option though care needs to be taken when considering the control of fluid flow. In-situ devices however are inherently autonomous (excluding maintenance), therefore fluid control is required for both capillary or channel preparation and sample injection. A pump will be required to take a sample from the monitored environment. With a view to minimise the number of components, a system of valves would enable the same pump to be used for sample injection. A HVPS would then be used to drive the separation. Alternatively the HVPS for the separation could be switched with a system of relays and therefore could also be used to electrokinetically inject the sample. For the design of in-situ CE systems, the notion of multi-functionality of components is of great importance since it minimises size, cost, complexity and power usage.

3.10. Dynamic Zeta-potential Modification Techniques

The separation enhancement routines described earlier in Section 2.4 require dynamic control of the EOF. CE practitioners often modify the capillary surface prior to running a CE separation and others permanently modify the channel surface in order to affect the EOF. These methods are non-dynamic, this section focuses on dynamic methods for modifying the zeta-potential using external electric-fields.

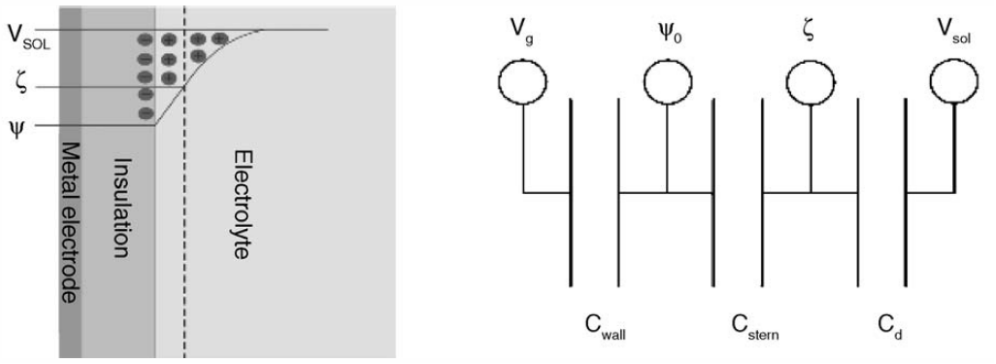

Figure 32: Simplified image of the double layer for an insulated metal electrode immersed in an electrolyte (left). Three-capacitor model representing the insulation/fluid interface (right) (taken from [41]).

Earlier in Section 2.3 the double layer structure on the channel walls which causes the EOF in the presence of an electric-field was described. A detailed description accompanied by computational models of the EDLs is given in Chapter 4. For simplicity, here the double layer will be assumed to be composed of a fixed layer (close to the channel wall), and a diffuse layer (extending from the fixed layer). This layout is shown in the left image of Figure 32. On the right of the figure, is a simple three-capacitor electrical representation of the EDL. The insulation can be represented as a having a linear potential distribution across it. The value of the wall capacitance can be approximated by Equation (16). It is dependent on the electrode area A, the insulation thickness d, and the relative permittivity ε_r of the insulation layer.

$$C = \frac{\varepsilon_0 \varepsilon_r A}{d} \tag{16}$$

Later in Section 4.1 models describing the potential distribution across the double layer are discussed. The potential distribution, and therefore the capacitance of the diffuse layer can be described by the Poisson-Boltzmann (PB) equation. Later the limitations of the PB equation are discussed but for the simplified explanation given here to describe the dynamic ZPM techniques, it is suitable. For a dilute symmetrical aqueous electrolyte, the capacitance of the diffuse layer is given by Equation (17) [59].

$$C_d = \left(\frac{2{z_i}^2 e^2 \varepsilon_0 \varepsilon_r c^\infty}{kT}\right)^{\frac{1}{2}} cosh\left(\frac{ze\psi_0}{2kT}\right) \tag{17}$$

Here, c^∞, k and T denote bulk concentration, Boltzmann's constant and temperature respectively. Commonly in the literature it is simplified to Equation (18) which is the case for a dilute aqueous solution at 25 ˚C [41]. The units of C_d in Equation (18) are μF cm^{-2}.

$$C_d = 228z\sqrt{c}cosh(19.5z\psi_0) \tag{18}$$

Most publications neglect the Stern capacitance because it is only significant in the electrical circuit model for solutions with large electrolyte concentrations or for dilute solutions with large polarisation [41]. Discounting the potential across the Stern layer, the change in zeta-potential affected by the voltage on the ZPM electrode is given by Equation (19) [41].

$$\Delta\zeta = \frac{C_{wall}}{C_d}(V_{ZPM} - V_{sol}) \tag{19}$$

As can be seen in Equation (19), the change in zeta-potential is directly proportional to the wall capacitance and therefore a material with a high dielectric constant is preferable. To keep the voltage required to significantly modify the zeta-potential low, a thin insulation layer is required, therefore the insulation material needs to have a high value of electrical breakdown strength. A list of typical breakdown strengths for commonly used materials for miniaturised CE systems is summarised in Table 8. There can be significant variation in the breakdown strength depending on fabrication method.

Table 8: List of typical values for breakdown strength of commonly used materials for miniaturised CE systems.

Material	Typical Breakdown Strength ($x10^6$ V m^{-1})	References
COC	30	[181]
PDMS	21	[182]
PEEK	190	[148]
PMMA	30	[148]
Polycarbonate	30	[148]
Polyimide	100-500	[183]
Polypropylene	140	[148]
Polystyrene	135	[148]
SU-8	440	[184]
Si	200	[185]
SiC	300-400	[185]
SiN	500	[186]
SiO_2	750	[49]

Van der Wouden *et al.* [187] discussed the charging dynamics of the EDL. The time, τ, for the EOF to develop in a microfluidic channel is given in Equation (20).

$$\tau = \frac{\rho_{fluid} d^2}{\eta} \tag{20}$$

It is clear from Equation (20) that the time taken for the EOF to develop for most microfluidic systems will be in the sub millisecond range. Provided the EOF is not switched at a high frequency, there will be no issues arising due to limitations on the EDL charging time.

To demonstrate the ability to modify the EOF, Buch *et al.* [49] fabricated a PDMS-based microfluidic system. The PDMS channel was reversibly sealed to a p-type silicon wafer and prior to sealing the channel, the silicon wafer was coated with 2 μm of silicon dioxide. The silicon wafer acted as the electrode which is referred to as the ZPM electrode in this thesis. Instead of directly controlling the voltage on the ZPM electrode, the authors chose to hold it at ground, see Figure 33. The average radial electric potential gradient along the channel was controlled using two HVPSs connected to the channel ends.

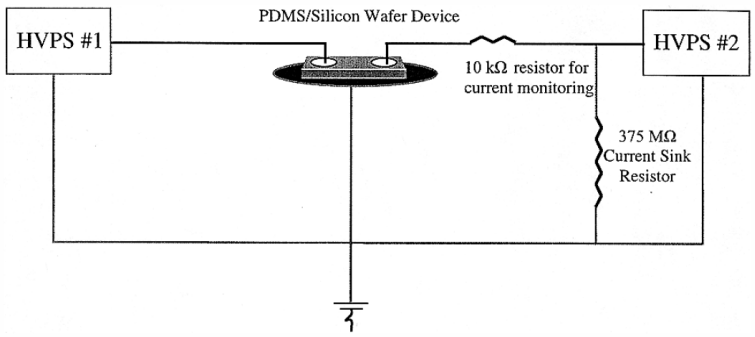

Figure 33: Illustration of hybrid PDMS-silicon wafer device created by Buch et al., to demonstrate field effect flow control (taken from [49]).

Whilst Kirby and Hasselbrink, authors of two papers discussing the zeta-potential of microfluidic substrates [53, 54], do not describe the methods of modifying the zeta-potential using an external electric-field, they do describe many other important aspects with regards to the zeta-potential which need consideration. These include the effects of pH, temperature, and counter-ion valence and size on EOF. The second paper considers the importance of the material forming the channel walls with a focus on numerous polymers.

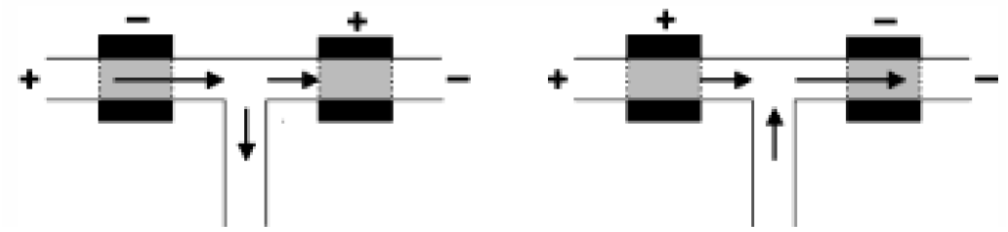

Figure 34: Schematic of T-intersection; the modification of the potential on the electrodes changes the pressure seen either side of the T-junction. In (a) the fluid travels down the main channel, whereas in (b) the fluid is pulled from the main channel (taken from [52]).

Hermes *et al.* investigated a fabrication method to develop a fluidic chip with an integrated electrode for the modification of the EOF [45]. With Pyrex as the substrate, using plasma enhanced chemical vapour deposition (PECVD), they deposited a variety of metals. They found that for their method, a combination of tantalum and platinum gave the best performance. Later processing steps, such as chemical mechanical polishing and high temperature annealing, required the metals have good adhesion and to exhibit minimal deformation at high temperature. The metal electrodes were insulated from the channel by a 400 nm thick insulating layer of SiO_2; the full process is described in detail in their paper [45]. The channel has dimensions for length, width and height of 15 mm, 45 μm and 45 μm respectively. The authors described further experiments performed on this device in two other papers [41, 187]. In the first publication they discuss their investigation into the effect the voltage on the integrated electrode, along the channel length, had on the EOF [41]. In the second publication they discuss the concept of using an AC electric-field for the separation voltage since this avoids hydrolysis. They cycled the potential on the integrated electrode with various phase differences, with respect to the electric-field in the channel, to find the optimum operating conditions to make fluid flow in a single direction with a varying electric-field [187].

Schasfoort *et al.* developed a device which they referred to as a 'flowFET' due to it having comparable functionality to a field-effect transistor (FET) [188]. Their interest was in using the effect to control fluid flow in integrated devices. To demonstrate this they controlled the flow down a side channel which fed off from the main channel. Their small dimensions enabled large electric-fields to be generated using small potentials. Using a potential of 50 V they were able to generated electric-fields strengths of 1.5×10^8 V m^{-1}. The explored the effect at pH 3.5 and pH 4.5, at lower pH values they demonstrated greater control over the EOF.

Another group whom used the ability to modify the EOF to aid and control fluid flow on microfluidic devices was Sniadecki *et al.* [51, 52]. Using a T-intersection, as shown in Figure 34, a flow was established in a channel using an electric-field, the channel which is connected perpendicular to this (as part of the T) will experience either a positive or negative pressure depending on the potentials applied to the electrodes in the main channel.

Vajandar *et al.* demonstrated the ability to control EOF pumping with porous silicon-silicon nitride membranes [38]. The silicon nitride layer was 500 nm thick. They showed the membrane enabled a EOF rate reduction of ~70 % for a positive applied potential and an enhancement of 15 % for a negative applied potential. They also showed that the effect on the EOF was only noticeable when the buffer pH was below pH 5.

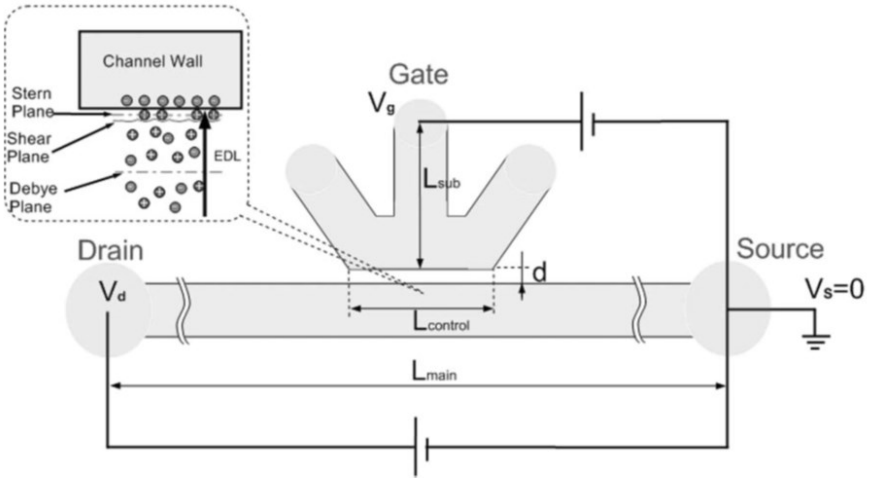

Figure 35: Illustration of microfluidic chip, showing the 'control' channel running parallel to the main channel. $L_{control}$, L_{sub} and L_{main} were 1 mm, 2.5 mm and 20 mm respectively (taken from [182]).

Instead of placing an electrode close to the channel surface to modify the zeta-potential, Horiuchi *et al.* fabricated a second channel (a 'control' channel) to run close to the main channel length [182]. Similarly to Schasfoort they also likened their device to a FET, an illustration of their system is shown in Figure 35. The gap between the channels was 1 μm, and flow control was observed using low gate voltages (~50 V).

Hayes *et al.* published a paper discussing fluid control in a CE microfluidic device using an electric-field [48]. The microfluidic device had two electrodes at 50 μm from the channel to apply the flow modifying electric-field. The authors showed results illustrating the effect the potential applied by these electrodes has on the sample migration time. Unfortunately the sample was composed of a single ionic species (N-(2-aminoethyl)-4-amino-3,6-disulfo-1,8-

naphthalimide, dipotassium salt) and therefore conclusions on the effect on electrophoretic separation cannot be drawn. Compared with other literature, the results presented by Hayes *et al*. were unexpectedly good in that the extent to which they were able to modify the EOF was greater even though some of their parameters would predict a poorer performance. For example they used a stronger buffer concentration (20 mM), this combined with a thick insulation layer of 50 μm would, at first glance, suggest a lower effect on the EOF than work by other authors. To compare the effectiveness of various publications, Buch *et al.*, whose work was discussed earlier, described a control factor which was given by the change of mobility per applied electric-field ($\Delta\mu_{EO}/\boldsymbol{E}_{rad}$) [49]. Buch *et al.* reported their highest control factor of $1.0\text{x}10^{-16}$ m^3 V^{-2} s^{-1}, and calculated a value of $2.1\text{x}10^{-16}$ m^3 V^{-2} s^{-1} for the work by Schasfoort *et al.* [188]. The work by Hayes *et al.* gave a control factor value of $3.3\text{x}10^{-15}$ m^3 V^{-2} s^{-1}; there are many possible reasons for the enhanced performance seen by Hayes *et al*. These include the fabrication method and materials, both of these affect the surface which is important in the development of the double layer [137].

Hayes's group investigated theoretical models and experimental methods for EOF control in capillaries [44, 46-48, 189]. In their work they used a conductive sheath or painted around a fused silica capillary. Their results confirmed that only a fraction of the capillary length needed to be modified in order to affect the EOF along the entire length. They showed experimental results for three cases; these were where the conductive paint coverage was: 0 %, 4 % and 60 %. With 4 % coverage, it was shown that for a given applied potential (– 10 kV), to the conductive paint, the sample migration time for a neutral marker was ~1.1 times slower than with 0 % coverage. Where the coverage was increased to 60 % (i.e. 15 times greater than 4 %), the sample migration time only increased by a factor of ~2.3; where the experimental conditions were the same as for the case with 4 % channel coverage [47]. To account for the non-linear relationship between the conductive paint coverage and effect on the EOF, Hayes *et al.* developed a model which accounted for the surface conductance along the inside of the capillary [47]. By accounting for the effect of the surface conductance, the model more closely matched experimental data. This work shows the importance of considering the surface conductance which directly affects the resultant zeta-potential and therefore the EOF. Further to this, Hayes *et al*. investigated the effect of pH on the EOF control, and showed similar results to Schasfoort *et al.* and Vajandar *et al.* in that the EOF control was only possible for pH values lower than pH 5 [38, 44, 188].

Lee *et al.* demonstrated the ability to enhance the separation resolution of laboratory-based CE systems using dynamic control of the zeta-potential [190, 191]. The separation capillary was placed inside a larger capillary. A higher concentration of buffer solution was placed in

the buffer reservoir at the start of the capillary compared to the concentration of the buffer in the capillary and at the end. The current flowing through the capillary was monitored throughout the experiment. Once the capillary was completely filled with the more concentrated buffer solution (due to the EOF), there would be no current change, hence making it possible to calculate the EOF. They demonstrated the separation of peptides and proteins showing the separation could be enhanced by direct control of the EOF through application of a potential to the external capillary surface.

Culbertson *et al.* originally used a pressure induced counter-flow to actively increase or decrease the electrokinetic migration of an analyte through a capillary [192]. They used the pressure flow to make a sample repeat its migration along the channel thus increasing the effective length travelled and therefore the separation. The undesirable effects of the parabolic flow on the separation were not considered, however in a later publication they replace the pressure driven flow with EOF, which they controlled with an external electric-field [193]. This method removed the complications of controlling the fluid with a pump and added the further benefit that the flow profile was always flat, and not parabolic. Using dynamic control of the EOF, Culbertson *et al.* improved the separation resolution of a capillary based CE system. Conductive silver paint was applied over the polyimide coating on the capillaries. Separate HVPS were connected to the capillary ends and a potential difference of 20 kV was maintained across the capillary for all experiments. The outer conductive layer (effectively the ZPM electrode) was held at ground. The potentials at both capillary ends were modified which directly changed *Vsol* (see Equation (19)) and therefore the zeta-potential (and EOF). They let the sample migrate through the capillary and then made the EOF move the sample back to the start of the capillary. Once it reached the start they let the sample migrate through the capillary again. This process was repeated numerous times, on each repeat, the sample became further separated.

The potential along the ZPM electrode at any one time is a single potential. The potential along the capillary however, varies along its length. The potential gradient which is often assumed to be linear is due to the large separation electric-field which drives the electrokinetic fluid flow. The difference between the potential on the ZPM electrode with respect to the potential along the capillary modifies the zeta-potential. This modification is non-uniform since the potential along the channel varies, and therefore the resultant zeta-potential is non-uniform along the channel length. The effects of a non-uniform zeta-potential were explored by Herr *et al*. [194]. Their work was not concerned with dynamic modification of the zeta-potential using external electric-fields. Instead they created a step change by using an EOF suppressing

polymer which was adsorbed onto varying fractions of the capillary wall. They also introduced a pressure driven flow alongside the electrokinetic flow. Their results showed that the resulting velocity profile and sample dispersion for a given location was a function of both the local zeta-potential and the system-averaged zeta-potential [194]. Lee *et al.* made use of changes in local zeta-potential to aid active mixing in a planar device [50]. They achieved rapid mixing using an alternating electric-field. The effect of variable zeta-potentials along serpentine and U-shaped micro-channels has been discussed by Saha *et al.* and Lee *et al.* [195, 196]. Lee *et al.* use the ability to locally control the EOF, to reduce the amount of band spreading around corners and U-bends in micro-channels. This was possible by modifying the velocity profile along the channel width such that the fluid on the outside of the corner moved faster than those on the inside of the corner. Since the outside fluid has a greater distance to travel this reduced the amount of broadening introduced by the corners.

3.11. Conclusions

The field of microfluidics is inherently multidisciplinary and whilst CE could be classed under chemistry, the miniaturisation of it has been investigated by a wide variety of research departments, typically engineering based. CE is an attractive analysis technique because of the detailed information it provides on its samples, which is why it has received significant attention. Since Andreas Manz first described the concept of a μ-TAS system in 1990, there has been a growing community investigating all aspects of miniaturising analytical systems, including CE.

It is clear that where research groups have taken a holistic approach, considering all aspects of the CE system design, there have been a number of successful outcomes. There are some in-situ CE systems that have been discussed, though an embedded solution has yet to be employed. There has been work on miniaturised CE systems using both chip and non-chip-based methods. The work on non-chip-based methods, typically with a shortened capillary, appeared earlier than the chip-based methods. The use of a capillary rather than a channel removes the requirement for a channel (the chip) fabrication, which enables more of an emphasis to be placed on the other and equally important aspects for the miniaturisation of CE. These include the detection system, HVPS and sample injection, which all need to be made portable for the entire system to be portable. The substantial amount of research on portable CE systems is large which has helped pave the way to in-situ CE systems and as

such it is expected that over the next few years there will be a shift such that more work focused on in-situ CE devices will start appearing in the literature.

Numerous research groups have investigated a wide range of fabrication methods and materials for miniaturised CE systems. Generally polymers are referred to as being easier and cheaper to fabricate than glass or silicon devices. Compared to glass or silicon, polymer materials tend to be more robust and therefore are more suited for in-field use. For some applications the use of polymers is limited due to the chemical resistance of the polymer. For example certain polymers would not be suitable for use with strong solvents. Since some fabrication methods are only compatible with certain materials, the choice of one informs the other. Over the last few years PDMS has become increasingly popular, primarily for the rapid prototyping of microfluidic structures and devices. Once a mould is created for the PDMS, the microfluidic can be created easily, and within one day, requiring only standard laboratory apparatus, such as a vacuum desiccator and oven. The substantial literature on fabrication methods for microfluidic chips means that it is now feasible to fabricate a microfluidic channel in a range of materials with only little process development required. Therefore the turnaround time from the design stages to a fabricated device can be reduced provided an in-depth survey of the appropriate literature is undertaken.

The majority of the work on the modification of the zeta-potential in microfluidic channels has been focussed on controlling fluid flow for electrokinetic transport applications, such as microfluidic pumping systems. There are no reports in the literature where the EOF has been modified dynamically in a microfluidic device to send a sample back along the channel. If the sample can be sent back along the channel, then the effective channel length can be increased without compromising the actual channel length. This would enable greater amount of separation within a shorter channel length. This method has been shown to work in a capillary, however a major difference is that in a capillary the entire outside of the capillary can be coated to act like an electrode. Therefore the zeta-potential on the entire inner-channel wall is modified. This is not so easily achieved in a microfluidic device, due to limitations of the fabrication methods. In the literature the ability to affect the EOF has been proven without complete channel coverage but the effects this has on the separation have not been investigated. Using computational modelling in Chapter 4, the consequences of EOF modification using a single electrode (i.e. only partial channel coverage) are investigated and the effects and limits this imposes on the separation enhancement methods are evaluated.

Chapter 4

Computational Modelling

Computational simulations provide the possibility of evaluating the effect of a range of parameters based on theoretical models and as such are a useful tool for exploring the theory and predicting device performance. Further to this they can be used to inform on design decisions, calculate the limits of operation, and infer an optimised solution. The designs of fluidic transport systems are becoming increasingly complex and as such the demand for computational models to describe these systems are becoming more important [197]. In this chapter there are a range of aspects for the design of a miniaturised CE system which are modelled. The models describing the EDL are discussed first. Following this, models for fluid flow to demonstrate the effect of the separation enhancement methods are presented.

4.1. Background Showing Evolution of Double Layer Models

There are a number of models available to describe the behaviour at an interface between an electrolyte and charged surface [65, 198]. These have been developed and adapted as the understanding of fluidic theories has evolved. The earliest EDL model was developed in the 1850s by Helmholtz by treating the double layer mathematically as a capacitor. A translation of the original publication [199] with notes is given in [200].

4.1.1. Helmholtz Model

As mentioned, Hermann von Helmholtz proposed that the double layer could be modelled as a capacitor [199, 200]. In this model the double layer is described as a monolayer of counter (oppositely charged) ions on a charged surface [201]; an illustration of this and the potential distribution can be seen in Figure 36.

The Helmholtz model implies a rapid potential drop across the EDL which does not agree with experimental data. Further to this, it does not consider the ion movement or adsorption of the solvent on the electrode surface [202].

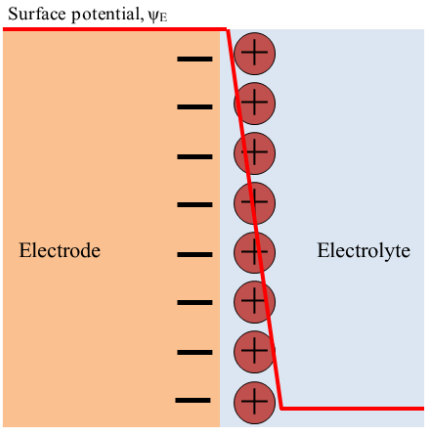

Figure 36: Illustration of the first model of the EDL as proposed by Helmholtz [203].

4.1.2. Gouy-Chapman Model

Between 1910 and 1913 the Helmholtz model was extended and developed independently by Louis Georges Gouy [204, 205] and David Chapman [206]; this improved model is known as the Gouy-Chapman model [65]. This model accounts for the diffusion layer at the surface, an illustration is shown in Figure 37.

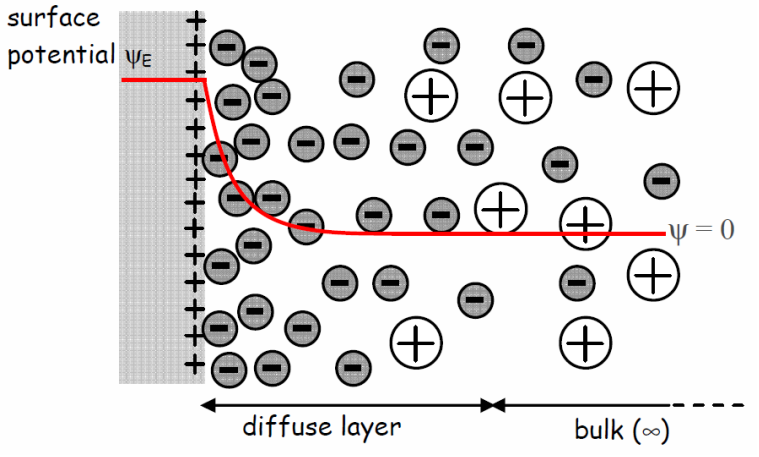

Figure 37: EDL as described by Gouy and Chapman (taken from [207]).

The Gouy-Chapman model is derived from the PB model; a combination of Poisson and Boltzmann equations [207]. The PB model uses a distribution of ionic species as described by the Boltzmann equation, shown in Equation (21). Here, c_i, c_i^{∞}, z_i *and* ϕ denote the concentration of ions i, the concentration of ions in the bulk, the ion valence and potential with respect to the bulk solution.

$$c_i = c_i^{\infty} e^{-\frac{z_i e \phi}{kT}} \tag{21}$$

Using Equation (21) the charge density, ρ, can be expressed as shown in Equation (22).

$$\rho = \sum_i z_i e c_i = \sum_i z_i e c_i^{\infty} e^{-\frac{z_i e \phi}{kT}} \tag{22}$$

The charge distribution is given by Poisson's equation as shown in Equation (23).

$$\vec{\nabla} \cdot \left(-\varepsilon \vec{\nabla} \phi\right) = \rho \tag{23}$$

Combining the Boltzmann distribution for charge density of ions (Equation (22)) with the Poisson distribution of charge (Equation (23)) yields the PB equation, shown in Equation (24).

$$\vec{\nabla} \cdot \left(-\varepsilon \vec{\nabla} \phi\right) = \sum_i z_i e \, c_i^{\infty} e^{-\frac{z_i e \phi}{kT}} \tag{24}$$

The most widely used model is the PB model, though due to its limitations there have been many modifications to it. Classic PB theory assumes a very dilute solution in which ions are represented by point charges with mean-field electrostatic forces [208]. Ions are significantly larger than point charges; a consequence due to the PB theory representing them as point

charges is that even in very dilute electrolytes, the predicted ion concentrations are severely exaggerated [207, 208].

No general analytic solution for the PB equation exists, however in certain cases it is possible to obtain an approximate solution [209]. One solution uses the Debye-Hückel approximation; this is explained in Section 4.1.4.

For the case of a symmetrical binary *z:z* electrolyte, the PB equation becomes the GC equation (see Equation (25)), a derivation is given in [30, 207].

$$\vec{\nabla} \cdot \left(-\varepsilon \vec{\nabla} \phi\right) = -2zec^{\infty} sinh\left(\frac{ze\phi}{kT}\right) \tag{25}$$

4.1.3. Gouy-Chapman-Stern Model

The GC model accounts for the diffuse layer of ions away from the channel surface, but does not consider the Stern (or Helmholtz) layer [207]. Stern suggested a two layer model for the double layer, the Stern layer close to the electrode surface and the diffuse layer which extended into the bulk solution, an illustration is shown in Figure 38. This can be represented electrically as two capacitors (representing Stern and diffuse layers) in series and was presented earlier in Section 3.10 to explain how the EOF can be modified [187]. The Stern layer consists of a high density of ions, tightly bound at the surface. The GC model assumed that ions behave as point charges and therefore there is no physical limit for the number of ions at the surface [207]. Since ions have finite size, the first ions in the diffuse part of the EDL cannot approach close than the diameter of the ions in the Stern layer. To overcome the problem of exaggerated ion concentrations due to the point-charge representation Kilic *et al.* [208] used a "packing parameter" to modify the PB distribution. The packing parameter is proportional to the hydrated radius of the buffer ions and concentration in the bulk (i.e. away from the surface). They referred to their equation as the Modified PB equation (MPB), shown in Equation (26); the packing parameter *v*, follows in Equation (27).

$$\vec{\nabla} \cdot \left(-\varepsilon \vec{\nabla} \phi\right) = -zec^{\infty} \frac{2sinh\left(\frac{z_i e\phi}{2kT}\right)}{1 + 2\nu sinh^2\left(\frac{z_i e\phi}{2kT}\right)} \tag{26}$$

$$\nu = 2r^3 c^{\infty} \tag{27}$$

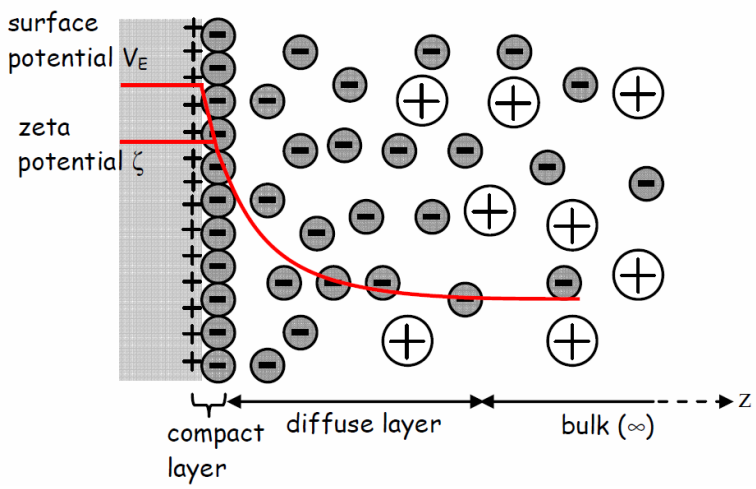

Figure 38: Gouy-Chapman-Stern model: Gouy-Chapman model of the EDL with Stern modification (taken from [207]).

4.1.4. Debye-Hückel Approximation

As stated earlier in Section 4.1.2, one method to obtain a solution to the PB equation is to use the Debye-Hückel approximation. In microfluidic systems, the use of the Debye-Hückel approximation has certain limitations. For example: as the electrode potential increases the error in the calculation becomes significant. The error for a range of zeta-potential values can be seen in Figure 39. A solution can be approximated for a flat electrode with a low potential using the assumption in Equation (28) [209].

$$exp\left(-\frac{ez_i\phi}{kT}\right) \approx 1 - \frac{ez_i\phi}{kT} \tag{28}$$

Using Equation (28), the PB equation, Equation (24), can then be written in the form shown in Equation (29).

$$\nabla^2\phi = \lambda_D^2\phi \tag{29}$$

The thickness of the double layer is often characterised using the Debye length (λ_D). This is the distance from the channel wall where the charge drops to e^{-1} (~37 %) of its maximum value [195], and can be calculated using Equation (30).

$$\lambda_D = \left(\frac{\varepsilon kT}{e^2\sum_i z_i c_i^{\infty}}\right)^{-\frac{1}{2}} \tag{30}$$

The plane of shear is located outside the Stern layer; this implies that the potential at the Stern plane will be slightly higher than the zeta-potential. Using the assumption that ϕ_s and ζ (location of Stern layer and shear plane) can be considered almost equal, combined with the expression for the Debye length, an approximate solution for Equation (29) can be given as Equation (31) [209].

$$\phi = \zeta exp\left(\frac{x}{\lambda_D}\right) \tag{31}$$

An analytical solution to Equation (29) is shown in Equation (32) for the case of a symmetrical electrolyte [209].

$$\phi = \frac{2k_BT}{ez} ln\left(\frac{1 + exp\left(-\frac{x}{\lambda_D}\right) tanh\left(\frac{ez\zeta}{4kT}\right)}{1 - exp\left(-\frac{x}{\lambda_D}\right) + tanh\left(\frac{ez\zeta}{4kT}\right)}\right) \tag{32}$$

To illustrate how the Debye-Huckel approximation is only valid for low zeta-potentials, the distributions for both the approximation and the full calculation were plotted, this is shown in Figure 39. For thin double layers, the approximations are based on the assumption that the ratio of the Debye length to the length across which the EDL electric-field exists is much less than unity [29]. Further to this, for small potentials, the approximation approaches the exact solution for sufficiently small ratios. As can be seen in Figure 39, for low electrode

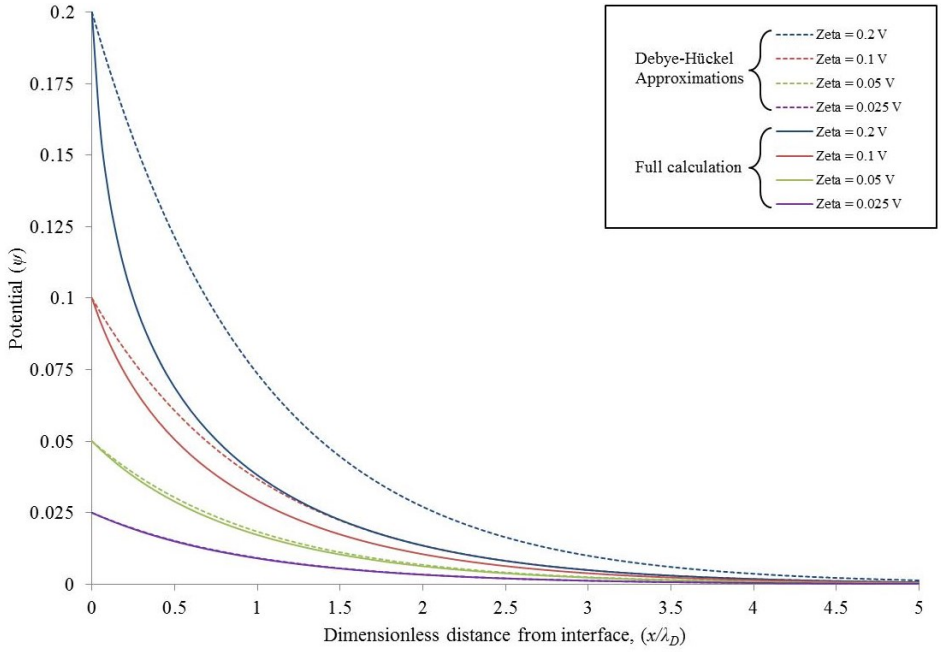

Figure 39: Graph illustrating differences in solutions for potential distribution using Debye-Hückel approximation (Equation (31)) and the full calculation (Equation (32)) [209].

potentials, the Debye-Hückel approximation is able to calculate the potential distribution reasonable accurately. As the electrode potential increases, the error in the approximation becomes significant and is no longer valid. While the electrical energy is small in comparison to the thermal energy, the approximation is valid, i.e. provided Equation (33) holds.

$$z_i e\zeta \ll kT \tag{33}$$

At room temperature, for a monovalent species, this translates as having a zeta-potential much less than 26 mV [30].

4.1.5. Grahame Model

A three layer model was developed by David C. Grahame in 1947 [210]; the model is divided by two planes, the inner Helmholtz plane (IHP) and the outer Helmholtz plane (OHP) [65]. Unlike Stern's model, Grahame's model accounts for the specific adsorption of ions; a specifically adsorbed ion loses its solvation and can move closer to the electrode. The IHP passes through the centre of these ions, as shown in Figure 40; the OHP passes through the centres of the solvated and non-specifically adsorbed ions [65]. Solvated ions at the electrode surface can have the same or opposite charge to the electrode, the bonds formed due to adsorption are stronger than for solvated ions. The charge of the solvated ions adsorbed on the electrode can significantly alter the potential distribution across the Helmholtz layer, a comparison of all the potential distributions of the models described here is given later in Section 4.1.7.

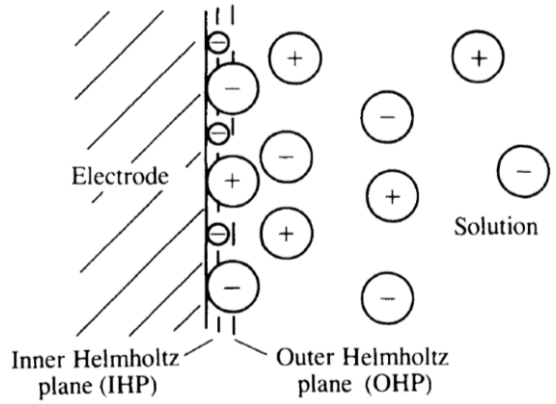

Figure 40: Grahame's representation of the double layer (taken from [65]).

4.1.6. Bockris, Devanathan and Müller Model

The physical nature of the interfacial region is considered by the Bockris, Devanathan and Müller model [65]. For example, in a dipolar solvent such as water, an interaction between the electrode and the dipoles will exist. A representation of the arrangement of ions and solvent molecules in the double layer is shown in Figure 41. In their paper published in 1963 [211] they discuss numerous known facts about the EDL which have been overlooked in earlier models. For concision, these facts have not been repeated here.

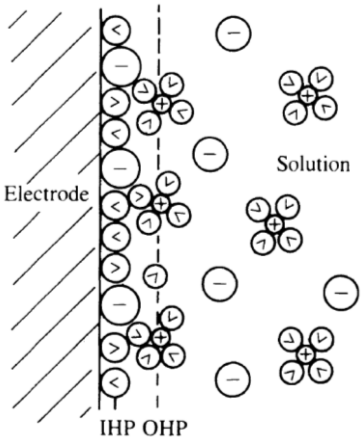

Figure 41: Representation of the arrangement of ions and solvent molecules in the double layer as described by Bockris, Devanathan and Müller (taken from [65]). The (^) symbol denotes water molecules.

The variation in the electrostatic potential with respect to distance x from the electrode for the Bockris, Devanathan and Müller model, alongside all the models described in this section are compared in Figure 42.

4.1.7. Summary of EDL Models

The potential distribution across the EDL described by the models varies greatly; this can be seen in Figure 42. From the description above, it is clear to see how the linear distribution predicted by the Helmholtz model becomes that predicted by the latter GC and the Stern models. The shape of the distribution of the Grahame and the Bockris, Devanathan and Müller model is significantly different. There are numerous distributions shown, these show the cases for different types of specifically adsorbed ions. To help describe these distributions a graph (graph f) describing the EDL for four cases of specifically adsorbed ions is included in Figure 42. If the adsorbed ions have a different sign to the electrode then the potential gradient in the Helmholtz layer increases, whereas if they are the same sign

then the potential gradient decreases [198]. In cases 1 and 2, the adsorbed ions are of opposite sign to the electrode surface, hence the steep potential gradient in the inner Helmholtz layer. In case 2, where there is appreciable specific adsorption, the adsorbed ions cause the potential at the inner Helmholtz layer to change sign and hence the potential distribution in the outer Helmholtz layer must compensate for this. Cases 3 and 4 have the same sign as the electrode surface and hence the gradient is less steep; in case 4 it is shown that this can cause a change of sign of the potential at the inner Helmholtz layer [198].

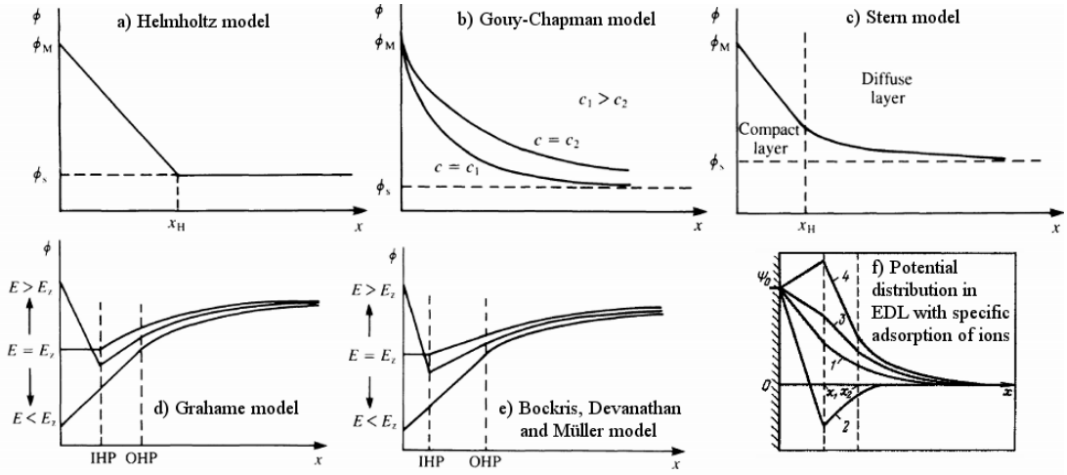

Figure 42: Variation of electrostatic potentials with respect to distance from electrode for the various double layer models, (figure composed of figures taken from [65] and [198]).

4.2. Modelling the Electrical Double Layer

The EDL model describes the behaviour of the double layer close to the interface between the channel wall and the electrolyte. In this work the GC solution to PB model was used as the starting point for the model. This model was chosen as a balance between the simpler models and the detailed models; this results in a more generic model. For example, the GC solution does not consider the solvation of ions at the electrode surface. To model this, a number of application-specific constraints would need to be introduced into the model. For flexibility, the model has been designed such that this can be interchanged later for a different model. This model describes the behaviour of molecules in the proximity of the channel wall. Initially, the case where an electrode is immersed in an electrolyte was considered. The PB equation in the form shown in Equation (25) was solved using COMSOL Multiphysics (version 4.2a) for two different values of bulk concentration. Notes on the modules used within COMSOL Multiphysics are given in Appendix C. The results from the simulation can be seen in Figure 43, alongside which is a figure taken from the

literature for confirmation that the model was solved correctly to produce realistic results. The model very closely matches the results published in the work by Pham *et al.* [207]. In the simulation, the electrodes were held at 0.05 V, in the graphs this can be seen for the case where x = 0 m. The PB model is an example of an electrical circuit model approach to describe the double layer. An alternative method is to solve the time-dependant Nernst-Planck equation, shown in Equation (34). This equation describes the ionic transport over time without distinguishing between the diffuse-charge layers [29], further details on the Nernst-Planck equation are given later in Section 4.3.1. It makes fewer assumptions than the circuit models and takes into account the diffusivity of the ions. As a result, it may be considered closer to first principles than the circuit models [29].

$$\frac{\partial c}{\partial t} = \nabla \cdot \left(D\nabla c - \boldsymbol{u_{fluid}} c + \mu_{ion} c \nabla \phi \right) \tag{34}$$

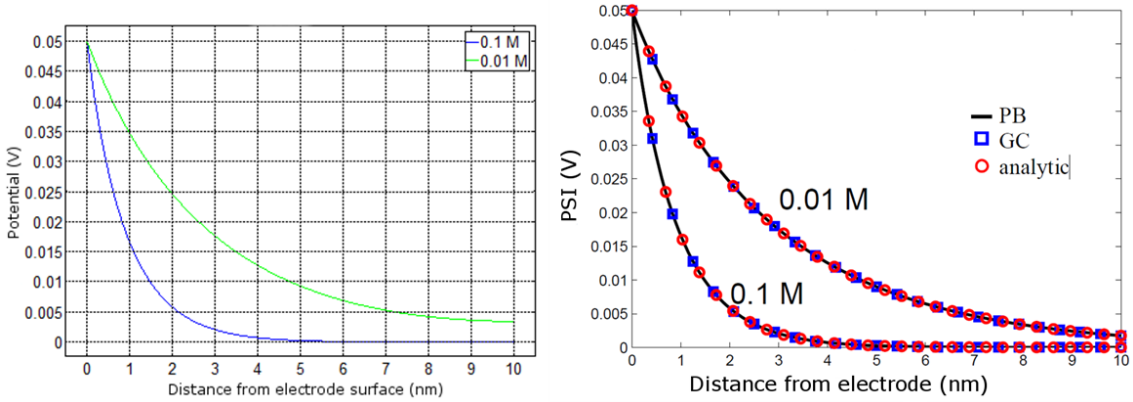

Figure 43: Simulation results showing solution to PB equation describing potential distribution away from an electrode surface for two values of bulk concentration (left). Figure taken from Pham et al. [207] showing their solution to the PB equation (right).

With the simple model proven, the next step was to expand the model for the case where instead of calculating the EDL from a conducting electrode into the bulk electrolyte, it was calculated where there is a dielectric channel wall between the electrode and the electrolyte. In the above case, the potential of the electrode (0.05 V) informed the boundary condition at x = 0 m for the entire electrode height (y). In the case of an insulating channel wall the potential along the electrode is known but the potential at the fluid/electrolyte boundary needs to be calculated. This is the potential dropped across the EDL which directly affects the EOF. An illustration of the model is shown in Figure 44, here the potential on the ZPM electrode informs on one boundary condition. The distribution across the dielectric is

calculated using Poisson's equation. The distribution across the EDL can be calculated using a number of models as described above, here the PB model was used.

Figure 44: Illustration of the model where there is a dielectric (the channel wall) between the electrode and the solution. The model for the EDL in the fluid can be interchanged depending on the requirements.

With a range of potentials on the ZPM electrode it is possible to calculate the potential at the dielectric-fluid interface. In Figure 45, the potential distribution for an electrolyte with a bulk concentration of 0.1 M is given, where the potential on the ZPM electrode is varied from 100 V to 500 V. The potential distribution in the EDL is small compared to the large ZPM voltage and so the EDL is shown in the right graph of Figure 45, where the axis has been scaled appropriately.

Buch *et al.* presented experimental results showing the change in EOF mobility for a range of applied electric-fields across a microfluidic channel wall [49]. Using their measured values for EOF mobility and Equation (7) it is possible to infer the effective zeta-potentials for the given applied electric-fields. These values and the model presented here (using a PB distribution) are shown in Figure 46. The model calculates the effect of the ZPM electrode

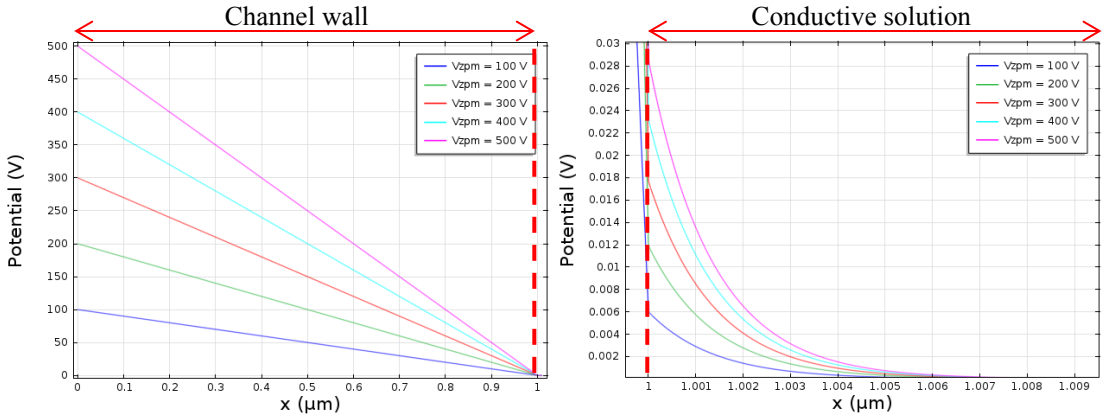

Figure 45: Simulation results showing the potential distribution across the 1 μm thick insulating channel wall and EDL for a range of potentials on the ZPM electrode (left). Potential distribution across EDL, axis have been rescaled (right).

on the zeta-potential, but needs to know the natural zeta-potential which as discussed earlier, in Section 2.4, is highly variable and subject to a wide range of factors. In the model shown in Figure 46, a value of –35 mV was used. Another point to note is that the values of zeta-potential inferred from the results by Buch *et al.* will all be offset by the natural zeta-potential which exists on the unmodified channel walls. Buch *et al.* used only a single electrode to modify the EOF. Therefore it is only the trend calculated by the model which is of interest here. It can be seen that it agrees with the results presented by Buch *et al.*

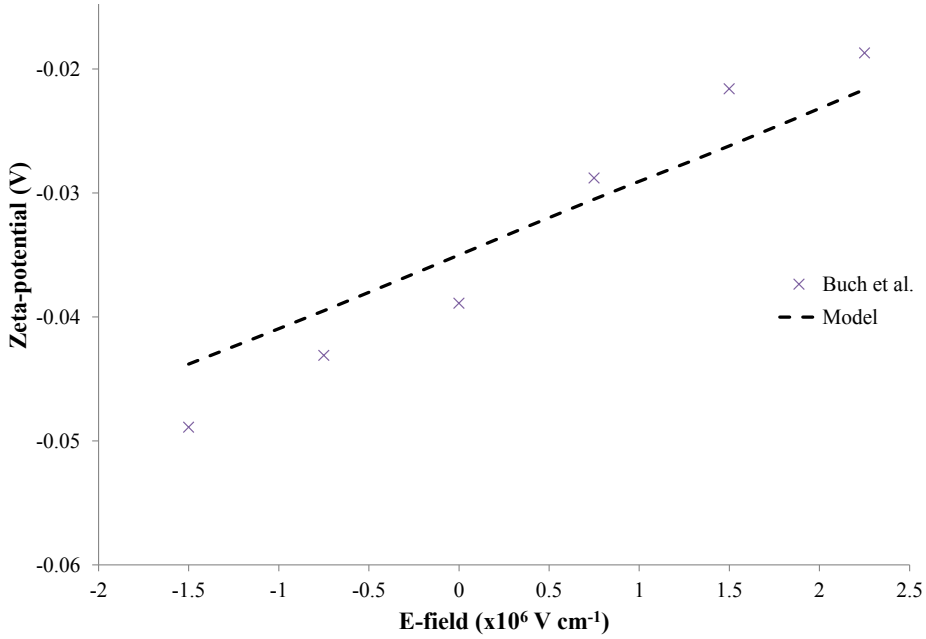

Figure 46: Graph showing zeta-potential inferred from results published by Buch et al. [49] showing good agreement with model.

Assuming the separation voltage (dropped along the channel) is linearly distributed then the value of V_{sol} will vary with respect to the length (y) along the channel. The ZPM electrode modifies the zeta-potential along the channel length depending on the difference between V_{zpm} and V_{sol} as described in Equation (19). Since V_{zpm} is a continuous electrode, it is a single potential which cannot vary along the channel length, therefore the change in zeta-potential must vary with respect to y. To account for this the model was modified to account for a varying V_{sol} along the channel length. The channel length in a microfluidic device is significantly larger than the insulation and EDL thickness, therefore this introduces a large aspect ratio into the model. Using finite element method (FEM), it is difficult and time consuming to solve large aspect ratios, therefore to describe the effect of the ZPM on the EDL in the presence of a separation electric-field, a short channel, or what could be considered a fraction of a channel is modelled.

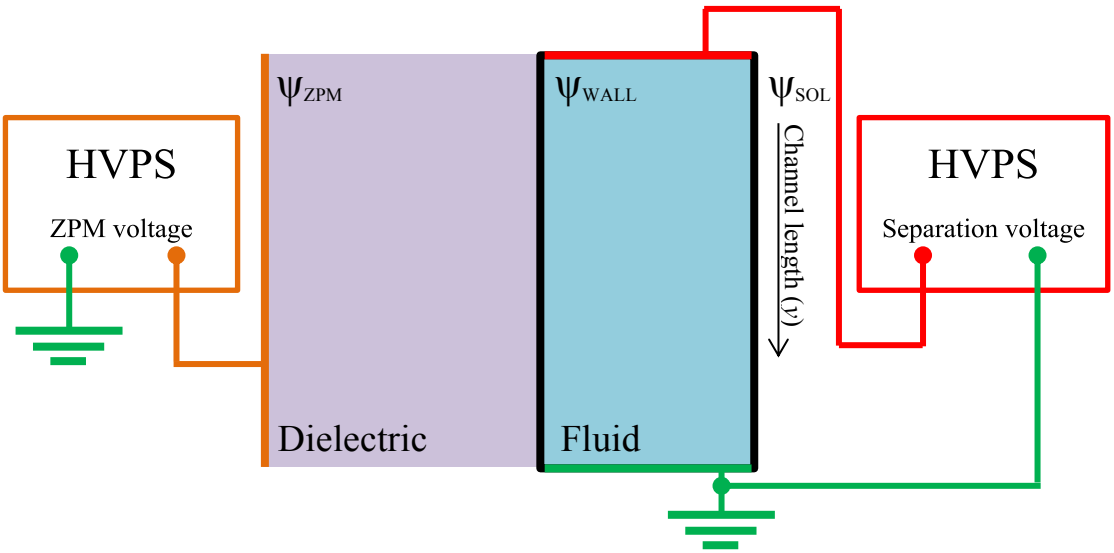

Figure 47: Illustration showing where the HVPS influence the model. The HVPS for the separation voltage generates a potential gradient along the channel, hence the solution potential ψ_{SOL} will vary with x.

An illustration showing how the model was setup is shown in Figure 47. It can be seen that the potential of the bulk electrolyte will vary along the channel length. The potential required to modify the zeta-potential strongly depends on the potential along the channel. The effect of the ZPM electrode potential on the EDL at different positions along a 1 mm length of channel is shown in Figure 48.

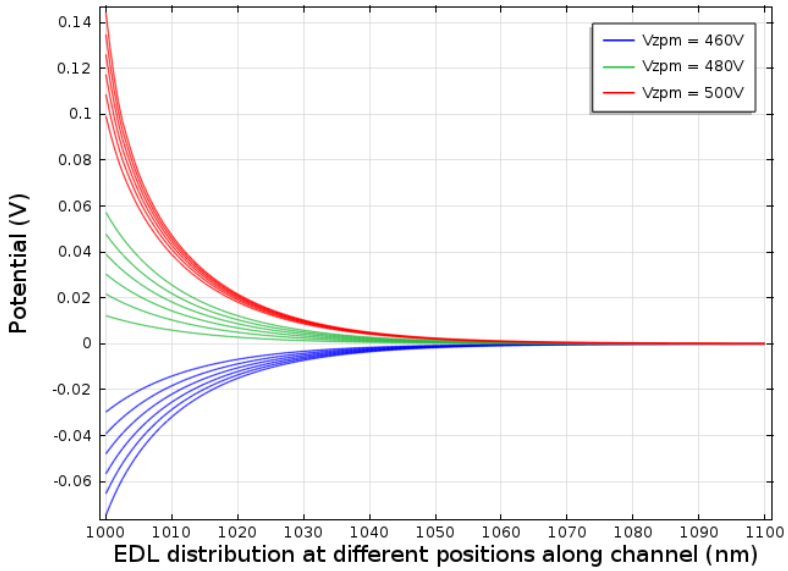

Figure 48: Potential distribution across EDL at different lengths along channel. Electric-field strength of 10 kV m^{-1}, generated along 1 mm section of channel length by applying 500 V to start of channel, and 490 V to end of channel. The multiple lines for each applied V_{ZPM} show the EDL distribution at even spaced lengths along the channel.

The electric-field was 10 kV m^{-1}, this was generated by making the potential 500 V at the start of the channel and 490 V at the end of the channel section. The EDL distributions shown for each applied potential on the ZPM electrode are evenly spaced along the channel length. It is clear that modifying the zeta-potential using this method yields a non-uniform zeta-potential along the channel length. Later the effect of non-uniform zeta-potential on the EOF and consequently the separation is investigated and modelled.

4.3. Theory for Fluidic Modelling

4.3.1. Nernst-Planck Model

The Nernst-Planck equation describes the flux of ions, in a fluid, subjected to a concentration gradient, fluid velocity and an electric-field; it was shown earlier in Equation (34). The equation is based on the mass conservation equation. The first term on the right-hand side of Equation (34), relates to the diffusion of the species; the second to the bulk movement of the fluid, this will include the EOF velocity term and any other fluid flow, for example: flow due to pressure gradients. The final term relates to the electrophoretic force acting on the species. In Section 4.4 the Nernst-Planck equation is solved to describe the behaviour of a mixed sample of charged species in a microfluidic device for a range of different separation conditions.

4.3.2. Modelling Diffusion

Molecules in a region of higher concentration will migrate towards regions of lower concentration due to diffusion [198]. The diffusion equation (Equation (35)) relates the diffusive flux to the diffusion coefficient and the concentration gradient.

$$\frac{\partial c}{\partial t} = -D_i \nabla^2 c \tag{35}$$

As can be seen from Equation (35), the extent of diffusion throughout an experiment is directly related to the experimental time, t. The diffusion constant, D_i is defined in one dimension as shown in Equation (36) [30].

$$D_i = \frac{(\Delta x)^2}{2\Delta t} \tag{36}$$

The one dimensional spreading of Cl^-, Cu^{2+}, Fe^{2+} and Fe^{3+} ions are shown in Figure 49. Due to their similar values of diffusivity, Cu^{2+} and Fe^{2+} diffuse by almost identical distances in the given time. With a larger value of diffusivity Cl^- ions diffuse a much greater distance in the same amount of time.

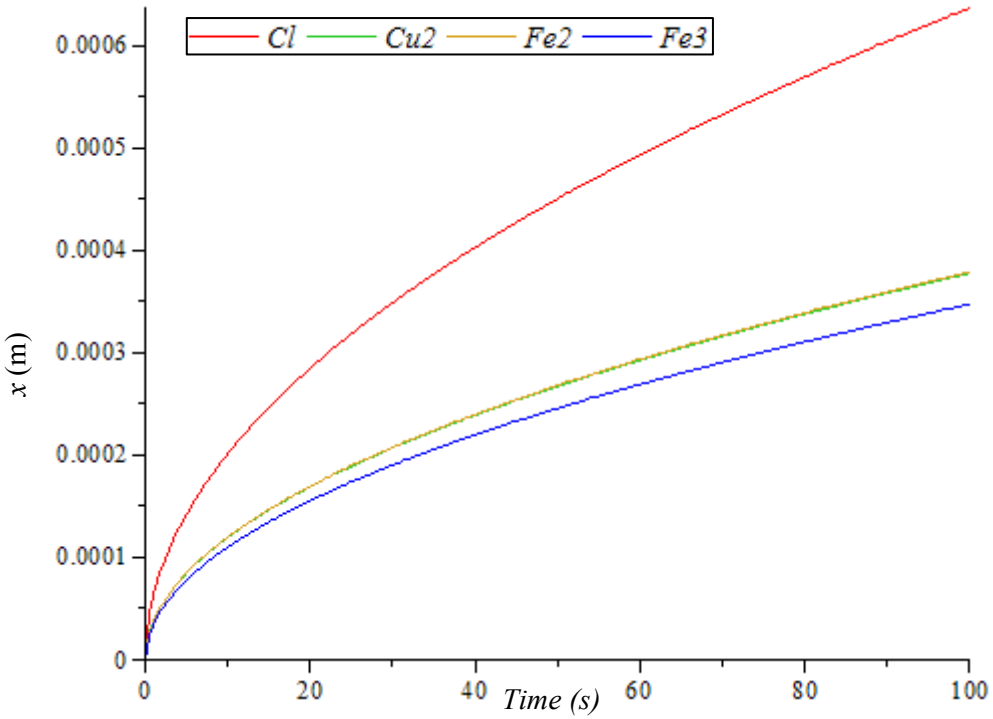

Figure 49: Graph showing extent of diffusion over time for a range of metal ions.

For good sample separation, the diffusive flux needs to be minimised. Diffusion is time dependent and therefore, reducing the duration of the experiment is one method for reducing the diffusion. The duration of CE experiments can be reduced by increasing the separation electric-field strength. This can be achieved either by increasing the separation voltage or shortening the capillary/channel. The experimental time can also be reduced by increasing the EOF velocity in favour of sample migration so that samples quickly migrate through the capillary/channel. Since the EOF affects all the species in the sample, this method could compromise the separation.

For a Gaussian distribution of a sample, the spreading due to diffusion, where the diffusivity is $1x10^{-9}$ m^2 s^{-1}, is shown in Figure 50. Both graphs (Figure 49 and Figure 50) show that the rate of diffusion lessens over time since the diffusion is proportional to the concentration gradient.

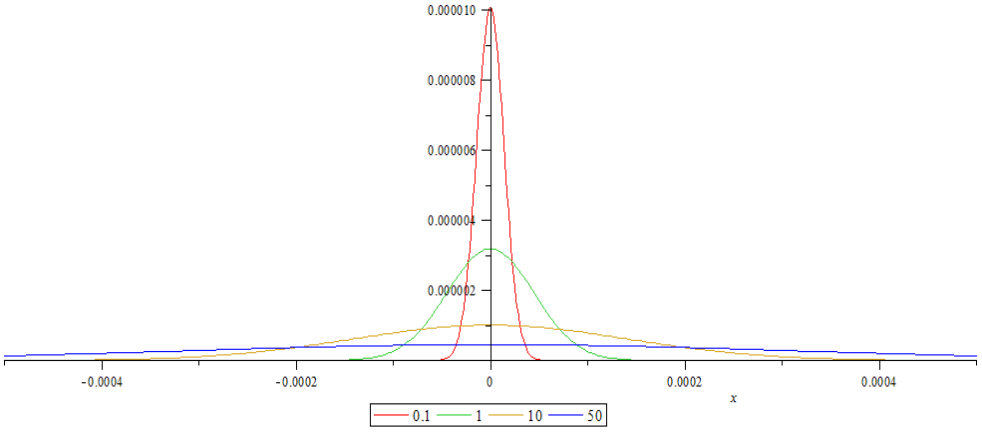

Figure 50: Broadening of a sample with a diffusivity of 1x10^{-9} m^2 s^{-1}, with a Gaussian distribution. Results presented for time (s) as shown in legend.

4.4. Microfluidic Modelling using Finite Element Method Analysis

The model described earlier in Section 4.2 demonstrates the effect of the potential applied to the ZPM electrode on the EDL thickness, the zeta-potential and consequently the EOF. The next part of the model describes the fluid flow through the microfluidic device. It can be used to predict the movement and separation of charged species in a channel subjected to an electric-field.

4.4.1. Modelling the Fluid Flow in a Microfluidic Channel

There are three mechanisms for charged species movement described by the model; these are due to the electrophoretic force, convective fluid flow (to account for EOF) and diffusion.

At the start of the simulation the initial concentration distribution of charged species are defined as a maximum concentration scaled by a Gaussian distribution about the point x along the length of the channel; the Gaussian distribution is of the form given by Equation (37).

$$a \cdot \exp\left(-\frac{(x-b)^2}{c_w}\right) \tag{37}$$

In the expression in Equation (37), the value a denotes the amplitude, b gives the position of the centre of the peak and c_w controls the width of the peak. The value of a was made equal to 1, since the expression is used as a scaling factor which is later multiplied by the initial

concentration of charged species. The value of b was set to $5x10^{-3}$, this sets the location for the centre of the peak to be 5 mm (i.e. this is where the injection channel crosses the separation channel). With a value for c_w of $1x10^{-9}$ the width of the peak at half the maximum value is about 200 µm. Using these values, the Gaussian function used in the simulation to describe the samples at the time of injection, can be seen in the graph in Figure 51.

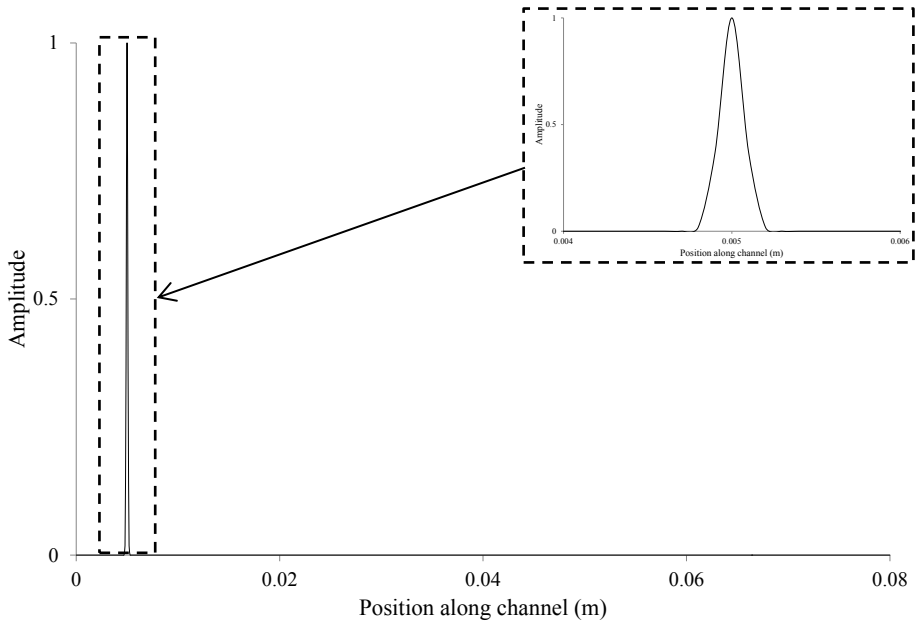

Figure 51: Graph of the Gaussian function defining concentration of ions in channel, using the following values: $a = 1$; $b = 5x10^{-3}$; $c_w = 1x10^{-9}$.

Numerous modules in COMSOL were setup to calculate different aspects of the model. This model is composed of the electrostatics, transport of diluted species, and laminar flow modules. The electrostatics module within COMSOL Multiphysics computes the electric-field in the fluid; this calculation is computed first in the simulation separately from the time dependant solving of the Nernst-Planck equations for efficiency. The electric-field dropped across the sample, and consequently the rest of the channel, will change throughout the experiment as the sample spreads and separates. Provided the sample and buffer are reasonably matched in terms of conductivity, it is assumed that the electric-field does not vary significantly throughout the experiment. Figure 52 shows how the electric potential varies along the length of the channel, for the following boundary conditions for $V(y)$: $V(0) = 750$ V and $V(0.08) = 0$ V. For a channel of 0.08 m length, this corresponds to an electric-field strength of 9375 V m^{-1}.

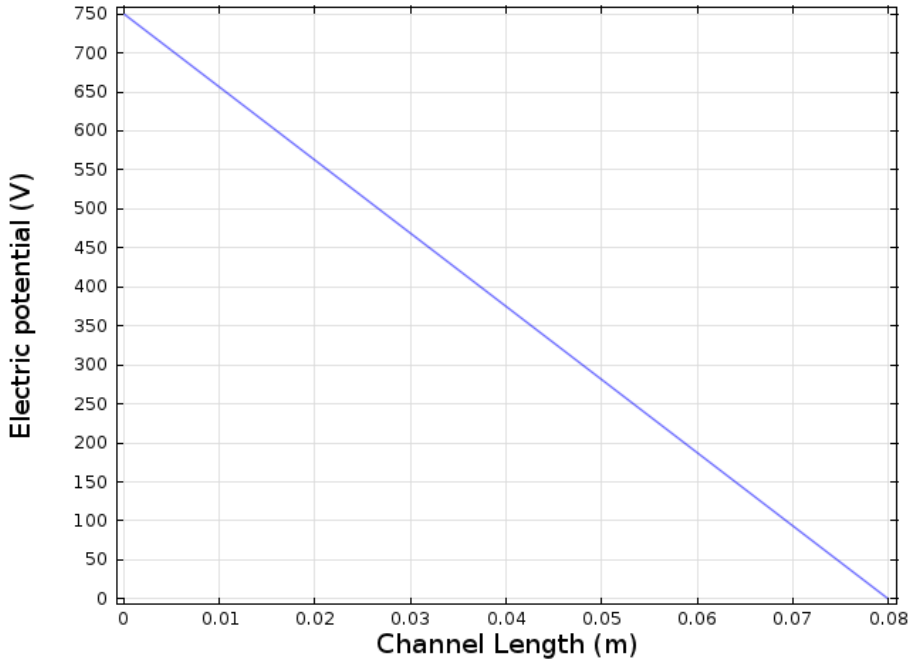

Figure 52: Variation in electric potential along the length of the channel.

The diffusion element of the model moves the ions irrespective of the presence of an electric-field. The electrophoretic force and EOF however, both act to move the groups of ions along the length of the channel at a velocity dependent on the magnitude and direction of the electric-field. Using the transport of diluted species module, the migration of the ions due to the electrophoretic force is computed based on the values of mobility for the ions, their valence and the electric-field. The convective flow term due to the EOF is calculated using the laminar flow module; the EOF was modelled as a flat flow profile.

4.4.1.1. Peak Shapes

The velocity at which the analytes migrate along the channel is made up of contributions from a variety of sources. Aside from the electrophoretic velocity, the main contributions come from the EOF and any pressure differences across the fluidic channel. The profile of these flows affects the distribution of analytes and therefore the resultant peak shape.

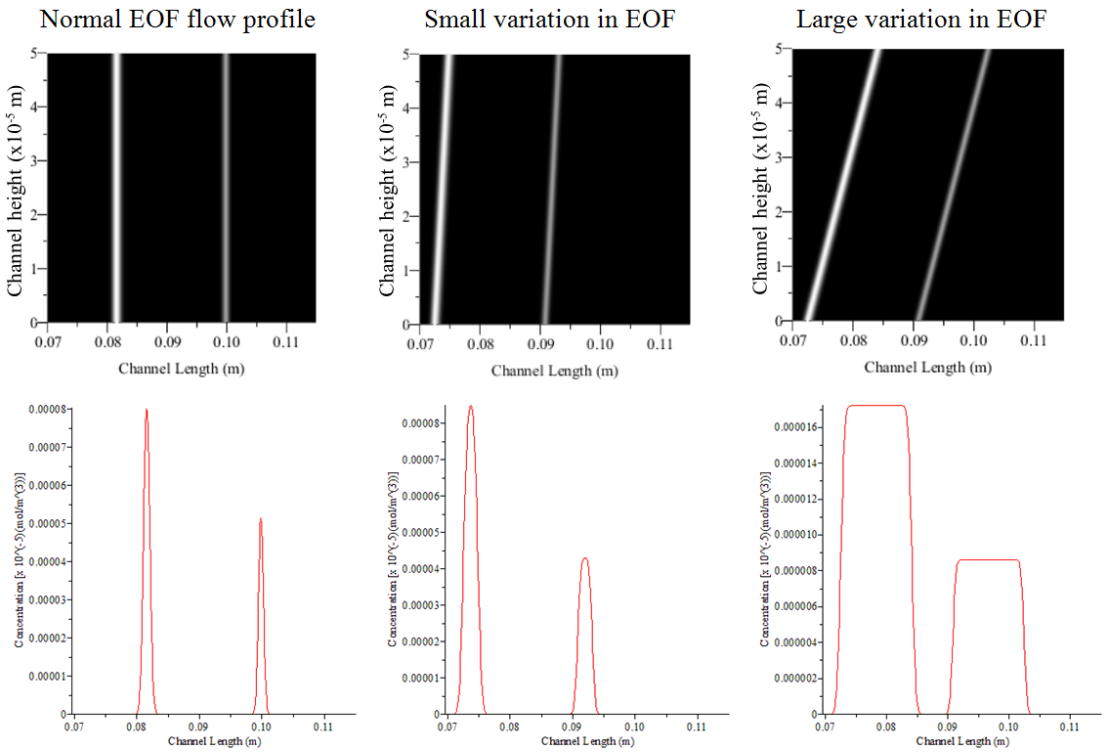

Figure 53: Analyte distribution (top) and resulting peak shapes (bottom) for three analytes (Cu^{2+}, Fe^{2+} and Fe^{3+}) travelling along a channel for three cases, for each an electric-field strength along the channel of 10 kV m^{-1} was assumed. In the first case (left) there is no variation in EOF velocity across the channel height, the EOF velocity is 1 x 10^{-4}. m^2 s^{-1} In the second case (middle) the EOF velocity varies linearly from 0.27 x 10^{-4} m^2 V^{-1} s^{-1} (bottom of channel) to 0.46 x 10^{-4} m^2 V^{-1} s^{-1} (top of channel). In the third case (right) the EOF velocity varies linearly from 0.27 x 10^{-4} m^2 V^{-1} s^{-1} (bottom of channel) to 1.21 x 10^{-4} m^2 V^{-1} s^{-1} (top of channel).

The effect on the analyte distribution and peak shape for three cases (sample: Cu^{2+}, Fe^{2+} and Fe^{3+}) is shown in Figure 53; it is assumed that there is no pressure difference across the channel. The first shows the case for a typical EOF profile which does not vary across the channel height and therefore the resultant peaks are Gaussian shaped. The second and third cases show the effect where the velocity profile varies across the channel height; in the example given the velocity is higher at the top of the channel. The result of the non-uniform EOF flow is that the peak shape becomes broader.

Figure 54 shows the effect of a low, medium and large parabolic flow profile on analyte distribution and peak shape for the case of three analytes (Cu^{2+}, Fe^{2+} and Fe^{3+}) travelling along a channel. The distributions and peak shapes are given after a short distance along the channel, by which point the Fe^{3+} is distinguishable from the Cu^{2+} and Fe^{2+}. With a parabolic flow profile, the velocity is highest at the centre of the channel. Two bands can be seen for

each flow profile. The band on the left represents the Cu^{2+} and Fe^{2+}, whereas the band on the right represents the Fe^{3+}. Due to the small difference in mobility between the Cu^{2+} and the Fe^{2+} ions, no separation is observable between them, unlike the Fe^{3+} which is clearly distinguishable. The corresponding peak shapes for each of the flow profiles can also be seen in Figure 54. Whilst the peaks started as a Gaussian distribution, the addition of the parabolic flow profile skews them. In the simulation results presented in this thesis the effects of pressure differences along the channel are not included. In a practical device it is desirable to minimise any pressure differences along the channel.

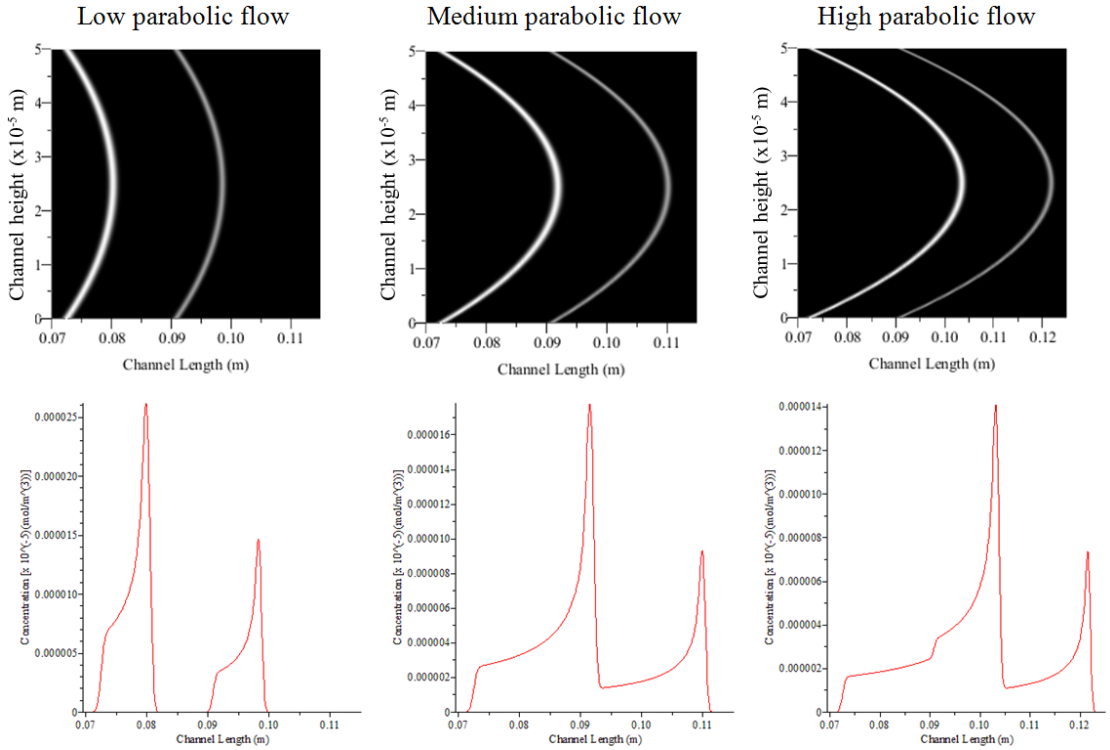

Figure 54: Analyte distribution (top) and resulting peak shapes (bottom) for three analytes (Cu^{2+}, Fe^{2+} and Fe^{3+}) travelling along a channel for three cases subjected to varying degrees of pumped flow. For each case an electric-field strength along the channel of 10 kV m^{-1} was assumed and pumped flow velocity at the channel wall was at 2.7 x 10^{-5} m^2 s^{-1}. In the first case (left) a low parabolic flow is present; the pumped flow velocity increased to 9.0 x 10^{-5} m^2 s^{-1} at the centre of the channel. In the second case (middle) a medium parabolic flow is present; the pumped flow velocity increased to 18.3 x 10^{-5} m^2 s^{-1} at the centre of the channel. In the third case (right) a high parabolic flow is present; the pumped flow velocity increased to 27.7 x 10^{-5} m^2 s^{-1} at the centre of the channel.

4.4.2. Modelling CE with Uniform EOF

The model is first described for the case where the zeta-potential has the same magnitude on all channel walls and therefore the EOF is uniform within the channel. Where a capillary is used, it is possible to easily modify all of the capillary walls. The work in this section describes this case; it is useful for comparison later to show the adverse effects that the separation enhancement methods induce. In Section 4.4.3 the model is adapted to predict the behaviour of the system where there is a difference in zeta-potential on the channel walls such as would be expected where a single ZPM electrode is used to modify the EOF.

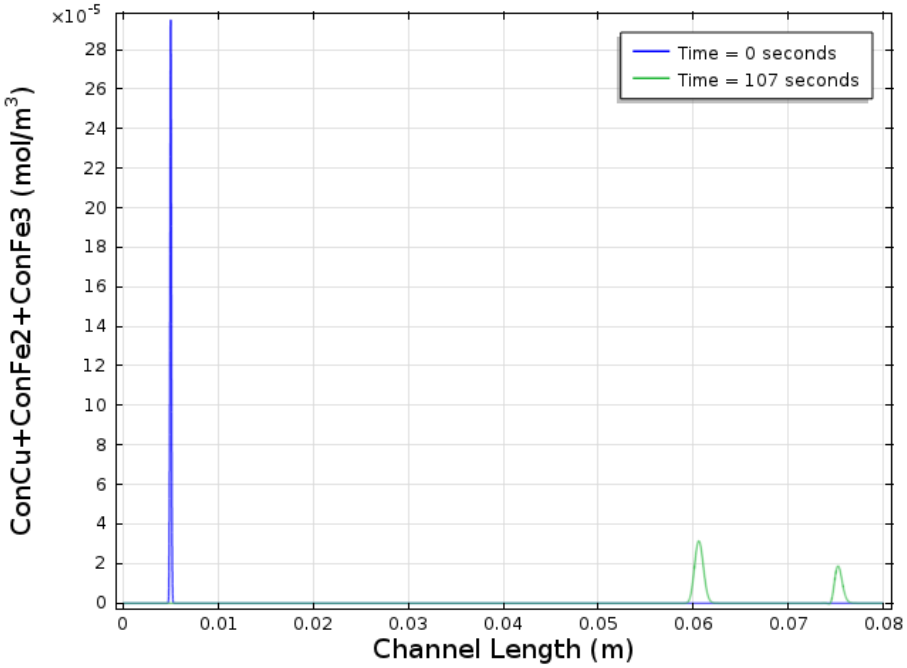

Figure 55: Graph showing the concentration of ions when injected (blue line) and their distribution 107 s after the injection (green line). The green peak at 0.075 m corresponds to the Fe^{3+} ions; the green peak just past 0.06 m represents the Cu^{2+} and Fe^{2+} ions.

The migration of the ions along the length of the channel is modelled first, for the case where the EOF is neglected. The sample of 10 mM of Cu^{2+}, Fe^{2+}, and Fe^{3+} is injected at x = 5 mm using the Gaussian distribution as described earlier by Equation (37). The results showing the position of the ions after 107 s are shown in Figure 55. It can be seen that the model predicts that part of the sample will have migrated to 5 mm from the end of the channel. This part of the sample has travelled further than the other parts, since it has a high mobility. Within the sample the Fe^{3+} ions have the highest mobility and so the peak at 0.075 m corresponds to the Fe^{3+} ions. The concentration at the start of the experiment shown by the

blue line in Figure 55 peaks at 30 mM since it shows the summation of the concentration of the three metal ions. The green line, showing the positions of the ion concentration at 107 s has significantly shallower peaks for two reasons; firstly the peaks have started to separate and so do not overlap perfectly (as they did at t = 0 s). Secondly the ion groups will spread out due to diffusion. This simulation run shows that if the EOF was supressed, then based on the differences in mobility alone it would be possible to separate ferric (Fe^{3+}) ions from cupric (Cu^{2+}) and ferrous (Fe^{2+}) ions. It also shows that under these conditions it would not be possible to separate cupric and ferrous ions in a 0.08 m length of capillary or channel. This is unsurprising given the similarity of their electrophoretic mobilities.

To account for the effect of EOF in the next simulation a typical value for EOF mobility was taken from the literature. The value used was 2.21×10^{-8} m^2 V^{-1} s^{-1}, which is representative of PDMS [212]. The addition of a secondary flow, the EOF, in the same direction as the electrophoretic flow makes it more difficult to separate the metal ions before they reach the end of the channel. The results of this simulation are shown in Figure 56, it can be seen that after 81 s the Fe^{3+} ions have reached x = 0.075 m and the mixture of Cu^{2+} and Fe^{2+} are 8 mm behind. For comparison, the results from the previous simulation shown in Figure 55, where the EOF was neglected, show that when the Fe^{3+} ions have reached x = 0.075 m, the Cu^{2+} and Fe^{2+} mixture is about 14 mm behind.

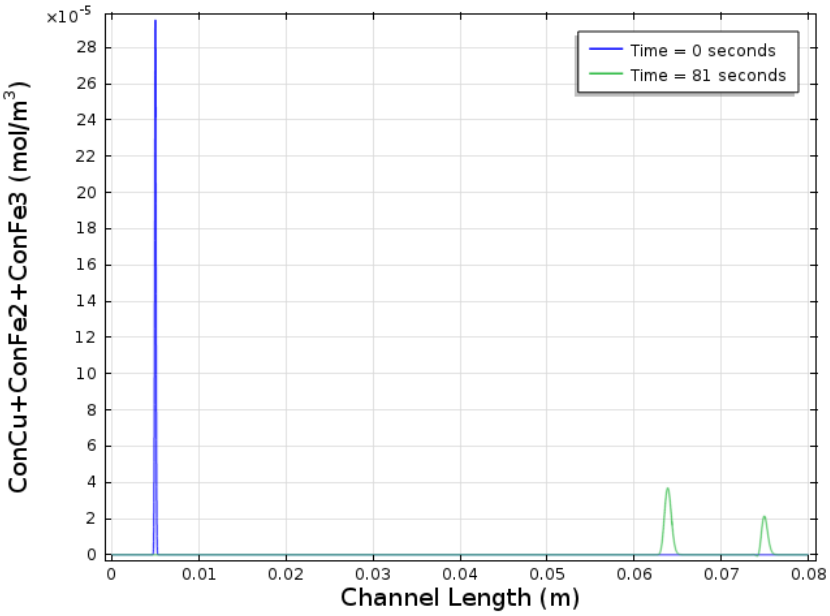

Figure 56: All parameters same as for simulation of Figure 55 except for inclusion of a typical EOF. The time taken for Fe^{3+} to reach the end of the channel is reduced to 81 s, which in turn has reduced the overall separation. Here the green line represents the ion concentrations at 81 s into the simulation.

To get the maximum separation for a sample of mixed ions the smallest difference in mobility needs to be considered. For the case of the three metal ions, Cu^{2+}, Fe^{2+} and Fe^{3+}, the smallest difference, as can be seen in Table 1, is between Cu^{2+} and Fe^{2+}. To get the maximum separation in a single run by modifying the EOF, the EOF would need to be set to be equal and opposite to the electrophoretic force on the Cu^{2+} ions. Matching the mobility of the EOF to that of the Cu^{2+} ions results in a net force of zero on the Cu^{2+} ions, therefore the Cu^{2+} ions will not migrate along the channel, except for some diffusion. The other ionic groups will move slowly along the channel as their velocity will be strongly retarded by the large negative value of EOF.

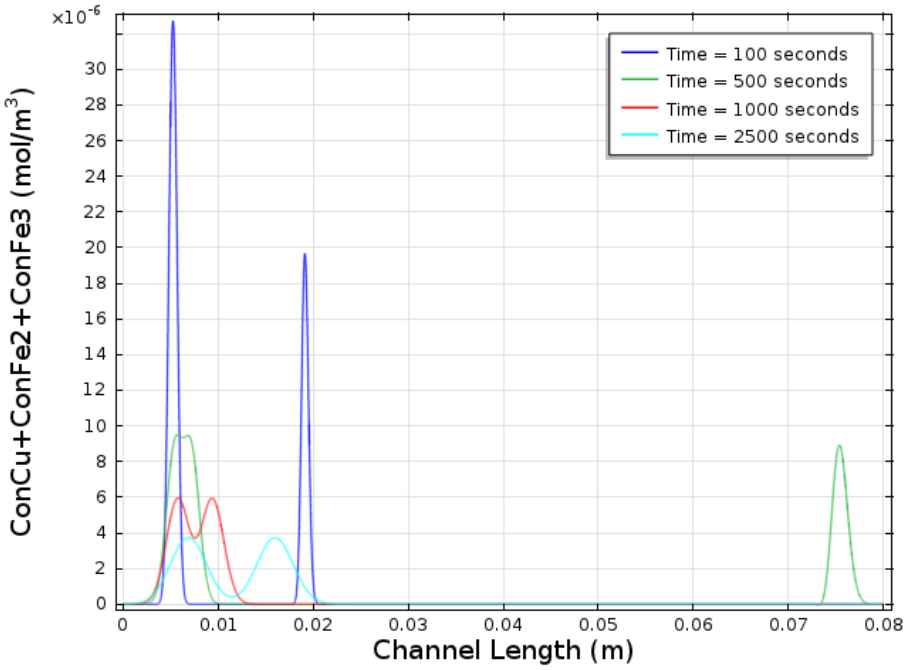

Figure 57: Simulation with EOF set to be about equal and opposite to the mobility of Cu^{2+} (EOF set to: -5.55x10^{-8} m^2 V^{-1} s^{-1}); temperature set to 298.15 K, time for each line displayed in seconds in legend.

The next simulation shows the case where the EOF mobility has been modified to –5.55x10^{-8} m^2 V^{-1} s^{-1} (this is slightly lower than the mobility of Cu^{2+}); the results can be seen in Figure 57. The EOF was not perfectly matched to the Cu^{2+} ions to enable them to migrate slowly towards the end of the channel. The temperature assumed for the simulation was 298.15 K; this is the same as that stated for the calculations of mobilities given in Table 1. In Figure 57, it can be seen that after 100 seconds, the Fe^{3+} ions have separated from the mixture of Cu^{2+} and Fe^{2+}. At 500 seconds, the Fe^{3+} ions have travelled to 0.075 m. At 1000 seconds, and 2500 seconds, it becomes possible to see the separation of Fe^{2+} from the Cu^{2+} ions. Under the given conditions, it is possible to separate Fe^{2+} ions from Cu^{2+} ions in a channel with a

length less than 1 cm. With a larger electric-field the separation would occur faster, and therefore there would be less time for diffusion and so the channel length could be further reduced.

To illustrate the importance of temperature on the migration of ions along the channel, another simulation was run in which the temperature was increased to 300 K, the results of which can be seen in Figure 58. Even with a weaker value of -5.54×10^{-8} m^2 V^{-1} s^{-1} for the EOF, the Cu^{2+} ions travel towards the start of the channel. Whilst control of the EOF to high precision is easily achieved in a simulation environment, such accuracy is practically impossible in real world experiments. The effect of temperature is an example of just one practical issue which requires consideration.

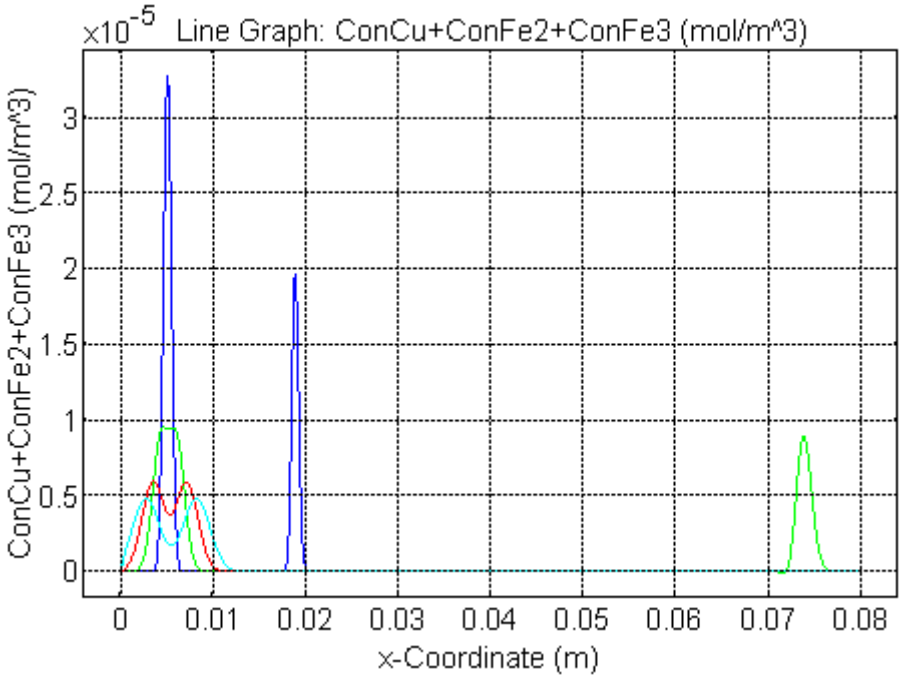

Figure 58: Simulation with EOF set to be about equal and opposite to the mobility of Cu^{2+} (EOF set to: -5.54×10^{-8} m^2 V^{-1} s^{-1}), temperature set to 300 K. Displayed times for graphs: blue = 100 s; green = 500 s; red = 1000 s; cyan = 1500 s.

In Section 2.4 two separation enhancement routines using dynamic ZPM were described. The first operated by matching the EOF to the sample migration velocity. The modelling of this has been described above. Here, a description of the second method (see Section 2.4.3) is given. Briefly, this method involved switching the EOF throughout an experimental run to cause the sample to migrate the channel length numerous times. Upon consecutive iterations the sample becomes increasingly separated. The EOF mobility is dynamically modified throughout the simulation; this has the effect of causing the sample to migrate along the

channel length in both directions and consequently leads to a longer retention time in the electric-field. The EOF value is modified as shown in the graph of Figure 59; it is defined as a square wave with a frequency of 228.6 Hz and amplitude of -1.112×10^{-7} m^2 V^{-1} s^{-1}. These values were chosen to make the sample migrate between x = 0.01 m and 0.07 m; the start position for sample injection was modified from 0.005 m to 0.01 m. The use of a square wave to define the timing for EOF switching means that there are two conditions for EOF which can be set. The first condition is travelling from the start to end of channel, and the second is the reverse. If the start point is at 0.005 m. then the sample will have to travel back to this point, however due to diffusion, there is a risk that over the course of the experiment, part of the sample would travel beyond this point and out of one of the channel ends. The simulation control is open loop in that the time for switching the EOF is known at the start of the experiment. In a real experiment, the use of detectors near the ends of the channel enable a closed loop system which would switch the EOF value when a sample nears the channel end.

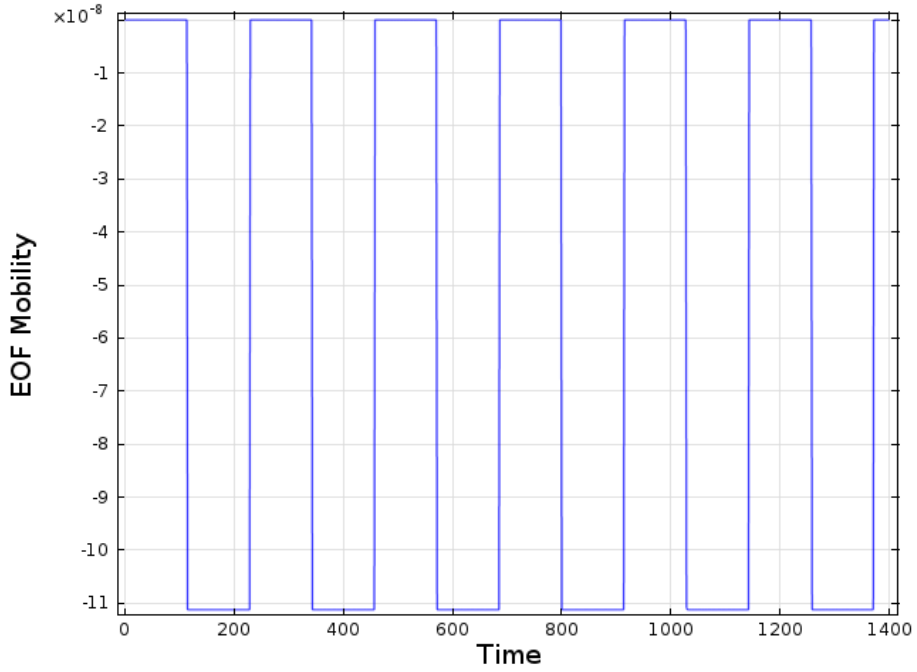

Figure 59: Graph showing EOF switching function to modify EOF during simulation. The square waveform has a frequency of 228.6 Hz and amplitude of -1.112×10^{-7} m^2 V^{-1} s^{-1}.

The sample in this simulation was Cu^{2+} and Fe^{2+} which have similar mobilities. After the sample travels along the channel once, there is no noticeable separation of the metal ions as shown by the blue line in Figure 60. At 114.3 s the sample reaches x = 0.07 m and the EOF is reversed such that the sample will travel back to x = 0.01 m by t = 228.6 s. At which point

the EOF is set to 0 again, and the sample is sent back down the channel. The sample next reaches x = 0.07 m, 114.3 s later (t = 342.9 s); it can be seen by the green line of Figure 60 that the Cu^{2+} and Fe^{2+} ions are still indistinguishable. The process of switching the EOF is continued and upon consecutive iterations the sample becomes increasingly separated; this effect can be seen in Figure 60. The simulation has also calculated how the sample will broaden due to diffusion. The extent of diffusion is related to the experiment time; the separation can be achieved faster and therefore with less diffusion by making the electric-field larger. A consequence of using a larger electric-field which needs consideration is the risk of Joule heating. Provided that the channel cross-sectional area is small and the buffer solution is not highly conductive then Joule heating will not be a problem in practice.

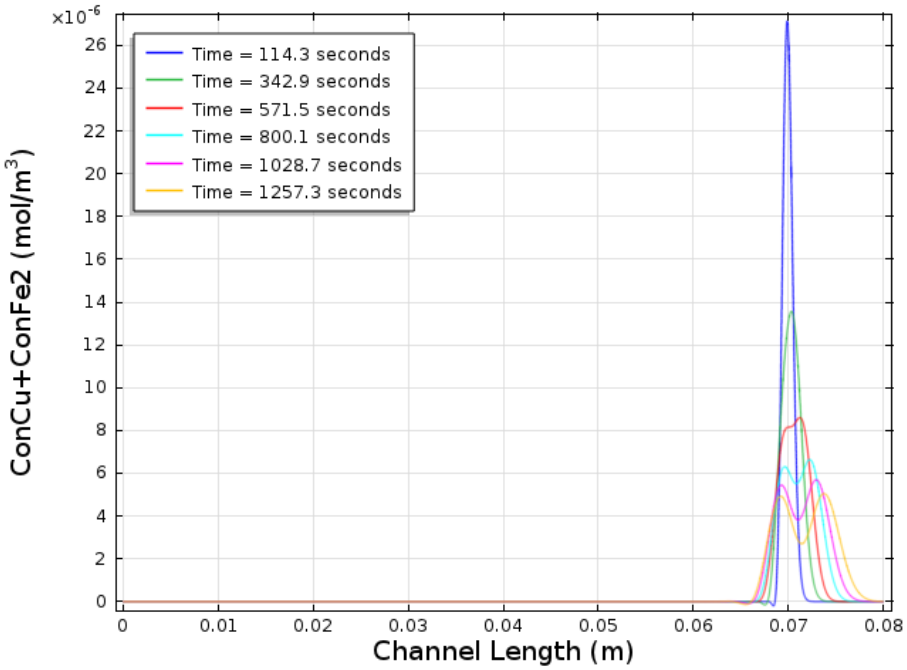

Figure 60: Simulation with EOF switched between two values numerous times throughout the simulation (as shown in Figure 59); temperature set to 298.15 K, time for each line displayed in the legend.

An alternative method to switching the EOF as the sample approaches the channel ends is to have two detectors close together to switch the EOF and keep the sample between the two electrodes. This technique was described earlier in Section 2.4.4; it could be considered a practical solution to mimic the effect of matching the EOF to the sample velocity, which as mentioned above would be difficult. After a certain number of switches, or time switching, the sample will be separated and can be sent to the end of the channel. Switching rapidly between these two detectors is an easily realisable method for matching the EOF to the mobility of the ionic sample. Using a closed-loop system, the EOF is switched when the

detector detects the presence of the sample. To simulate the effect of rapidly switching the EOF, a simulation was run which modified the EOF using a sine wave as shown in Figure 61.

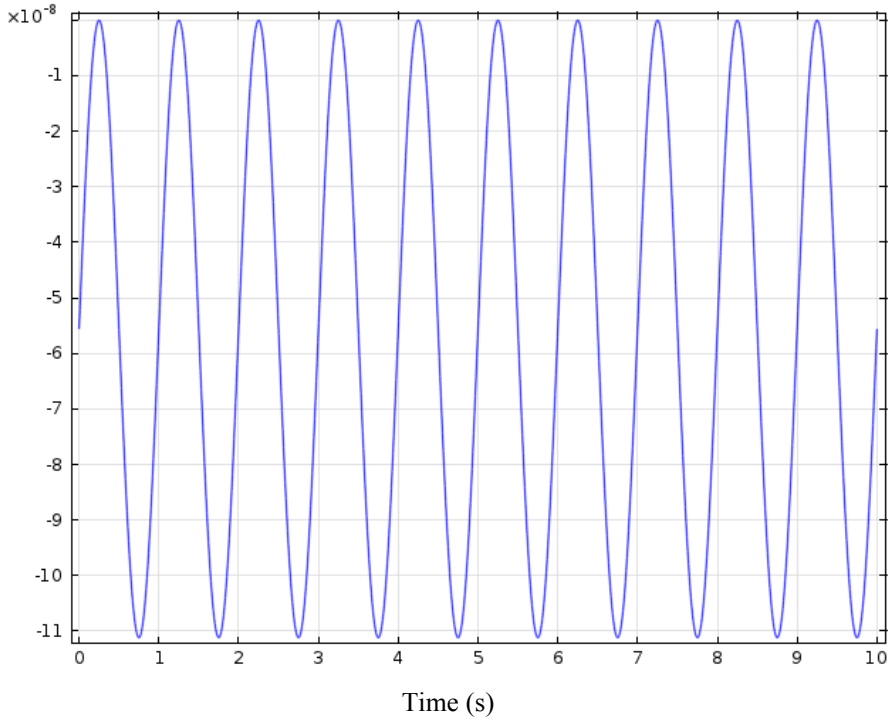

Figure 61: Graph showing EOF switching function to modify EOF during simulation. The sinusoidal waveform has a frequency of 1 Hz.

Unlike the switching waveform shown earlier in Figure 59, the average EOF is slightly less than for Cu^{2+}; this means that the entire sample will migrate along the channel length. The sample will migrate slowly along the length of the channel and so will separate before it reaches the end of the channel.

After 500 seconds which corresponds to 500 switching cycles of the EOF it can be seen in Figure 62 that the sample is starting to separate and has travelled less than 4 mm. After 1000 seconds the peaks are even further separated. The peaks are clearly distinguishable by 1500 seconds and even more so by 2500 seconds; the sample has travelled less than 15 mm. This clearly demonstrates the importance of these separation enhancement schemes particularly for miniaturised CE devices.

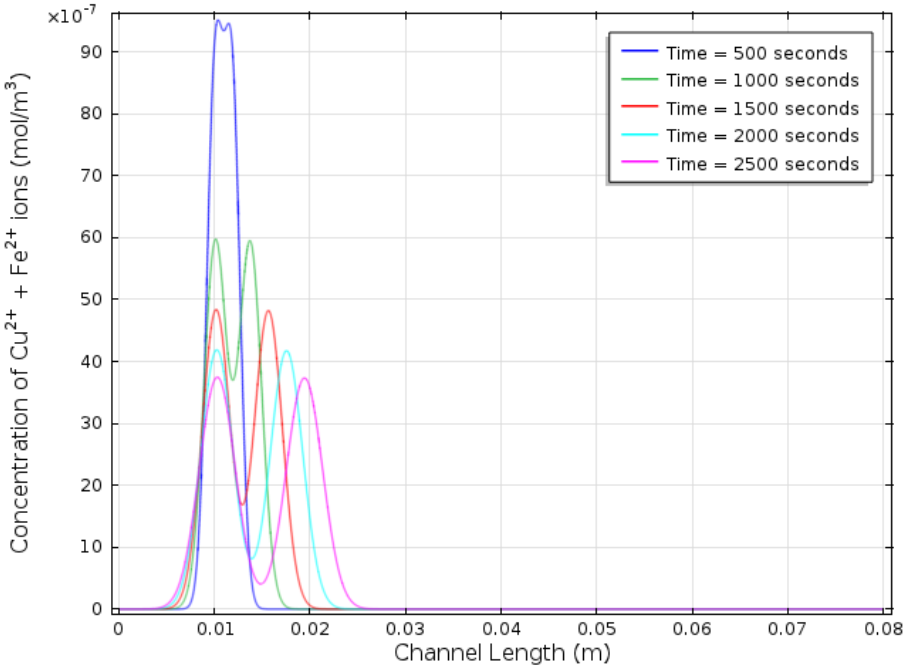

Figure 62: Simulation with EOF switched rapidly between two values numerous times throughout the simulation (as shown in Figure 61); temperature set to 298.15 K, time for each line displayed in the legend.

4.4.3. Modelling CE with Non-uniform EOF

In the previous section the effect of modifying the EOF on the separation was described for the case where the modification was the same on all channel walls. Dynamic control of the EOF enables separations to be achieved in shorter channel lengths. In this section the effects on EOF where the zeta-potential is modified along a single channel wall are investigated. It is advantageous, for fabrication purposes of a planar device, if only one ZPM electrode near a channel wall is required. In such a case it is only possible to dynamically modify the zeta-potential on the channel wall nearest the ZPM electrode. The other walls maintain their natural zeta-potential, however it is still possible to increase, decrease and reverse the EOF. To maximise the effect of the ZPM electrode on the EOF, it is beneficial to modify the larger channel surface. In the case of a rectangular channel, the channels should be wide and shallow. Our model assumes that channel depth << width, therefore the effect on the EOF from the vertical sidewalls at this stage has been neglected. The 2D model is illustrated in Figure 63, the boundary conditions for the EOF mobility at the top and bottom channel walls are shown.

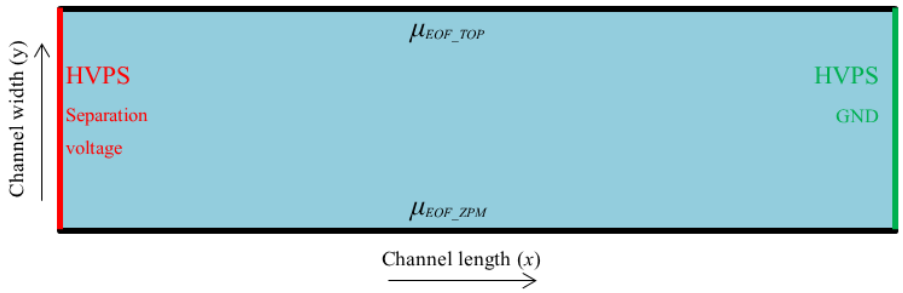

Figure 63: Illustration describing geometry and locations of boundary conditions for the microfluidic model.

To investigate the effect of modifying the EOF mobility at a single channel wall, the mobility along the top of the channel wall was kept constant at $-1x10^{-8}$ m^2 V^{-1} s^{-1} and the mobility along the bottom channel wall was varied. The EOF mobility along the bottom channel was modified from 9 $x10^{-8}$ m^2 V^{-1} s^{-1} to $-11x10^{-8}$ m^2 V^{-1} s^{-1}. These values were chosen to give a difference in EOF mobility (from the top wall EOF mobility) of +/– $10x10^{-8}$ m^2 V^{-1} s^{-1}. The results from this simulation are shown in Figure 64.

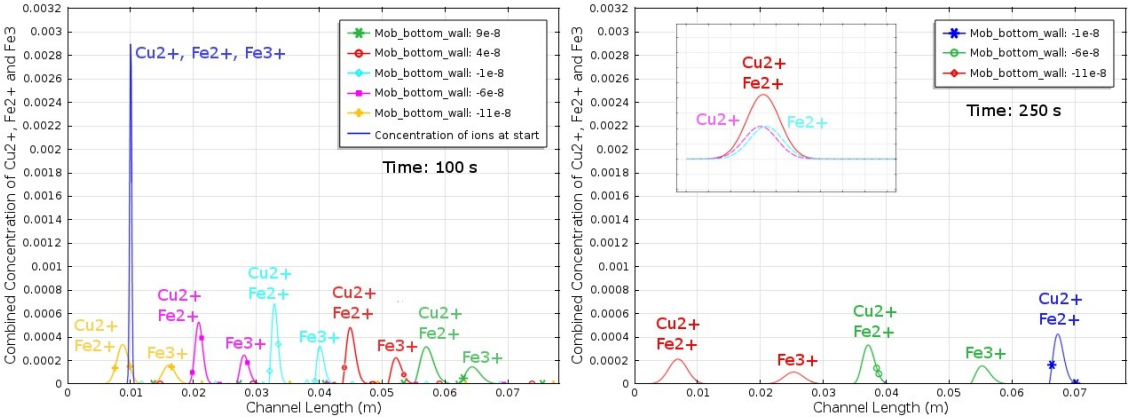

Figure 64: Simulation results showing the effect on separation of different values of mobility on the bottom channel wall (see legend). EOF mobility on top channel wall kept constant (-1x10^{-8} m^2 V^{-1} s^{-1}). Left: concentration of ions after 100 s. Right: concentration of ions after 250 s; inset graph: Cu^{2+} and Fe^{2+} starting to separate, but it is small due to small difference in mobility.

Two observations can be made from these results. Firstly they show that using a single electrode, to execute the separation enhancement routines described earlier in Section 2.4, it is possible to improve the amount of separation within a given channel length. The second observation is that there is increased broadening of the peak as the difference in top and bottom wall EOF mobility increases. To highlight this effect, the ratio of peak height to width of Cu^{2+} and Fe^{3+} ions after 100 seconds for a range of differential EOF mobility

values, are shown in Figure 65. It can be seen that as the difference between the EOF mobility of the bottom channel wall (near the ZPM electrode) and the fixed top channel wall increases, the peak height decreases, and the peak width increase. The decrease in the ratios means that the peak is becoming broader which is undesirable for a separation system and consequently places a limit on the technique. As can be seen in the inset graph of Figure 64, where the difference in electrophoretic mobility is small (such as between Cu^{2+} and Fe^{2+}), this additional peak broadening makes it difficult to attain separation. To reduce the amount of broadening, the difference in sample velocity across the channel height/width needs to be minimised. The optimum case would be where the sample velocity is uniform; in this case the broadening would be caused only by diffusion. The broadening from both diffusion and differential-wall mobilities must be overcome for the sample to separate.

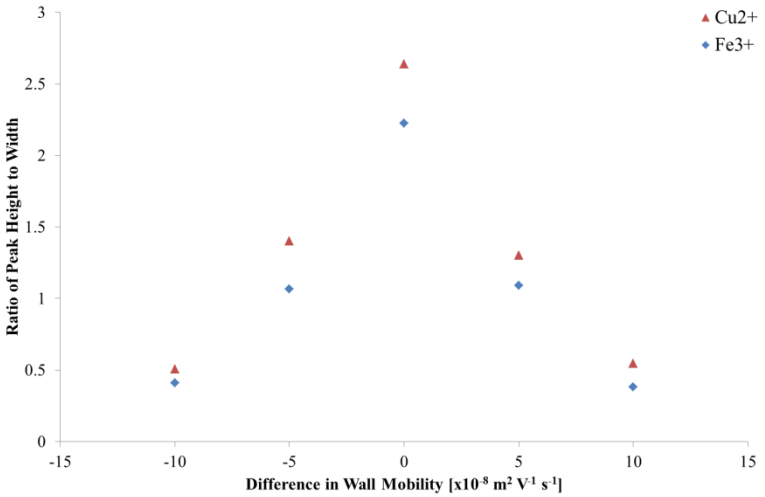

Figure 65: Ratio of peak height to width of Cu^{2+} and Fe^{3+} ions after 100 seconds for a range of differential EOF mobility values.

A selection of results generated by the model discussed in this section were summarised in a paper and presented at the 26th European Conference on Solid-state Transducers [55].

4.4.4. Dispersion Induced by Difference in EOF

Non-uniform EOF induces sample dispersion. This has been modelled analytically with a view to inferring limits on design. The time-varying concentration of ions in a channel can be described using Equation (38) [213]. This is a modification of the Gaussian distribution as given earlier in Equation (37).

$$C_i(x,t) = \frac{c_0}{\left(\sqrt{4\pi D_i t}\right)} e^{-\left(\frac{\left(x-(x_{start}+u_{ion}t)\right)^2}{4D_i t}\right)} \tag{38}$$

For the case where the sample is a mixture of ions, the concentration of the individual ions can be summed. For example, if the sample is a mixture of Cu2+, Fe2+ and Fe3+ then Equation (38) becomes Equation (39).

$$\begin{aligned} C_i(x,t) = {} & \frac{C_{cu2\_start}}{\left(\sqrt{4\pi D_{cu} t}\right)} e^{-\left(\frac{\left(x-(x_{start}+u_{cu2}t)\right)^2}{4D_{cu2} t}\right)} + \frac{C_{fe2\_start}}{\left(\sqrt{4\pi D_{fe2} t}\right)} e^{-\left(\frac{\left(x-(x_{start}+u_{fe2}t)\right)^2}{4D_{fe2} t}\right)} \\ & + \frac{C_{fe3\_start}}{\left(\sqrt{4\pi D_{fe3} t}\right)} e^{-\left(\frac{\left(x-(x_{start}+u_{fe3}t)\right)^2}{4D_{fe3} t}\right)} \end{aligned} \tag{39}$$

With the ion velocity is dependent solely on the ion mobility and the EOF is neglected, it can be shown that when t = 107 s the response (given in Figure 66) matches that given earlier for the same conditions predicted by the FEM model in Figure 55.

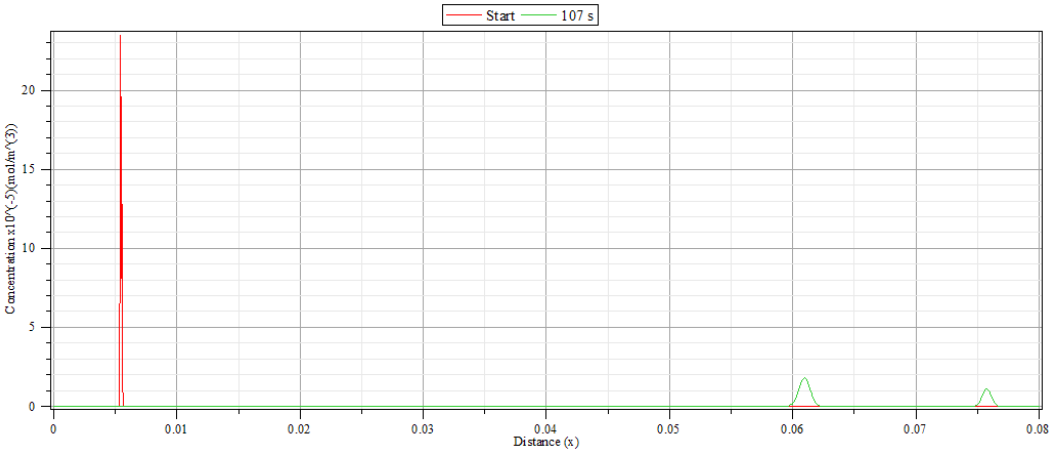

Figure 66: Graph showing the concentration of ions when injected (red line) and their distribution 107 s after the injection (green line). This shows good agreement with the FEM model presented earlier (Figure 55).

In order to account for a uniform EOF, Equation (38) can be modified by adding in an EOF velocity term as shown in Equation (40).

$$C_i(x,t) = \frac{c_0}{\left(\sqrt{4\pi D_i t}\right)} e^{-\left(\frac{\left(x-(x_{start}+(u_{ion}+u_{EOF})t)\right)^2}{4D_i t}\right)} \tag{40}$$

To model a non-uniform EOF, i.e. an EOF which varies along the channel width, the EOF velocity can be defined as a function of y in which case, Equation (40) is written as shown in Equation (41).

$$C_i(x,y,t) = \frac{c_0}{\left(\sqrt{4\pi D_i t}\right)} e^{-\left(\frac{\left(x-(x_{start}+(u_{ion}+u_{EOF}(y))t)\right)^2}{4D_i t}\right)} \quad (41)$$

If desired, the EOF velocity profile could be shaped to include a pumped-flow profile which could arise from pressure differences along the channel. Here, the variation in EOF along the channel width is varied as a linear change with width. This profile allows the modification of the velocity at the walls and enables the effect of a difference in EOF wall mobilities on the sample dispersion to be shown.

Figure 67 shows electropherograms for three cases. In each case a sample of Cu^{2+}, Fe^{2+} and Fe^{3+} is sent along a channel where on one wall (the top) the EOF mobility remains constant at $1x10^{-8}$ m^2 V^{-1} s^{-1}. The EOF mobility at the bottom channel wall (modified by the ZPM) is set to $1x10^{-8}$ m^2 V^{-1} s^{-1}, $1.1x10^{-8}$ m^2 V^{-1} s^{-1} and $1.5x10^{-8}$ m^2 V^{-1} s^{-1} for cases A, B and C respectively. The electropherograms show the ion concentration distribution at the start and after 80 seconds. It can be seen that after 80 seconds the Fe^{3+} ions have separated from the Cu^{2+} and Fe^{2+} ions. As the EOF mobility on the bottom wall is increased to $1.5x10^{-8}$ m^2 V^{-1} s^{-1}, i.e. the difference in EOF wall mobilities increases, the sample dispersion increases. Even with the large amount of dispersion shown in case C of Figure 67 it is still possible to separate the Fe^{3+} ions from the Cu^{2+} and Fe^{2+} mixture.

Equation (42) describes a condition for defining separation for a sample of two species, species a and b. They can be considered separated at the time where the difference between the positions of the species is greater than their broadening distance, x_b. Dispersion due to a varying EOF velocity across the channel width and diffusion both contribute to the broadening distance. The difference in velocities is directly related to the difference in electrophoretic mobilities of the species. The difference in the electrophoretic mobility of the species places a limit on the 'tolerable' broadening.

$$(u_a - u_b) \cdot t > x_b \quad (42)$$

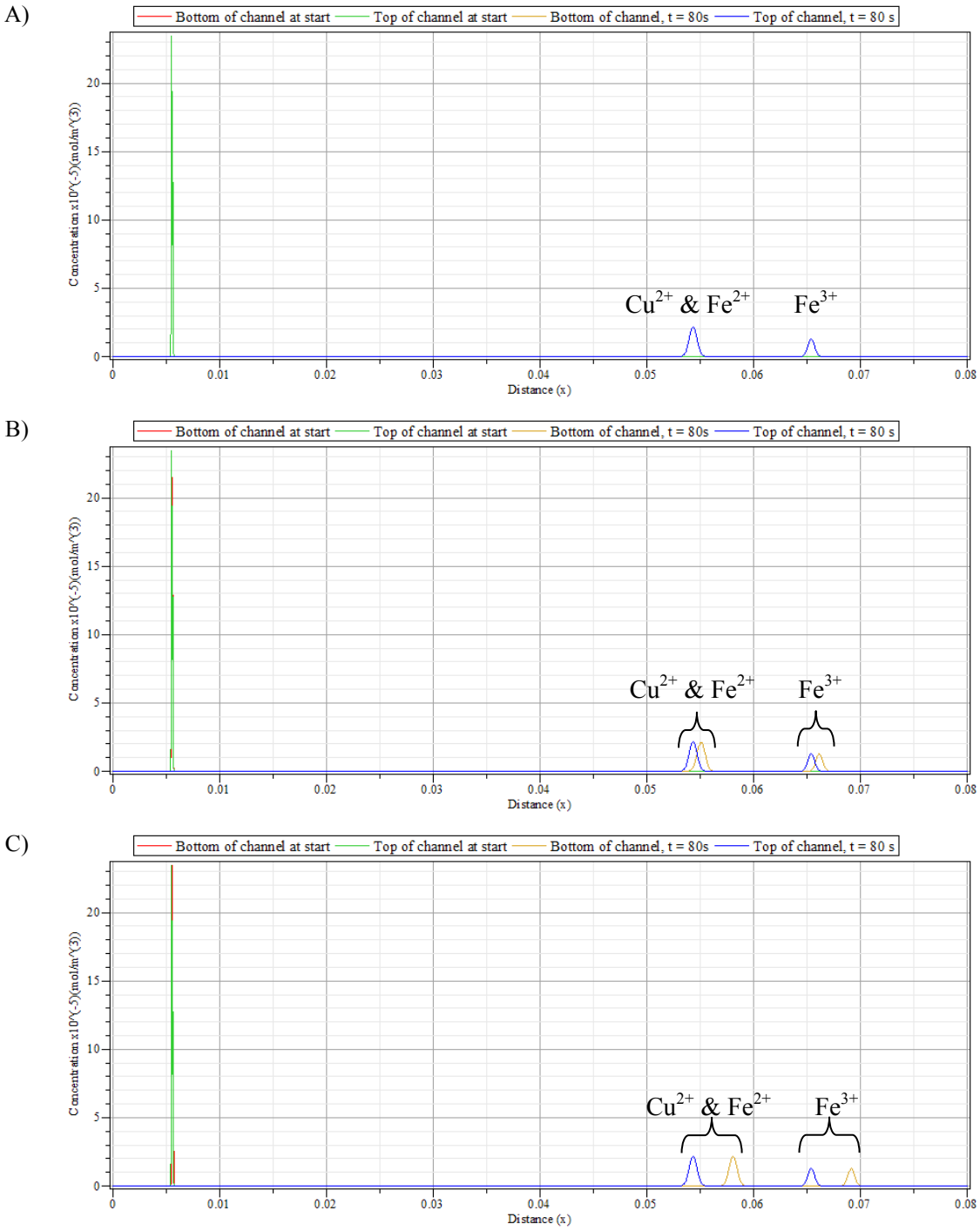

Figure 67: Electropherogram of a sample of Cu^{2+}, Fe^{2+} and Fe^{3+} shown at start and after 80 seconds in electric-field of 9375 V m^{-1}. For all cases the EOF mobility on the top channel wall is $1x10^{-8}$ m^2 V^{-1} s^{-1}. The EOF mobility at the bottom channel wall (modified by the ZPM) is set to $1x10^{-8}$ m^2 V^{-1} s^{-1}, $1.1x10^{-8}$ m^2 V^{-1} s^{-1}, and $1.5x10^{-8}$ m^2 V^{-1} s^{-1} for cases A, B and C respectively.

The contribution to the broadening distance due to the differences in EOF velocity across the channel width is given by Equation (43).

$$x_{\Delta EOF} = \left(u_{EOF\_top} - u_{EOF\_bottom}\right) \cdot t \tag{43}$$

Diffusion was described earlier in Section 4.3.2. The total broadening distance is a combination of Equations (36) and (43). To show how these equations describe the limit on the difference in velocity across the channel, a numerical example is described. In the case of Cu^{2+} and Fe^{3+}, the following condition needs to be met to separate the species.

$$\left(u_{fe3} - u_{cu2}\right) \cdot t > \Delta u_{EOF} \cdot t + \sqrt{2D_i t} \tag{44}$$

If the channel is 0.1 m long, and the electric-field is 10 kV m^{-1} and an average EOF mobility of $1x10^{-8}$ m^2 V^{-1} s^{-1} is assumed then the Fe^{3+} ions will take ~124 seconds to travel from the start to the end of the channel (i.e. t = 124 s). Using Equations (4) and (5) with the values for diffusivity from Table 1, the difference in EOF wall mobilities is $1.46x10^{-8}$ m^2 V^{-1} s^{-1}. Using these values the concentration distribution was calculated. The EOF mobility on the top and bottom channel walls was $2.7x10^{-9}$ m^2 V^{-1} s^{-1} and 1.73 $x10^{-8}$ m^2 V^{-1} s^{-1} respectively. These were calculated such that the average EOF mobility would be $1x10^{-8}$ m^2 V^{-1} s^{-1} and the difference between the values is $1.46x10^{-8}$ m^2 V^{-1} s^{-1}. The resulting electropherogram is shown in Figure 68, it can be seen that at the point where the peaks corresponding to the Fe^{3+} species finishes, the Cu^{2+} species begins. Due to the Cu^{2+} species directly following the Fe^{3+} species, it would not be possible to distinguish between them, unless the detector was capable of identifying the species.

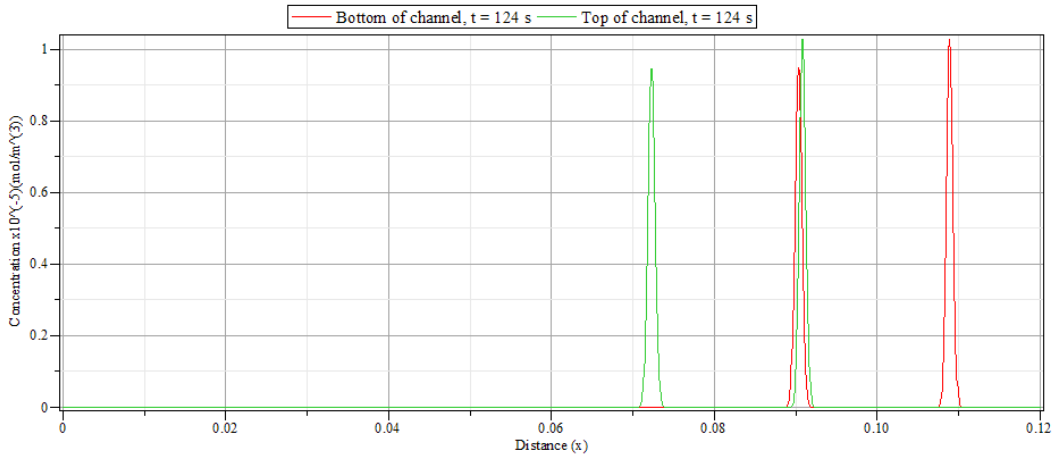

Figure 68: Electropherogram showing minimum amount of broadening (due to difference in EOF velocity along channel width and diffusion) which would prevent separation of Cu^{2+} and Fe^{3+}.

4.5. Conclusions

This chapter has detailed a range of models and simulations which aid the design of a microfluidic system to perform the separation enhancement methods. An overview of the existing models from the literature which describe the potential distribution across the EDL has been presented. From this a model was developed to predict this potential distribution for the case where there is an external electric-field applied across an insulating channel wall in the presence of a second electric-field along the channel. Comparing the model's predicted zeta-potential, taken from the EDL distribution, with inferred values of zeta-potential from experimental results, based on published results in literature, the model was shown to accurately predict the zeta-potential.

Later in Chapter 6 a discussion on a number of devices which were fabricated in parallel with the development of the model is given. Based on the fundamental CE theory, as described in Section 2.2, device 1 was fabricated with a long channel length; on this device the fundamental CE theory was evaluated. The effect of the ZPM electrode on the zeta-potential, as described in Section 4.2, and consequently the EOF as described in Section 4.3 was explored by monitoring the EOF on device 3.

From the modelling of the EDL, it was clear that the thickness of the insulation layer was an important factor affecting the ability to modify the EOF. The model showed that a large portion of the electric-field would be dropped across the insulation layer, and therefore for devices 3 and 4 a thin insulation layer of ~1 μm would be suitable.

Another aspect of the model solved the time-dependant Nernst-Planck equations to predict the separation under a range of conditions. Keeping the requirements of planar fabrication in mind, the model was modified to investigate the effect of dynamically modifying the zeta-potential on a single channel wall rather than the ideal case which would be complete channel coverage. For both cases, the effectiveness of the separation enhancement routines was explored.

Two factors which contributed to the sample dispersion have been investigated. The first factor was diffusion, where molecules migrate from a region of higher concentration to that of a lower concentration. The second contributing factor arose as a consequence of using a single planar electrode (resulting in partial channel coverage) for the modification of the zeta-potential (and the resulting EOF) as opposed to having full channel coverage. The relationship between this second factor and the difference in the EOF mobility between the covered and uncovered channel walls has been discussed. It was shown that a larger

difference in the EOF mobilities between the channel walls resulted in larger sample dispersion. This dispersion acts against the separation and as a consequence places limitations on the separation capability of the system. Using an analytical model, an equation for the maximum 'allowable' difference in velocity across the channel has been developed. This relationship can be used to calculate the operational limits for the system.

Chapter 5

Detection System

The separation enhancement methods required a detection system to inform the control system. The control system relies on detectors warning when the ions reach the extremes of the channel as well as informing on the state of separation. In this chapter the design of the detection system is discussed. Simulation of the electronic circuits was performed using a SPICE simulator. SPICE is a general purpose electronic circuit simulation program developed at the Electronics Research Laboratory, University of California, Berkeley [214]. Details on the developed SPICE simulation for the circuitry of the detection system are given. This was used to aid the design and predict performance. The detection system was tested on selected prototype devices; the results from this are given in the appropriate section discussing the prototype devices in Chapter 6.

5.1. Background on Detectors for Miniaturised CE Systems

As has already been mentioned, CE is a method of separating ionic species based on the differences in their values of electrophoretic mobility. A detector is required to inform the user when an ionic species passes a certain point, usually some distance along the capillary, near the outlet. If the time for a species to travel from the injection point to the detector is known (from which the mobility can be deduced), then it is possible to identify what species has been detected. For the project the detector was only required to inform the user and control system that an ionic species has arrived at a particular point along the channel. Identification and quantification of the ionic species can be conducted later in the device using a separate ECD system.

Usually, choosing the correct detector for use in CE analysis is crucial to ensuring optimum performance in terms of: the limit of detection; analyte identification; differentiation between similar analytes; reliability; accuracy and precision. The type of detector used often depends on the sample that is being analysed. For example, many optical methods are of little or no use if the analytes to be separated are not highly coloured or cannot be marked, for example by fluorophores, to make them fluoresce for detection by a UV detector.

UV detection of metal ions can be performed indirectly by complexation of the metal ions. Whilst this adds additional processing steps, the complexation process also modifies the electrophoretic mobility of the ions, and therefore the difference in mobility of the metals ions can be increased making it easier to separate them [90]. Various ligands can be used as complex-forming compounds to enable indirect UV detection of metal ions [90, 215]. The metal ions of interest to the project, as listed in Table 1, includes the metal ions of chromium, copper, iron, manganese and nickel; a complexation process for these is discussed in [90]. Kelly *et al.* discuss the use of CE for corrosion analysis, they report on the analysis of metal ions, including aluminium, manganese and copper [117]. A detailed discussion on optical detection is given in Section 5.1.1.

A contactless conductometric detection system was described by Kubáň *et al.* [21]. This system was shown capable of detecting chromium ions without the requirement of any sample pre-treatment, other than dilution [21]. The limit of detection for the conductometric system was measured as 10 μg L^{-1} for the Cr^{3+} ions [21]. Prest *et al.* discussed the analysis of numerous metal cations, including: chromium, cobalt, iron, manganese, nickel and zinc [216]. The ions were detected using a conductometric detection method, the detection limits for each of the ions was measured; the limits ranged from 0.5 - 5 mg L^{-1} [216]. Electrochemical detection methods are discussed in further detail in Section 5.1.2.

As research has progressed toward the concept of the μ-TAS (micro-total analysis system), a term first described by Manz *et al.* [217], there has been much discussion on the success of different detector types and their compatibility with miniaturisation. For a truly miniaturised CE device optical methods are less suitable due to the reduction in sensitivity brought about by the reduction of the detector window size. As discussed earlier in Section 3.2, ECD systems stand to gain an increase in sensitivity from miniaturisation with associated reduction in working electrode size, due to enhanced flux toward the electrode surface [89].

Often with miniaturised systems, researchers use external detector systems. For a truly miniaturised system the entire detector system also needs to be miniaturised. For optical detection methods this would require miniaturising the laser/diode light source and the

receiver. ECD electrodes are typically well suited to miniaturisation. As well as the miniaturisation of the detectors themselves, the control system which controls and monitors the detectors needs to be miniaturised.

For the separation system within the project, the detectors are not within the main focus of interest. However an investigation on detection systems was required to aid the experimental validation of the separation enhancement methods. The control system requires information from detectors to determine when electric-fields need to be switched. This meant that the specification of the detection system was lenient.

5.1.1. Optical Detection

The simplicity of shining a laser or light beam onto a channel and measuring the response has kept optical detection methods popular, with LIF being one of the most widely used methods for CE systems [218]. Further to this, optical systems are inherently electrically decoupled from the high voltages applied to the separation channel in CE [218]. Vogt *et al.* discussed the typical limits of detection for various detection methods for use with CE. The detection limit for indirect UV absorption was quoted in the region of 10^{-4} – 10^{-8} mol L^{-1}; for fluorescence detection the range was from 10^{-5} – 10^{-9} mol L^{-1} [90]. In 2004, Guijt *et al.* [173] stated that high pressure (or performance) liquid chromatography (HPLC) used optical detection methods much more so than any other method and that ECD techniques such as amperometry were only employed about 5 % of the time. Whilst optical methods have proven popular with HPLC, ion chromatography on the other hand, has tended to favour conductometric detection methods [173].

Whilst optical detection (fluorescence and adsorption) has been used by numerous groups with CE, the reported work on optical methods for the detection of metal ions typically uses complexing agents to modify the species to be detected. The molecules that complex to the metal ions enhance the extinction coefficient at the detection wavelength. For example, for the detection of Cu^{2+} ions, Norkus *et al.* used β-cyclodextrin; they showed that the extinction coefficient of the complex was 50 M^{-1} cm^{-1} (wavelength maximum: 660 nm) [219]. Another Cu^{2+} complex, (4-chloro-2-{[1E)-quinolin-2-ylmethylene)]amino} (4-Cl-2-QMAP)) was discussed by Avcibasi *et al.*; the values for wavelength maximums measured varied between 460 nm to 555 nm depending on the supporting solvent used [220]. For their system, the detection limit for Cu^{2+} in water was calculated as 1.6 x 10^{-5} mol L^{-1} [220]. Säbel *et al.* reported on the complexing of Zn^{2+}, Cu^{2+} and Co^{2+} with zincon and measured the extinction coefficients; detection limits were found to be in the high nanomolar range [221]. For the

other metal ions of interest to this project such as: for Fe^{2+}, Kim *et al.* used 1,10-phenanthroline [222]; for Ni^{2+}, El-Mossalamy *et al.* used a thiazolazo compound [223]; and for Al^{3+}, Kim *et al.* used anthraquinone [224]. These examples illustrate a small fraction of the work on the complexation of ionic species for optical detection. The use of complexing agents for optical detection of metal ions is useful for specific CE applications, however there are limitations. It introduces the requirement for a range of complexing agents for each of the individual ionic species. Whilst surveying the literature on optical detection of the metal ions of interest to this project, some of the reported complexing agents were capable of complexing with a number of the ionic species [221]. However, a single complexing agent suitable for all of the metal ions was not found. Further investigation would be required to identify potential solutions. A further disadvantage of using complexing agents is that they will alter the redox potential; this would have consequences for the electrochemical detection which is discussed in Section 2.4.4.1.

One of the main drawbacks of LIF is that detection usually requires analytes to be marked with fluorophores. Aside from the obvious disadvantage (i.e. the requirement to use fluorophores), they tend to be 'bulky', therefore they can cause the analytes to exhibit similar mobilities [218]. This increases the difficulty of separating the analytes and consequently schemes such as longer separation channels may need to be employed. For this project it was desirable to minimise or remove the requirement for any sample pre-treatment. Since the metal ions of interest to the project do not naturally fluoresce, this made optical detection methods less appealing.

5.1.2. Electrochemical Detectors

There are three types of ECD schemes commonly used in CE that are applicable to miniaturised CE analysis. These are potentiometry, conductometry and amperometry. Put simply potentiometry is the measurement of potential for given current conditions, conductometry is the measurement of conductance and amperometry is the measurement of current at a given potential. Each of these detector schemes has various methods for implementation depending both on the application and the CE device.

A very simple method of incorporating an amperometric detection scheme is presented by Schwarz *et al.* [225] in which only two electrodes are required. In conventional amperometry, a potential is held, with respect to a reference electrode, and a current is measured between two electrodes – the counter and working electrode. To achieve results with only two electrodes, Schwarz *et al.* [225] used a working and an electrophoretic ground

electrode; the latter served as the counter and the reference electrode. The amperometric detection technique strongly relies on the redox characteristics of the analyte molecules, consequently it may not be suitable for all separation applications [173].

Both optical and electrochemical methods can be used for detection of a range of metal ions including those of interest to the project as listed in Table 1 [90]. For conductometric detection methods, the typical limits of detection are 10^{-4} – 10^{-8} mol L^{-1}, whereas for potentiometric detection, the range is 10^{-3} – 10^{-8} mol L^{-1} [90]. Amperometric detection was shown to be more sensitive than the other electrochemical and optical methods, with detection limits between 10^{-5} – 10^{-11} mol L^{-1} [90]. The primary requirement for the detection system in this work was to identify that when an ionic species had reached the detection window, and to inform the control system. As discussed in Section 2.4.4.1, following the separation enabled by the work in this thesis, the metal ions were to be analysed by electrochemical methods.

An improvement in the signal to noise ratio, which enables a lower limit of detection, can be gained by decreasing the electrode size; as the electrode size is reduced the electroactive species diffusion changes from planar to hemispherical diffusion. The result of this is an improvement in the collection efficiency at the surface of the electrode [226]. A disadvantage is that the magnitude of the current signal decreases and for accurate measurements electronic shielding may be required.

5.1.3. Detector Placement

Another consideration for the design of a detection system is the placement of the detector electrodes. There are three schemes regarding the placement of ECD electrodes which are commonly discussed [227]. The detector can be placed in-channel, off-channel, or at the end of the channel. Each position carries its own advantages and disadvantages, these are discussed below.

5.1.3.1. In-channel

As the name implies, with in-channel detection the detector electrodes are placed inside the channel and as a result are subjected to the electric-field across the channel. To make a measurement with an ECD system, the ECD system needs to be electrically separated from the potential applied to the fluidic channel. Therefore to make a measurement in the channel, a decoupler is often required. One common method of decoupling the system is to make a

path to ground immediately before the ECD system, using an electrode [74]. Some researchers have found ways to make measurements without requiring a decoupler. Martin *et al.* [74] developed a miniaturised electrically isolated potentiostat to make the measurements. This highly portable potentiostat is powered by a 9 V battery. When the ions pass the end of the channel they experience post-capillary broadening; in-channel detectors have the advantage that the measurement is taken before the ions experience this [89]. Commonly, amperometric methods are used with in-channel detection which requires careful selection of the electrode material; often noble metals are used. With continual use the surface of the working electrode will become fouled, affecting the detector performance. However, the lifetime of these electrodes, and subsequently the CE device, has been significantly increased by the incorporation of PAD [89]. The process of PAD combines amperometric detection with anodic cleaning and cathodic reactivation of the noble metal electrode surface. This ensures an electrode surface which is continuously self-cleaned and remains active [89].

Another method to overcome the problem of surface fouling, is described by Lin *et al.* [228]. They developed an in-channel ECD scheme where the electrode can be drawn out once the electrode becomes fouled. Moving the electrode a small amount ensures that a fresh electrode surface is available to be used by the detector. Once this surface becomes fouled, the electrode is drawn out a little more and the process is repeated until the electrode is fully removed. One drawback of this process compared with the PAD method is that it requires human interaction to move the electrode, unless a system for autonomously moving the electrode was employed.

An in-channel detection scheme is described by Coltro *et al.* [229], which has the electrodes placed on the channel, separated by a layer of insulation; CCD was used in this case. Whilst CCD is less sensitive than other methods, it has the advantage that there is no risk of electrode fouling. A further advantage is that there is inherent electrical isolation from the large separation electric-field.

5.1.3.2.End-channel

In this method the electrodes are placed outside the channel and therefore do not require decoupling from the high separation field. Wu *et al.* [227] claim that from their review of the literature, a majority elected to use end-channel amperometry as the detection mode for their CE devices. As well as the insulation from the separation voltage, it is easier to fabricate end-channel devices since there is no requirement to get an electrode into the very narrow

channels. Since the metal electrode is placed at the end of the channel care must be taken to ensure that it does not block the channel or upset the fluid flow. For accurate measurements, good electrode alignment is required which can often cause complexities with regards to positioning the electrodes. A similar method as used by Lin *et al.* to enable easy cleaning/replacement of the electrode surface was presented by Liu *et al.*[230]. Here a channel was created across the end of the separation channel, through which a metal wire electrode was placed (an illustration is shown in Figure 69). The electrode channel is an extra channel positioned outside of the separation channel which enables the electrode to be moved, exposing a fresh surface.

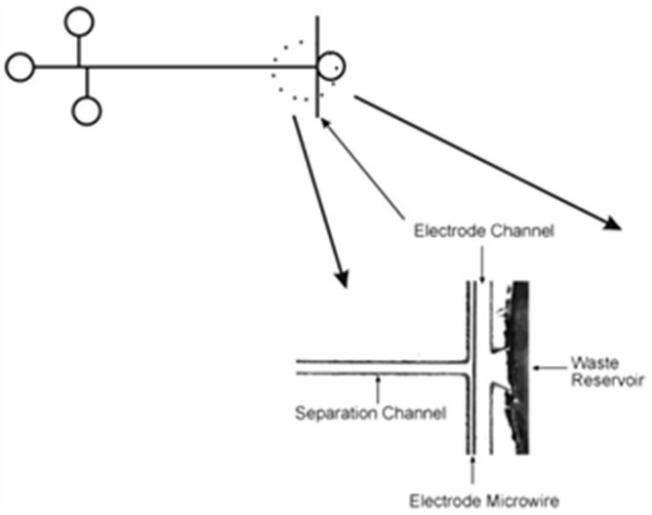

Figure 69: Schematic illustrating placement of the electrode alignment channel (taken from [230]).

5.1.3.3. Off-channel

Here the detection is conducted outside of the channel/capillary. With an off-channel EC detection scheme, isolation from the separation voltage is achieved by creating a current path to ground between the capillary/channel and the electrode. A common method to achieve this is to introduce a fracture into the separation capillary [218], though one problem which can occur from this is the generation of backpressure. A fracture is essentially a mechanically formed crack in the capillary. With capillaries it is possible to create a fracture by carefully mechanically stressing the capillary such that a crack (the fracture) is generated. The crack which will become filled with the conductive buffer solution provides an electrical current path from inside the capillary to the outside; the point at which the crack meets the outside of the capillary is grounded. Wallingford *et al.* [231] showed that providing the EOF is strong enough and that the length from the fracture to the detector is

kept minimal, then there is only a small loss of efficiency. Figure 70 shows an example of an off-column ECD system.

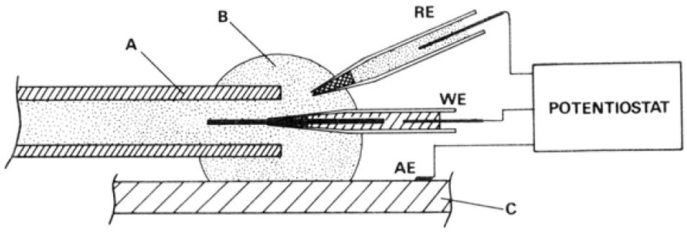

Figure 70: Example of an off-column ECD system. A: Fused silica capillary, B: Buffer solution, C: Stainless steel plate, RE: Reference electrode, WE: Working electrode, AE: Auxiliary electrode (taken from [231]).

5.1.4. Detector Design

Two detectors were required to demonstrate the separation enhancement routines described in this thesis. These detectors needed to be placed at either end of the channel to notify the control system when the ions reach the channel ends. Further to this, the detectors need to provide information on the amount of separation between the ions. The detectors discussed in this report have not been designed to identify the ions, but simply to detect their presence.

Theoretically it would be possible to identify the ions based on their electrophoretic mobility alone. The actual identification and quantification of the individual ionic species is not specifically required by this detection system due to the incorporation of thick-film metal ion sensors at a later stage in the device, as discussed in Section 2.4.4.1. The sample is analysed in greater detail following separation. These thick-film sensors were designed by Cranny *et al.* [10, 13]. The advantages of using these sensors over relying on timed electrophoretic methods are improved accuracy and reliability. This is especially important for the application specified by the project where the sample could be contaminated with numerous unknown ions. The sample would be from a corroding component/structure in an unknown environment.

To isolate the detection system from the separation electric-field and due to its suitability to miniaturisation combined with it ease of implementation, it was decided to design a CCD for the separation system.

5.1.4.1. Conductivity Detection: Theory of Operation

The basic principle of operation for conductivity detection systems is to place two electrodes with a varying voltage ($V_{\sim}$) across them into the solution being analysed and measure the current ($I_{\sim}$) through the electrodes. The cell constant (K) which has units of m^{-1} describes the relationship between the voltage and current. The value of the cell constant is related to the area of the electrodes and spacing between them. The relationship between, current, voltage, cell constant and conductivity (κ) is given by Equation (45).

$$I_{\sim} = \frac{V_{\sim}}{K} \times \kappa \tag{45}$$

Using Ohm's law this can be simplified to the expression shown in Equation (46).

$$\kappa = \frac{I_{\sim}}{V_{\sim}} \times K = \frac{K}{R_{SOL}} \tag{46}$$

Here, R_{SOL} denotes the resistance of the solution and is the reciprocal of the solution conductance.

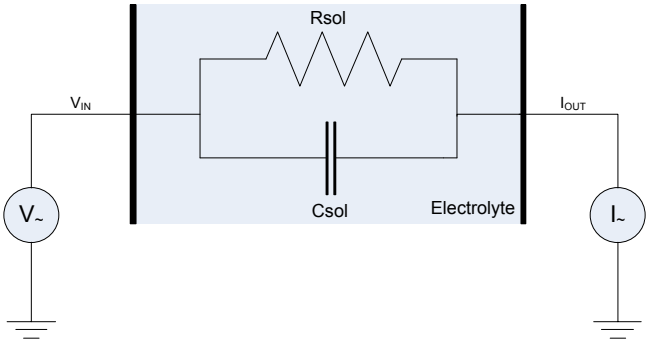

Figure 71: Simple model of two-electrode contact conductivity detection.

As the equivalent electrical model in Figure 71 depicts, the impedance of the electrolyte has both resistive and capacitive elements in parallel, the solution capacitance, C_{SOL}, accounts for the dielectric behaviour of the electrolyte. At high frequencies the capacitive term may dominate the detector behaviour; it can be calculated using Equation (47).

$$R_{SOL}.C_{SOL} = \frac{\varepsilon_0 \varepsilon_r}{\kappa} \tag{47}$$

The conductivity and R_{SOL} are related by the cell constant as shown in Equation (48).

$$\kappa = \frac{K}{R_{SOL}} \tag{48}$$

It is clear from Equation (48) that a large cell constant results in a greater response to a change in conductivity.

5.1.4.2.Four-Electrode Configuration

Above a simplified two electrode configuration has been described for a detector where the electrodes are in contact with the solution being measured. In the description the effect of the double layer on the electrode surface due to the difference in charge density between the electrode and electrolyte has been left out. For the detection system used in the experiments presented later, a four-electrode configuration was used. The signals in and out of the detector system and an electrical model of this can be seen in Figure 72.

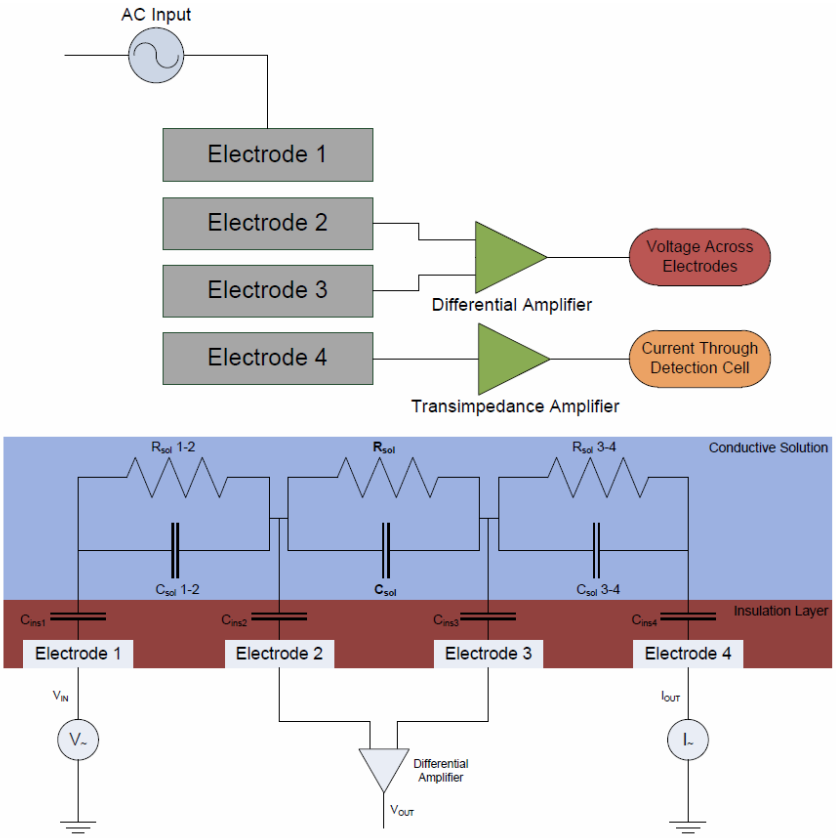

Figure 72: Four-electrode detection. Top: Illustration of input and output signals. Bottom: Electrical model.

One of the main advantages of the four-electrode configuration is that the output voltage is independent of the electrode insulation. The voltage dropped across R_{SOL} is measured using high-input impedance differential amplifiers; therefore almost no current passes through the insulation over electrodes 2 and 3. The voltage drop measured is therefore due almost entirely to the voltage dropped across R_{SOL}. The current through the detection cell is

measured by passing the current from electrode 4 through a transimpedance amplifier. The ratio of V_{OUT} to I_{OUT} gives us the resistance of R_{SOL}. The capacitors in parallel with the solution resistance also need to be considered, their influence will be frequency dependant.

5.2. Development of the CCD Electrical Model

The circuitry for the detection system was simulated using LT Spice IV. The model for the four-electrode configuration was simplified to exclude the solution capacitance in parallel with the solution resistance, following a model used by Laugere *et al.* [232]. This simplification is valid providing the solution is reasonably conductive. The electrical equivalent circuit model with and without parasitic capacitors can be seen in Figure 73. The four electrodes which feed into the detection circuitry are labelled det_1 to det_4. Typically for the dimensions used in CCD on planar devices the parasitic capacitances contribute a negligible effect and so can be excluded from the model. Since they made little difference to the computational time for the LT Spice IV simulations performed here, they were kept in the model. As well as giving a more accurate description of the system, they make the LT Spice IV model more flexible in the CCD configurations it can describe.

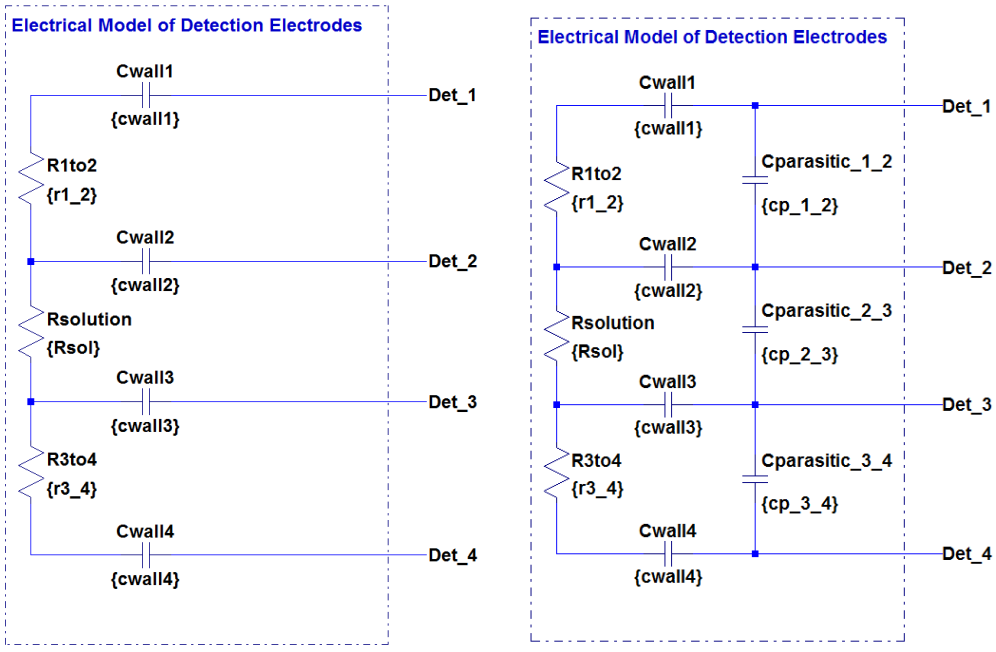

Figure 73: Equivalent circuit model of CCD: without parasitic capacitors (left), and with parasitic capacitors (right). The addition of the parasitic capacitors is an extension onto work by Laugere et al. [232].

An illustration of CCD electrode layout A, which was the design for the first of the two CCD electrode layouts used by the fabricated devices (Devices 2 and 3) discussed in Sections 6.7.2 and 6.8.2 respectively, is shown in Figure 74. During one redesign, discussed in Chapter 6, the layout of the CCD electrodes became smaller; this layout was used on Device 4, the fabrication of which is discussed later in Section 6.11.2. The main reason for this was to enable a larger area of the channel to be exposed to the ZPM electrode. The second design, layout B, is shown later in Figure 75. The layouts used by the prototype devices and the insulation thickness are summarised in Table 9. It should be noted that due to fabrication issues discussed later, the planned insulation thickness of the second prototype device was significantly larger. Further to this, the insulation thickness of the insulation layer for Device 4 was originally intended to be 1 μm, however due to issues regarding failure of the insulation layer this was increased to 5 μm; details on the failure are discussed later in Section 6.11.3. In this section, simulation results for the 5 μm insulation thickness are presented.

Table 9: Summary of the layouts used by the various prototype devices and their associated insulation thicknesses.

Device	CCD electrode layout	Insulation thickness (μm)
1	No detector	
2	A	1
3	A	1
4	B	1, 5

The values of wall insulation capacitance were calculated based on the wall thickness and material in contact with the detector electrode area using Equation (16).

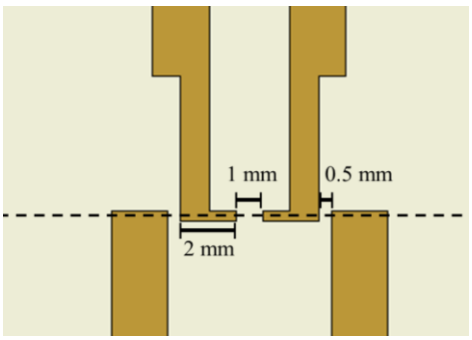

Figure 74: CCD electrode layout A: Layout of CCD electrodes. Channel represented by dashed line. Electrode dimensions: width = 2 mm; gap between outer and inner electrodes = 0.5 mm, and gap between inner electrodes = 1 mm.

Using the third prototype device as an example, the insulation material was SU-8 which has a relative permittivity of ~4.1 [233]. With an insulation thickness of 1 µm, an electrode width of 2 mm and a channel width of 300 µm, the wall capacitance for each electrode is 21.8 pF. As can be seen from Equation (49), as the value of capacitance increases the impedance (Z_c) decreases; a low value for impedance is desirable since it results in a larger voltage drop across the solution resistance ($R_{solution}$ in Figure 73). The change in voltage across $R_{solution}$ is monitored, a voltage increase suggests a decrease in resistance which in turn suggests an increase in conductivity. Such a detection event would arise for a group of metal ions passing the detector.

$$Z_C = \frac{1}{2\pi f C} \tag{49}$$

When the CCD electrode layout was changed from A to B, the result was that the electrode area was reduced. This smaller electrode area meant that the wall capacitance was reduced and consequently the impedance increased. Therefore the sensitivity of the detectors was decreased. For this work, the function of the detectors was simply to detect the presence of ions not to quantify them. As discussed earlier in Section 2.1, an ECD system designed by Cranny *et al.* was intended to be implemented into the system [13]. An illustration of the redesigned layout (layout B) for the CCD electrodes, used in the fourth prototype device, can be seen in Figure 75. The outer pair of electrodes is wider than the inner pair and therefore has a different capacitance. If the insulation thickness is 5 µm, using the dimensions given in Figure 75, the value for the capacitance is 1 pF for the outer electrodes and 0.44 pF for the inner electrodes.

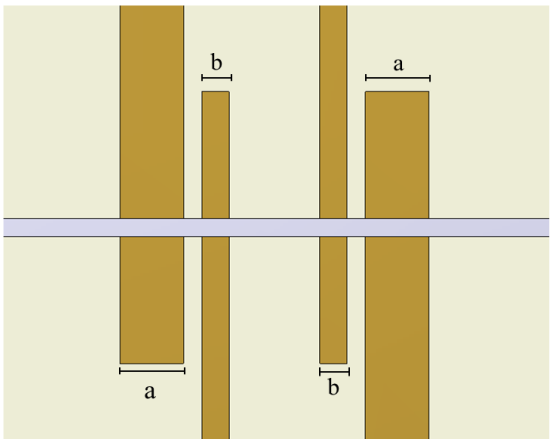

Figure 75: Schematic showing microfluidic channel over CCD electrodes for the fourth prototype design. Dimensions: a = 700 µm; b = 300 µm; channel width = 200 µm; gap between outer and inner electrodes = 200 µm; gap between inner electrodes = 1 mm. The range of overlap between electrodes (where the channel can be placed) is 3 mm.

The value of the parasitic capacitances depends on the distance between electrodes, the thickness of the electrodes and the length of the parasitic area. It can be seen in Figure 76 that there are three areas between the four electrodes where parasitic capacitances may occur.

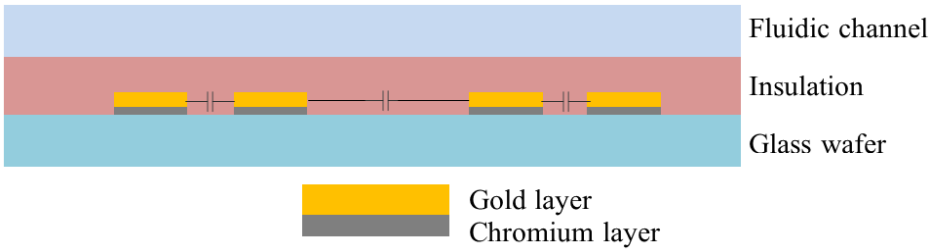

Figure 76: Cross-section of the device along the channel length illustrating the potential for parasitic capacitances between electrodes.

For CCD electrode layout A, the gap between the outer and inner electrodes, and between the inner electrodes was 0.5 mm and 1 mm respectively, as shown in Figure 74. The thickness of the Cu layer on the PCB used for the second prototype device was 35 µm. For the third prototype device, the thickness of the Cr and Au layers were 20 nm and 200 nm respectively. The fourth prototype device had a gap of 0.2 mm between outer and inner electrodes; the distance between the inner electrodes was the same as for the earlier prototypes, 1 mm. Later the thickness of the Au layer was reduced to 100 nm for the fourth prototype device. A summary of the wall and parasitic capacitances for all the prototype devices can be seen in Table 10; the values of parasitic capacitances are significantly lower than the wall capacitances.

Table 10: Summary of wall and parasitic capacitances for prototype devices.

Device	Wall outer electrodes	Wall inner electrodes	Parasitic outer-inner electrodes	Parasitic inner electrodes
1	No detector			
2	21.8 pF	21.8 pF	0.76 fF	0.381 fF
3	21.8 pF	21.8 pF	5.2 aF	2.6 aF
4	1 pF	0.44 pF	76 aF	1.5 aF

Using Equation (50), the resistance of the solution can be calculated provided the resistivity, ρ_{SOL}, of the buffer solution and the channel dimensions are known. L denotes length and A denotes the cross-sectional area.

$$R_{SOL} = \frac{\rho_{SOL} L}{A} \tag{50}$$

The resistivity will decrease as a group of metal ions pass the detector and will cause the resistance at that point in the channel to decrease, this will be reflected as a decrease in voltage across that part of the channel. This decrease in voltage is measured by a differential amplifier, the circuit for which is shown in Figure 77.

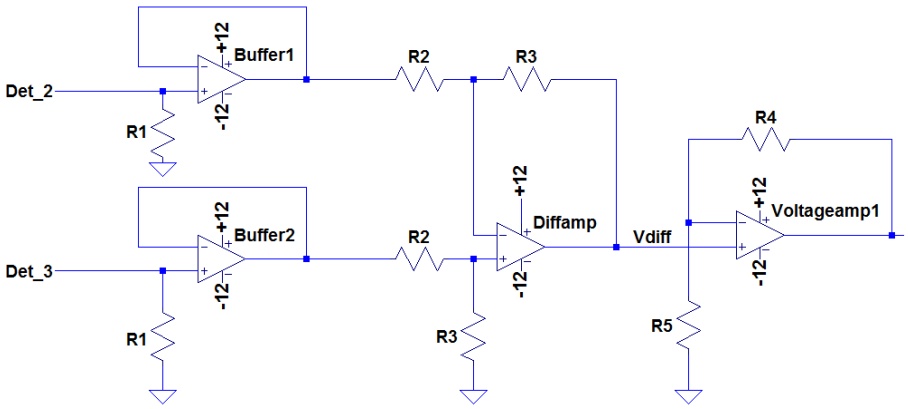

Figure 77: Circuitry for differential amplifier, Det_2 and Det_3 represent the inner pair of electrodes.

The inner electrodes are connected to points labelled Det_2 and Det_3 on the circuit in Figure 73. They are both independently connected unity gain buffers. The buffers have high input impedance and low output impedance. Therefore negligible current is drawn from the electrodes and thus they are used to prevent the detection circuitry affecting the measurement. Following the buffering stage, the difference between the two signals is amplified by the differential amplifier. In case further amplification was required a non-inverting voltage amplifier was included following the differential amplifier stage. The gain, G, of the amplifier is given by Equation (51) where $R_{feedback}$ and R_{ground} are the resistances of the feedback and ground resistors.

$$G = 1 + \frac{R_{feedback}}{R_{ground}} \tag{51}$$

As well as a decrease in voltage, because the resistivity of the fluid in channel is reduced around the detector electrode, the current through the detection cell will increase as a group of ions pass. This increase is current is measured by the transimpedance amplifier circuit shown in Figure 78.

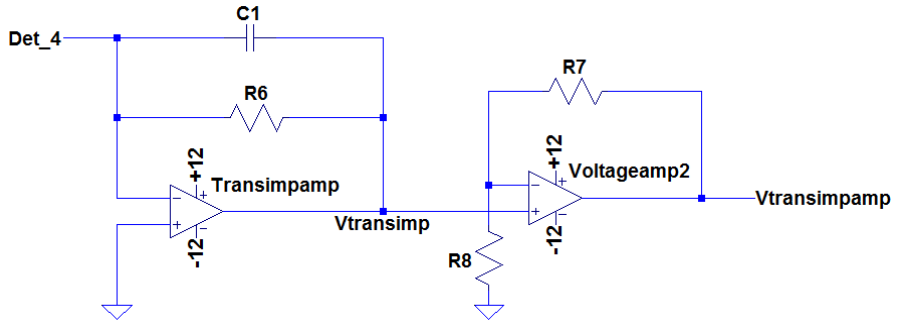

Figure 78: Circuitry for transimpedance amplifier, Det_4 represents one of the outer electrodes.

The virtual earth theorem states that the inverting input to the transimpedance operational amplifier will effectively be at zero volts because the non-inverting input is tied at ground. Assuming that the input impedance to the operational amplifier is sufficiently high, all the current from the detection cell passes through the feedback resistor (R6) of the transimpedance amplifier. The voltage at the output will be the product of the current and feedback resistor. A non-inverting voltage amplifier follows the transimpedance amplifier to provide additional amplification as was the case for the differential amplifier.

5.2.1. Simulating the CCD Circuitry

Assuming a value for resistivity of the buffer solution of 10 Ω m (this corresponds to a conductivity of 0.1 S m^{-1}) the frequency response of the equivalent electrical circuits for the three prototype electrode layouts was calculated; these can be seen in Figure 79, Figure 80 and Figure 81. The detector circuitry remained the same; the changes between devices consisted of electrode size, shape, spacing and insulation thickness.

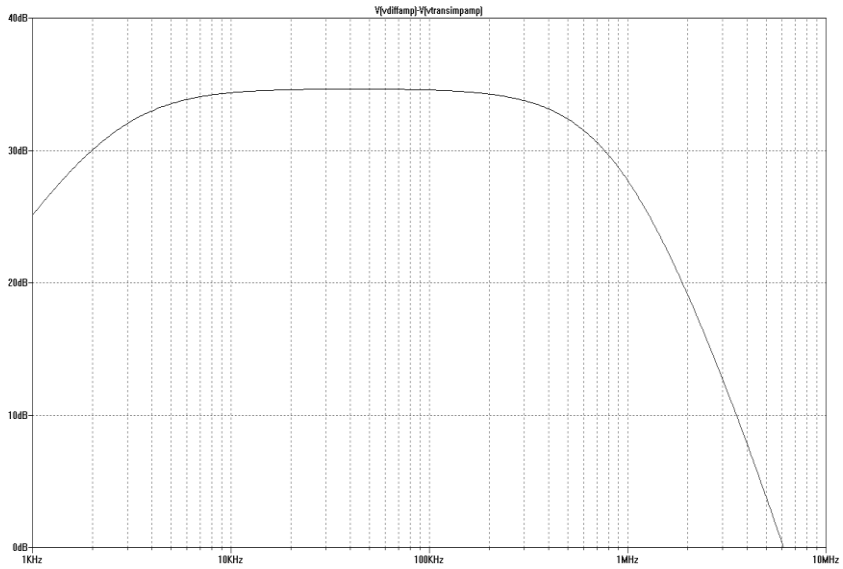

Figure 79: Frequency response of CCD layout for second prototype device, (assuming solution conductivity of 0.1 S m^{-1}).

The frequency response for the second and third prototype devices is similar. This is because the electrodes layout was the same, the only differences between the devices was that the third had a slightly shallower channel and thinner electrodes. The second prototype device, designed on a PCB had electrodes with a thickness of 35 μm, which were thicker than the third prototype device which had electrodes of 240 nm thickness. In the model only this thickness influenced the size of the parasitic capacitances. For the dimensions used the parasitic capacitances, as expected, showed no noticeable effect.

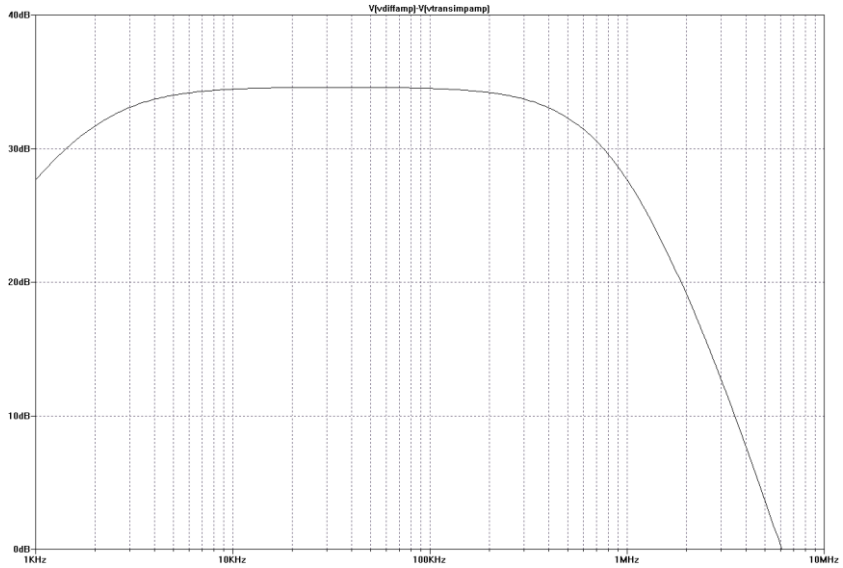

Figure 80: Frequency response of CCD layout for third prototype device, (assuming solution conductivity of 0.1 S m^{-1}).

The frequency responses shown in Figure 79 and Figure 80 show a large flat band for linear operation ranging from about 10 kHz to 200 kHz. The detection system was operated at 10 kHz. An operating frequency of 10 kHz was chosen since it was the lowest frequency which was in the flat band of the frequency response. The passing of an ionic species through the detection window modifies the impedance of the channel (i.e. the values of resistance and capacitance in the conductive solution, as shown in the bottom illustration in Figure 72). This in turn affects the frequency response, by moving the cut-off frequency. For the initial testing with the detection system this was desirable to operate in the flat band of the frequency response since in this region the system behaves in a linear fashion, and would be less affected by changes in the solution impedance. This was important in the earlier prototype systems to help minimise the unknowns. Further to this, the original data acquisition system (NI DAQmx 6016) could sample at a maximum of 200 kHz. Later, another data acquisition system (NI USB-6251) with a better specification which was capable of sampling at 1.25 MHz was purchased. This sampling frequency was spread across all of the monitored channels. Each detector on the chip required the use of two channels; one for the differential amplifier and the other for the transimpedance amplifier. The larger the sampling frequency is, compared to the signal frequency, the more accurately the data can be captured. With two channels in use, the two individual 10 kHz signals could be sampled at 100 kHz each. This translates as 10 points to represent and reconstruct a sinusoidal wave. For full functionality and system control, two detectors would be required at either end of the channel. Therefore, the 200 kHz would eventually need to be spread across 4 channels, further reducing the sampling resolution. To monitor the CCDs a LabView program was developed, details on this are given in Appendix D.

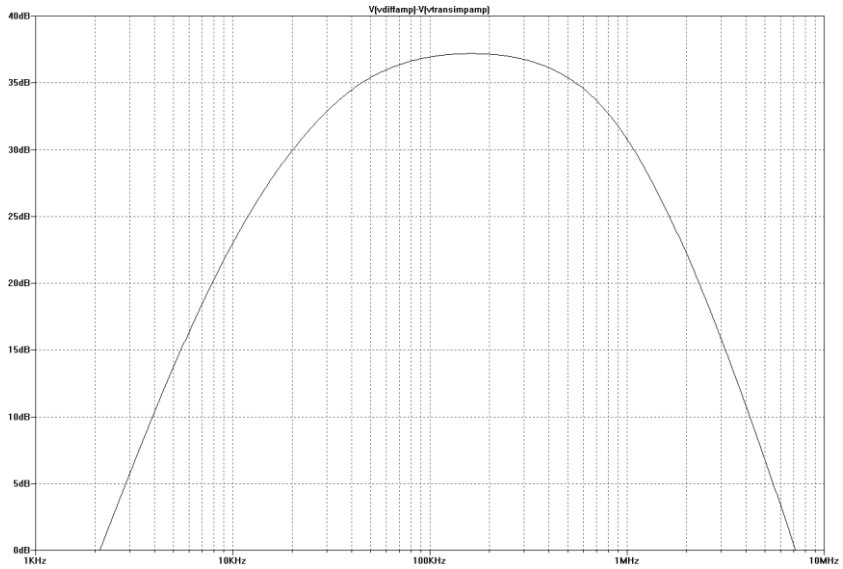

Figure 81: Frequency response of CCD electrode layout as for fourth prototype device, (assuming solution conductivity of 0.1 S m^{-1}).

The flat band for the detector circuitry using the fourth prototype device with electrode layout B ranges from 100 kHz to 200 kHz, shown in Figure 81. The function of the detector is to identify that there is a group of ions passing the detector. Since the change of resistivity also changes the frequency response, it is possible to operate the detector at a frequency outside the flat band, if required. Figure 82 shows the effect that the increasing resistivity has on the cornering frequency for the response of the detector cell. The effect of increasing the resistivity, is that the voltage seen by the differential amplifier increases. If the detector is operated at a frequency below 1 MHz it can be seen that the increase in resistivity will also cause the gain to increase thereby making the differential amplifier system more sensitive. Essentially this enables a trade-off between linearity and sensitivity.

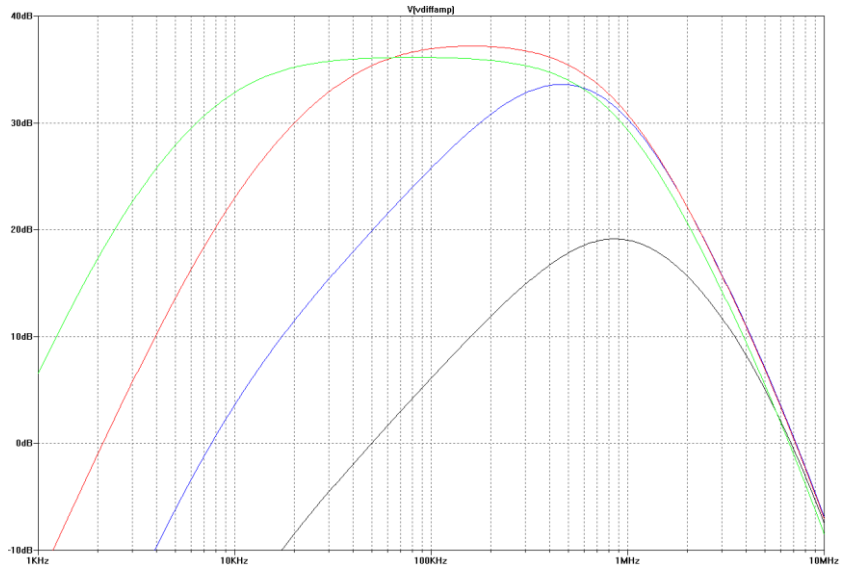

Figure 82: Frequency response of differential amplifier part of the CCD with electrode layout as for fourth prototype device illustrating effect of changes in solution resistivity. Values of solution resistivity: black = 0.1 Ω m; blue = 1 Ω m; red = 10 Ω m; green = 100 Ω m.

For the transimpedance amplifier however, an increase in solution resistivity causes a decrease in current and consequently the measured voltage. The frequency response of the transimpedance amplifier in Figure 83 shows that for certain frequencies the gain also drops with an increase in solution resistivity, this further improves the sensitivity. The gain drop at the higher frequencies is attributed to the transimpedance amplifier, whereas at the lower frequencies, the change in gain is also due to the change of time constant in the equivalent electrical model. With the detector operating at 10 kHz, the response should be linear for resistance changes from 0.1 Ω to 10 Ω.

To simulate the effect of a change in solution resistivity on the detector response where the detection system was operated at 10 kHz, a transient analysis of the models was performed. A summary of the resulting changes in RMS for the three simulated devices is given in Table 11

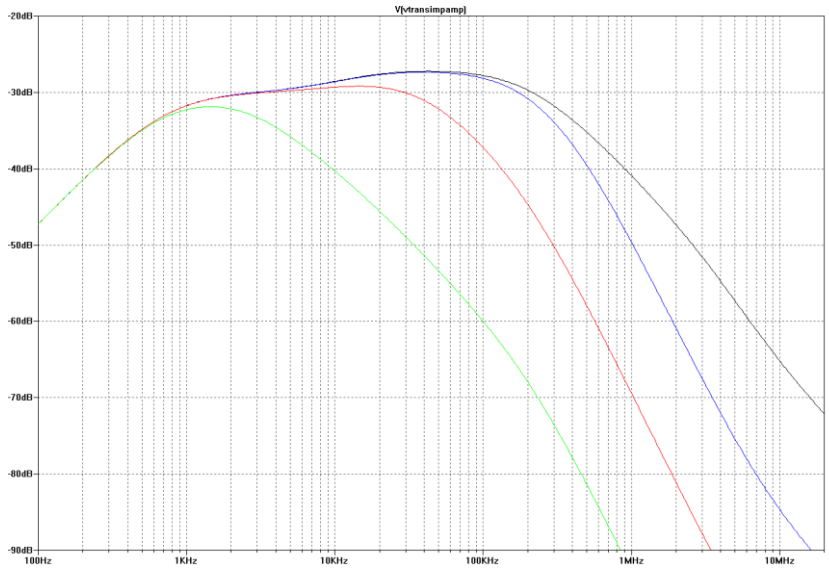

Figure 83: Frequency response of transimpedance amplifier part of the CCD with electrode layout as for fourth prototype device illustrating effect of changes in solution resistivity. Values of solution resistivity: black = 0.1 Ω m; blue = 1 Ω m; red = 10 Ω m; green = 100 Ω m.

As the resistivity increases from 1 Ω m to 10 Ω m, the RMS of the response increases from 1.230 V to 3.338 V. For the transimpedance amplifier for the second device, the RMS voltage drops from 0.636 V to 0.168 V as the resistivity increases from 1 Ω m to 10 Ω m.

A similar set of simulations were run for the third device which had the same electrode layout as the second device. The main differences were that the third device had a shallower fluidic channel, which lowered the channel resistance, and a reduced electrode thickness, which further reduced the parasitic capacitances. For a change in solution resistivity from 1 Ω m to 10 Ω m, the RMS voltage of the responses for the differential amplifier and the transimpedance amplifier, change from 1.652 V to 3.373 V, and from 0.597 V to 0.117 V respectively.

The fourth device used CCD electrode layout B and therefore had smaller electrode areas. Further to this it should be noted that the channel width was reduced to 200 µm. Both of which had the effect of reducing the wall capacitance and therefore increasing the impedance. The larger impedance reduced the detector current through the detection cell. This consequently reduced the signal measured by the transimpedance amplifier. The issue was further exacerbated with the increase in insulation layer thickness from the originally planned 1 µm to 5 µm. The simulation of the detection system for the fourth prototype device, shown here, shows the case for the larger insulation layer to reflect the true expected behaviour of the system. The RMS voltages of the responses for the differential amplifier

and transimpedance amplifier change from 0.097 V to 0.904 V and from 0.026 V to 0.024 V respectively for a change in solution resistivity from 1 Ω m to 10 Ω m. The effect of the thicker insulation layer severely reduces the sensitivity of the transimpedance amplifier's contribution to the detector response. However the combined responses of the differential and transimpedance amplifiers are suitable for the requirements imposed by the prototype system. It should also be noted that the amplitude of the input voltage all these simulations was set at 1 V. This voltage could be increased during the practical experiments if greater sensitivity was required.

Table 11: Summary of simulated values for change in RMS for the differential and transimpedance amplifiers for a change in solution resistivity.

	RMS response of differential amplifier (V)		**RMS response of transimpedance amplifier (V)**	
Solution resistivity:	1 Ω m	10 Ω m	1 Ω m	10 Ω m
Device 2	1.230	3.338	0.636	0.168
Device 3	1.652	3.373	0.597	0.117
Device 4	0.097	0.904	0.026	0.024

Following simulations the detection circuit was built on prototype board and briefly tested to verify it worked. Following this, a PCB was designed which would both make the detection system more mechanically robust and was in preparation for the fully miniaturised system. A photograph of the PCB detection circuitry is given in Figure 84.

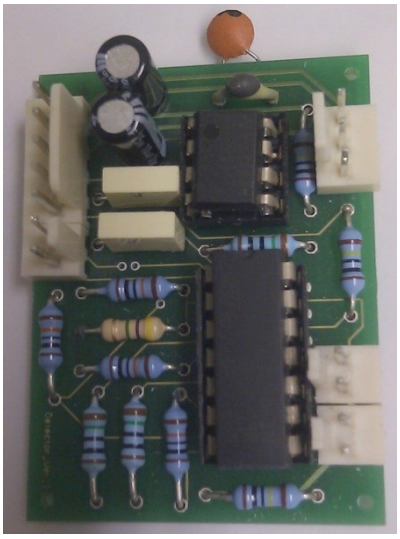

Figure 84: Photograph of assembled PCB developed for the detection system.

5.3. Conclusions

For the demonstration of the separation enhancement methods a detection system was required. After investigating the advantages and disadvantages of numerous detection systems, it was decided that a four-electrode CCD system would be appropriate. Before building, the electronic circuitry for the CCD system was modelled in LT Spice. An equivalent electrical circuit of the detection cell was interfaced to the model to describe the behaviour of the detection system for changes in conductivity.

Before the fabrication of the microfluidic devices which incorporated the detection system (devices 2, 3 and 4), the planned electrode layouts were simulated. This simulation gave verification that they should perform as required. The fabrication of the microfluidic devices is described in detail in Chapter 6. The size/layout of the electrodes and thicknesses of the insulation layer for the fabricated devices were discussed in Section 5.2. For device 2 and 3, whilst the electrode layout was the same, the decrease in electrode thickness, from device 2 to 3, reduced the parasitic capacitance. For device 4, it was desirable to reduce the electrode area; the simulation revealed the effect of this and verified that whilst the performance of the detection system would decrease, it would remain fit for purpose.

The detection system was simulated for a range of conditions relating to the prototype devices. The simulations showed that a four electrode CCD system was sensitive enough to detect the levels of conductivity changes that would be seen in the experiments on the prototype devices. The design of these prototype devices and the consequences of fabrication issues are described in the next chapter. The detrimental effect of the compromises taken due to fabrication issues on the sensitivity of the detection system was also investigated. It was shown that even with the undesirable thicker insulation layer that the detection system would be capable of detecting the expected changes in conductivity.

Chapter 6

Experimental Work and Device Fabrication

6.1. Introduction

During the course of this research a range of experiments were conducted. Many of these required the fabrication of microfluidic devices, and over the course of this research a total of four microfluidic devices were constructed. These were fabricated in parallel with the development of the computational models, described earlier in Chapter 4. The experiments described in this chapter both aided the development of the computational model and evaluated whether certain design aspects, such as the detection system, were fit for purpose. A summary of the aims of the various experiments performed on a laboratory based CE instrument and the fabricated devices is given in Table 12.

This chapter starts with an overview of material considerations and typical fabrication methods for miniaturised CE systems. This is followed by a description of each of the experiments described in Table 12, establishing their reason, and thus their design. Most of the experiments required a fluidic device and the design of such devices is described.

Table 12: Summary of the aims for the experiments performed.

Experiment number	Aims
1	Characterise electrophoretic dyes. • Measure and compare the apparent electrophoretic mobility for fluorescein and eosine dyes with values reported in the literature.
2	Confirm ability to move ionic species along a microfluidic channel using an electric-field under conditions similar to those reported in literature [128-131, 234]. Evaluate the suitability of chosen channel materials, dimensions and fabrication methods.
3	Setup and test of experimental control systems: • detectors, • micro-pump-based fluidic control system, • high voltage power supplies.
4	Characterise ability to modify EOF with a planar ZPM electrode.
5	Evaluate performance of detection system.
6	Demonstrate separation and detection of low concentration of metal ion sample (e.g. $CuCl_2$).
7	Evaluate performance of detection system with reduced electrode area and demonstrate ability to enhance separation of metal ions using: • matched EOF separation enhancement method (as described in Section 2.4.2), • switched EOF separation method (as described in Section 2.4.3).

6.2. Discussion on Material Considerations for Microfluidic CE Devices

There are a wide range of materials which have been discussed in the literature for use in miniaturised CE systems [235, 236]. Silicon has been the material of preference for substrates for electronic microchips for many years. Using current state-of-the-art technology, transistors are routinely fabricated on silicon wafers with micro-fabrication technology capable of creating line widths of the order of nm [237]. As such, the technology has received a substantial amount of interest and funding over many decades and still continues to advance to smaller feature sizes. The methods to fabricate and process microstructures on silicon have been developed to a high calibre [236]. The dimensions used with microfluidic devices are typically orders of magnitude larger than those used at the forefront of micro-fabrication technology and as a result the processes are well understood [237]. On silicon wafers, numerous devices can be produced with almost identical mechanical, electrical, optical and chemical characteristics [238]. Whilst they require

specialist and expensive tools, machines and equipment, it is now relatively simple to create a microfluidic device in glass or silicon using these well-established methods [239].

As well as being a desirable material for microfluidic systems, glass has been used in biological and chemical experimental apparatus for many years [240, 241]. It has good stability and is highly non-reactive to a large variety of chemicals, such as strong acids and bases, and alcohols. A further advantage is that it is optically transparent which allows the use of optical detection systems [24]. Glass has good electrical insulating properties and this is another reason that it is often the material of choice for miniaturised CE applications. Standard CE machines commonly use a fused silica capillary; a significant amount of research has been done using these and as a result there is a plethora of information available on fused silica capillaries [32, 79]. Fused silica capillaries are often coated (externally), usually with polyimide, to improve their mechanical robustness [46].

Aside from silicon and glass, a vast range of polymer materials have been investigated in the literature for microchip CE fabrication [212]. A list of polymers commonly used include: PDMS; PMMA; PEEK; polystyrene; COC or COP (cyclic olefin polymer), and polycarbonate [85, 123, 148, 236, 242]. Polymers have gained increasing popularity for a number of reasons; primarily their flexibility in terms of fabrication and their low cost. Further advantages are that they tend to be relatively robust and some have medium to high chemical resistance to a large range of chemicals [242].

PDMS is a flexible polymer and due to its low surface free energy it behaves in a hydrophobic manner without any surface treatments [85]. PDMS is commonly employed for rapid prototyping of devices [236]. The Sylgard™ 184 kit can be used for creating PDMS; it contains the PDMS elastomer and a curing agent which are mixed 10:1 respectively. The mixing usually introduces bubbles into the viscous polymer which must be removed before curing. Removal of the bubbles can be achieved by placing the mixture into a vacuum desiccator [243]. Once bubble-free the polymer is poured into a mould and cured. The curing process takes 24 hours if left at room temperature, but can be reduced to just 10 minutes by elevating the temperature to 150 ˚C [244]. Contamination can be a problem for PDMS, since samples tend to adsorb to the channel surface and can be difficult to remove [245]. This has meant that PDMS is often viewed as a material for prototypes and disposable instruments.

COC has shown excellent chemical resistance to a range of acids and bases, as well as alcohols and polar solvents, though it can be attacked by non-polar organic solvents, for example hexane or toluene [242]. Whilst PMMA, polycarbonate and polystyrene do not exhibit such strong chemical resistance they are still useful for miniaturised CE chips as a

more economical choice. For most applications, the sample and buffer solution will not be highly aggressive and will not adversely react with the polymer microfluidic devices. Provided the contamination caused by the sample can be reliably removed without the need for aggressive chemicals, then the chemical resistance is less of an issue. An advantage of a material with good chemical resistance is that aggressive chemicals can be used to clean the channels, thus ensuring the device is reliably cleaned before every run.

The zeta-potential will vary depending on a number of factors, including: the channel material, buffer solution, fabrication method, and wall coatings [43, 88]. Wang *et al.* presented their EOF measurements for a range of polymers fabricated using various methods [212]. They presented a table of EOF mobility values for a range of buffer solutions/micro-channel substrates. The table can only be used to give a feel for the EOF behaviour for given buffer solutions and micro-channel combinations due to the complex nature of EOF. To accurately depict the effect on the EOF, the table should have also considered buffer pH and buffer concentration. Further to this the cleaning or preparation regime can have a significant effect of the EOF and therefore should be noted.

6.3. Typical Fabrication Methods for Microfluidic CE Devices

Fabrication can introduce numerous difficulties resulting in both material and labour costs. Further to this, many of the fabrication methods require specialist equipment and cleanroom facilities. To avoid these issues some researchers buy their microfluidic devices from specialist companies. Pittman *et al.* [163] purchased their microfluidic device from Micralyne; it was fabricated in Borofloat glass and consisted of a 85 mm channel with a cross-sectional width of 50 μm and depth of 20 μm. Micralyne Inc. supply micro-machined silicon and glass chips, they typically either use a deep-reactive ion etching (DRIE) process or a wet etch (such as KOH) [246]; more information on these methods is given later in Section 6.3.2.

The end application strongly dictates the methods employed for the fabrication of microfluidic devices. For example, an autonomous in-situ device requires minimal user interaction and therefore the use of interchangeable disposable microfluidic channels is undesirable. In point-of-care devices, where a user is present, the replacement of microfluidic channels is only a minor inconvenience; further to this, the risk of cross-contamination of samples can be eliminated. In medical applications for example, cross-contamination of samples is unacceptable. For the corrosion monitoring application outlined

earlier in Chapter 2, there is a desire for an autonomous in-situ device. The requirements of an autonomous in-situ device mean that minimum maintenance is important and therefore regular microfluidic channel replacement is unsuitable. Earlier in Section 2.1 it was shown that reasonably large concentrations of metal ions were expected and therefore it was not expected that the error produced due to surface contamination would be significant. Therefore flushing the channel with buffer solution prior to each experimental run should be adequate [247, 248]. Further to this, the closed-loop control system would be resilient to the variation in EOF caused by any surface contamination.

The fabrication methods directly affect the end device performance and behaviour since each method renders different channel surfaces or topographies. The EOF is related to the quality and resulting chemistry of the channel surface. Pugmire *et al*. investigated the effect of different gas phases during a laser-ablation fabrication process [138]. Amino, hydroxyl, carboxylic and phenolic functional groups could be generated on the channel surface by the use of oxygen or nitrogen. As well as highlighting that the fabrication process is important, this showed that it is possible to modify the natural zeta-potential during the fabrication. One example of the EOF dependence on fabrication method for a PMMA substrate was shown by Wang *et al.* The EOF mobility was ~2.2 x 10^{-8} m^2 V^{-1} s^{-1} when the substrate was processed with a laser cutting technique but 50 % larger at ~3.3 x 10^{-8} m^2 V^{-1} s^{-1} when a hot embossing technique was used.

6.3.1. Moulding

Moulding is a fabrication technique suited to a wide range of polymers [226]. It has become highly popular for the fabrication of PDMS-based microfluidic devices [249, 250]. There are numerous variations on the methods used but essentially a master is created in a harder material over which the PDMS is poured and set. The master defines the structure of the microfluidic device. A recent review on various techniques for rapid prototyping was discussed by Sollier *et al.* [251].

A common method of moulding microfluidic channels in PDMS is to create a mould from a photoresist, such as SU-8, on a glass wafer [252-254]. The thickness of the layer of photoresist determines the thickness of the mould and therefore the channel depth. SU-8 is a negative photoresist. Negative and positive photoresists results in different profiles, an illustration of this is shown in Figure 85. The profile takes this shape due to the diffraction of UV light in the gap between the mask and the photoresist. Therefore the resulting profile of an SU-8 resist may exhibit curved sidewalls as shown in (b) of Figure 85.

Figure 85: Illustration showing different in resulting profiles for (a) positive and (b) negative photoresists, (image modified from: [255]).

In Figure 86 an illustration of the fabrication steps for the creation of a SU-8 mould and the moulding process is given. First a wafer (for example: glass or silicon) is cleaned to remove any surface contamination. A photoresist layer is spun onto the wafer; the spin speed determines the layer thickness and therefore the channel height. The photoresist is soft baked to remove the solvents in the photoresist and then exposed to a UV source via a mask which defines the mould pattern. SU-8 is a negative photoresist and so the areas not exposed to UV will get removed by the development process. After exposure to UV the SU-8 is hard-baked for a few minutes, depending on layer thickness. Following development, the mould is prepared, though a second hard-bake process is recommended, this helps ensure all the solvent is removed from the SU-8. The resulting SU-8 layer will be more mechanically and chemically robust [256]. On top of this SU-8 mould, the polymer, (for example PDMS) is poured and cured. Once cured it is removed from the mould, the result being a polymer containing a moulded open channel, which needs to be closed for use. In the case of PDMS, its elastomeric nature allows it to be reversibly bonded to a number of substrates provided the surfaces are suitably flat. If a permanent bond is required, this can be achieved using an oxygen plasma to active the silanol groups on the PDMS surface, following which the PDMS piece can be directly bonded to PDMS or glass [247].

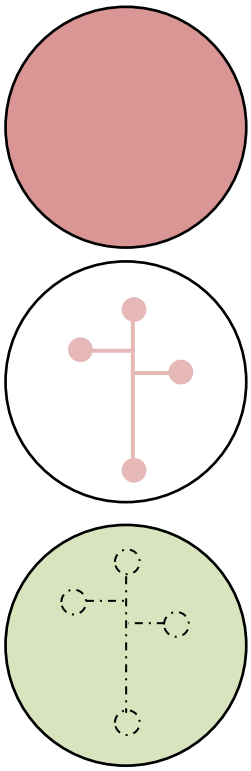

Spin a thick photoresist onto a clean wafer. Thickness determines channel depth.

For example, SU-8 onto a glass wafer.

Cure the photoresist and expose to UV via a mask and develop.

This will result in the master wafer.

Pour on polymer and then cure.

Remove polymer substrate from master wafer.

Figure 86: Process for creating a photoresist mould and open-channel device. Following this process, the device needs to be sealed to a flat substrate to close the channels.

A variation on this moulding technique is injection moulding. This is another relatively simple method for the rapid mass production of 3D microstructures of various geometries [251, 257]. In Figure 87 it can be seen that the mould is created by placing a former (which defines the channel pattern) inside a chamber. The device material is then injected into the mould at pressure and at an elevated temperature. The injected material, which is usually a polymer, cures as the temperature slowly cools, taking the shape of the mould. Injection moulding is suitable for a wide range of polymers and unlike many other fabrication methods is more applicable for large-scale fabrication requirements [242].

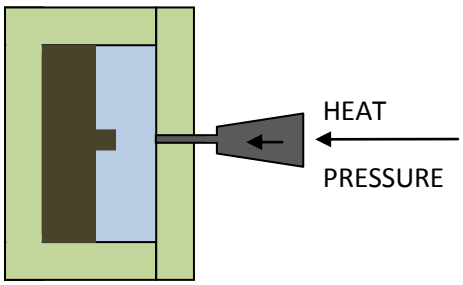

Figure 87: Cross-section illustration of injection moulding. The brown region represents the former and the blue represents the injected polymer.

A similar method to moulding is hot embossing, a process in which a pattern is stamped into a polymer substrate. Here the temperature of the substrate is raised above its glass transition temperature and pressed into a hard mould. Mühlberger *et al.* used a hot embossing technique with multiple polymers, focussing on PMMA and PEEK [148]. Their aim was rapid development of new polymer materials for the development of a label-free method for analyte detection in micro-channels. The latter was achieved by using an ECD system. The devices they fabricated had cross-sectional areas (width x height) of 50 µm x 50 µm.

A double-sided PCB was used as a mould by Harris *et al.* who sandwiched it between two pieces of PMMA at a temperature of 125 ˚C using a force of ~15000 N [258]. This yielded two open channels which were brought together and sealed using solvent bonding.

6.3.2. Micromachining

The term micromachining is rather broad but here it is used refer to microfabrication techniques such as lithography and etching. Some of the other methods described here use multiple fabrication technique, but at the expense of increased fabrication complexity.

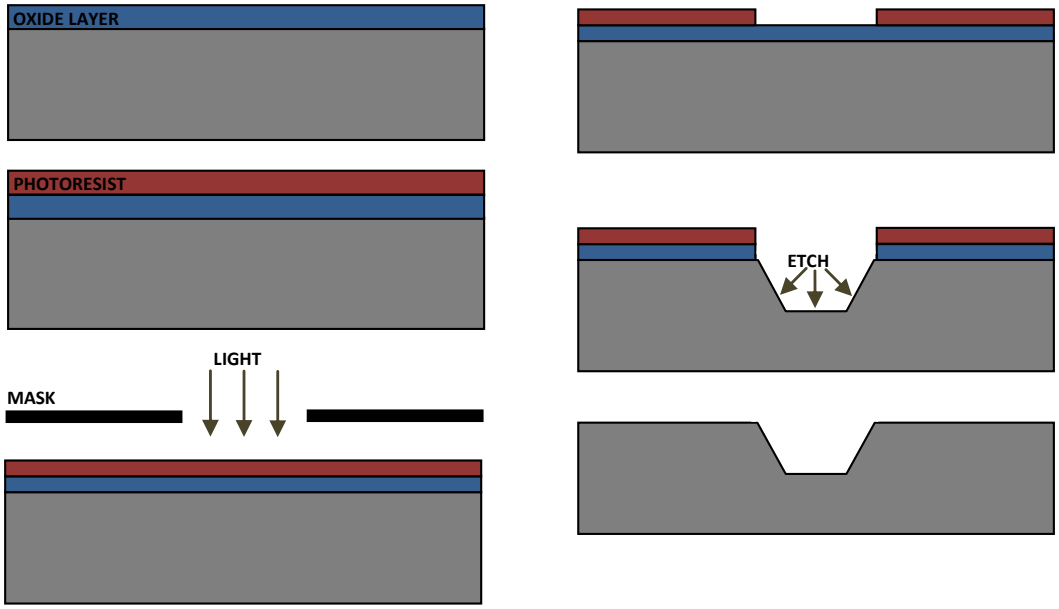

Figure 88: Simplified micromachining method for creating a channel in silicon (based on a figure in [259]).

Campana *et al.* stated that micromachining is defined as the "sculpturing" of silicon (and silicon-compatible materials), for the production of devices which have no direct electrical function [259]. This is true of chip-based CE devices whereby the creation of a micro-

channel is required as a structure on which electrophoretic separations are performed. Typical processing steps for creating a channel by micromachining are shown in Figure 88.

Depending on the type of etch performed, different cross-sectional profiles will be produced. For example an isotropic etch of silicon can be achieved using a mixture of hydrofluoric, nitric and acetic acid [239]. In the etch reaction the nitric acid oxidises the silicon which can then be etched by the hydrofluoric acid. Typically etch rates are between 0.1 and 100 μm min^{-1}; the etch rate is controlled by varying the ratio of the acids [239]. The result of a wet isotropic etch is shown in Figure 89. If the etchant is potassium hydroxide, the etch rate is heavily dependent on the orientation of the silicon. For example, the {100} planes are etched 100 times faster than the {111} planes and the {110} planes are etched about twice the rate of {100}planes [260]. The significant difference in etch rates can be exploited to enable the fabrication of V-shaped grooves as illustrated in Figure 89.

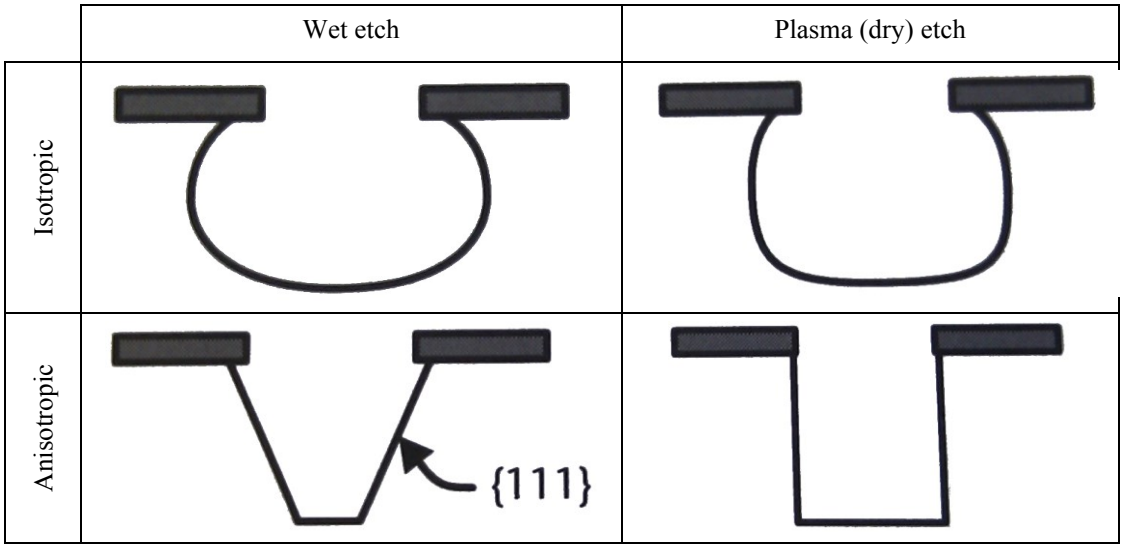

Figure 89: Illustration showing cross-sections of trench profiles for four different types of etch method, (image modified from [239]).

In plasma etching, chemically reactive neutrals and ions are generated and accelerated toward the substrate. If the etch process is enabled by ion bombardment rather than just a chemical reaction the process is referred to as reactive ion etching [239]. The density of ions and effect of the ion bombardment can be increased through the use of RF electromagnetic fields; this is referred to as inductively coupled plasma reactive ion etching. Deep reactive ion etching enables the fabrication of high-aspect-ratio trenches with almost vertical sidewalls. An extension to this method, known as the Bosch process operates by repeatedly switching between an etch cycle and a deposition cycle [239]. An illustration of this method is shown in Figure 90. During the etch cycle SF_6 is used to etch through the silicon. During

the deposition cycle a polymer is deposited all over the silicon. During the next etch cycle, the polymer exposed directly to the plasma is quickly removed, following which the silicon etch continues. The polymer on the sidewalls is etched at a lower rate and so protects the sidewalls from being attacked, thus rendering an almost vertical sidewall [239].

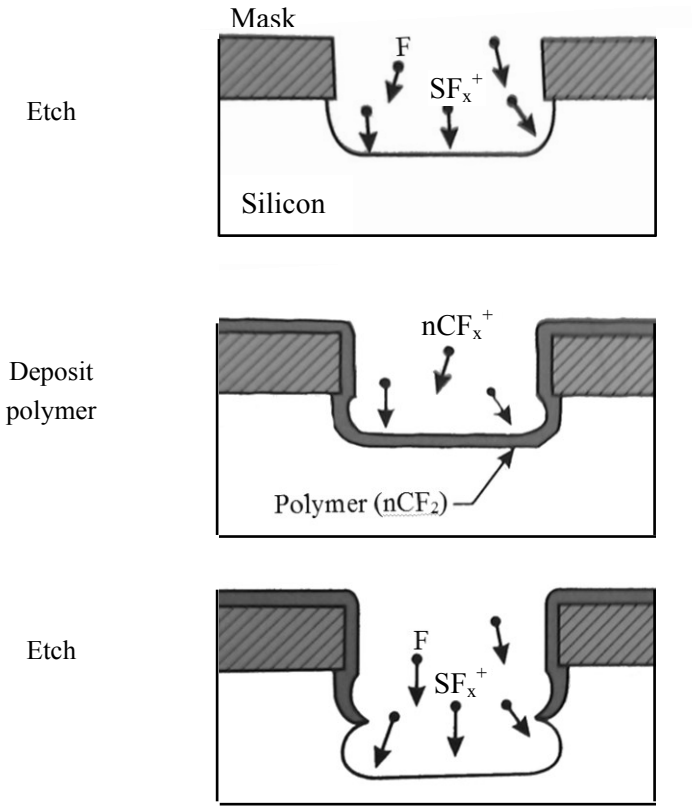

Figure 90: Illustration of Bosch process. There are two steps, the etch step which uses SF_6 and the polymer deposition step which uses C_4F_8. The deposited polymer protects the sidewalls from the etching step, (image modified from [239]).

6.3.3. Milling

Milling a channel using a milling tool is a quick and simple method to create a channel. The minimum channel dimensions are limited by the diameter of the milling-bit, though suitably narrow tools can be purchased to fabricate a channel width down to ~100 µm. Unfortunately as milling-bits get smaller, they become more fragile and prone to breaking, which can make the milling of narrow and deep channels difficult and costly.

Prest *et al.* who developed a system for ITP, milled a microfluidic device in PMMA with a channel cross-section of width 200 µm and depth 300 µm [128, 131]. There has been

criticism on the surface condition following milling; the abrasive action of the tool on the substrate can leave an uneven surface. Depending on the substrate material, methods have been developed to smooth surfaces following milling. Methods using solvents (such has acetone/ethanol) have been developed to both smooth and seal or bond the device to another substrate [261, 262]. The use of diamond tools with ultra-precision machining can result in channel surfaces with a low roughness of a few nanometres RMS [263].

6.3.4. Screen-printing

This method is not widely used but is of interest for convenient portable microfluidic systems. In a publication by Dong *et al.* they described how they printed a microfluidic device on a bare PCB [226]. An advantage of using a PCB is that electrodes can be patterned easily and accurately on the substrate. Whilst multiple researchers have used screen-printing to define detection electrodes, Dong *et al.* used it to define the walls for a network of fluidic channels [226]. The printing of carbon, and silver/silver chloride electrodes was demonstrated. The channel walls were created by printing and UV curing between 5-6 layers of a UV curable dielectric. Further details on the fabrication steps are given in their paper [226]. To seal the open screen-printed channel, a flat sheet of PDMS with inlet and outlet ports was pressed onto the top. Wang *et al.* printed silver ink CCD electrodes onto PMMA sheets [264]. These were then cut into cover sheets and sealed to PMMA channel plates, which were fabricated using a moulding technique.

6.3.5. Powder-blasting

Schlautmann *et al.* [265] and Guijt *et al.* [266] fabricated a planar CE device in glass using a powder-blasting technique. The technique was capable of creating microstructures below 50 – 100 μm outside of a cleanroom at low cost. In this method, a fine powder, such as Al_2O_3, is accelerated toward the surface material which as a result is removed by the erosion process. To define the channels, a patterned photosensitive resist foil was placed on the surface; this was capable of withstanding the powder-blasting. The foil was later removed using either a 10 % KOH or 100 % HNO_3 etch, followed by cleaning in an ultrasonic cleaner to remove any loose particles. There needed to be a balance between the size of the particles used and the required resolution. Smaller particles gave better resolution but slower etch rates [265, 266].

6.3.6. Channel Formers

A novel method of fabrication was devised during this research investigation. This method was presented and well received at the 5th Asia-Pacific Conference on Transducers and Micro-Nano Technology (APCOT 2010) [267]. There are two implementations of the method. In the first a wire is submerged in PDMS and physically removed following the curing of the PDMS. In the second a strand of a sacrificial material is produced and submerged within PDMS which is then cured, after which the strand is dissolved. Both methods produce sealed channels without any requirement for bonding. A detailed description can be found in Appendix E.

The advantages of this method were that a microfluidic device could be fabricated with a short turn-around time and without the requirement of a cleanroom. For the patterning of complex micro-channels, further investigation would be required; methods to pattern the sacrificial material would need to be devised.

6.3.7. Conclusions on Fabrication Methods

A brief discussion on a number of fabrication methods commonly employed for the fabrication of microfluidic CE devices has been given. In this project, it was necessary to construct four devices. Each of there were designed to demonstrate a variety of aims, such as confirming understanding of the theory and its practical application to physical devices, and to demonstrate the separation enhancement concepts. Different fabrication techniques were used throughout the project. Devices 1 and 2 used a milling technique to create the microfluidic channels, whereas Devices 3 and 4 used a moulding technique. More details on the device fabrication are given in the relevant sections (Sections 6.6 through 6.11).

As discussed in Section 3.10, the channel material will directly affect the EOF, which in turn directly affects the electrophoretic separation; therefore the selection of materials for the microfluidic channels is important for CE systems, particularly miniaturised systems where the channel length is shorter. To control the EOF, researchers have investigated a number of methods such as modifying the channel walls using coatings and modification of the buffer solution; this was discussed earlier in Section 6.2. A benefit of the separation enhancement methods investigated in this thesis (described in Section 2.4) is that they give greater flexibly in the material choice since the EOF is modified by the application of an external electric-field. In terms of material selection, this reduces the importance of the natural (unmodified) zeta-potential, channel coatings and buffer solution composition. Instead consideration can

be given to factors such as: the breakdown strength; the relative permittivity and ease of fabrication. A table summarising the breakdown strengths of numerous materials was given in Table 8 (in Section 3.10). In Equation (19) (Section 3.10), it can be seen that a large channel wall capacitance would result in a large change in the EOF for a given applied potential. Therefore the material for the channel wall would ideally have a large relative permittivity and hence a large wall capacitance. In this work, the ease of fabrication was an important consideration; the devices were designed to demonstrate the separation enhancement concepts and verify aspects of the computation models rather than be a fully optimised design. The reasons behind material choices for each of the devices are discussed further in the relevant sections discussing their fabrication (see Table 13).

The following materials are commonly used for the fabrication of electrodes in miniaturised CE systems: carbon, copper, gold, palladium or platinum [89]. For chip-based CE systems, metals are often preferred as they can be easily evaporated or sputtered [89]. Often gold and platinum are used due to their high resistance to electrochemical degradation [59]. The adhesion of gold and platinum to glass or silicon is poor, and therefore adhesion layers (such as chromium or titanium) is required [239, 268]. Since titanium is more electrochemically robust than chromium it is also more difficult to etch. To overcome this issue, a photolithography patterning technique called lift-off can be used [239]. Palladium is sometimes considered for use as an electrode for CE systems due to its ability to absorb hydrogen produced from the electrolysis of water at the electrophoretic ground [74].

6.4. Overview of Proposed Device and Prototypes for Design Optimisation

To fabricate a device capable of demonstrating the separation enhancement methods as described in Section 2.4 a number of devices were first fabricated to aid design optimisation. The modelling of the insulated ZPM electrode in Section 4.2 showed that control of the EOF required thin insulation layers of the order 1 – 5 μm. To fabricate a suitably thin insulation layer microfabrication techniques are required. Since the cleanroom facilities at the University of Southampton are suited to wafers up to 150 mm, with allowances for the space required for the buffer and sample reservoirs it was decided that a channel length of 0.08 m would be appropriate. A long channel length was desirable since it is favourable for separation as discussed earlier in Section 2.2. Whilst it would have been possible to create a longer length of channel by designing it meander rather than being straight, this was undesirable as it would increase the amount of sample broadening [195]. In Sections 4.3 and

4.4 the ionic species transport and diffusion in a fluidic channel was modelled with a channel of 0.08 m. With these design decisions in mind, to demonstrate the separation enhancement methods a microfluidic device was required which had a channel length of ~0.08 m where along the channel length there was a ZPM electrode insulated with a thin (1 – 5 μm) insulation layer. In terms of material choices for the devices, the dynamic control of the EOF gave a significant amount of flexibility (as discussed in Section 6.3.7). Figure 91 shows an illustration of an envisioned device which would be suitable for demonstrating the separation enhancement techniques.

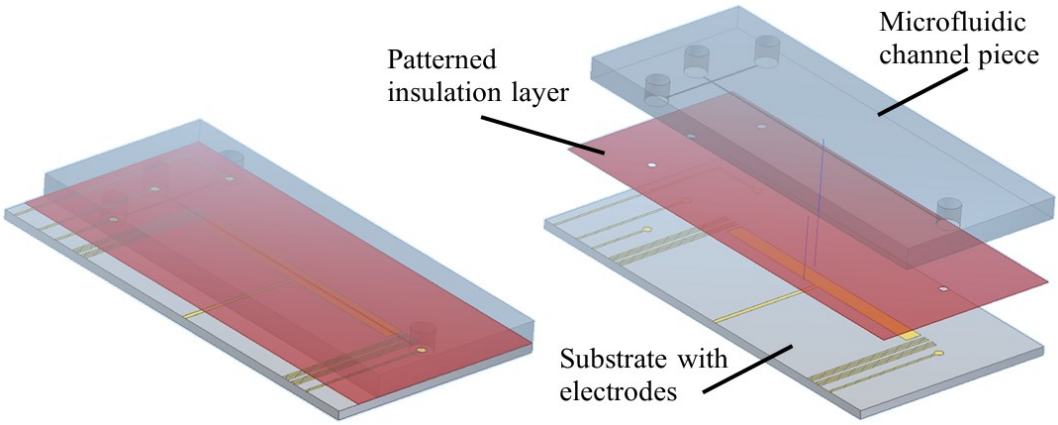

Figure 91: Left: Illustration of envisioned device for demonstrating separation enhancement methods. Right: Exploded view of the envisioned device.

As discussed in Section 6.1, seven experiments were devised; the aims of the experiments were summarised in Table 12. In the following sections (Section 6.5 to 6.11) an overview and the aims of each experiment are discussed in detail. The experiments performed on the devices informed on the design optimisation. Experiments 2 – 7 required the fabrication of microfluidic devices; a table linking the experiments to the corresponding devices is given in Table 13. As well as containing a reference to the section where the fabrication of the device is discussed, Table 13 also references the relevant sections where the theory related to the experiments is described. Since the requirements of the devices were strongly dictated by the experiments, the aims and requirements of the experiments are described prior to the description of the device fabrication. The results and outcomes from the experiments have been analysed; the results from some of the earlier experiments influenced decisions for the ensuing experiments. Experiment 1 uses a commercial CE instrument to characterise electrophoretic dyes. This experiment was required since the dyes were used in many of the other experiments. Experiment 2 which was performed on Device 1 was designed to verify basic CE theory (as discussed in Section 2.2) and demonstrate electrophoresis on a planar CE device. The experience gained from the fabrication of Device 1 combined with the

results from the modelling (Section 4.2) showed that thin insulation layers (and therefore microfabrication techniques) would be required. It was anticipated that this fabrication process would be quite time consuming and Device 2 was fabricated as an engineering prototype on which the ancillary hardware could be setup and tested. Therefore Experiment 3 was used to test the control system which was designed to monitor the detectors and control the designed computer controlled-HVPS. This HVPS was for applying the potential along the channel, and the potential to the ZPM electrode. Further to this, Experiment 3 verified the functionality of the micro-pumps. This meant that Experiments 4, 5 and 6 could commence shortly after the completion of the fabrication of Device 3. Of these experiments, the first experiment (Experiment 4) was designed to characterise the effect of the potential applied to the ZPM electrode on the EOF. Experiment 5 investigated the limits of detection for the CCD system (the design of which was discussed in Sections 5.1.4 and 5.2). The final experiment on Device 3 was used to demonstrate the separation of a sample of metal ions. The results from this experiment were compared with those generated by the microfluidic model discussed in Sections 4.3 and 4.4 to verify that the model was capable of describing the microfluidic behaviour (in particular the electrophoretic separation). Finally, Experiment 7 was designed to demonstrate the separation enhancement methods as described in Section 2.4 and modelled in Section 4.4.

Table 13: Table linking experiments to corresponding devices.

Experiment number	Experiment Title	Device number	Theoretical work	Fabrication description
1	Characterisation of electrophoretic dyes	-	Sections 2.2 and 2.3	-
2	Control of ionic species in microfluidic device	1	Sections 2.2, 2.3, 3.2, 4.3.1 and 6.3	Section 6.6.2
3	Setup and test control system	2	Sections 2.5 3.2, 3.8, 3.9 and 5.1.4	Section 6.7.2
4	Modification of EOF with planar ZPM electrode	3	Sections 3.10, 4.1, 4.2 and 6.3	Section 6.8.2
5	Evaluate detection system	3	Sections 5.1.4 and 5.2	Section 6.8.2
6	Demonstrate separation and detection of metal ions	3	Sections 2.2, 2.3, 4.3 and 4.4	Section 6.8.2
7	Demonstrate separation enhancement methods	4	Sections 2.4, 3.10, 4.2, 4.3, 4.4, 5.1.4 and 5.2	Section 6.11.2

6.5. Experiment 1: Characterisation of the Electrophoretic Dyes

6.5.1. Aims of Experiment 1

The primary aim of Experiment 1 was to measure the apparent mobilities of electrophoretic dyes. These highly coloured electrophoretic dyes were required to demonstrate numerous aspects on the fabricated devices and to aid the experiments. The experimental conditions were closely matched to those described by Pérez-Ruiz *et al.* [234]; the buffer solution was 50 mM with 10 mM β-cyclodextrin. In their work they calculated the values of apparent mobility for a number of electrophoretic dyes over a range of buffer pH values [234]. The apparent mobility was calculated by measuring the sample velocity and dividing by the electric-field strength. The sample velocity has contributions from both the electrophoretic velocity and the EOF velocity. Earlier in Section 2.3, Equation (9) showed the relationship between the electrophoretic velocity, electroosmotic velocity and the applied electric-field, from this it is possible to calculate a value for electrophoretic mobility.

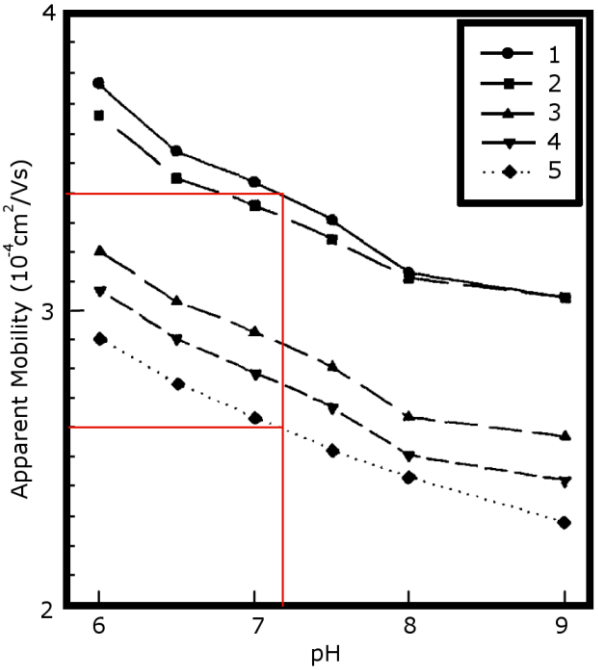

Figure 92: Graph depicting the dependence of the apparent mobilities of the dyes on the pH of the buffer; (1) fluorescein, (2) dichlorofluorescein, (3) rose bengal, (4) erthrosine, (5) eosine (modified from [234]). Red line highlights apparent mobilities for fluorescein and eosine at pH 7.2 (i.e. the pH value used in the experiments described in this thesis).

The graph in Figure 92 shows a sample of the results published by Pérez-Ruiz *et al.* [234]. From this graph, the values for apparent mobility can be estimated over a range of buffer solution pH values. The red lines highlight the values of apparent mobility for fluorescein and eosine at pH 7.2; they are 3.4 x 10^{-8} m^2 V^{-1} s^{-1} and 2.6 x 10^{-8} m^2 V^{-1} s^{-1} respectively. The ratio between the values of apparent mobilities of fluorescein to eosine is 1.31. This ratio is a useful value which will be used later in this section and Section 6.6. It enables a comparison of results without the requirement of measuring the exact value of the EOF velocity.

6.5.2. Experiment 1: Verification of the Apparent Mobilities of the Fluorescent Dyes

To verify the values of apparent mobility of the fluorescein and eosine dyes, a series of experiments were conducted on a commercial CE instrument – the Prince Technologies PrinCE-560 instrument with a TraceDec CCD system [269]. The separation conditions were closely matched to those described by Pérez-Ruiz *et al.* [234], such that:

- the buffer solution used was a 50 mM phosphate buffer with 10 mM β-cyclodextrin (pH 7.2). The β-cyclodextrin was added to aid the separation of the dyes using a process called host-guest complexation. Complexation modifies the molecular mass of a substance which alters the charge density and therefore its mobility [234].
- a separation voltage of 20 kV was applied along the fused-silica capillary.
- the concentrations of the dyes were 50 mM.

For Experiment 1 the following four runs were performed consecutively on the PrinCE instrument:

1. electrophoresis with capillary filled with buffer solution,
2. electrophoresis of a sample of 50 mM fluorescein,
3. electrophoresis of a sample of 50 mM eosine,
4. electrophoresis of a mixed sample of 50 mM fluorescein and eosine.

The buffer run served two functions, as well as cleaning the capillary it confirmed that the buffer itself showed no peaks in the detector trace. As samples pass the detection window of the TraceDec detection system, the difference in the conductivity between the buffer and sample is detected which results in a peak on the electropherograms. The electropherograms of the four runs can be seen in Figure 93. The purpose of running the experiment with a

single dye was to identify the migration time of that dye from the injection point to the detector. As can be seen in Figure 93 the fluorescein sample caused a peak at 14 minutes whereas a sample of eosine caused a peak at 19 minutes. When both dyes were run at the same time (shown by the red trace in Figure 93) the fluorescein and eosine could be easily identified and were significantly separated. If the buffer and single dyes runs were not performed before the two dye run, then the peak at 19 minutes (corresponding to eosine) would not be convincing. The CCD system detects changes in conductivity between the sample and background buffer.

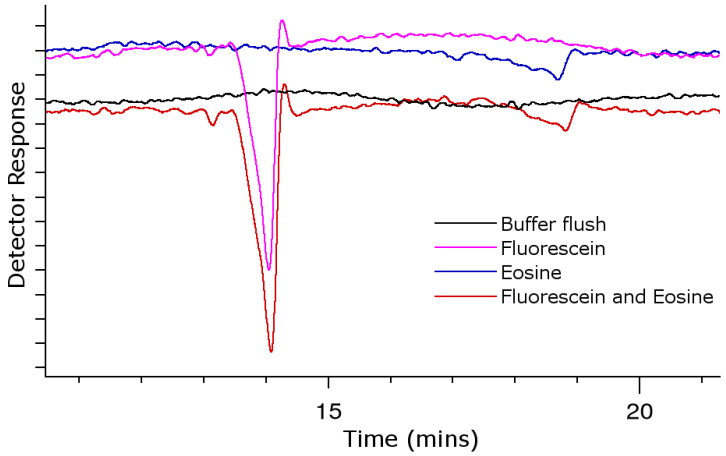

Figure 93: Separation of fluorescein and eosine using a commercial CE (PrinCE-650) instrument.

6.5.3. Outcomes from Experiment 1

This experiment verified that the two electrophoretic dyes could be separated using an electric-field. The ratio between the values of the measured apparent mobilities of fluorescein to eosine was calculated as 1.36. This is comparable with the value of 1.31 calculated from the work by Pérez-Ruiz *et al.* [234].

6.6. Experiment 2: Confirm Control of Ionic Species in a Microfluidic Device

6.6.1. Aims of Experiment 2

With the behaviour of the dyes confirmed in Experiment 1, the aims of this experiment were to confirm the ability to move an ionic species along a planar microfluidic channel and to evaluate the fabrication method which produced this microfluidic device.

A discussion on the fabrication of the microfluidic device (referred to as Device 1), which occurred at an early stage in the project, is given in Section 6.6.2. There was no intention of investigating the effect of modifying the EOF with this device and hence no ZPM electrode features in the design or device. The experimental conditions including the ionic species (sample) and buffer solution were closely matched to those of Pérez-Ruiz *et al.* [234]. The main difference was that a PMMA device was used in place of fused-silica capillary to host the buffer solution. The work by Pérez-Ruiz *et al.* used fluorescent dyes; this was useful for this experiment since it removed the requirement of a detection system.

In Section 2.2 it was shown that the migration time of an analyte is proportional to the electric-field and its electrophoretic mobility. In this experiment the aim was to measure the ratio of apparent electrophoretic mobilities of the fluorescent dyes and compare with the values from the results published by Pérez-Ruiz *et al.* [234]. It was anticipated that the EOF would be significantly different given that a microfluidic channel was used in place of a fused-silica capillary [270].

6.6.2. Fabrication of Device 1

Due to its low cost, quick turnaround time (from design to fabricated device) and expertise offered by colleagues, a milling technique was used to create an open channel of 270 mm in length in PMMA. The PMMA was supplied by Aquarius Plastics Ltd. [271]. The channel width and depth were 300 µm and 30 µm respectively. The width and depth were chosen to closely match work by Prest *et al.* [128-130] whom also used a milling technique. The minimum width was limited to 300 µm due to the milling tool used; whilst a 100 or 200 µm milling bit could have been purchased it was decided that 300 µm would be suitable. Smaller milling bits are known to be fragile which can often create issues with fabrication. To aid the separation it was decided to create the microfluidic device with a relatively long channel

length compared with those typically used by other researchers working on miniaturised CE systems [131]. The channel length was limited by the dimensions of the milling machine. The work area on the milling machine had a maximum length of 300 mm; hence the channel length was limited to 265 mm. The remaining 35 mm was required to define the buffer reservoirs and allow spacing to the edge of the device. The option of using meandering channels to significantly increase the channel length was deemed unnecessary as it would introduce unwanted complications, for example, increased sample dispersion [195]. A 3D drawing of Device 1 can be seen in Figure 94. A technical drawing of the PMMA piece which contained the microfluidic channels for Device 1 can be seen in Figure 95. Device 1 was composed of two parts, this drawing shows the main part, the milled PMMA piece. The other part was a PMMA piece of similar dimensions without the channels or reservoirs milled into it. To seal the milled channels, the PMMA pieces were bolted together using nylon nuts and bolts. Nylon nuts and bolts are not electrically conductive and so were used in place of metal nuts and bolts as a safety precaution. If the microfluidic channels leaked, the nuts and bolts could be connected to the high voltage applied to the channels via the conductive buffer solution.

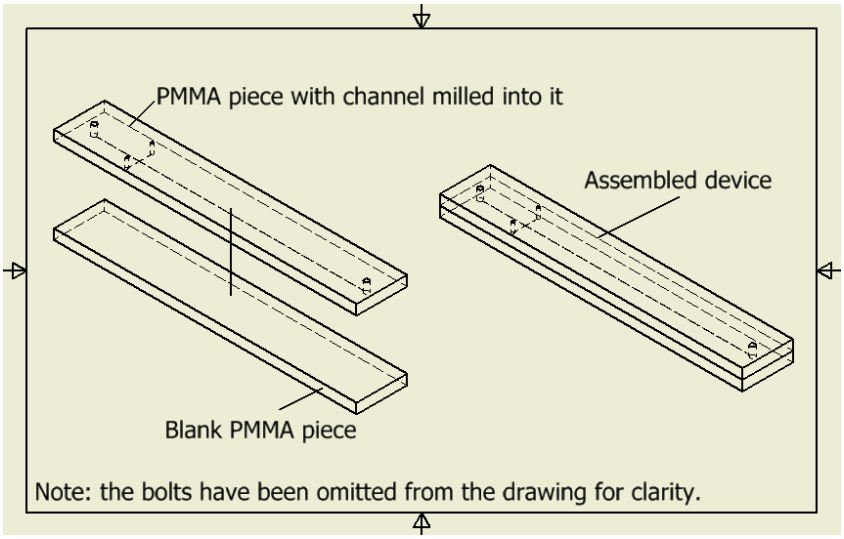

Figure 94: 3D drawing of Device 1; the dimensions are given in Figure 95.

The holes through the milled piece of PMMA at the extreme ends of the channel define the buffer and buffer waste reservoirs. The drawing (Figure 95) also shows the inclusion of a second channel that crosses the main channel. This is the sample injection channel where through the application of pressure, small sample volumes could be directly injected into the main separation channel.

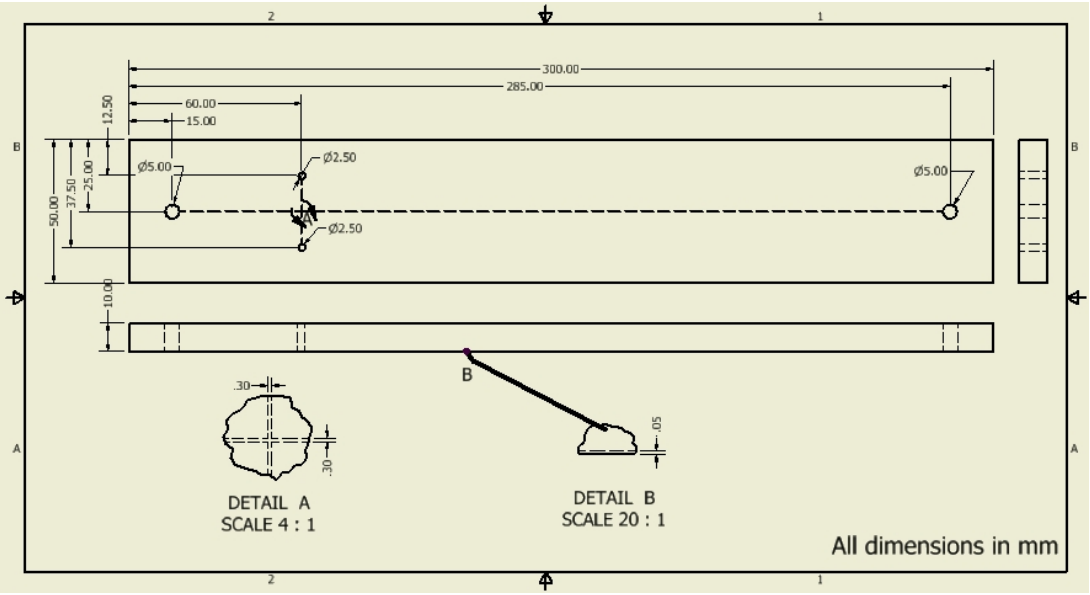

Figure 95: Technical drawing for the milled PMMA piece for Device 1.

6.6.3. Refinement of Device 1

After the two prepared PMMA pieces were bolted together the channels were filled with buffer solution. Initially, filling of the channels was achieved by applying pressure to the buffer reservoir. Later the filling was achieved by applying a negative pressure to the buffer waste reservoir using a syringe. Once the device was filled, it became apparent that the nuts and bolts were spaced too far apart and that they would be insufficient for sealing the device. In the areas between the bolts the fluid was able to leak from the channel. To overcome this problem and to enable the aims of the device to be achieved, more bolts were added along the length of the device, an image of the device can be seen in Figure 96. As well as adding extra bolts, a thin layer of petroleum jelly was applied between the PMMA pieces. Care was taken to ensure that no petroleum jelly entered and blocked the microfluidic channel. A small quantity of petroleum jelly was applied around the PMMA piece away from the channel. The pieces were then gently pressed together and the spreading of the petroleum jelly could be seen. Where there was not sufficient coverage of petroleum jelly, more could be added by separating the pieces and repeating the process. With these modifications the device no longer leaked.

Figure 96: Photograph of Device 1 after refinements.

6.6.4. Experiment 2: Ionic Species Migration along Channel Subjected to Electric-Field

Highly coloured electrophoretic dyes, fluorescein and eosine, were used to investigate the ability to electrokinetically transport fluid through the PMMA microfluidic channel. The primary advantage of using dyes was that a detection system was not required. Fluorescein and eosine were selected for use in this experiment since they had the greatest difference in apparent mobilities and therefore would be the easiest to separate [234]. Further to this their colours are different; fluorescein is a bright yellow, whereas eosine is pink. The buffer solution and dyes used were selected based on work by Pérez-Ruiz *et al.* [234]. The buffer solution used in this experiment was a 50 mM phosphate buffer with 10 mM β-cyclodextrin (pH 7.2).

The methodology for this experiment was:

1. *Buffer flush*: At the start of each experiment the channels were flushed with buffer solution. A 50 mM phosphate buffer solution containing 10 mM β-cyclodextrin was flushed through the channel by applying a negative pressure to the buffer waste reservoir.
2. *Electrokinetic buffer flush:* 1250 V was applied along the 265 mm channel resulting in an electric-field strength of 4717 V m^{-1}; this electric-field was applied for 20 minutes to electrokinetically flush the buffer through the separation channel, after which the high voltage was turned off.
3. *Sample injection:* A volume of 20 µL of sample injected at the start of the microfluidic channel.
4. *Apply electric-field:* 1250 V applied along the 265 mm channel resulting in an electric-field strength of 4717 V m^{-1}.

5. *Measure progress of sample:* To measure the apparent mobility of the dyes as they migrated along the channel, the position of the dyes were recorded against time. From these measurements an average velocity could be calculated which is directly proportional to the apparent mobility.

Initially a sample of 50 mM fluorescein was used for the experiment described above. In Figure 97, it can be seen that the fluorescein dye migrates along the channel when subjected to an electric-field. The black dashed line represents the midpoint of the channel. This experiment verified the expectation that it was possible to electrokinetically move a fluid along a channel in one direction. Further to this, it revealed that there were no unexpected issues (due to surface chemistry, etc.) between the materials and chemicals used.

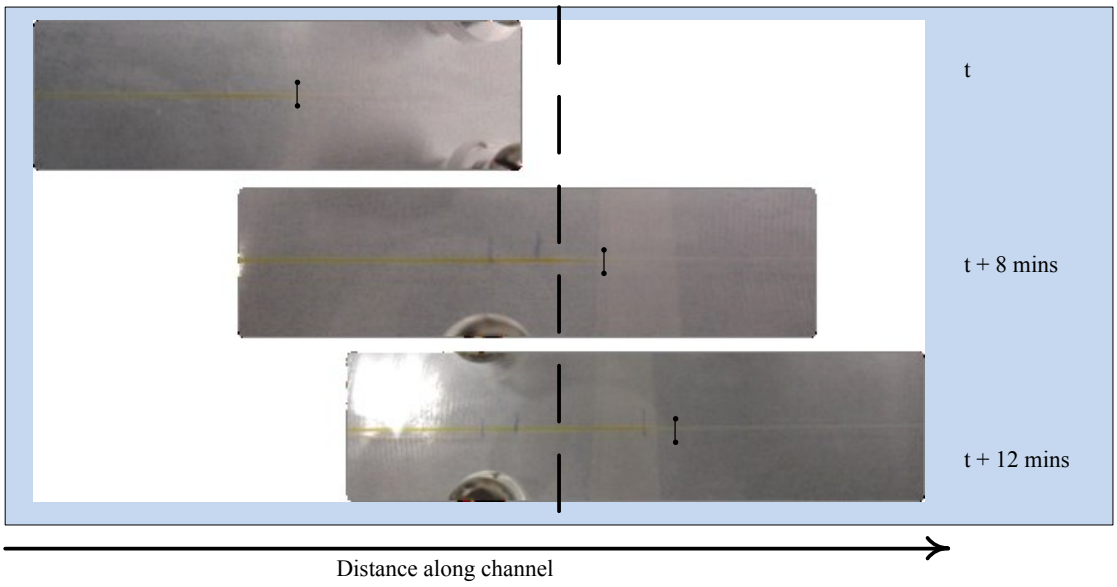

Figure 97: Time-shots of fluorescein dye moving through the channel when subjected to an electric-field.

Following the experiment with fluorescein, the same methodology was applied for a sample of 50 mM of eosine. The apparent velocity of fluorescein was measured as 1.08 x 10^{-4} m s^{-1} whereas for eosine it was 0.83 x 10^{-4} m s^{-1}. Assuming a linear potential drop along the channel, the apparent mobility values for fluorescein and eosine were calculated as 2.3 x 10^{-8} m V^{-1} s^{-1} and 1.8 x 10^{-8} m V^{-1} s^{-1} respectively. This results in a ratio of apparent mobility of fluorescein to eosine of 1.28. The values of apparent mobility measured Pérez-Ruiz *et al.* were 3.4 x 10^{-8} m V^{-1} s^{-1} and 2.6 x 10^{-8} m V^{-1} s^{-1} for fluorescein and eosine respectively [234]. This results in in an apparent mobility of 1.31; therefore the results from the experiment on Device 1 are in good agreement with reported work.

For microfluidic systems fabricated in PMMA it has been reported that the EOF is lower than for glass-based systems [270]. The apparent mobility accounts for the contribution from the electrophoretic mobility and the EOF mobility. This explains why the values for apparent mobilities measured on the PMMA device, were lower than from the experiment by Pérez-Ruiz *et al*. [234] where a fused silica capillary was used. Many researchers have stated values of EOF mobility for different polymers, but the experimental conditions and fabrication method play an important role in the determination of the EOF mobility for polymers. For example, in Figure 98, Ford *et al*. [272] state that the EOF of PMMA is fairly stable over a wide range of pH values; above pH 7 it is approximately 1.9 x 10^{-8} m^2 V^{-1} s^{-1}, whereas Mühlberger *et al.* [148] estimated a larger value of 3.5 x 10^{-8} m^2 V^{-1} s^{-1}. At a pH of 7.2, the value of EOF mobility in a fused silica device was reported as being ~4.4 times larger than that measured in a PMMA device, as shown in the graph in the left of Figure 98. As discussed in Section 6.2, the value of EOF mobility is dependent on a number of factors, including the buffer solution and device processing steps. The EOF mobility was expected to be lower in a PMMA device compared with the fused-silica capillary. Given the lower EOF mobility in a PMMA device, a lower apparent velocity would also be expected; this is in agreement with the results from Experiment 2 [272]. At lower pH values, the difference in the EOF mobility for fused-silica and PMMA device reduces. Therefore the difference in apparent velocity when using lower pH buffer solutions would also be expected to be smaller.

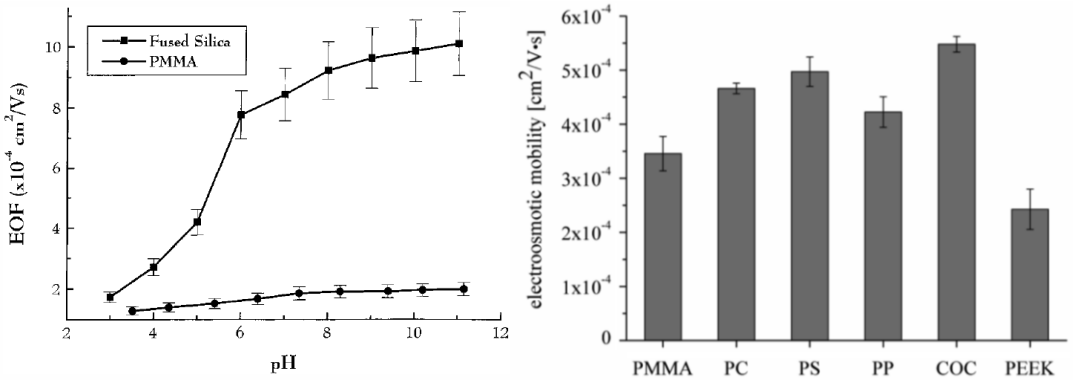

Figure 98: Variation in EOF mobility over range of pH values for PMMA and fused silica (left) (taken from [272]). Values of EOF mobility measured for a range of different polymers (right) (taken from [148]).

Although there was no reason to think that reversing the field would not have an effect on the flow, an experiment was done just to confirm this as extra characterisation of the device and materials. To confirm that electric-field direction controlled the fluid flow direction, an experiment was conducted where the electric-field direction was switched after the

electrophoretic dye had migrated halfway along the channel length. For this experiment the following steps were performed:

1. *Buffer flush*: At the start of each experiment the channels were flushed with buffer solution. A 50 mM phosphate buffer solution containing 10 mM β-cyclodextrin was flushed through the channel by applying a negative pressure to the buffer waste reservoir.
2. *Electrokinetic buffer flush:* 1250 V was applied along the 265 mm channel resulting in an electric-field strength of 4717 V m^{-1}; this electric-field was applied for 20 minutes to electrokinetically flush the buffer through the separation channel, after which the high voltage was turned off.
3. *Sample injection:* A volume of 20 μL of eosine injected at the start of the microfluidic channel. Eosine was selected since it was darker than the fluorescein and therefore easier to observe visually.
4. *Apply electric-field: E*lectric-field strength of 4717 V m^{-1} applied to channel.
5. *Monitor progress of sample:* The position of the dye was monitored visually as it migrated along the channel.
6. *Reverse electric-field:* Once the dye had reached halfway along the channel (indicated by the bolts in Figure 99b) the electric-field was reversed.

As can be seen in the sequence of photographs in Figure 99, during step 4, the eosine travelled from the start (Figure 99a) to the halfway along the channel (Figure 99b). The reversal of the electric-field (step 6) caused eosine to migrate back along the channel (Figure 99c) confirming that the eosine was responding to the electric-field direction.

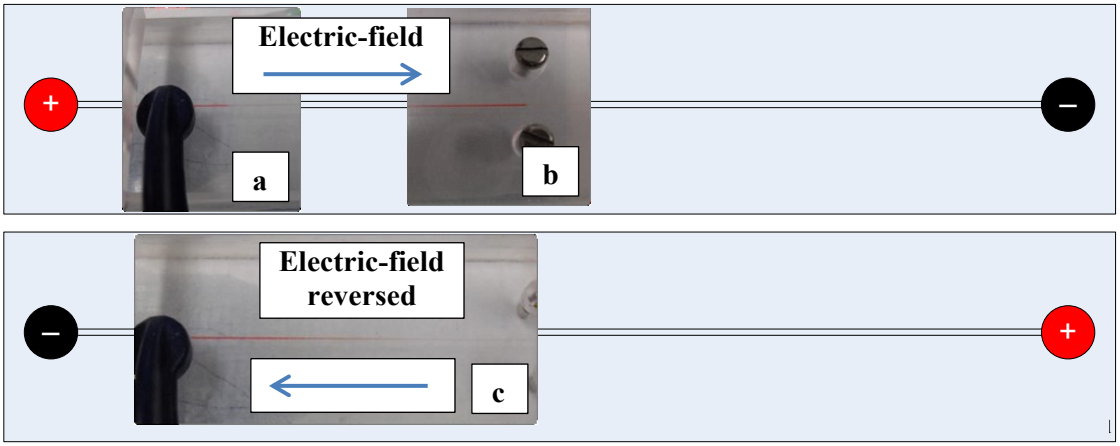

Figure 99: Illustration with photographs showing eosine dye moving along channel and switching direction when the electric-field was reversed. (a) shows the eosine as it migrates along the channel. (b) shows the eosine reaching halfway along the channel at which point the electric-field was reversed. The migration of the eosine back along the channel is shown in (c).

6.6.5. Outcomes from Experiment 2

These experiments revealed issues with the fabrication method, particularly with the sealing of the microfluidic channel, although the primary aim of this device was to investigate the ability to electrokinetically transport ionic species in a microfluidic channel. This aim was successfully achieved and the measured ratio between apparent mobilities of 1.28 was in good agreement with the value calculated from the literature of 1.31 [234] and of that measured experimentally, as described in Section 6.4 which was 1.36.

Another result from these experimental investigations was that it became apparent that the construction technique would be unsuitable for later aims of demonstrating the separation enhancement methods (described in Section 2.4). These require an electrode to be placed close (<1 μm) to the microfluidic channel, thereby enabling control of the EOF. To fabricate a device with an electrode close to the channel requires a thin insulation layer, which can be achieved using microfabrication techniques.

The use of electrophoretic dyes was useful since it enabled the aims of the device to be met without the requirement for a detection system. It was clear however, that the detection system was a key component which should be included in later devices. The use of a detector would reduce the amount of error in the measured data, particularly the timing of events which were determined by visual inspection, which can be subjective.

6.7. Experiment 3: Setup and Test of Experimental Control Systems

6.7.1. Aims of Experiment 3

The primary aims for Experiment 3 were to test the functionality and suitability of the ancillary hardware designed for the testing of the whole system and the associated control software. This included the:

- computer controlled HVPS (discussed in Section 6.7.4),
- CCD system (as described in Section 5.1.4.2)
- microfluidic micro-pumping system (discussed in Section 6.7.3) .

As discussed in Section 6.6.5, to achieve the aims imposed by Experiments 4-7, it was clear that the fabrication method used for Device 1 would not be suitable and that microfabrication techniques would need to be employed. It was anticipated that it would take a significant amount of time to complete the fabrication of a device suitable for performing all the later experiments on. With this in mind Device 2 was fabricated to address the aims of Experiment 3. This allowed for the development and testing of the ancillary hardware, which was required for later experiments, to be run in parallel with the design and fabrication of Device 3, which was created to address Experiments 4, 5 and 6. This meant that upon completion of the fabrication of Device 3, the testing system would be ready, with minimal alteration required. It should be noted that whilst the fabrication methods are vastly different for Devices 2 and 3, the detection and ZPM electrode layout, and channel dimensions were the same. The physical layout of the devices should be as close as possible to reduce the chances of introducing more degrees of freedom For example, for testing the micro-pump system, it was important to keep the channel dimensions the same, since they significantly affect the hydraulic resistance as discussed in Section 3.2.

An additional aim of Experiment 3 was to investigate the effect of applying a high voltage to the ZPM electrode even though the insulation layer would be significantly thicker than that presented by other researchers working on EOF modification using electric-fields [49].

6.7.2. Fabrication of Device 2

Since the cleanroom equipment was designed for processing wafers up to 150 mm diameter, devices were designed with this constraint in mind. The channel length of Device 2 was significantly shorter than the channel length of Device 1. The reduction in channel length was also a step toward a smaller and therefore more portable device. A 3D drawing of Device 2 can be seen in Figure 100.

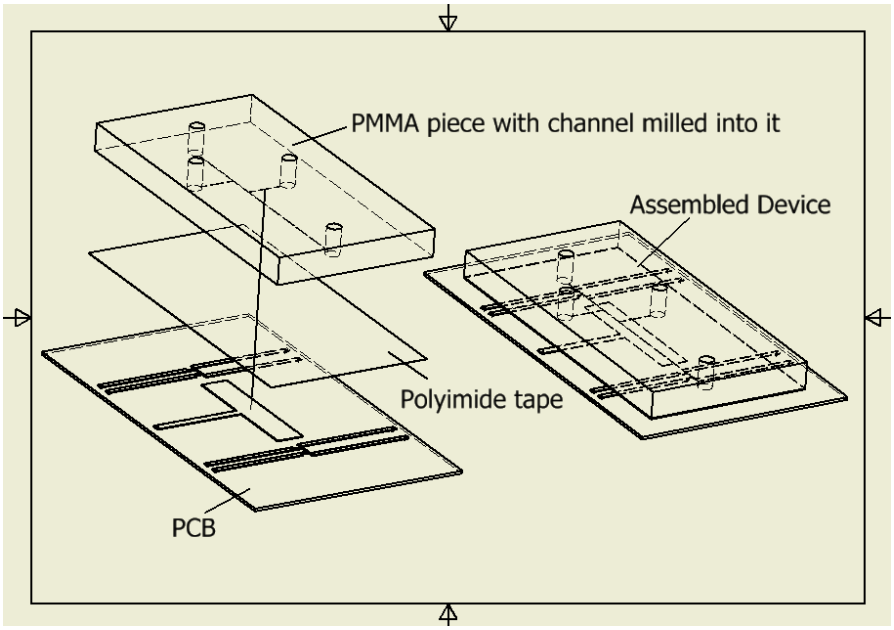

Figure 100: 3D drawing of Device 2. The dimensions for the PMMA piece are given in Figure 101; the dimensions of the detector electrode layout were given in Section 5.2.

The device was composed of two parts, a PMMA piece containing the open microfluidic channel, and a PCB which was processed and sealed to the PMMA piece to close the channel. The microfluidic channel was milled into a piece of PMMA; a technical drawing of the piece can be seen in Figure 101. The separation channel had a length, width and depth of 85 mm, 300 µm and 50 µm respectively. The channel from the sample injection reservoir was offset by 10 mm along the separation channel with respect to the sample waste channel. This enabled larger volumes of sample to be injected (compared with Device 1) which is normally undesirable in CE [33, 78]. However for testing purposes it was useful to have a large volume of sample; one of the tests discussed later in Section 6.7.4, shows the detector response to electrophoretic dyes. The use of a large sample volume enabled the visual verification that the detector responded to the ionic species being transported along the channel.

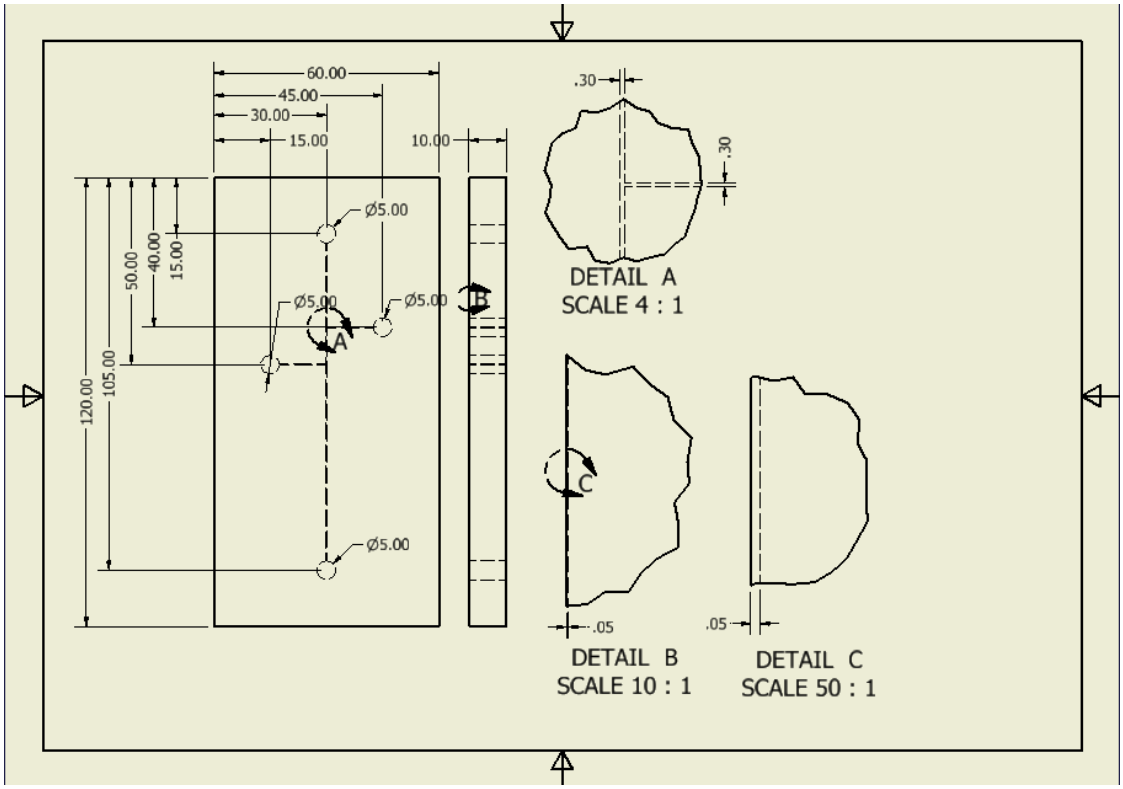

Figure 101: Technical drawing of PMMA channel piece for Device 2. Detail A shows channel width is 300 µm. Detail B and detail C show channel depth of 50 µm.

The reservoirs of the PMMA channel piece were all tapped to create a thread, so that it was possible to securely attach a fluidic connector between them and the micro-pump. This was important to enable the testing of the micro-pump-based fluid control system.

An image of the second piece, the PCB, can be seen in Figure 102. The PCB contained electrodes for the detection system, and a ZPM electrode along the channel length. The detector electrode dimensions for Device 2 were discussed earlier in Section 5.2. Using double sided polyimide tape (100 µm thick Kapton® supplied by Katco [273]), the PCB was attached to the PMMA channel; this sealed the microfluidic channels. Whilst the electrodes on the PCB had a height of 35 µm, the lack of planarity did not cause issues with regards to sealing the channel since the polyimide tape was first sealed to the PMMA piece and then placed onto the PCB where it would rest on the copper electrodes. A consequence of using double sided polyimide tape was that a layer of adhesive was present along the bottom channel wall and in direct contact with the fluids within the channel. The thickness of this layer was less than a few microns. Since this is much less than the smallest channel dimension, the risk of blocking the channel with adhesive was low, however the effect of the adhesive on the EOF properties was unknown. Whilst this was undesirable, the primary aims of Device 2 were to test the setup of the detection and microfluidic pumping system.

Therefore it was anticipated that the adhesive on the tape would not cause any significant issues which would prevent the aims of the device being met. An image of the assembled device can be seen in Figure 102.

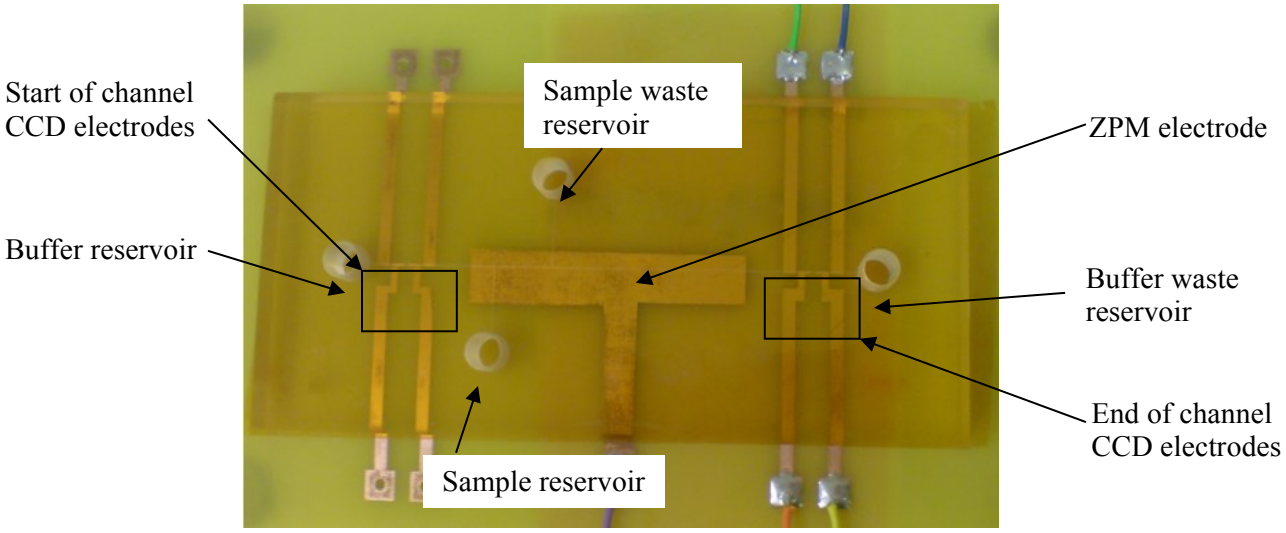

Figure 102: Photograph of the Device 2, channel milled into PMMA and sealed with double-sided polyimide tape to a PCB. The PCB includes detection electrodes at both channel ends and a ZPM electrode.

As a safety precaution, a rig was constructed to prevent accidental access to the reservoirs whilst the high voltage was applied. This rig was placed on top of the PMMA piece which housed the microfluidic channel. An image of the rig can be seen in Figure 103 alongside which is a photograph of the high voltage connector which sits in the rig to connect the HVPS to the fluid. The electrode holder was capable of holding 4 SHV connectors; two for the separation electric-field and two to enable electrokinetic sample injection.

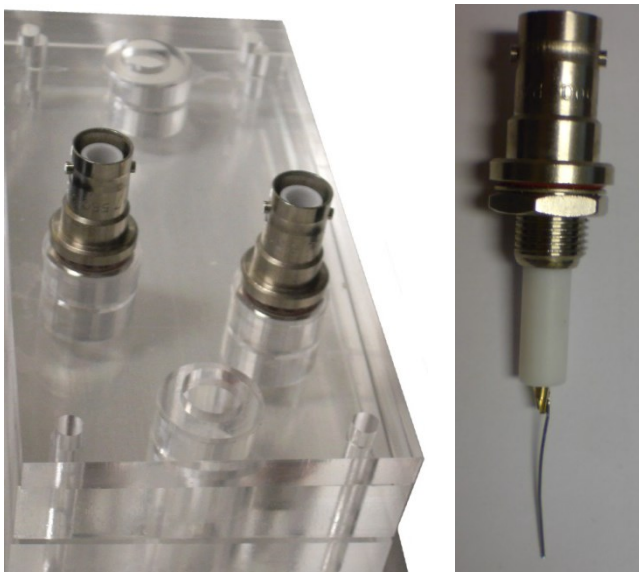

Figure 103: Left: rig manufactured to prevent accidental access to the fluidic reservoirs whilst high voltages were applied, showing the rig mid-assembly. Right: the high voltage connections which were placed in the holes created in the PMMA piece.

6.7.3. Experiment 3: Suitability of Micro-pump for Sample Injection and Flushing of Buffer

A micro-pump (model: mp-6) was purchased from Bartels Mikrotechnik [180]. For convenience it can be controlled by the mp-x controller. The mp-x controller is relatively large and primarily for evaluation purposes. Whilst the mp-x controller is quite large and would not be considered portable, the micro-pumps can be controlled by a microcontroller. This pump was chosen because of its small size (30 mm x 15 mm x 3.8 mm) and mass (2 g) in anticipation for later implementation into a portable device [274]. The operation of the pump is based on two piezo-electric actuators [274]. The operational lifetime is specified as >5000 hours. Typical flow rates (for water) were stated as 7 ml min^{-1} and the maximum back pressure was 600 mbar [274].

The micro-pump was connected to Device 2 using a push-fit-to-screw-terminal connector. Before connecting the micro-pump, the channels were first filled with deionised water. This was achieved by submerging the device in deionised water and placing it in a vacuum desiccator. As the pressure in the desiccator was reduced, the air in the channels was forced out and displaced with the deionised water.

Once the channels were primed, the micro-pump was connected to the sample waste reservoir where it created a negative pressure to flow fluid through all the channels. This

caused the fluid from the buffer, sample and buffer waste reservoirs to travel through their respective channels to the sample waste channel. By placing fresh buffer solution in the buffer, sample and buffer waste reservoirs, it was possible to flush all the channels with buffer solution using this buffer flushing scheme; an illustration of this is shown in Figure 104a. After flushing the channels with buffer solution for at least 10 minutes, the sample could be hydrodynamically injected by pipetting the sample into the sample reservoir. With a radius of 5 mm and depth of 10 mm (as shown in Figure 101), it is possible to estimate that the volume of the sample injection reservoir was ~200 µL. The injected sample filled 10 mm of the separation channel (of cross-sectional area 1.5 x 10^{-8} m^2), therefore the volume of sample injected was ~0.15 µL. Whilst the values for injection volume vary significantly in the literature, this value of 0.15 µL is comparable with that used by other researchers; typically in the region of 0.01 µL – 50 µL [161, 275]. The use of electrophoretic dyes enabled the injection scheme to be visually observed. Within 30 seconds the sample injection channel and sample waste channel would be coloured by the dye; the other channels continued to be flushed with buffer solution; an illustration of this is shown in Figure 104b.

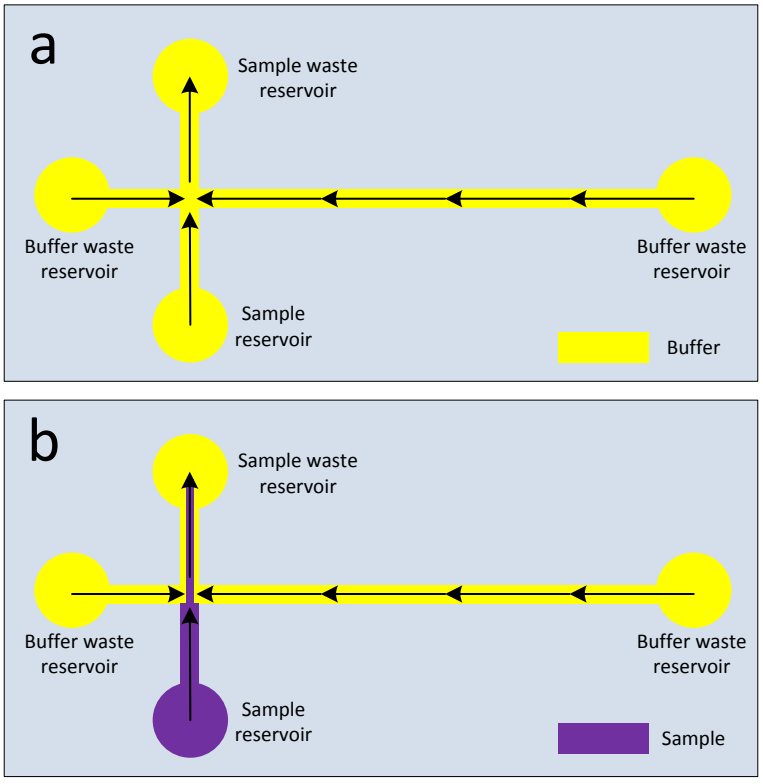

Figure 104: Illustration of the buffer flushing scheme (a) and hydrodynamic sample injection scheme (b).

6.7.4. Experiment 3: Integration and Testing of Detection System and HVPS into the Test Platform

The designed detection system involved the construction of two PCB detection circuits (discussed earlier in Section 5.2.1). There were two outputs per PCB, one from the transimpedance amplifier and another from the differential amplifier. These four signals were fed into a National Instruments DAQmx-6016 card and processed using LabView software. The thickness of the polyimide tape (100 μm) resulted in a small value of wall capacitance seen by the detectors. This was undesirable but did not prevent the setting up of the LabView program to enable the acquisition, filtering, processing and storage of the four signals from the two contactless conductivity detectors. The design of the detection system was discussed earlier in Section 5.2. Based on the frequency response of the SPICE simulation it was decided to operate the detectors at 10 kHz since the response is flat over a range of frequencies either side of this frequency. The detectors were interfaced to a computer running LabView software via a National Instruments DAQmx-6016 data-acquisition card. Once the signals were acquired, they were passed through a 2^{nd} order software band-pass filter with a high- and low-pass cut-off frequency of 9 kHz and 11 kHz. Following the filtering stage the RMS values of the signals were calculated which reduced the amount of data to store. Further to this, calculating the RMS alleviates issues regarding the phase differences between the waveforms. The ratio of the RMS values gives an indication of the conductance of the channel between the electrodes.

As well as a detection system two computer controlled HVPSs were required: one to supply a potential for the separation electric-field and a second to provide the potential to the ZPM electrode to modify the EOF. To enable the switching of the EOF direction, the latter HVPS needed to be dual polarity.

The computer controlled HVPS contained two high voltage modules, one to generate the separation electric-field and the other to generate the ZPM potential on the ZPM electrode. The power supply designed was based on HV DC-to-DC converters supplied by Applied KiloVolt Ltd. For the separation electric-field, the HP005PAA025 module was used; this enabled the application of 5 kV, with a maximum current of 2 mA [276]; as stated earlier in Section 3.7. the current flow in CE systems is typically in the range of μA and therefore this module was deemed suitable. The HV DC-to-DC converters required a supply voltage of +24 V, to provide this voltage an AC-to-DC converter (V-Infinity VSBU-120) was used. This board and the HV DC-to-DC converter boards were placed in an enclosure. A panel meter (DATEL DMS-40LCD-0/1-5-C) to monitor the voltage, and HV connectors were

placed on the enclosure and connected to the converters. The panel meter required a supply voltage of 5 V which was also provided by the AC-to-DC converter. The HV DC-to-DC converters were controlled using LabView software (further details given in Appendix D), via the output ports of the National Instrument data acquisition card (DAQmx-6016) used to monitor the CCD as discussed above.

With this HV module, over a channel of 85 mm in length, separation electric-fields up to 58.8 kV m^{-1} could be applied. For the electric-field to enable the modification of the EOF, the HP005ZIP025 module was used; this could output a potential of +/– 5 kV [277]. For a 1 μm insulation layer, this HVPS would allow an electric-field of 5 x 10^9 V m^{-1}. Based on work by Buch *et al.* where the electric-field across the insulation layer from a number of researchers was summarised, the typical values of electric-field across the insulation layer ranged from 2.4 x 10^6 to 3.7 x 10^8 V m^{-1} [49]. The National Instruments DAQmx-6016 card had two output ports which were configured to control the output from the high voltage modules. A programming voltage of 0 to 10 V set the output from 0 V to the full scale output from the HV DC-to-DC converters.

To demonstrate the functionality of the test platform equipment, a sample of fluorescein and eosine were sent along the microfluidic channel. The first system tests were performed using the electrophoretic dyes for two reasons. Firstly the ability to see the position of the dyes in the channel made it possible to ensure that the sample had successfully crossed the sample injection point along the channel. Secondly it was possible to visually verify that the detector responded as the sample passed the detection window. In this experiment the buffer solution was a 50 mM phosphate buffer with 10 mM β-cyclodextrin (pH 7.2) as used in earlier experiments, discussed in Sections 0 and 6.6. The following steps were performed for a sample of 1 mM fluorescein; following which they were repeated with a sample of 1 mM eosine:

1. *Buffer flush:* the buffer solution was flushed for >10 minutes using the buffer flushing schemes as described in Section 6.7.3.
2. *Sample injection:* a sample was injected for 60 seconds, using the sample injection scheme discussed in Section 6.7.3; resulting in a 10 mm plug in the separation channel.
3. *Apply electric-field*: the separation electric-field was generated by applying a potential of 700 V along the channel length (0.085 m) yielding an electric-field strength of 8235 V m^{-1}.
4. *Measure detector response:* the response from the detector was recorded.

The response in Figure 105 showed that the detector was able to detect a concentration of 1 mM of fluorescein and eosine. It also indicated that it would not be possible to separate the two dyes with a single run along the channel. This was expected given that the channel length was relatively short.

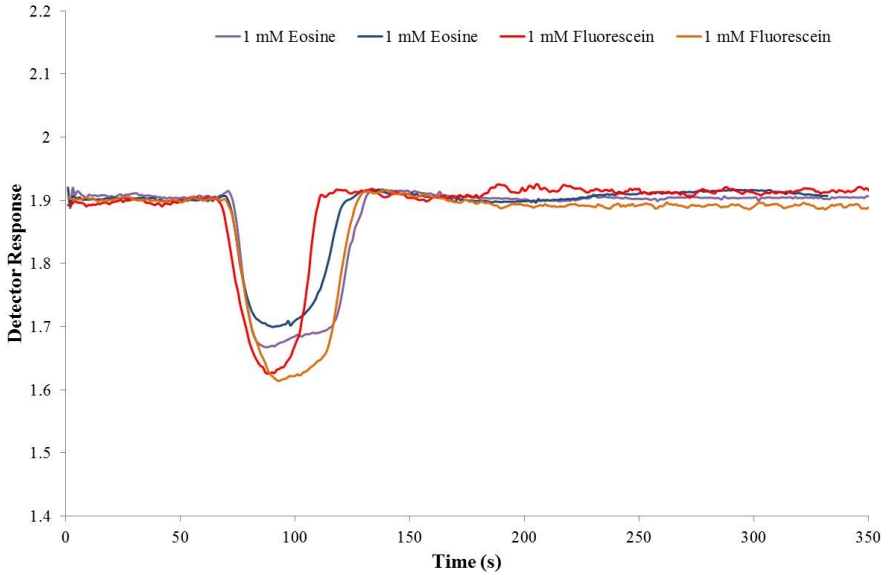

Figure 105: Electropherograms of four runs on Device 2, two showing the response for 1 mM fluorescein, and the other two showing the response to 1 mM eosine.

Figure 105 shows a set of results where the two dyes arrive at the detector at approximately the same time. Preliminary experiments with Device 2 showed that it was susceptible to significant temporal variability. The variability was attributed to differences in reservoir heights between experimental runs; a consequence of which would be an induced pressure driven flow along the channel, the velocity of which would be related to the fluid height in the reservoir. Earlier in Section 4.4.1.1, the effect of pressure driven flow on peak shapes was discussed; since the peaks do not show significant skewing, it was assumed that the pressure differences were small. Pressure differences were minimised by ensuring that the height of fluid in the reservoirs was the same for all reservoirs to avoid any pressure differences at the start of each experiment. Further to this, a channel cleaning scheme was run prior to each experiment. This cleaning scheme consisted of flushing the channel with buffer solution for 10 minutes. This helped clean the channels and removed any remaining sample solution from the channels.

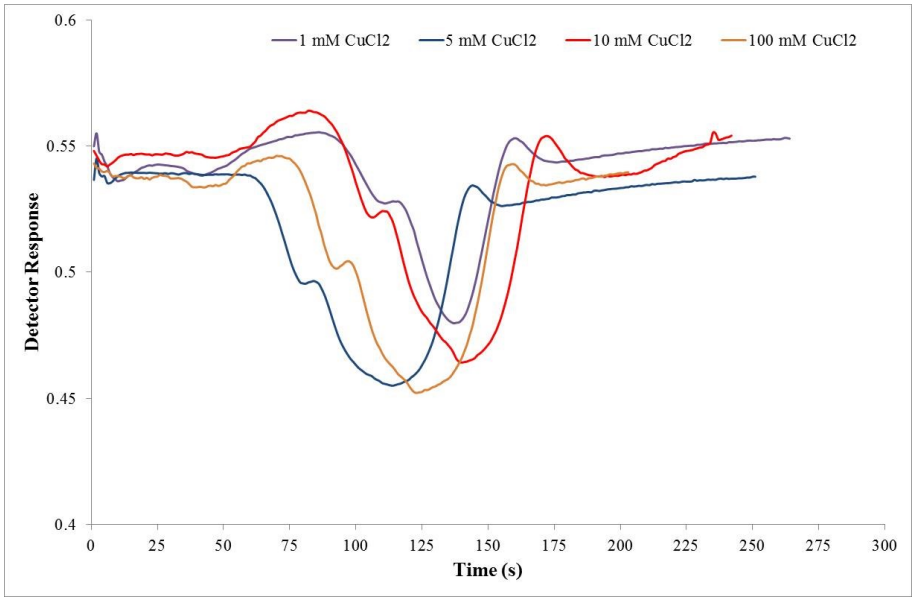

Figure 106: Electropherogram showing the detection of different concentrations of $CuCl_2$.

The methodology described above was also used to test a range of concentrations of a sample of $CuCl_2$. In Figure 106, the electropherogram shows that the detector is able to detect a sample of 1 mM $CuCl_2$. Prior to this experiment a sample of 0.1 mM was sent through the channel using an electric-field, but it was not possible to detect this. Increasing concentrations of $CuCl_2$ showed peaks with greater heights. The graph also shows that a higher concentration of $CuCl_2$ results in a broader peak. This could be attributed to diffusion, the extent of which is known to be proportional to the concentration gradient. There was some variation in the arrival time of the sample at the detector. As described earlier in this section, steps were taken to minimise the variation. Comparing the elution time with the concentration, there is no discernible correlation, therefore although the local EOF conditions (with respect to the sample) would be affected by sample concentration (as discussed earlier in Section 4.2); it was not the dominating cause of variability in this experiment. Whilst undesirable, due to the closed-loop nature of the proposed enhancement techniques, these variations would not be a significant issue. The four electropherograms in Figure 106 each consist of two overlapping peaks since the sample of $CuCl_2$ dissociates into Cu^{2+} and Cl^- ions. An explanation for the two peaks is that each peak shows the separation of the Cu^{2+} ions from the Cl^- ions. As discussed earlier, both anions and cations can migrate along the capillary or channel in the presence of a strong EOF.

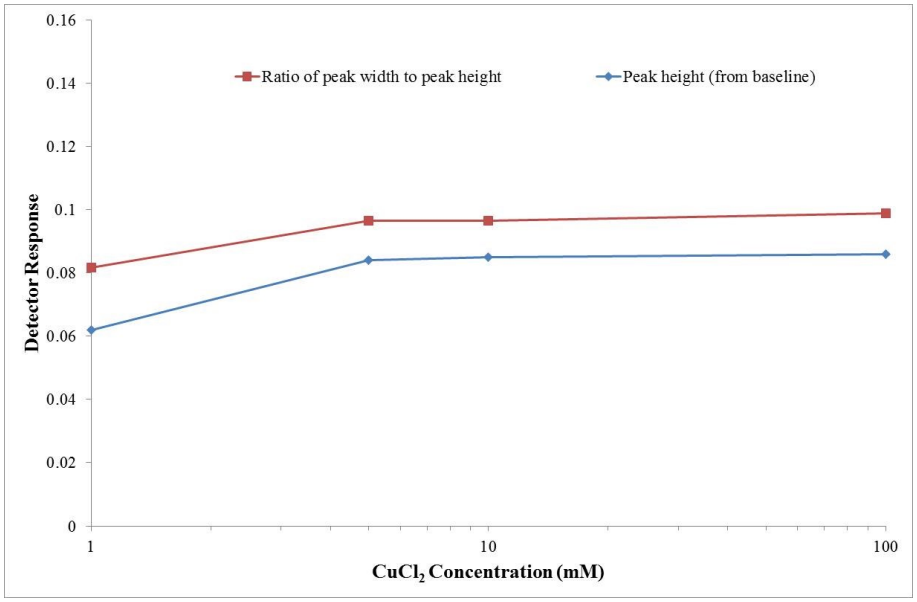

Figure 107: Graph showing detector response to an increase in $CuCl_2$ concentration. Plots for both the ratio of peak width to height, and the peak height (from baseline) are shown.

It was not deemed necessary to investigate the detection limits for this device since the use of polyimide tape as the electrode insulation layer meant that it was relatively thick. The detector response to an increasing $CuCl_2$ sample concentration (from 1 mM to 100 mM) is shown in Figure 107. As well as showing the peak height (from the baseline) the Figure 107 also shows a plot for the ratio of peak-width to height, since this is more reflective of the actual concentration. From a concentration of 5 mM to 100 mM a linear response can be observed. As discussed earlier in Section 2.1, the typical concentrations of metal ions in crevices are about 21 mM for ferric ions, and 79 mM for cupric ions. Therefore given that with a 100 um thick polyimide layer detection of 1 mM of Cu ions was possible and that the limits of detection would improve with the decrease in thickness of the insulation layer, this demonstrated that the detection system was fit for purpose. In the next section the limits of detection for the detector are discussed. The main difference between the detector systems on devices 2 and 3 was the insulation thickness. The electrode layout and detection circuitry remained the same. It was expected that the thinner insulation layer on the next device (Device 3) would show improved performance.

6.7.5. Experiment 3: Investigating Effect of ZPM Electrode on Migration Time

Further to the primary aims requested of this device, an investigation was launched to ascertain the effect of applying a potential to the ZPM electrode even though the insulation was significantly thicker than that presented by other researchers investigating EOF modification using external electric-fields [48, 49, 188].

Using a 50 mM phosphate buffer solution (pH 7.2), and a sample of fluorescein, the experiment consisted of the following steps:

1. *Buffer flush:* the buffer solution was flushed for >10 minutes using the buffer flushing schemes as described in Section 6.7.3.
2. *Sample injection:* a sample of fluorescein was injected for 30 seconds, using the sample injection scheme discussed in Section 6.7.3; resulting in a 10 mm plug in the separation channel.
3. *Apply electric-field*: the separation electric-field was generated by applying a potential of 700 V along the channel length (0.085 m) yielding an electric-field strength of 8235 V m^{-1}.
4. *Measure detector response:* the response from the detector was recorded.

The above steps were conducted for two cases. In the first, –100 V was applied to the ZPM electrode. In the second, +100 V was applied to the ZPM electrode. The results from these experiments can be seen in Figure 108, which shows that applying –100 V to the ZPM electrode decreased the migration time of the fluorescein dye, compared to applying +100 V. It was encouraging to see that the potential applied to the ZPM electrode had some effect on the migration time, and therefore the EOF. The change in EOF that could be affected with this device meant that whilst it was possible to enhance and reduce the migration time, it was not possible to reverse the direction of the EOF.

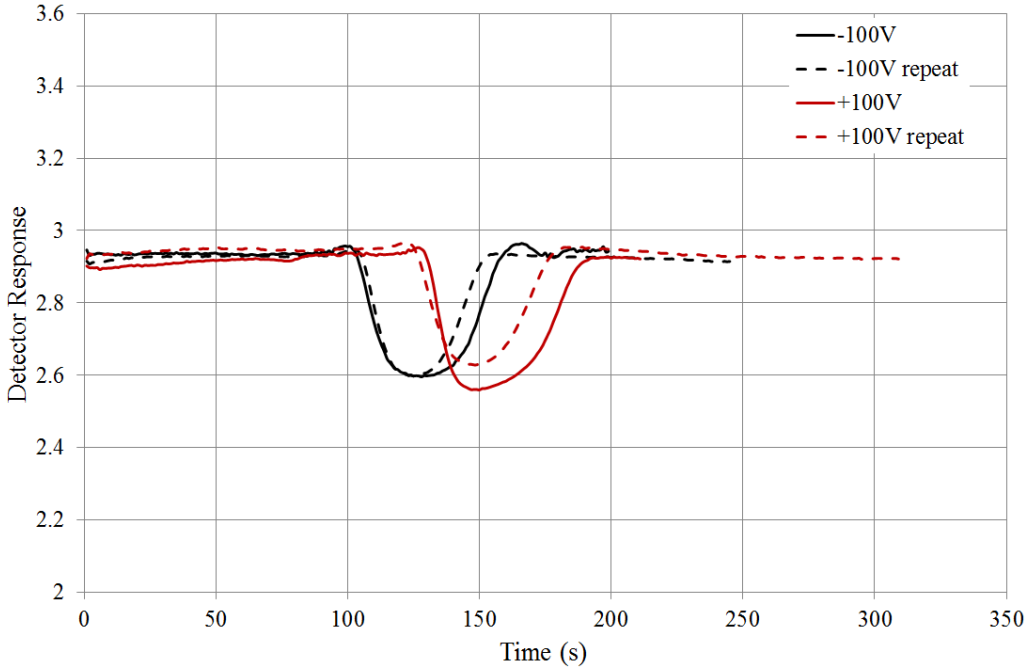

Figure 108: Electropherograms for a sample of fluorescein showing different arrival times of the sample at the detector, for different potentials on the ZPM electrode.

The design of this device and experimental results, alongside a discussion about the separation enhancement methods were presented by the author at an oral presentation at the 13th International Meeting on Chemical Sensors (IMCS-13), Perth, Australia [278].

6.7.6. Outcomes from Experiment 3

Device 2 served as an engineering prototype to test the setup of the detection system, HVPS and fluid pumping system in parallel with the fabrication of Device 3. The channel dimensions were identical to those of Device 3 the primary difference was that the insulation layer between the electrodes and microfluidic channel was significantly larger. The use of a thinner insulation layer would be beneficial for both the detection system and the control of the EOF via ZPM. Proving the detection system on Device 2 was a good indicator that it would work when implemented into Device 3.

The main function of the detection system was to detect the presence of ions in the channel. This was required to inform the control system when to switch the direction of the EOF. As discussed in Section 2.4.4.1., the identification of the ions was to be performed following separation using electrochemical methods. On Device 2, it was possible to show that the detectors were able to detect the presence of ions in the channel through the 100 µm thick insulation layer.

A computer controllable HVPS was built which enabled the development of a control system which was integrated with the detection system. As described earlier in Section 6.7.4 the HVPS consisted of two HV DC-to-DC modules; one to supply the high voltage for the separation electric field, and the other to provide the voltage to the ZPM electrode. The potential output from the HV DC-to-DC converters was controlled using the output ports from the National Instruments DAQ card. A potential from the ports between 0 – 10 V set the output of the HV DC-to-DC converters from 0 V to their full-scale voltage. This system was able to autonomously control both the separation voltage and ZPM voltage. Further to testing the device with basic CE operation, the LabView program was modified so that it could switch the EOF a predetermined number of times. The event to trigger the switch was when a dye entered the detection window. This control system would be capable of autonomously sending a sample between the detectors a controllable number of times. To perform this autonomously the LabView program was written such that it would switch the potential on the ZPM electrode when the detectors saw a peak; this would signify that a sample was entering a detection window. Each switching event would be triggered when the differential of the detector response exceeded a threshold value. After a set number of events the sample would be passed through the end detector to evaluate the effect that the number of cycles has on the separation. Images of the LabView program designed to perform this routine are included in Appendix D.

Whilst it was believed that the insulation layer may be too thick to significantly affect the zeta-potential through application of a voltage on the ZPM electrode, an experiment was run to investigate this. It was shown that it was possible to alter the zeta-potential slightly but not to reverse it for the conditions used.

The micro-pump was proven to be capable of flushing the microfluidic device by setting it up to create a negative pressure on the sample waste reservoir. Using dyes it was possible to observe that all the channels were flushed, however, it was noticed that due to the larger hydraulic resistance of the longer separation channel, the fluid flow along it was less than along the shorter sample injection channel.

6.8. Experiment 4: Characterise Ability to Modify the EOF with a Planar ZPM Electrode

6.8.1. Aims of Experiment 4

The aim of Experiment 4 was to investigate the ability to control the EOF using a planar ZPM electrode. The tests for Experiment 4 were conducted on Device 3, the fabrication of which is discussed next. Device 3 was designed to investigate Experiments 4, 5 and 6; the latter two being discussed in Sections 6.9 and 6.10 respectively. The aims of the experiments were summarised earlier in Table 12, Section 6.1.

6.8.2. Fabrication of Device 3

The electrode layout for Device 3 was the same as for Device 2, however the fabrication method was significantly different to enable the placement of the ZPM and detection electrodes close (~1 μm) to the microfluidic channel.

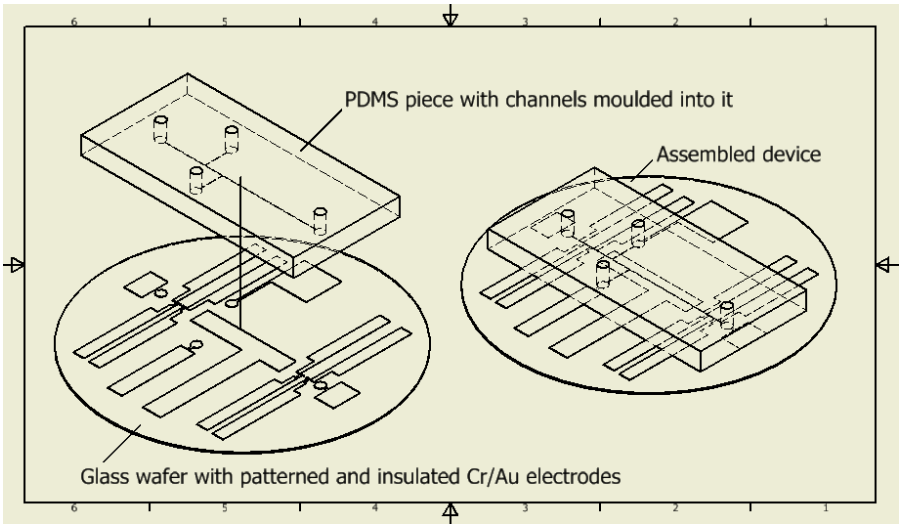

Figure 109: 3D drawing of Device 3; the dimensions for patterned glass are given in Figure 111 and the dimensions for the PDMS piece are given in Figure 114.

A 3D drawing of Device 3 can be seen in Figure 109. The device was composed of two parts: a glass wafer onto which metal electrodes were patterned and a moulded PDMS piece which housed the microfluidic channels. An advantage PDMS has over many other polymers is that due to its elastomeric nature, it is possible to reversibly seal the PDMS to flat surfaces. A reversible bonding method was deemed highly advantageous at this stage in the development since it would enable modifications to be made easily and without the

requirement to manufacture a new device for each design change. An additional advantage of being able to remove the channel from the wafer was that it gave direct access to the channel. This was useful for removing blockages within the channel [89]. For early stage testing purposes it was decided that the reversible bonding would be useful since it makes it possible to disassemble the device for cleaning. A method for permanently bonding the PDMS channel to SU-8 is described in Appendix F

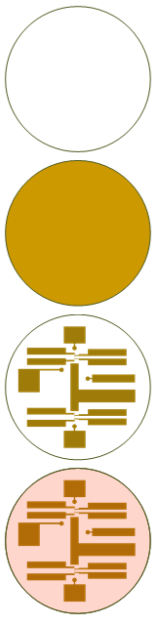

Start with clean glass wafer.

Evaporate Cr and Au onto glass wafer.

Spin photoresist, bake and expose via mask, develop then etch Au and Cr.

Spin, pre-exposure bake, expose (via mask), post-exposure bake, develop, and hard-bake insulating layer of SU-8.

Figure 110: Process to pattern gold electrodes and SU-8 insulation layer on a glass wafer.

The glass wafer was fabricated using standard lithographic techniques in a cleanroom. The process for patterning the glass wafer with metal electrodes and insulating them is illustrated in Figure 110 and described in detail below:

1. *Clean wafers:* To clean the wafers, they were immersed in fuming nitric acid for 15 minutes, following this they were rinsed thoroughly with DI water and dried.
2. *Metal deposition:* Gold is known to have a poor adhesive strength to glass; therefore, to get good adhesion, an adhesive layer is typically used [239]. Chromium and titanium are commonly used to improve the adhesion of gold to glass and silicon [239]. For Device 3, a 20 nm layer of chromium was evaporated onto the glass, immediately following this 200 nm of gold was evaporated.
3. *Process the photoresist*: To define the electrodes a photoresist was spun onto the metallised wafer, the steps for this process were:
    a. Bring the AZ9260 photoresist to room temperature.

- *Typically, photoresists are stored at cooler temperatures to prolong their lifetime. They need to be brought to room temperature before use since their viscosity is strongly related to temperature and the viscosity is related to the resulting thickness of the spun on layer.*

b. Put the metallised glass wafer in an oven at 210 ˚C for a dehydration bake; this removes moisture from the wafer.

c. Spin the positive photoresist AZ9260:

- Spin at 500 rpm (acceleration of 250 rpm/sec) for 5 seconds.
- Spin at 4000 rpm (acceleration of 1750 rpm/sec) for 60 seconds.
- Spin at 500 rpm (deceleration of 1750 rpm/sec) for 5 seconds.

d. Bake the wafer at 110 ˚C for 120 seconds.

e. Expose the wafer to UV light for 30 seconds via an acetate mask (technical drawing shown in Figure 111).

f. Develop the resist using AZ400K developer in a 1:3 ratio to DI water; this removes the resist which was exposed to the UV.

4. *Wet etch metal:* The areas where there was no photoresist to protect the metal layers became etched during the etching process; this left the electrode pattern on the glass wafer.

a. *Gold etch:* the gold etchant used was a KI etchant diluted 1:2 with DI water. The gold etch took approximately 45 seconds.

b. *Chrome etch:* the chrome etchant was a standard solution containing acetic acid and ceric ammonium nitrate, used neat. The chromium etch took approximately 30 seconds.

c. Following each etch step the wafers were thoroughly rinsed with DI water.

5. *Remove photoresist:* The AZ9260 photoresist was removed by immersing the wafer in AZ100 remover for 60 seconds. A photograph of the glass wafer with the patterned gold electrodes is shown in Figure 112.

6. *Process the thin insulation layer:* To insulate the ZPM and detection electrodes a thin layer (~1 μm) of SU-8 was spun onto the surface. The steps for processing this insulation are described below:

a. Bring TI PRIME (adhesion promoter) and SU-8 photoresist to room temperature.

b. Dehydrated the wafer in an oven at 210 ˚C.

c. Spin TI PRIME layer:

- Spin at 500 rpm (acceleration of 100 rpm/sec) for 5 seconds.

- Spin at 2000 rpm (acceleration of 500 rpm/sec) for 60 seconds.
- Spin at 500 rpm (deceleration of 500 rpm/sec) for 5 seconds.

d. Bake TI PRIME layer on hotplate at 120 ˚C for 120 seconds.

e. Spin SU-8 (SU-8-2000.5) photoresist:

- Spin at 500 rpm (acceleration of 100 rpm/sec) for 5 seconds.
- Spin at 5000 rpm (acceleration of 300 rpm/sec) for 30 seconds.
- Spin at 500 rpm (deceleration of 500 rpm/sec) for 5 seconds.

f. Pre-exposure bake: bake resist on hotplate at 65 ˚C for 60 seconds, and then ramp temperature up to 95 ˚C and bake for a further 180 seconds.

g. Expose wafer and resist to UV light with i-line filter via an acetate mask for 25 seconds.

h. Post-exposure bake: bake resist on hotplate at 65 ˚C for 60 seconds, and then ramp temperature up to 95 ˚C and bake for a further 180 seconds.

i. Develop the photoresist in EC solvent. This process takes 20-30 seconds during which the solution was agitated.

j. Rinse wafer with IPA.

k. Blow dry with nitrogen.

l. Hard bake wafer at 150 ˚C for 60 minutes.

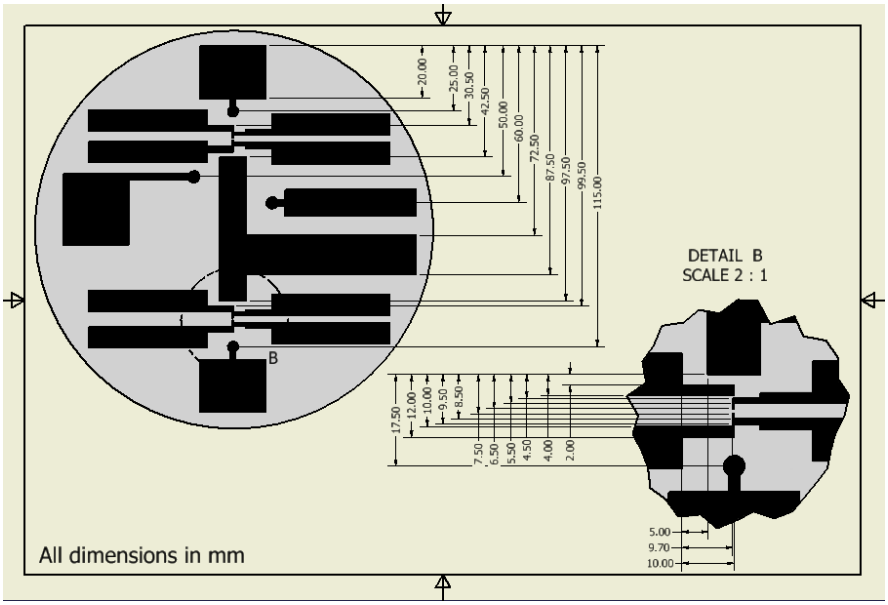

Figure 111: Technical drawing of acetate mask for Device 3 for defining metal electrode pattern.

A thin insulation layer benefits the detection system by providing larger wall capacitances and enables a greater effect on the zeta-potential (and consequently the EOF) by the potential on the ZPM electrode.

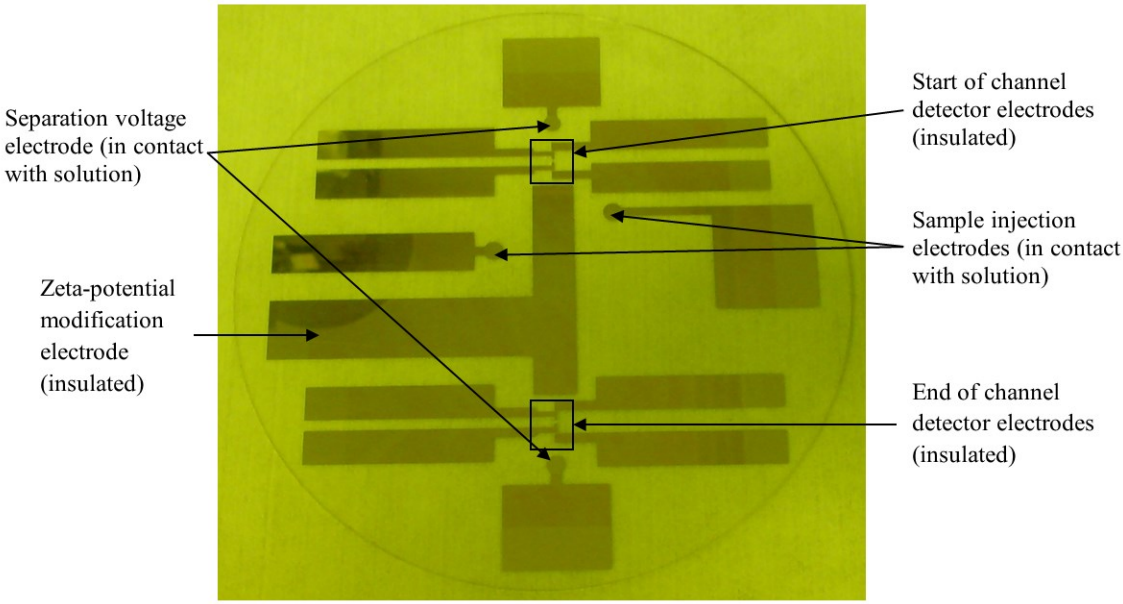

Figure 112: Glass wafer with electrodes patterned in chromium-gold covered with a layer of patterned SU-8.

To fabricate the moulded PDMS piece containing the microfluidic channels the Dow Corning Sylgard™ 184 two part elastomer kit was used. Originally a mould was created using the Connex 350 3D printer. A technical drawing of the mould can be seen in Figure 113. Unfortunately the high surface roughness of the resulting mould prevented the moulded PDMS pieces from adhering to the insulated metal-patterned glass wafer surface. It was decided that the quickest method to proceed to produce a suitable mould would be to create one using SU-8 on a glass wafer given that the necessary fabrication skills for this task had been gained in the development through the processing of the glass wafer.

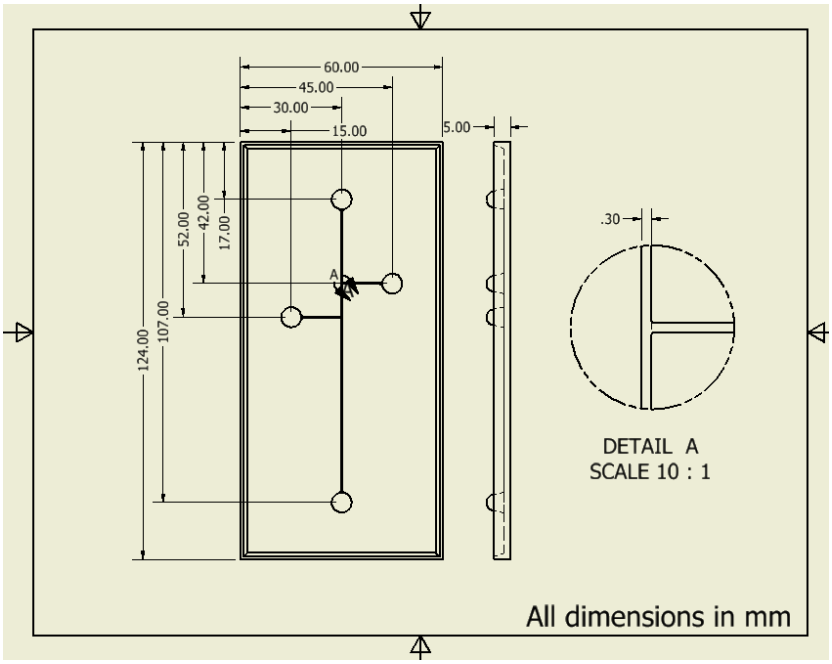

Figure 113: Technical drawing of the mould which was 3D printed.

A similar process as used for the fabrication of the thin insulation layer (described in step 6 earlier in this section) was used for the creation of the SU-8 mould which was required for the fabrication of the PDMS piece. The differences in the process were that:

- step 6e was changed to:
  - Spin SU-8 (SU-8-50) photoresist:
    - Spin at 500 rpm (acceleration of 100 rpm/sec) for 5 seconds.
    - Spin at 3000 rpm (acceleration of 300 rpm/sec) for 30 seconds.
    - Spin at 500 rpm (deceleration of 500 rpm/sec) for 5 seconds.
- Step 6f was changed to:
  - Pre-exposure bake: bake resist on hotplate at 65 ˚C for 5 minutes, and then ramp temperature up to 95 ˚C and bake for a further 15 minutes.
- Step 6g was changed to:
  - Post-exposure bake: bake resist on hotplate at 65 ˚C for 1 minute, and then ramp temperature up to 95 ˚C and bake for a further 4 minutes.
- Step 6i was changed to:
  - Develop the photoresist in EC solvent. This process takes 60 seconds during which the solution was agitated.

A technical drawing of the mask used for the UV exposure of the SU-8 for the PDMS mould is shown in Figure 114.

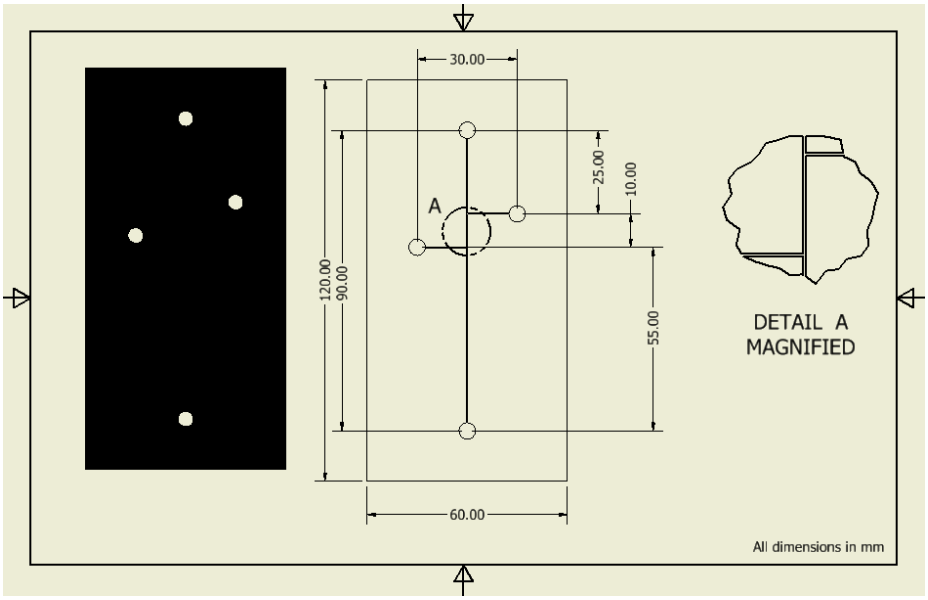

Figure 114: Technical drawing of the mask to pattern the SU-8 for the PDMS mould.

Once the mould was prepared, the next step was to use it with the PDMS to create the microfluidic channel. The process for creating the PDMS piece was:

1. *Prepare the PDMS:* The PDMS was prepared by mixing in a 10:1 ratio the PDMS elastomer and curing agent (Sylgard™ 184 silicone elastomer kit). The mixing process introduced bubbles into the PDMS mixture; these were removed by placing the mixture into a vacuum desiccator.
2. *Pour PDMS into mould:* Following the removal of the bubbles, the mixture was poured onto the SU-8-on-glass mould.
3. *Cure the PDMS:* The PDMS filled mould was then placed into an oven at 150 ˚C for 10 minutes. The curing temperature and time were based on information from the Sylgard™ 184 silicon elastomer kit datasheet [244].

The microfluidic reservoirs were formed by punching a hole through the PDMS piece after the moulding process. Following the fabrication of the PDMS piece, it was carefully positioned over the glass wafer and pressed down gently to seal the channel.

The PDMS piece was designed to have similar dimensions to Device 2, with a width of 300 µm, a depth of 50 µm and a length of 85 mm.. On Device 2, the microfluidic reservoirs were tapped which allowed the connection to the micro-pump via a tapped connector. The elastomeric nature of the PDMS meant that it did not possess the mechanical strength to

support a thread and so to connect the PDMS pieces to the micro-pump, a tapered fluidic connector was gently pushed into the reservoirs.

6.8.3. Experiment 4: Modification of EOF using Planar ZPM Electrode

To prove the concepts described in this thesis, control of the EOF needed to be characterised and evaluated. To achieve this, the potential on the ZPM electrode was varied whilst the effect on the EOF was measured by monitoring the migration time of an ionic species. The ionic species used in this experiment was the electrophoretic dye, eosine. It was selected due to its strong red-pink colour which makes its position in the microfluidic channel easy to identify. The buffer solution used was a 50 mM phosphate buffer with 10 mM β-cyclodextrin (pH 7.2).

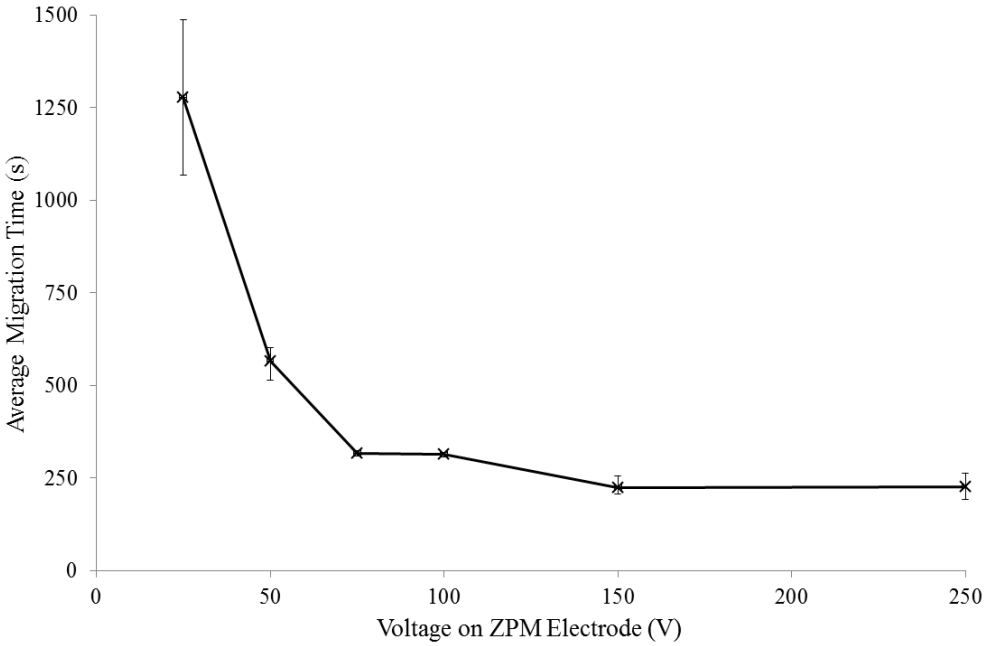

Figure 115: Effect of voltage on the ZPM electrode on the migration time for eosine.

The experimental methodology was:

1. *Buffer flush:* At the start of the experiment the device was flushed with buffer solution using the micro-pump to create a negative pressure on the sample waste reservoir. This process was similar to the pumping process described in Section 6.7.3 except that the tapped adapter was replaced with a tapered one.
2. *Electrokinetic buffer flush:* A potential of 300 V was applied along the channel to generate an electric-field (3750 V m^{-1}) to flush the buffer solution through the channel for at least 10 minutes.

3. *Sample introduction:* 100 μL of the sample was injected into the sample injection reservoir using a micropipette.
4. *Sample injection:* An electric-field was applied between the sample injection reservoir and sample waste reservoir until it could be seen that the sample had spread across the sample injection part of the separation channel. The voltage applied to the sample injection reservoir was 300 V and took ~30 seconds to complete the injection.
5. *Apply electric-field*: An electric-field was applied along the separation channel; the voltage applied to create this field was 300 V, resulting in an electric-field strength of 3750 V m^{-1}.
6. *Measure migration time:* With the electric-field established along the separation channel the dye moved towards the end of the channel. The time taken for the migration from the injection point to the detector at the end of the channel was recorded for each ZPM voltage tested.

After one migration time was recorded for an applied ZPM voltage, another two were obtained by repeating steps 4 to 6. Following each group of three experiments, the process was repeated for each ZPM voltage tested.

The results from this experiment can be seen in Figure 115. They show that as the voltage on the ZPM electrode is increased from 25 V to 250 V, the EOF increases, as evident by the decrease in the recorded migration time. The characteristics of the graph are as expected. There are limits at both extremes, with a low and high voltage applied to the ZPM electrode. As the voltage on the ZPM is made lower eventually there will be a point where the EOF approaches zero and after this a further reduction in the ZPM voltage will reverse the EOF. The migration time increases as this point is approached until eventually the ions no longer move down the channel. At the other extreme, as the voltage is increased there is a limit to how much the double layer can physically be enhanced (and therefore the EOF). It can be seen in Figure 115 that good control of the EOF can be obtained by setting the ZPM voltage between 25 V and 150 V.

Using the same starting conditions as above, another experiment was run to show the effect of applying a large negative voltage to the ZPM electrode. A sample of eosine was injected into the channel and with no potential on the ZPM electrode and 350 V across the channel; the sample migrates toward the buffer waste reservoir. After a short period of time a potential of -350 V was applied to the ZPM electrode, this had the effect of reversing the EOF and the dye could be seen moving back up the channel. Before the sample got back to

the sample injection point, the ZPM was turned off. This experiment was recorded using a video camera. A series of images taken from the video can be seen in Figure 116. In the figure:

(a) shows the sample injected at the start of the experiment just before the separation electric-field is applied.

(b) after 1 minute the sample had travelled some distance along the channel, after which the EOF was reversed (by applying -350 V to the ZPM electrode).

(c) after 20 seconds the dye had moved back toward the point of injection at which point the ZPM voltage was turned off thus returning the EOF back to its original state.

(d) after 2 minutes the sample travelled further along the channel,

(e) with the EOF reversed again, the sample is sent back to the position shown in image (e).

(f) the voltage applied to the ZPM electrode was then turned off and after a further 4 minutes and 10 seconds, the sample has travelled further along the channel.

(g) for the final time the EOF was reversed, this time for 3 minutes, in which time the dye travels back to the injection point.

(h) the sample was then sent down the entire length of the channel, it can be seen leaving the channel and entering the buffer waste reservoir.

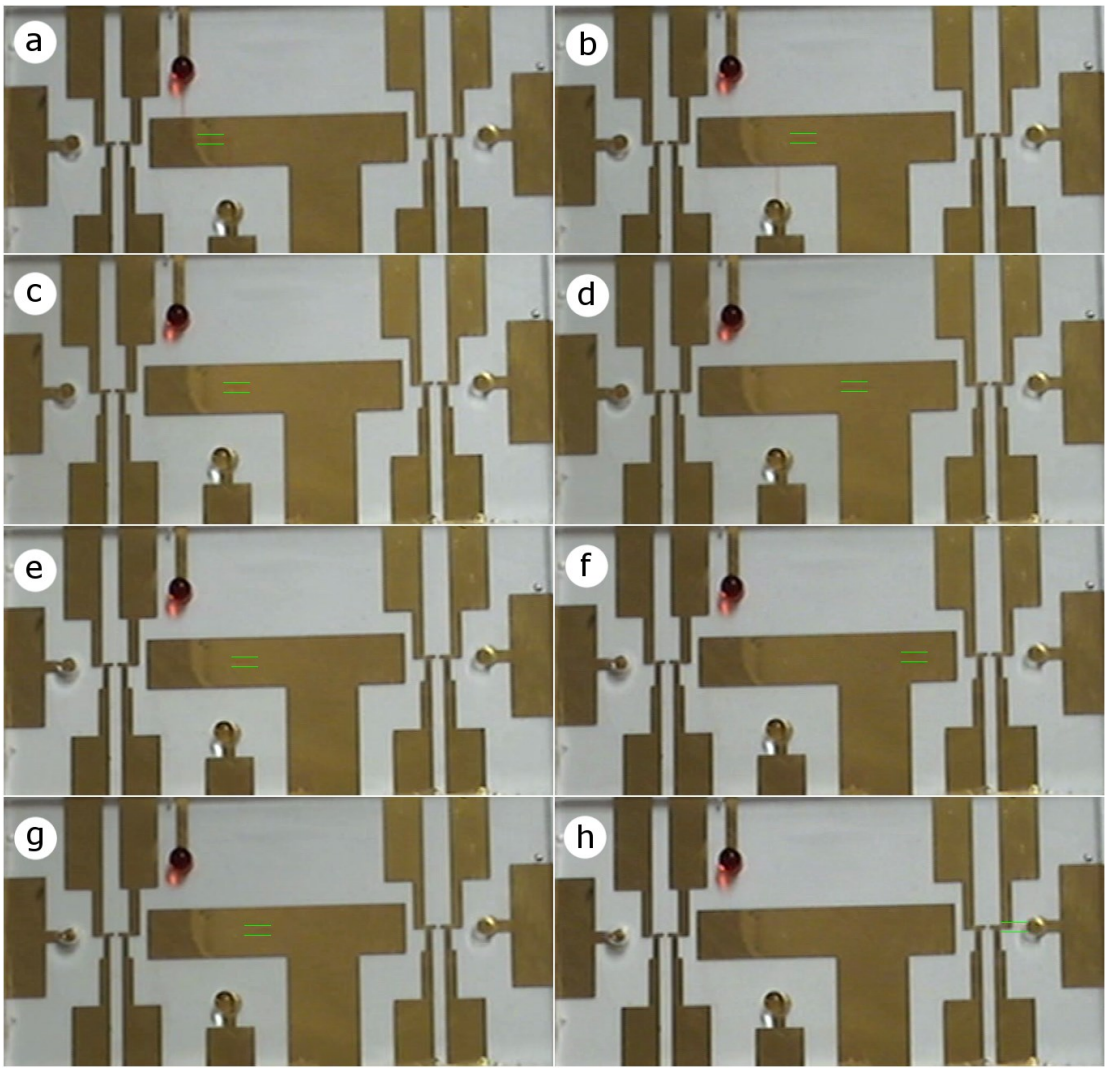

Figure 116: Photographs showing migration of eosine dye in both directions along the channel; (a) t = 0 s, (b) t = 60 s, (c) t = 80 s, (d) t = 200 s, (e) t = 285 s, (f) t = 535 s, (g) t = 715 s and (h) t = 1130 s. Dye position highlighted by two green bars either side of the channel.

The sample was not sent further back along the channel length than to the end of the sample injection area. This was to ensure that the sample could not leave the separation channel, due to pressure differences with respect to the sample injection channel.

6.8.4. Outcomes from Experiment 4

Standard microfabrication techniques were investigated and used for the development of Device 3. This device was composed of two parts: a glass wafer, onto which metal electrodes were patterned and selectively insulated; and a PDMS piece containing microfluidic channels. One advantage of PDMS was that it could be reversibly sealed to the

wafer. The electrodes were patterned on a glass wafer using a wet etching technique. With this device the ability to modify the EOF was characterised. It was shown that the EOF could be enhanced, reduced and even reversed using a single planar electrode.

6.9. Experiment 5: Evaluate Performance of Detection System

6.9.1. Aims of Experiment 5

The aim of Experiment 5 was to investigate the limits of detection for the CCD system. Following which it would be possible to verify whether the detector would be fit for the purpose; i.e. capable of detecting ionic species with concentrations down to the mM region, as discussed in Section 2.1.

6.9.2. Experiment 5: Measuring the Limits of Detection for the Detection System

Earlier in Section 6.7 the setup of the detection system and the post-acquisition processing within the LabView software environment was discussed. To measure the limit of detection of the detector implemented into Device 3, its response to a range of concentrations of sodium chloride (NaCl) was measured. The concentration was stepped up from 500 μM to 1 M. For each level of concentration the following steps were conducted:

1. *Flush channels with deionised water:* the channels were flushed with deionised water using the pumping scheme as described in Section 6.7.3.
2. *Flush channels with NaCl:* the channels were flushed with the required concentration of NaCl using the pumping scheme as described in Section 6.7.3.
3. *Measure detector response:* the response from the detector was recorded.

Following step 1, the detector response was monitored to ensure that the detector response had returned to the start value. A graph of the detector response can be seen below in Figure 117. NaCl was used since this project places an emphasis on a device for marine applications. Sea water has a chloride concentration of approximately 0.6 M; in this region it can be seen that the detector gives a significant response. The inset graph of Figure 117 shows that for concentrations from 200 μM to 1 mM of NaCl the detector response varied from 3.20 to 3.30. At higher concentrations the response will reach a maximum, however only NaCl concentrations up to 1 M were tested since it was the lower limit of detection

which was of greater interest. With the detection system and LabView program set up as discussed in Sections 5.1.4 and 6.7.4, it was difficult to measure changes in detector response below a 0.1 step. At low concentrations (< 1 mM), the amplitude of the signal from the transimpedance amplifier became comparable with the amplitude of the electrical noise (sources of electrical noise are discussed below). A simple method to improve the limit of detection would be to increase the amplitude of the input signal; this was deemed unnecessary since the concentration levels of ions found in corroding crevices is usually > 1 mM as discussed in Section 2.1.

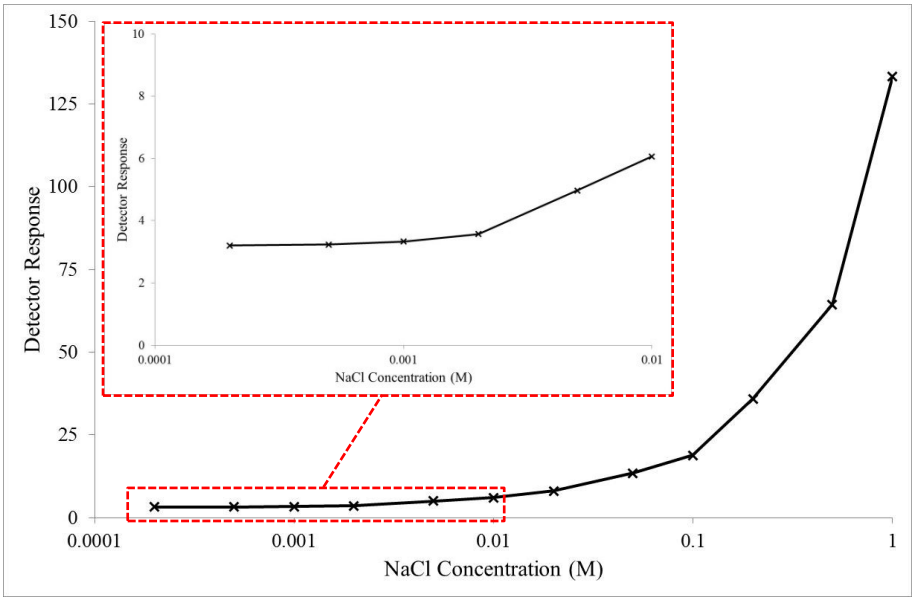

Figure 117: Detector response for range of values of NaCl concentration filling the channel. Inset graph shows response at lower concentrations on an expanded scale.

Electrical noise results in a fluctuation in electrical signals; there are a number of sources of electrical noise such as thermal, shot and flicker noise [279]. A limit on the detection system occurs where the change in the level of the signal being monitored becomes comparable to the amplitude of the electrical noise level. Therefore it is not possible to determine if the variation in the signal is due to electrical noise, or because of a change in the signal being monitored (due to a change in conductivity). Thermal noise (or Johnson noise) occurs due to thermal agitation of charge carriers (e.g. electrons) within electrical conductors [279]. Defects such as impurities within conductive channels which may develop during semiconductor processing steps can lead the generation of flicker noise (or 1/f noise) [280]. Flicker noise is only important at low frequencies; for example less than 2 kHz for bipolar transistor [280]. Another source of noise is shot noise, which occurs due to the discrete nature of electric charge; typically shot noise is insignificant when compared with other

noise sources such as thermal and flicker noise [281, 282]. Inductors and capacitors make electronic circuits susceptible to noise (e.g. crosstalk) from electromagnetic sources [283, 284]. To reduce the inductive and capacitive coupling of the electromagnetic signals the electronic circuitry may be placed in shielded housing, which is connected to ground [285]. This diverts the electromagnetic interference to ground via a low-impedance path. In addition to this, shielded cables are also often used to reduce the pickup of electromagnetic interference [285]. For the detection circuit which was operated at 10 kHz, transit time noise can be neglected since it is only important at frequencies at and above the VHF range [286]. Further to this, avalanche noise can also be neglected since it is produced when junction diodes are operated at the onset of avalanche breakdown and there are no diodes in the detection circuitry operating in this region [286]. Another type of noise is burst noise (or popcorn noise), the main characteristic of burst noise is that it consists of step-like transitions between two or more discrete levels [287]. The main characteristic of burst noise is that it consists of step-like transitions between two or more discrete levels [287]. The design of the detection circuitry was described in Section 5.2, of the noise sources discussed here, thermal and electromagnetically coupled noise are considered to the main contributors which should be minimised in order to improve the limits of detection.

To calibrate the limits of detection in terms of conductivity, the conductivity for the different concentrations of NaCl were measured using two conductivity probes. The conductivity probes were purchased from Hanna Instruments Ltd., they were models HI 98303 and HI 98304. These are capable of measuring to 0.1999 S m^{-1} and 1.999 S m^{-1} respectively [288]. The conductivity of NaCl solution was measured for concentrations ranging from 200 μM to 1 M, and the results displayed in Figure 118 show a trend comparable to that of Figure 117. The detector was able to measure a change in conductivity for concentrations above 1 mM. At a concentration of 1 mM, the conductivity was measured as 0.01 S m^{-1}, therefore this is the limit of detection for the detection system on Device 3. This demonstrated that the detection system would be capable of measuring the ion concentrations typical with crevice corrosion as discussed in Section 2.1.

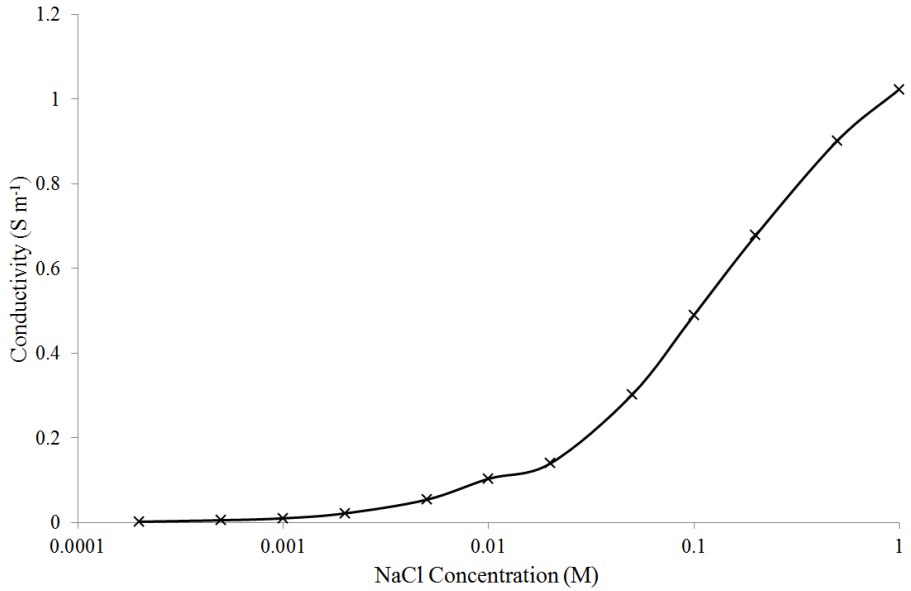

Figure 118: Plot showing the variation in conductivity for a NaCl solution versus its concentration measured with conductivity probe.

The same methodology as described earlier in this section was used to investigate the effect of increasing the concentration of $CuCl_2$. The change in conductivity for a range of values of concentration from 200 µM to 1 M was measured, the results of which can be seen in Figure 119. Above 0.1 M the response plateaus which means that the detector is capable of measuring changes in $CuCl_2$ concentrations from 200 µM to 0.1 M. The inset graph in Figure 119 shows that for a concentration change from 200 µM to 500 µM no change in the detector response was observed. The values of Cu ions in a corroding crevice were expected to be approximately in the tens of mM (as discussed earlier in Section 2.1), in this region the detection system gives a good response and therefore this detection system is appropriate for the application.

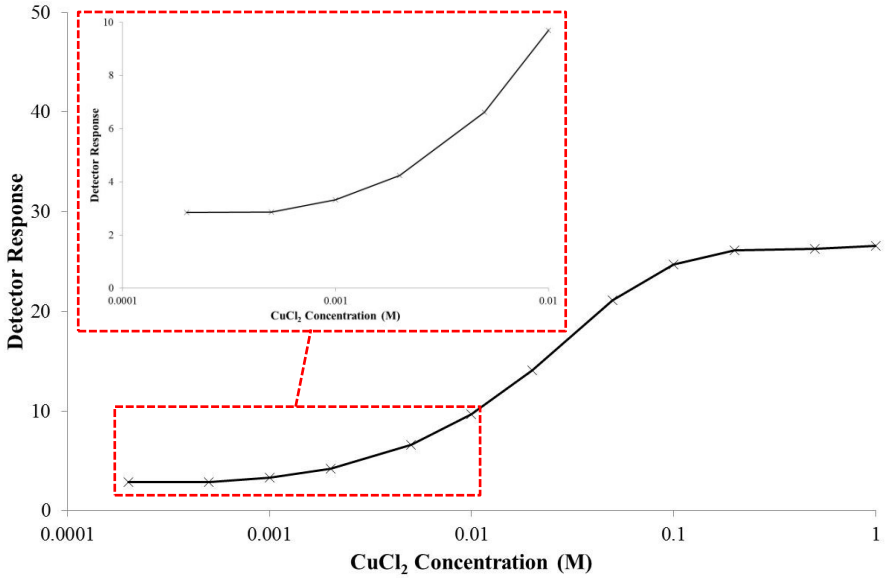

Figure 119: Detector response for range of values of $CuCl_2$ concentration filling the channel. Inset graph shows response at lower concentrations on an expanded scale.

The change in conductivity versus $CuCl_2$ concentration was measured using the Hanna Instruments Ltd. conductivity probes (models HI 98303 and HI 98304 as described earlier in this section), a graph showing the relationship can be seen in Figure 120.

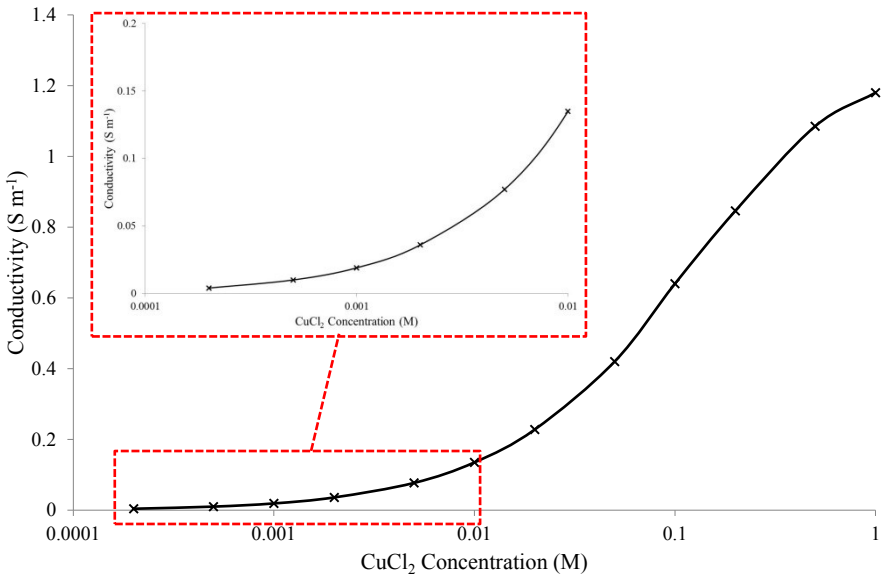

Figure 120: Plot showing the variation in conductivity for a $CuCl_2$ solution versus its concentration measured with conductivity probe. Inset graph shows conductivity at lower concentrations on an expanded scale.

6.9.3. Outcomes from Experiment 5

The limits of detection were measured using NaCl; a chloride salt being chosen since this anion would typically be the more prevalent in the envisioned application area of marine corrosion monitoring. It was demonstrated that the detection system was capable of measuring copper and sodium chloride ion concentrations down to 1 mM; this corresponds to a lower limit of detection of 0.01 S m^{-1}. For the ions of interest, the concentrations typically seen in corroding crevices will be higher than this value, as discussed in Section 2.1.

6.10. Experiment 6: Demonstrate Separation and Detection of Low Concentration of a Metal Ion Sample

6.10.1. Aims of Experiment 6

The aim of Experiment 6 was to separate and detect a sample of low concentration of metal ions. Following this, the results could be compared to the computation model described in Chapter 4.

6.10.2. Experiment 6: Separation and Detection of $CuCl_2$

An experiment investigating the separation and detection capability of Device 3 was devised. It was useful to compare the results of the separation of a low concentration of metal ions (example sample being 10 mM $CuCl_2$) with the computation models discussed in Section 4.4.

Originally the experiment was carried out with a 50 mM phosphate buffer solution (pH 7.2); however this caused the sample of $CuCl_2$ to precipitate out of the solution. To overcome this issue the buffer was substituted with deionised water for this experiment. This was not ideal since the conductivity of deionised water is lower than that of the $CuCl_2$ sample; as can be seen from in inset graph in Figure 120 the conductivity of a sample of 10 mM $CuCl_2$ is 0.02 S m^{-1}. A further concern is that the pH of deionised water is easily modified and is not considered a good buffer. Based on work by Wharton *et al*. a sample concentration of 10 mM $CuCl_2$ was used since it is comparable to the concentration levels of $CuCl_2$ expected within a corroding NAB crevice (as discussed earlier in Section 2.1) [7]. As discussed in Section 2.4.4, Nie *et al.* used buffers with CTAH and TMAH added, for the separation of

metal ions, including $CuCl_2$. It was felt that the use of this buffer would increase the complexity of the chemistry in the channel and introduce a number of unknowns. For example, the effect of the complexation of the Cu^{2+} ions alters their mobility and conductivity. Further to this, it could not be reliably predicted how the surfactants in the buffer solution would affect the PDMS channel walls [43, 88].

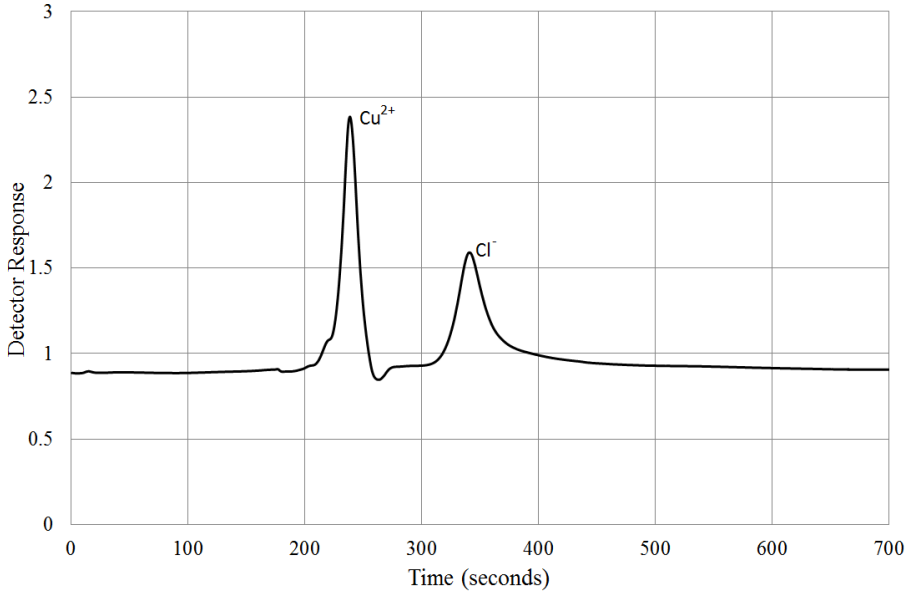

Figure 121: Electropherogram showing separation of 10 mM $CuCl_2$. The detector response has been inverted unlike earlier detector responses. This was done because in the literature electropherograms are usually a plot of changes in conductivity rather than resistivity.

The experiment consisted of the following steps:

1. *Flush channels with deionised water:* the channels were flushed with deionised water using the pumping scheme as described in Section 6.7.3.
2. *Electrokinetic flush:* A potential of 350 V (resulting in an electric-field strength of 4375 V m^{-1}) was applied along the channel to flush the solution through the channel for at least 10 minutes.
3. *Sample introduction:* 100 µL of the sample was injected into the sample injection reservoir using a micropipette.
4. *Sample injection:* An electric-field was applied between the sample injection reservoir and sample waste reservoir for ~30 seconds.
5. *Apply electric-field*: An electric-field was applied along the separation channel; the voltage applied to create this field was 350 V, resulting in an electric-field strength of 4375 V m^{-1}.

6. *Monitor detector:* With the electric-field established along the separation channel the sample moved towards the end of the channel. The change in conductivity of the solution within the detection window was monitored by the detection system.

Using the above method, the separation of $CuCl_2$ into Cu^{2+} and Cl^- ions was achieved in a single run. A large EOF velocity was observed; this caused the Cl^- ions to travel along the channel against the direction of their electrophoretic velocity. The Cu^{2+} ions migrated in favour of the EOF and the Cl^- ions opposed it; this made the separation possible in a short channel length.

As discussed in Section 6.7.3, once the sample is injected into the sample injection reservoir it becomes diluted. Since the volume of the sample reservoir on Device 3 was ~200 μL, the 100 μL of 10 mM sample of $CuCl_2$ would be diluted. The solution was not mixed within the sample injection reservoir and hence the exact concentration of $CuCl_2$ is not known precisely, based on the reservoir volume compared with the injected volume it is estimated to be reduced to ~5 mM. The injection and electrophoretic separation of the sample causes a further reduction in the ionic concentration. Comparing the electropherogram in Figure 121 with the concentration curve for $CuCl_2$ in Figure 119 the concentration of ions within the detection window can be inferred. The peak response in the electropherogram for Cu^{2+} ions was 2.4. From Figure 119, this value suggests a concentration of ions <200 μM.

To demonstrate that the model described in Section 4.4 (based on the Nernst-Planck equation (Equation (34)) in Section 4.3.1) was able to accurately describe the separation of the ionic sample it was used to calculate the separation for the conditions that produced the result of Figure 121. As can be seen in Figure 121 the peak corresponding to the Cu^{2+} ions arrives at the detector (which is located about 50 mm from the sample injection point) at ~250 seconds and the Cl^- ions arrive ~100 seconds later. A computer simulation of this experiment showed that a greater difference between the arrival of the Cu^{2+} and the Cl^- ions would be expected. For this experiment, the channel was filled with deionised water which has a lower conductivity than the sample. Therefore the electric-field dropped across the sample is less than the electric-field dropped across the rest of the channel. This result highlights a consequence of not matching the conductivity of the buffer solution to the sample, as discussed earlier in Chapter 3. Effectively the EOF is enhanced and the separation voltage is decreased. Using the known values of electrophoretic mobility for Cu^{2+} and Cl^- and taking the arrival times shown in Figure 121 it is possible to calculate the effective field dropped across the sample, as discussed in Section 2.2. From this, it is also possible to infer the EOF mobility. The resulting value of effective electric-field strength across the sample

was 425 V m^{-1} and the EOF mobility was 4.475 x 10^{-8} m^2 V^{-1} s^{-1}. Earlier in Figure 98 (Section 6.6.4) it was shown that typical values for the EOF mobility of a range of polymers were in the region of between 2 and 5.5 x 10^{-8} m^2 V^{-1} s^{-1}; the calculated value for Device 3 from this experiment was within this range. Using the inferred values for the E-field drop across the sample, and the EOF, the model was adjusted and the simulation was re-run, the result can be seen in Figure 122. It should be noted that the graph in Figure 121 shows the detector response (i.e. concentration) against time, whereas the simulations plot the concentration against distance along channel (at specified times). As well as showing that the Cu^{2+} ions arrive at the detector at 250 seconds and ~100 seconds before the Cl^- ions, it also shows that due to the higher coefficient of diffusivity for the Cl^- ions the corresponding peak is broader than the peak for the Cu^{2+} ions. Both of these observations are in agreement with the results given by Device 3, shown in Figure 121.

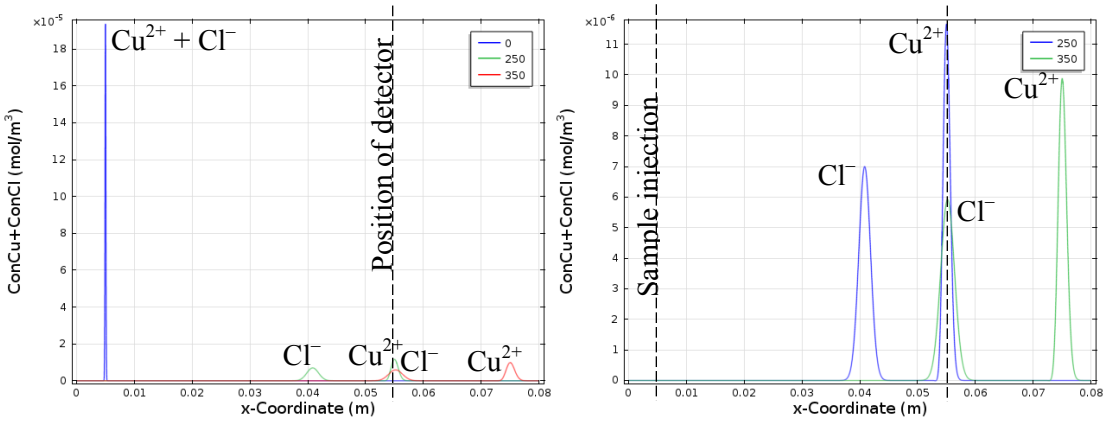

(a) (b)

Figure 122: Simulation (based on model discussed in Section 4.4) validating the ability of the model to predict the separation of a mixture of charged species (experimental data shown in Figure 121). Both graphs show same data, however (a) includes the sample at the start whereas (b) has been scaled to show a greater detail at lower concentration levels. The time (given in seconds) at which the concentration is evaluated is shown in the legend.

A selection of results from this device alongside a description of the project and the microfluidic device design were presented on a poster at a Marine Energy Systems Day (2011), University of Southampton, UK, and at the Joint Academic Research Programme for Defence Exploitation Event (2011), Dstl Porton Down, Salisbury, UK [289, 290].

6.10.3. Outcomes from Experiment 6

A sample of $CuCl_2$ was separated into Cu^{2+} and Cl^- ions and detected. The computation model, as described earlier in Section 4.4, was modified to demonstrate that it was able to describe the behaviour of a real sample.

Over the course of the experiments, the Cr layer beneath the Au disintegrated which meant that the gold electrodes no longer adhered to the glass wafer. Ti readily forms a protective oxide layer and is highly resistant to corrosion and electrochemical degradation therefore, a proposed solution to avoid the loss of the Cr adhesion layer was to replace it with a Ti adhesion layer [291]. Both Cr and Ti are commonly used as adhesion layers for gold in microfabrication processes [239, 268, 292, 293]. For the fabrication of Device 4, a Ti adhesion layer was used; however since it is more difficult to etch Ti, this change meant that the fabrication process was altered. For Device 3, the Cr layer was etched after the etching of the Au layer. To pattern the Ti layer, in place of a metal etch process, a lift-off process was used; this lift-off process removed both the Ti and Au layer in a single step. A detailed discussion on the fabrication of Device 4 is given in Section 6.11.2.

6.11. Experiment 7

6.11.1. Aims of Experiment 7

During the development of Device 3 a fabrication method was created which enabled the dynamic control of the EOF such that it could be increased, decreased and reversed. This control was enabled using a single planar electrode. Experiment 7 was to investigate the effect of the smaller detector electrode area, as discussed earlier in Section 5.2. The smaller area of electrodes was desired in preparation for the development of a later envisaged device with a significantly shorter channel length. Further to this, the channel width was reduced to 200 μm. Once the new limits of detection were calculated, the proposed separation enhancement methods, as described in Sections 2.4.2 and 2.4.3, were to be demonstrated. Device 4 was designed and fabricated to address the aims of Experiment 7.

6.11.2. Fabrication of Device 4

Device 4 was composed of two parts: the first being a moulded PDMS piece containing the channels; the second being a glass wafer on which metal electrodes were patterned and insulated. A 3D drawing of Device 4 can be seen in Figure 123.

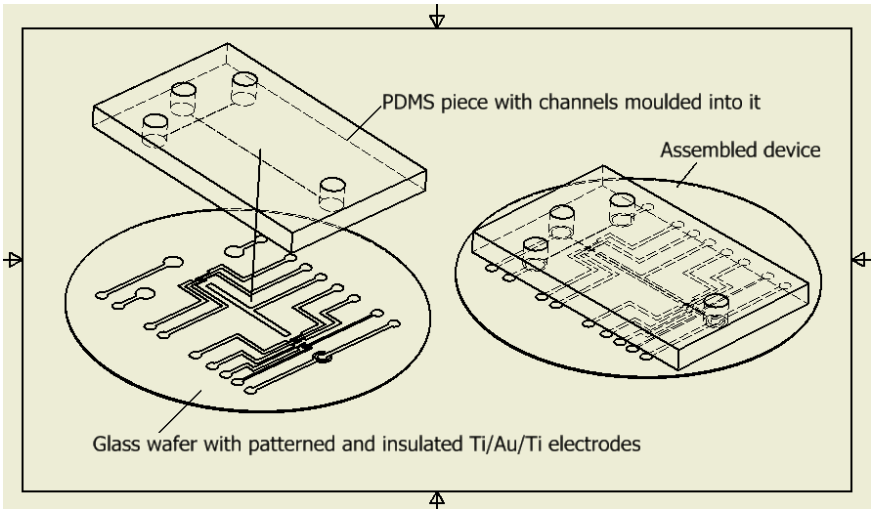

Figure 123: 3D drawing of device 4. The dimensions for the PDMS piece are given in Figure 124 and the dimensions for the patterned glass wafer are shown in Figure 127.

The fabrication method for the PDMS piece was similar to that of Device 3 (as discussed in Section 6.8.2). One difference was that a different mask pattern was used for exposure step during the lithography process. A technical drawing of the new mask pattern for the PDMS mould can be seen in Figure 124.

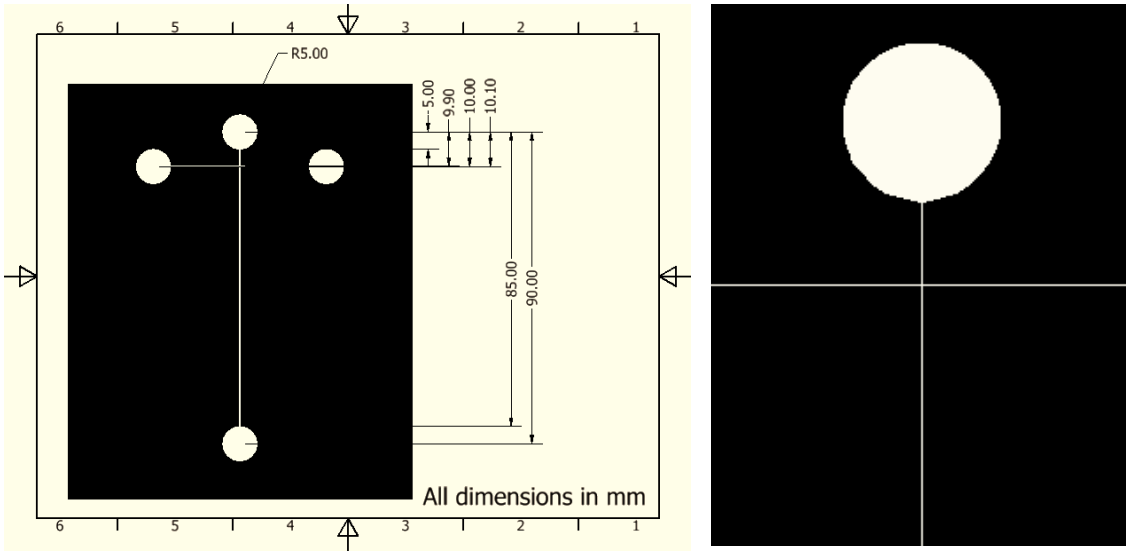

Figure 124: Left: Technical drawing of mask for PDMS mould for Device 4. Right: enlarged image showing the channels at the sample injection point.

Unlike for Device 3, where the reservoirs were formed by punching holes into the PDMS, for Device 4 the reservoirs were formed during the curing process. To achieve this, a mould holder and reservoir former were fabricated, an illustration of which is shown in Figure 125. After processing the SU-8 layer on a glass wafer, the glass wafer was cut and secured into the holder. The reservoir former was then lowered onto the glass wafer after which the PDMS could be poured over the mould. The curing process of the PDMS was performed at 80 ˚C for 45 minutes, after which the PDMS was removed from the mould and placed in an oven at 150 ˚C for a further 10 minutes to ensure it was fully cured.

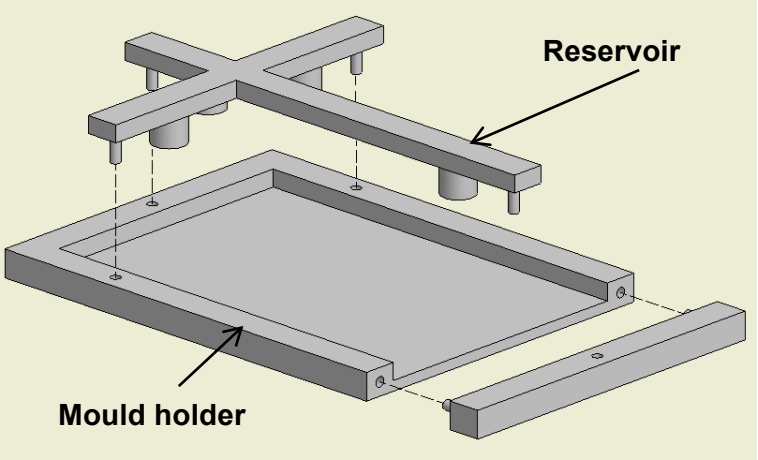

Figure 125: Drawing of mould holder and reservoir former.

The profile of the SU-8 mould on the glass wafer was measured using a KLA-Tencor P11 contact surface profilometer; the resulting profile can be seen in Figure 126. The profiler was run at 5 evenly spaced intervals along the channel length; the average step height measured was 47.2 µm ± 2.74 %. The resulting profile shows that the SU-8 mould is smooth along both the sidewalls and the top.

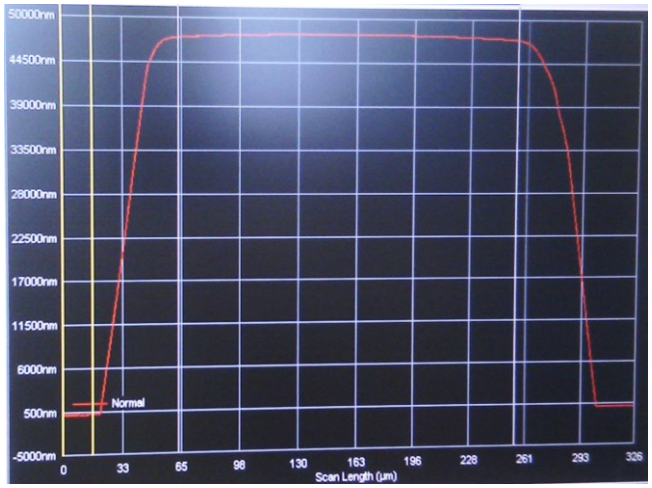

Figure 126: Profile of the SU-8 mould on a glass wafer.

A method to prevent the disintegration of the metal electrodes (Cr/Au) observed during experiments with Device 3 was to replace the Cr adhesion layer with a Ti adhesion layer. Further to this it was decided to place a thin Ti layer on top of the Au electrode to help protect it from electrochemical degradation, as discussed earlier in Section 6.10.3. Even though this resulted in the Au layer being sandwiched between two layers of Ti, the Au layer was still required to ensure the resistivity of the electrodes remained low. A disadvantage of using Ti is that it is difficult to wet etch. To address this issue a photoresist lift-off process was used to pattern the Ti/Au/Ti electrodes. The advantage of using a lift-off process is that it possible to use the same process for the patterning of a number of metals. Therefore if it was later shown that another material was required, the only change in the fabrication process would be the deposition of the new material.

A step-by-step guide of the lift-off process is given below:

1. Bring the negative photoresist, AZ nLOF 2070, to room temperature.
2. Dehydrated glass wafer in an oven at 210 ˚C.
3. Spin the AZ nLOF 2070 photoresist:
   - Spin at 500 rpm (acceleration of 100 rpm/sec) for 10 seconds.
   - Spin at 6000 rpm (acceleration of 1000 rpm/sec) for 30 seconds.
   - Spin at 100 rpm (deceleration of 1000 rpm/sec) for 6 seconds.
4. Pre-exposure bake: resist is baked on hotplate at 115 ˚C for 60 seconds.
5. Exposure: the resist is exposed to UV with i-line filter via mask for 6 seconds; drawing of the acetate mask shown in Figure 127.
6. Post-exposure bake: resist is baked on hotplate at 115 ˚C for 60 seconds.
7. Development: Using AZ 726 MIF developer, the photoresist is developed. This process takes 110-120 seconds during which the solution should be agitated.
8. Descum: Oxygen plasma (50 sccm) with RF power of 100 W for 30 seconds.
9. Deposit metal layers:
   a. the Ti adhesion layer (5 nm) was evaporated at a rate of 0.2 Å s^{-1},
   b. the Au layer (100 nm) was evaporated at a rate of 1 Å s^{-1}.
   c. the final Ti layer (15 nm) was deposited at a rate of 0.3 Å s^{-1}.
10. Remove (lift-off) the resist by submerging the wafer in NMP (n-methylpyrrolidone) and leaving for 12 hours.
11. Rinse wafer with acetone then IPA.
12. Blow dry with nitrogen.

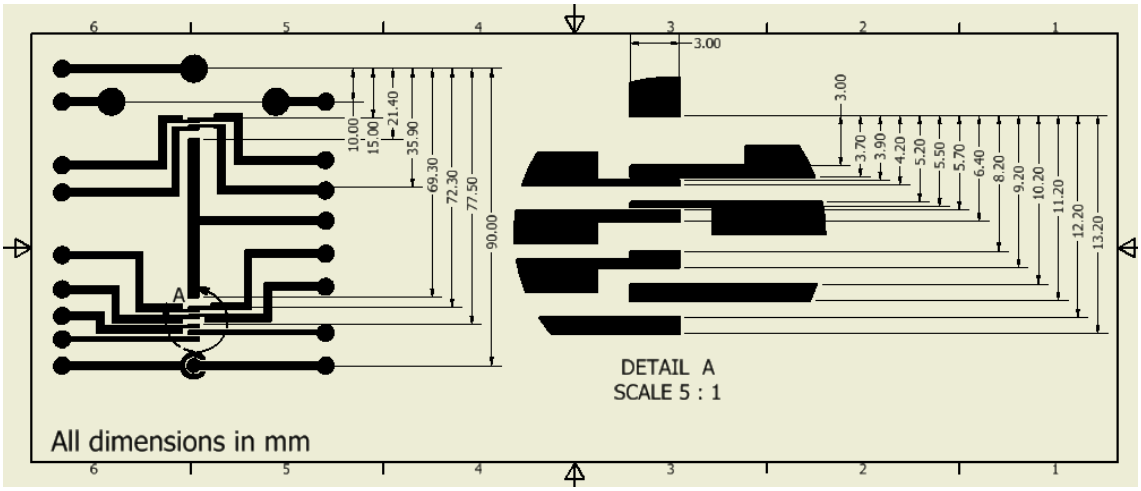

Figure 127: Technical drawing of acetate mask for Device 4 for defining metal electrode pattern.

Once the metal had been patterned on the glass wafer, the electrodes were insulated with a 1 µm layer of SU-8 using a similar process as described for Device 3 in Section 6.8.2. The only difference between the processes were the acetate masks used; the mask for patterning the SU-8 insulation layer for Device 4 can be seen in Figure 128.

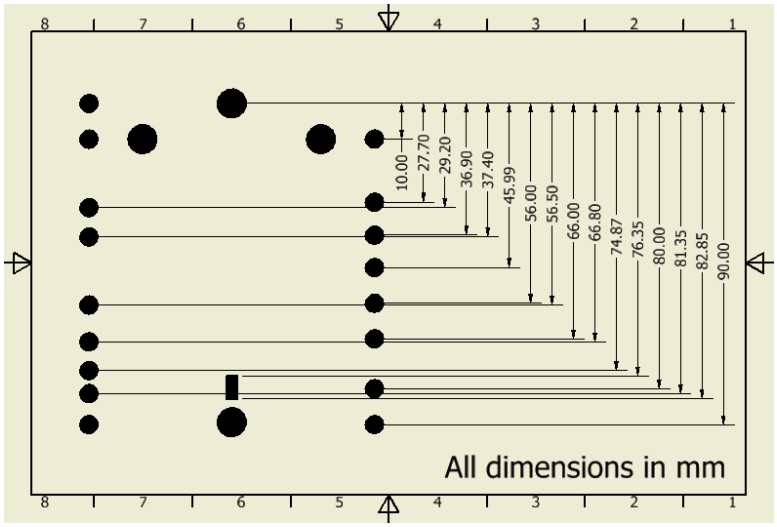

Figure 128: Technical drawing of acetate mask for SU-8 layer.

With the application of a gentle pressure to the PDMS piece, it was reversibly sealed to the insulated glass wafer. A labelled image of the resulting device can be seen in Figure 129.

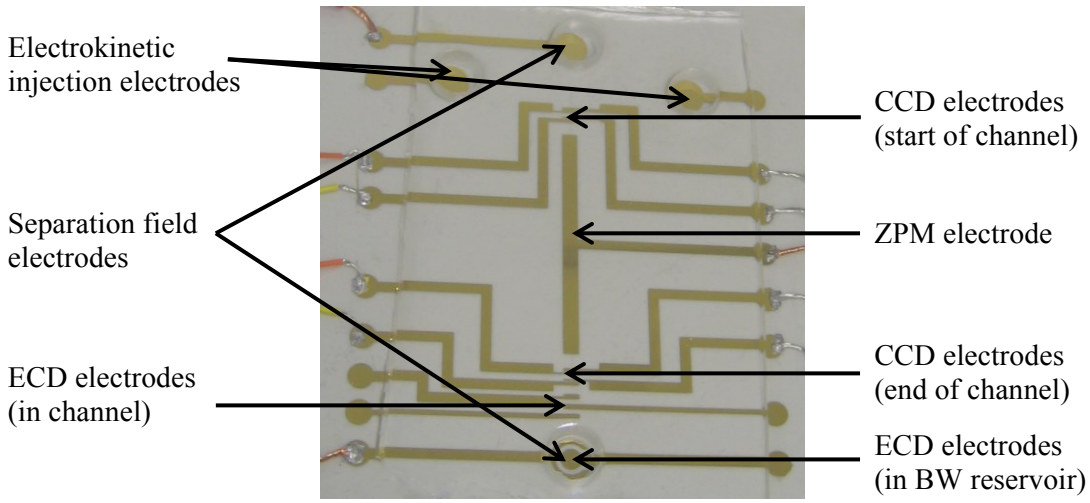

Figure 129: Photograph of Device 4, showing the patterned Ti/Au/Ti wafer with an SU-8 insulation layer, on top of which a PDMS piece containing the channels is reversibly sealed.

6.11.3. Reliability Issues with Device 4

A number of reliability issues prevented the aims of the testing on Device 4 from being achieved. The primary issues encountered included the generation of bubbles in the microfluidic channel and the failure of the insulation layer.

6.11.3.1. Refinement of Device 4

The in-channel ECD electrodes (shown in Figure 129) were not insulated and were positioned further along the channel than the second CCD. It was planned that following separation, the separated sample species could be electrochemically characterised in channel whilst they are at their most concentrated; when the sample leaves the channel it becomes diluted in the buffer waste reservoir. It was a concern that some electrochemical techniques that may need to be used to detect certain ion species within the buffer solution might encourage hydrolysis to occur at the ECD electrodes which would result in the generation of gas bubbles which could block the channel. For example, the electrical potentials applied to the electrodes during a voltammetric detection technique could include those potentials at which hydrolysis occurs for a particular solution pH. To mitigate for this possible problem, two different electrode patterns were designed for the photolithography mask that either included or excluded the in-channel ECD electrodes. Both designs however contained two electrodes in the buffer waste reservoir. Since the ECD system would only be active when

the electric-field was turned off, one of these electrodes had dual functionality. It would be an electrode for both applying the electric-field along the channel and as one of the ECD electrodes. For the ECD system, the two patterned electrodes in the buffer reservoir would act as the working and counter electrode, with a third electrode (the reference electrode) positioned in the reservoir.

During the first few experimental runs, even when there was no external connection to any of the ECD electrodes, it was noticed that bubbles were being produced at the in-channel ECD electrodes. The production of bubbles at the in-channel ECD electrodes only occurred in the presence of an applied separation electric-field (i.e. a potential applied to the separation electrodes). The potential difference along the channel induces a potential on the electrodes hence leading to a potential difference between the electrodes which results in electrolysis; this in turn causes the generation of the bubbles (as discussed earlier in Section 3.2). This issue highlights the importance of decoupler systems for ECD in CE systems as discussed in Section 5.1.3.1. To overcome this issue, a new wafer was fabricated which used the mask where the in-channel ECD electrodes were omitted, a drawing of this mask is given in Figure 130.

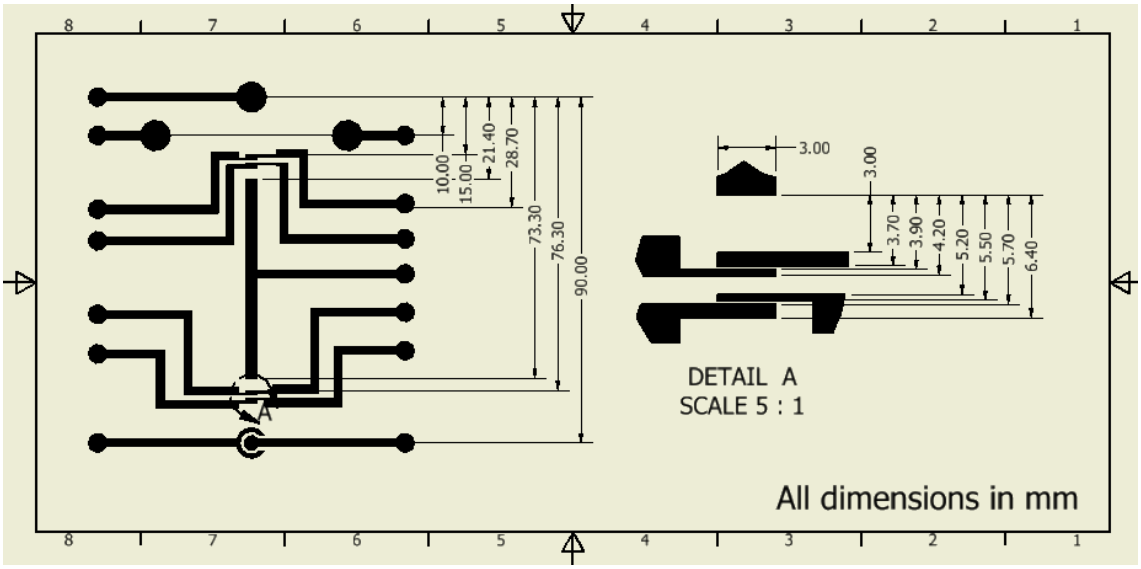

Figure 130: Technical drawing of acetate mask for Device 4 for defining metal electrode pattern, in this design the in-channel ECD electrodes were omitted.

A different mask was also required for the SU-8 insulation layer; a drawing of which is given in Figure 131. Whilst the in-channel electrodes would have been beneficial for the detection system, their removal would not prevent the aims set for Experiment 7 being achieved.

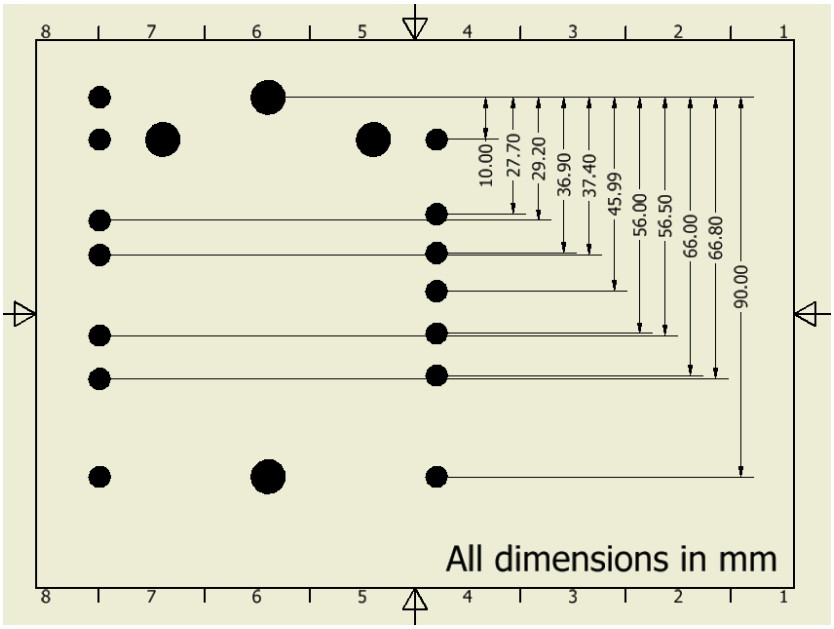

Figure 131: Technical drawing of acetate mask for SU-8 layer where the in-channel ECD electrodes were omitted.

6.11.3.2. Failure of the Insulation Layer

After a few preliminary experimental runs with Device 4 in which a maximum of 300 V was applied to the separation electrodes, the current flow through the channel would fall to zero. Upon closer inspection of the separation channel, bubbles could be observed; usually these would either be located over or in close proximity to an electrode along the channel. Since all the electrodes along the channel of the device were insulated by a thin layer (~1 μm) of SU-8, there should have been no bubble generation. Earlier in Table 8 (in Section 3.10) the typical breakdown strength for SU-8 was listed as 440 x 10^6 V m^{-1} [184]. For a 1 μm thick insulation layer this equates to a maximum workable voltage of 440 V. Here, the insulation failed even though the potentials applied to the buffer and buffer waste reservoirs were 300 V and 0 V respectively. The voltages at the sample injection reservoirs were left floating during these preliminary experiments. The insulation layer for Device 4 was fabricated using the same method as used for the insulation layer for Device 3; however the SU-8 insulation layer on Device 3 appeared more robust than the insulation layers later fabricated on Device 4. For these reasons, the failure of the insulation layer at these potentials was unexpected.

The SU-8 layer was fabricated following a recipe from the manufacturing company (MicroChem Corp.) and it has been used successfully by numerous researchers [184, 294-296]. Since the SU-8 layer was fabricated in a cleanroom using different equipment (in terms of manufacturers and specifications) to those used by MicroChem Corp. it meant that

producing a perfect replica of the SU-8 layer meeting the specifications specified by the manufacturers might not be possible. Therefore some deviation in the properties would be expected, however the SU-8 underperformed significantly in these experiments. There have been numerous reports on the successful use of SU-8 in microfluidic devices; for example Sikanen *et al*. reported that their SU-8 microfluidic channels performed from day to day, exhibiting no aging effects over long term use (several weeks of daily use) [294]. Wu *et al.* discussed the use of a SU-8/PDMS hybrid microfluidic device for the monitoring of lactate [297]. Ou *et al*. reported on the improved heat dissipation of a hybrid SU-8/PDMS over a PDMS/PDMS device which enabled the use of higher electric-fields [296]. SU-8 has also been successfully used for electrowetting on dielectric (EWOD) microfluidic devices [298]. Kumar *et al.* reported that SU-8 was advantageous since it simplified the fabrication process due to the SU-8 layer acting as both the dielectric layer and the hydrophobic layer; usually in EWOD devices a hydrophobic layer, such as polytetrafluoroethylene (PTFE) is required on top of the dielectric layer [298]. Dielectric failure can occur electro-wetting systems due to the inherently porous nature of the fluoropolymer films (such as PTFE), hence a two-layer dielectric stack is often employed [299].

Since the breakdown strength of the SU-8 layer appeared to be lower than expected, it was decided to increase the insulation layer thickness to 5 μm. To produce this layer, a two layer SU-8 process was used where a thickness of 2.5 μm is spun onto the wafer and processed (including a hard-bake), after which the process is repeated. The steps for this process were similar to those used for the insulation layer for Device 3, described in Section 6.8.2, step 6. The only difference was that step 6e was changed to:

Spin SU-8 (SU-8-2) photoresist:

- Spin at 500 rpm (acceleration of 100 rpm/sec) for 5 seconds.
- Spin at 1000 rpm (acceleration of 300 rpm/sec) for 30 seconds.
- Spin at 500 rpm (deceleration of 500 rpm/sec) for 5 seconds.

This process successfully created an insulation layer with a thickness of ~4.5 μm. The layer thickness was measured using a KLA-Tencor P11 contacting surface profilometer. Whilst this was slightly less than desired it would mean that the SU-8 should be able to survive a potential drop across it of ~2 kV.

The disadvantage of a thicker insulation layer was that it would reduce the sensitivity of the detection system. Earlier in Section 6.7.4 the detection system was proven for a 100 μm

thick polyimide insulation layer, based on this and SPICE simulations discussed in Section 5.2.1 the detection system was believed capable of meeting the specification.

With a thicker insulation layer on the device a small number of preliminary tests were conducted. Unfortunately, the device failed after a couple of experiments. This prevented any conclusive experimental data being collected from the device. The failure was attributed to dielectric breakdown of the SU-8 insulation layer. An image of the failure site can be seen in the left image of Figure 132. The watermarks show where the channel ran (horizontally) across the electrode. The optical fringing effects suggest that the SU-8 has delaminated from the electrode at the point of failure. The SU-8 resist at the failure site was brown in places suggesting that it may have burnt due to the high current flow through the surface at breakdown. The image on the right of Figure 132 shows the electrode after cleaning in fuming nitric acid. The fuming nitric acid removes the SU-8 layer. This meant that a new insulation layer could be put down on the patterned wafer for testing. The fabrication of new SU-8 insulation layers using the same process on the patterned wafer was attempted, however during the testing stages, the device would fail in the same manner within a few experiments.

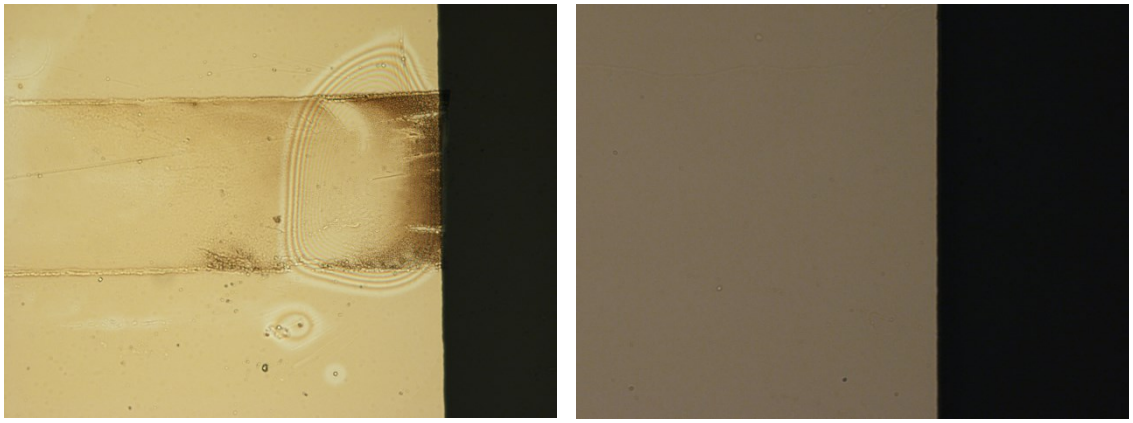

Figure 132: Image of the CCD detector electrode after failure, before (left) and after (right) stripping SU-8 insulation layer.

The device functioned for a number of experiments, therefore it was suggested that the failure could be caused by the ingress of buffer solution into the SU-8. There were a number of factors which could cause this:

- during an experimental run, the SU-8 could expand due to an increase in temperature,
- formation of cracks or gaps in the SU-8 layer during the fabrication; these can occur for a number of reasons.

- if the SU-8 does not reach room temperature before processing, due to its high viscosity at lower temperatures, bubbles can become trapped in the SU-8,
- bubbles could form during the spin coating process and if not given enough time to escape would become trapped in the insulation layer when baked,
- thermal shock could occur if the SU-8 is not given enough time to relax after baking.

To rule out the first option, the temperature was monitored using a single channel digital temperature measuring instrument (Testo 925). The temperature probe was placed at various locations in close proximity to the microfluidic channel during numerous experimental runs. There was no variation in temperature observed during the experimental runs.

During the fabrication of the insulation layer, it was suggested that following the spinning step, the wafer should rest for 30 minutes prior to the pre-exposure bake. This modification however caused issues when the second layer of SU-8 was spun onto the wafer. During the pre-exposure bake the solvent in the SU-8 seemed to have attacked the underlying layer, an image showing the wafer after this can be seen in Figure 133.

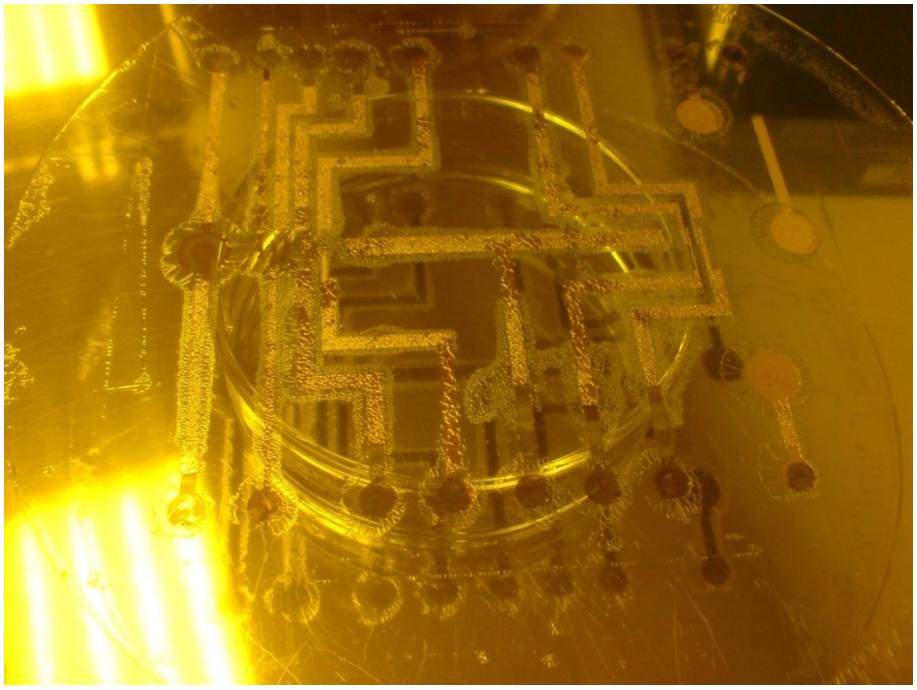

Figure 133: Photograph of wafer (in yellow room) following the pre-exposure bake for the second layer of SU-8.

SU-8 comes in a range of viscosities, each specified for a range of layer thicknesses for a given range of spin speeds. Using a high viscosity SU-8 it was possible to spin a thicker insulation layer in a single run. The fabrication of this layer was executed with care taken to

avoid large or sudden thermal changes. After each processing step the layer was given time to recover and relax; ensuring that the layer reached room temperature before continuing. The layer thickness was measured to be ~6.7 μm. This device was tested but still failed after a few experimental runs and so it was decided to try a different insulation material, even though SU-8 was reported to have the required electrical properties. In EWOD applications, the failure of dielectric layers has received significant interest [299]. Usually in EWOD applications, there are two layers of dielectric [300]. One of the layers provides the required dielectric breakdown strength, and the other provides the surface properties [298, 300]. For example, PTFE has hydrophobic properties favourable for EWOD, however because of its low dielectric breakdown strength it is usually used with another dielectric, such as parylene C [298]. Raj *et al.* reported on dielectric failure in EWOD devices where ionic species were able to permeate through the dielectric layer [299]. It is possible that a similar mechanism contributed to the failure of the SU-8 dielectric in Device 4. Since SU-8 is hydrophobic and has a good breakdown strength, Kumar *et al.* explored the possibility of using it for EWOD applications; since it would remove the requirement for multi-layered dielectrics [298]. The thickness of their SU-8 layers varied from 0.5 μm – 5 μm and they used voltages up to 220 V, therefore their 0.5 μm SU-8 dielectric layer was capable of surviving a voltage greater than the SU-8 layer used on Device 4 [298]. A search of the literature has showed numerous cases discussing successful use of SU-8 as a dielectric layer; therefore it is clear that further research into the use of SU-8 as a dielectric is required to identify the cause of failure [294, 296, 297].

Schasfoort *et al.* successfully used a 0.4 μm silicon nitride insulation layer for EOF control in microfluidic devices [188]. Buch *et al*. used a 2 μm silicon dioxide insulation layer in their work where they investigated the effect of buffer solution strengths, pH, etc. on the ability to modify the EOF [49]. It was decided that in place of the photoresist layer, a 5 μm layer of silicon nitride would be sputtered onto a freshly prepared patterned glass wafer. It was sputtered in stages of 2 μm, 2 μm and then 1 μm. This is a significantly thicker layer than is usually sputtered for other applications. Unfortunately due to stresses in the sputtered layer it “wrinkled”, an image of this can be seen in Figure 134. This route required further process development; however this was not possible within the time frame of the project. If PECVD is used instead of sputtering the stress could be controlled by alternating the plasma excitation frequency [239]. The presence of pinholes in the dielectric layer would severely reduce the electrical performance of the layer; therefore a further consideration for the development of a PECVD process for the fabrication of a silicon nitride layer would be to use a multilayer process. The advantage of a multilayer process is that it removes issues with

pinholes since pinholes in one layer will be covered by the overlying and subsequent layers [301].

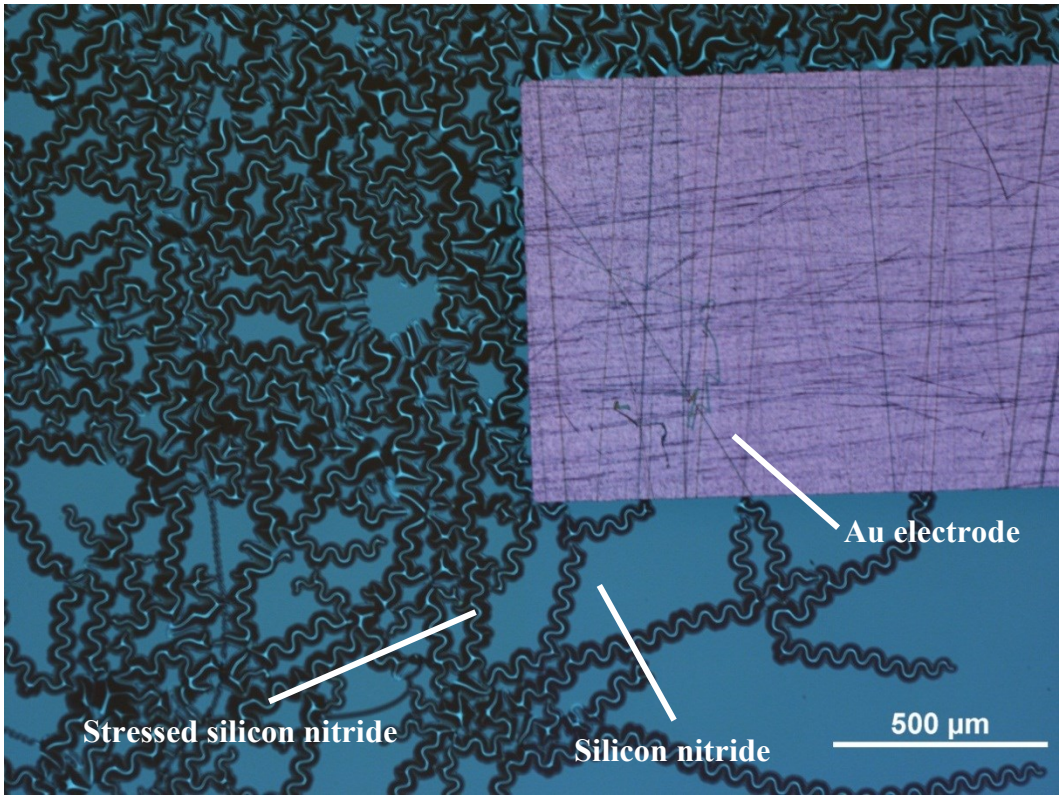

Figure 134: Image showing effect of stress in silicon nitride layer.

6.11.4. Outcomes from Experiment 7

Despite checking the specification of the SU-8 insulation layer numerous problems were encountered during experimental runs. A number of approaches including increasing the layer thickness and varying the fabrication method were attempted. During the fabrication of Device 3 an SU-8 layer was successfully fabricated which survived the numerous experimental runs. Therefore the numerous issues with the SU-8 layer were unexpected; it was not possible to determine the exact cause that prevented the SU-8 from performing as per its specification with Device 4. Given that the failure did not occur instantly, but after a period of time, it is believed that buffer solution was able to ingress into the SU-8 layer; over time this could cause the effective thickness of the layer to decrease and could explain the failure.

The primary aim of Device 4 was to experimentally demonstrate the separation enhancement methods. SU-8 was primarily chosen for its ease of use and quick turnaround time from design to fabricated device. The material selected for the insulation layer however, could be

replaced with a number of materials. A silicon nitride layer was sputter coated onto the wafer, however this layer was highly stressed and could not be used. Time restrictions prevented the aims of Device 4 from being achieved. The next step should be the investigation of using PECVD to deposit a low-stress silicon nitride or silicon oxide film. There are a number of parameters which would need to be investigated and optimised in order to fabricate a suitable low-stress silicon nitride film. These parameters include: deposition temperature, gas pressure, gas phase composition and the RF frequency [302-304]. For example, Claassen *et al.* showed that silicon nitride layers deposited at temperatures up to 550 ˚C showed compressive stress behaviour, whereas layers deposited at temperatures above 550 ˚C showed tensile stress behaviour [302]. Further to this they showed that depositions with a high RF frequency (>4 MHz) produced layers which exhibited tensile stress behaviour, whereas low frequencies (<4 MHz) resulted in layers with compressive stress behaviour [302]. Alternatively a silicon oxide layer could be deposited, for example Bulla *et al.* discussed the use of PECVD with (tetraethylorthosilicate) TEOS for the deposition of oxide layers up to 4.2 µm [305]. For film thicknesses over 0.7 µm they used a multilayer process which consisted of successive deposition steps of 0.5 µm to avoid issues with the film cracking [305]. Following an investigation into the fabrication of a suitable silicon nitride insulation layer the separation enhancement methods could be experimentally investigated and compared with the computation models.

6.12. Conclusions

In Section 6.4 an overview of the proposed device for the demonstration of the separation enhancement methods was described. In order to develop this device, several iterations of the design were produced. The first two devices were fabricated as stepping stones towards the fabrication of the envisioned device. Device 3 was designed to closely match the design criteria of the envisioned device however due to unforeseen issues, as discussed in Section 6.10.3, a fourth device was fabricated. Compared with the proposed device discussed in Section 6.4, Device 4 bears significant similarities in terms of device layout, insulation layer thickness, and channel and device dimensions. A number of experiments were conducted on the devices. The results from the evaluation of the various prototype devices aided decisions regarding the fabrication methods which would be required for the envisioned device. The requirements imposed by the experiments placed various restrictions which informed the selection of the fabrication method. There were a large number of differences between the first proposed prototype device, Device 1, and the proposed device (discussed in Section

6.4). Device 1 was fabricated using PMMA and the channel length was intentionally designed to be longer than what might normally be expected for a miniaturised CE system (as discussed in Section 3.3.1) in order to have a reasonable chance of demonstrating electrophoretic separation. To test the detection system, and the micro-pumps, Device 2 was fabricated; this device was also made in PMMA, using the same micromachining technique as used for Device 1, however, the channel sealing technique was significantly different as discussed in Section 6.6.2. To predict the performance of the micro-pump on the proposed device, the channel dimensions of Device 2 were chosen to be comparable. Further to this it also included electrodes for the detection system. Prototype devices 2 and 3 had identical layouts for the ZPM and detection electrodes, although Device 3 was fabricated using microfabrication techniques on a glass wafer in a cleanroom. On the glass wafer of Device 3 electrodes for applying the potential along the separation and sample injection channels were patterned. An advantage of using microfabrication techniques was that a thin insulation layer could be produced, thus resulting in an insulation thickness comparable with that of the envisioned device Unlike the earlier devices, the channels for Device 3 were fabricated in PDMS to address issues regarding the sealing of the channel, as discussed in Section 6.8.2. Compared with Device 3, the area of the detection electrodes on Device 4 was smaller so that the ZPM electrode could be extended over a larger length of channel. The materials for the electrodes of Device 4 were Ti and Au since, as discussed in Section 6.10.3, deficiencies with the Cr adhesion layer resulted in a move to using Ti as the adhesion layer. Further to this, a Ti layer was placed on top of the Au layer because of the electrochemical properties of Ti, such as high electrochemical stability, as discussed in Section 6.10.3. The channel overlap length between the sample injection and separation channels was also reduced; shorter sample lengths are favourable for separation. Further to this, the reduction in injected sample length enabled a longer length of channel to be in close proximity to the ZPM electrode. When the fabrication issues regarding the failure of the insulation layer are overcome, Device 4 would be expected to be capable of demonstrating the separation enhancement methods.

As discussed in Section 3.2, miniaturised CE systems require numerous components, including HVPSs and detection systems. Experiments 1 and 2 were required to test basic electrophoresis theory. The use of electrophoretic dyes enabled a range of tests without the requirement for a detection system. Before using these electrophoretic dyes within the microfluidic devices, their values of apparent mobility were calculated using a laboratory-based CE instrument and compared with values reported in the literature. Experiments on Device 1 showed that the EOF was less than observed when using a fused silica capillary;

this is in good agreement with many researchers who have shown that EOF in polymers (such as PMMA) is less than that for fused silica [294].

The primary aim of Experiment 3 was to enable the testing of the pumping system, and to act as a platform on which to test and demonstrate the HVPS and detection system. Using electrophoretic dyes, it was possible to visually verify that the micro-pump was capable of pulling fluid through all channels of the device. Software was written in LabView which was able to control two HVPS; one for the separation electric-field and the other for the ZPM electric-field. The LabView program was further developed to monitor the two detection systems. A control system which would be capable of autonomously controlling the switching-based separation enhancement method was devised. This system was based on the monitoring of the change in concentration; upon detecting a significant change, the EOF would be reversed. Following this, the other detector would be monitored until a concentration change is observed, which would then trigger the HVPS to be set to the original value. Using a counter this processes could be repeated a set number of times. Although outside the initial aims of Experiment 3, the effect of a change in ZPM was investigated. Even in the presence of a thick insulation layer, a small change in the EOF rate was observable.

For Experiment 4, the effect of the ZPM electrode on the EOF was characterised by monitoring the migration time of an electrophoretic dye for a range of potentials applied to the ZPM electrode. As well as decreasing and increasing the EOF, the ability to reverse the EOF was also demonstrated.

The aims of Experiment 5 were to measure the limit of detection of the detection system. It was shown that the detector was capable of measuring changes in concentration down to 1 mM. This demonstrated that the detection system would be suitable for the corrosion monitoring application described in this project, since the change in concentration caused by the release of metal ions during crevice corrosion is significantly higher than this value.

The ability to separate and detect a low concentration (10 mM) of $CuCl_2$ was demonstrated on a fabricated microfluidic device. The computation model discussed in Section 4.4, was shown to be capable of accurately predicting the separation between the Cu^{2+} and Cl^- ions for the given experimental conditions.

A number of issues were encountered with the insulation layer used for Device 4 which was designed to address Experiment 7. A range of potential issues with the SU-8 insulation have been discussed. During the fabrication process, a number of attempts to overcome these

issues were made. It was not possible to successfully fabricate the device with the SU-8 insulation layer which did not fail during the testing. It was decided to attempt to sputter a silicon nitride insulation layer; however without the required process development this introduced further fabrication issues. It was not possible within the timescale of the project to perform Experiment 7 on Device 4.

Chapter 7

Conclusions and Future Work

7.1. Summary of Work

This investigation formed part of a larger project looking at in-situ corrosion monitoring with an emphasis on metal crevice corrosion in marine environments. This work was concerned with the separation of mixed species of ions in a miniaturised fluidic system, which is an important part of the full corrosion monitoring system (discussed in Section 2.1.1). To this end, several metal corrosion systems were targeted, reducing the number of species of interest and in particular the NAB system was of interest. In the case of NAB, during corrosion a number of metal ions are released and by monitoring the evolution of the concentration of these, in particular the cupric and ferrous/ferric ions it is possible to infer the phase of corrosion of the component. The concentrations of these key metal ions released into the crevice environment during corrosion were expected to be >20 mM, based on previous work reported in the literature, as discussed in Section 2.1. Therefore this work concentrated on the separation of these species by way of example, although the techniques developed can be generally applied.

Analysing general mixtures of metal ions is a difficult task, but measuring individual species when separated from other species is a more practical approach, particularly when there is a limited choice of species; specific detectors can be designed for the ions of interest. In this case, a separate project developed electrochemical thick-film detectors for the ions of

interest. Separation to a level where these detectors can operate thus becomes an important part of the overall system. The electro-analytical method selected to achieve this separation was CE. The separation capability of CE is directly related to the capillary length; for portable or in-situ systems, shorter lengths are desirable. Thus the primary aim of the work presented in this thesis has investigated novel separation enhancement methods for miniaturised planar CE systems without compromising device size. Two methods to achieve this which use dynamic EOF modification techniques have been considered and discussed in Sections 2.4.2 and 2.4.3.

- The first method involves reusing the channel length by switching the EOF between two values to cause a sample to migrate along a section of the channel multiple times.
- The second method closely matches the EOF to the sample velocity such that the sample migrates along the channel due primarily to the difference in electrophoretic mobility of the sample constituents.

A control system for the separation enhancement methods has been considered. This uses a feedback loop similar to a closed-loop system, which gives significant advantage over non-feedback methods in that it is less susceptible to unwanted experimental variation.

A detailed review of the literature on miniaturised CE was carried out and this formed the basis of a journal review paper [66]. From this, the importance of a holistic approach became clear. The following aspects of miniaturised CE systems were considered in detail:

- HVPS,
- detection systems,
- power supplies,
- device materials,
- fabrication methods.

Further to this, related work on EOF modification using electric-fields was investigated. The dynamic EOF modification techniques require that an electrode is placed close to the fluidic channel walls as discussed in Section 2.4.1. The project requirement for the system to be planar introduced difficulties with regards to fabrication of a device where all the channel walls are in close proximity to an EOF controlling electrode. However, EOF modification is possible without full channel coverage at the expense of some unwanted sample dispersion. Using computational modelling, the consequences of using one electrode next to a channel

wall has been compared with the ideal case where the modifying electrode is placed in close proximity to all channel walls.

Models describing the EDL have been developed and solved for a range of conditions to describe the effect of the ZPM electrode. The values measured by the model have been compared with experimental results published in the literature and showed good correlation, as discussed in Section 4.2. Computation modelling has been used to investigate and describe the behaviour of a microfluidic system incorporating the developed separation enhancement routines. Since a planar electrode system would be subjected to increased sample dispersion compared with a capillary system, the limits of the separation enhancement methods have been explored and modelled.

To meet the needs of the control system, it was clear that a detection system would be required. The main requirement of the detection system was to detect metal ions with concentrations >20 mM. The system did not need to identify the ionic species since the use of an ECD system would later be used for identification. It was decided that a CCD system would be suitable to meet the requirements. The circuitry and an electrical equivalent circuit of the detection electrodes/fluid interface were simulated; this identified a suitable operating frequency for the fabricated detection system which was implemented into three of the four fabricated microfluidic devices. The development of the design for the CCD system was discussed in Sections 5.1.4 and 5.2.

A number of experiments were conducted with the aim of experimentally validating aspects of the theory, and modelling outputs, as listed in Table 12 (in Section 6.1), with the overall aim of constructing a working separation system. Some of these required the design and fabrication of microfluidic devices and ancillary hardware; this included the CCD system, a HVPS system and the incorporation of a micro-pump. After confirming basic electrokinetic fluid flow, the CCD system was proven to be fit for purpose; the limit of detection was measured as >1 mM, discussed in Section 6.9. Using an electrophoretic dye, the ability to increase and decrease the EOF was demonstrated on a planar CE device. Further to this, as discussed in Section 6.8, the reversal of the EOF was achieved; an electrophoretic dye was successfully controlled to migrate back and forth along the channel multiple times.

A number of difficulties were encountered with the fabrication of a microfluidic device to experimentally verify the separation enhancement methods as a whole as detailed in Section 6.11.3. Where possible, numerous aspects of the model have been verified either with experimental data from the fabricated microfluidic devices or by comparison with data extracted from results published by other researchers. This gives confidence that with

investigation into a suitable fabrication method, an enhancement in the separation of a sample as described by the model would be achieved. Such a device will be of significant interest for the development of portable and in-situ CE systems. The salient advantage for miniaturised portable CE systems is the ability to effectively increase the channel length without compromising the device size.

Whilst the separation enhancement routines can be implemented on standard CE instrumentation, for example by coating a capillary with conductive paint, the primary reason for their development and this investigation, which has focused on planar systems, is for the development of portable and in-situ CE devices. These devices are limited in terms of their channel length which means that the separation of samples with similar electrophoretic mobilities is difficult. Methods to overcome these difficulties, commonly reported in the literature, usually take the form of a chemical modification techniques. Either by modification of the channel walls using a coating to control the EOF, or alternatively the EOF can be controlled by modifying the buffer solution composition [42]. Another chemical modification method (sample complexation) works by modifying the sample to increase the difference in the electrophoretic mobilities of the constituents. The clear advantages of the separation enhancement routines developed in this work are that they remove the requirement for the complex chemistry. This is important since it makes the device more flexible in the range of analytes it is able to analyse, with minimal device reconfiguration. The chemical modification methods tend to be both device-material and sample composition dependent and consequently they result in a highly application specific device, and the proposed techniques here mitigate against this.

7.1.1. Main Contributions

A number of aspects of the fluidic model needed development in order to describe the behaviour of a CE system incorporating the separation enhancement methods. Whilst this model may be used to describe separation within standard CE systems, its use as a tool to aid the design and development of miniaturised CE systems, which incorporate the separation enhancement methods, is of greater interest. Firstly, a model describing the effect of the potential applied to the ZPM electrode on the EDL (and therefore the zeta-potential) was required. Following this a model describing the separation of a sample where the EOF is varied, effectively yielding a variable channel length was developed.

A classical model for the EDL was adjusted to describe the effect of the ZPM electrode on the zeta-potential in a fluidic channel subjected to an electric-field, as discussed in Section

4.2. The ionic distribution in the EDL is complex and there are a number of accepted models that have been used here to give an approximation for the potential distribution across the EDL. Further to this, the EDL model has been developed to account for the presence of an electric-field along the channel length which affects the dynamic modification of the zeta-potential. The makeup of the EDL depends on a number of factors and therefore it is highly application specific, however, numerous researchers have successfully used the various EDL approximations to model the EDL for a range of scenarios. With that in mind flexibility was built into the model so that the EDL representation can be interchanged for another depending on the application and accuracy required.

Using planar technology, it is difficult to fabricate a microfluidic device with a ZPM electrode that has complete channel coverage. With this in mind the effect of modifying the zeta-potential, and consequently the EOF using just a single electrode along one of the four channel walls was investigated. It has been shown that a difference in values of zeta-potential between the channel walls induces a proportional amount of sample dispersion, discussed in Section 4.4.3. Like diffusion, this dispersion effect acts against separation and is therefore undesirable. A certain amount of sample dispersion is deemed acceptable provided that it does not prevent separation within a given channel length. This amount of acceptable dispersion has been defined and used to infer limits on the maximum difference in EOF wall mobility. This can be translated such that based on a minimum difference in sample mobility a minimum channel length can be deduced.

Control systems have been described (Section 2.5), including a discussion on a novel system which effectively enables the matching of the EOF to the mean velocity of the sample. This system overcomes a number of issues which cause variability in real world testing, in contrast to laboratory conditions where variability can be controlled to some degree. For a feasible portable or in-situ CE system, the separation method needs to robust; hence a closed-loop control system is favourable. Such a control system requires the inclusion of a detection system at the end of the separator channel. This detection system is required to detect the presence of the ionic species; the system does not need to identify the species since this can be performed by a specific detector after the separation. This removes the time element often used to identify the sample constituents as separation is now detected independently of time. This makes the device resilient to experimental variability. Further to this, the requirement to completely separate a sample could be removed. For example, the ECD system discussed in Section 2.4.4.1 can distinguish between Cu^{2+} and Fe^{2+} provided there is no Fe^{3+} present. Therefore the separation system would only need to separate Fe^{3+} from the Cu^{2+} and Fe^{2+}; the separation of Cu^{2+} and Fe^{2+}, which is difficult and time

consuming due to their similar mobilities would not be required, and thus the analysis time would be significantly reduced.

7.1.2. Publications

A number of peer-reviewed and other publications have been produced during the course of this research to disseminate key results to the wider research community. These are listed in Appendix B.

7.2. Recommendations for Future Work

The future work has been divided into three sections. In the first, the work required to address the immediate issues encountered with device fabrication are discussed. Following this, in Section 7.2.2, a discussion on the work required to finalise the device such that it could be used by the applications specified for this project as discussed earlier in Section 2.1 is given. Finally in Section 7.2.3, alternative applications of the techniques and additional work are considered. Some applications would require little or no alteration to the envisaged end device whereas others would require some modifications.

7.2.1. Short-term Future Work

The project started in October 2008, at which time access to the cleanroom (Southampton Nanofabrication Centre) was limited due to the rebuild of the cleanroom following a fire in October 2005. Following the rebuild, the cleanroom was opened for use from September 2009, though officially opened on 28th January 2011. The limitations this placed on the equipment and facilities available strongly influenced the fabrication of the microfluidic devices, for example, hydrofluoric acid was not available. Further to this there were numerous difficulties and problems which arose during the initial setup of the equipment which often resulted in delays in the processing. Devices 1 and 2, the fabrication of which is discussed in Sections 6.6.2 and 6.7.2 respectively were fabricated without the use of a cleanroom. The requirement of a thin insulation layer to prove the separation enhancement methods meant that microfabrication techniques such as those employed in a cleanroom would be required.

An outcome of the studies discussed throughout this thesis is a number of key design parameters; these are useful for the design of an optimal device. The key design parameters

are the channel length and the insulation layer thickness which can be used to infer material restraints on the insulation layer. In Section 2.4.3 the advantages of a long channel length for CE systems were discussed, however for portable or in-situ devices shorter channel lengths are preferable. The separation enhancement methods were designed to address the issues of reduced channel lengths on the separation resolution of CE systems. As well as enabling separation in shorter channel lengths, the methods are better suited to short channel lengths since this enables the generation of large electric-fields at lower electrical potentials. For the demonstration of the separation enhancement methods a channel length of 80 mm was selected. This value was selected since a long channel length was desired however it was limited due to the requirement to fabricate on a 150 mm wafer (further details on the requirements of the design were discussed earlier in Section 6.4). It is possible to get an electric-field strength of 10 kV m^{-1} along a channel of length 80 mm by applying 800 V along the length. To get the same strength electric-field in a shorter device, since the required potential scales proportionally with the channel length, a lower potential can be used (i.e. a 40 mm channel would require a potential of 400 V for an electric-field of 10 kV m^{-1}). As discussed in Section 4.2, the potential along the channel directly affects the degree of modification of the zeta-potential for a given potential on the ZPM electrode. Therefore in a shorter channel, the potential difference along a channel can be made small without compromising the separation electric-field strength; with a smaller potential along the channel length, the amount of variation of the effect of the ZPM electrode on the zeta-potential along the channel length is reduced. For the matched EOF enhancement technique discussed in Section 2.4.2, the use of a short channel would require greater precision for the dynamic control of the EOF. For the switching EOF technique discussed in Section 2.4.3, a shorter channel length would mean that a greater number of switching events would be required.

In Chapter 6, due to issues encountered with device fabrication it was not possible to conduct Experiment 7. The task of fabricating a device to prove the separation enhancement methods was underestimated and therefore an in-depth investigation into a suitable fabrication method needs to be explored. The main difficulty encountered was due to the underperformance of the insulation layer. The dimensions of Device 4 were chosen as a combination of the results from the modelling (as discussed in Sections 4.2 and 4.4) and from a practical fabrication perspective. Since SU-8 was shown to be unsuitable (as discussed in Section 6.11.3.2) it should be replaced with a suitable material such as silicon nitride or silicon dioxide. In Section 6.11.3.2 an attempt at sputtering silicon nitride was discussed, due to the limited time available it was not possible to develop a suitable process

for the deposition of a low stress silicon nitride layer. As a consequence the resulting layer was highly stressed and unusable. In the short-term future work, the use of PECVD should be investigated for the deposition of a suitable insulation layer for example silicon dioxide or silicon nitride. In Section 6.11.4 a number of methods for minimising the stress of silicon nitride and silicon dioxide layers were discussed. Briefly, the growth temperature, pressure, gas composition and RF frequency need to be optimised. In Section 6.11.3.2 the use of a multilayer process to avoid potential issues with pinholes in the dielectric layer was discussed.

With this issue solved there are a number of experiments which should be run with a view to addressing Experiment 7. First the effect of the reduced electrode area of Device 4 compared with Device 3 should be evaluated to confirm that the detection system is fit for purpose. The testing methodology for this would bear significant similarity to that used for Experiment 5**.** The ancillary hardware (including the detection system, HVPS and micro pumps) required to fully test the prototype system has been fully developed; for the demonstration of the separation enhancement methods, these need no further work, later in Section 7.2 miniaturisation of the hardware is discussed. A computer controlled HVPS which has been integrated with the detection systems has been prepared. This system is able to autonomously control both the separation voltage and ZPM voltage. Originally it was planned to test the prototype system by sending the sample between the detectors a varying number of times. In preparation, to perform this autonomously the LabView program was modified so that it would switch the potential on the ZPM electrode when the detectors saw a peak, this would represent a sample entering a detector window. Each switching event would be triggered when the differential of the detector response exceeded a threshold value. After a set number of events the sample would be passed through the end detector to evaluate the effect that the number of cycles has on the separation. The main aims of Experiment 7 were to investigate the separation enhancement methods described in this thesis. Experiment 7 consisted of two parts:

1. demonstration of the switching EOF concept (described in Section 2.4.3 and modelled in Section 4.4),
2. demonstration of the matched EOF concept (described in Section 2.4.2 and modelled in Section 4.4).

For the first set of tests, the effect of switching the EOF can be investigated by performing the following tests (see Table 14), with a sample (for example: $CuCl_2$).

Table 14: Set of experiments to determine effect of number of switches in separation.

Test number	Number of Switching Events	Effective Distance Travelled (mm)
1	0	68
2	2	188
3	4	308
4	6	428
5	8	548
6	10	668
7	12	788
8	14	908
9	16	1028

Following the experiments, the effect of the number of switches on the separation between the Cu^{2+} ions and the Cl^{-} ions should be evaluated. Test 9 yields an effective channel length of 1 m which is comparable to a laboratory-based CE instrument. For comparison, it would be useful to perform electrophoresis with similar test conditions as for Test 9 using a 1 m length of capillary (without dynamic EOF modification/switching). The EOF of the capillary based system should be closely matched to the average EOF generated by the switching of Test 9. The EOF can be set by modifying the pH of the buffer solution. This comparison would give an experimental indication of the degree of addition sample dispersion, induced by the EOF modification technique.

For the second part of Experiment 7, the effect of the ZPM electrode on the EOF would first need to be characterised. This could be achieved using the same experimental methodology as used for Experiment 4. Following the characterisation, a number of runs with a sample (for example $CuCl_2$) should be conducted, where the EOF is modified. Where the EOF set to a value to match the mean sample velocity of $CuCl_2$, there should be a significant improvement in the separation recorded.

The use of $CuCl_2$ as a sample for Experiment 7 is useful for demonstrating the separation enhancement methods since it is relatively easy to separate. Following these experiments, the sample should be changed to a mixture of Cu^{2+}, Fe^{2+} and Fe^{3+} ions. Due to the similarity in the electrophoretic mobilities of these ions, there will be less separation attained. Further to this, the issue of matching the EOF to the sample velocity becomes more critical. Following these experiments, the results should be compared with the predictions from the model.

7.2.2. Addressing the Corrosion Monitoring Application

Whilst the hardware for conducting the experiments has been prepared, further development of the system to make it truly portable is required. The electronics for the CCD system can be made portable simply by changing the power source to a battery. For further miniaturisation, the PCB for the detection system circuitry could be significantly reduced. A control system needs to be developed and implemented onto a microprocessor. This control system is required to monitor the detectors, identify peaks and control the potentials on both the separation and ZPM electrodes which is easily achievable using a microcontroller. Further to this the HVPS would need to be made portable, initially, the use of a commercial HV DC-to-DC converter, such as those supplied by EMCO High Voltage Corp. could be used for this purpose. Following the separation of the sample, the ECD system needs to identify the species as discussed earlier in Section 2.4.4.1. The electrodes to achieve this have been incorporated into the buffer waste reservoir. The ECD detection system, along with the CCD system, HVPS and control system could be implemented onto a single PCB.

Later for an in-situ system, adjustments to the control system would be required to enable it to periodically control the micro-pump to acquire a sample. For real-world testing, this sample would need to be passed through a filter before separation. The control system would need to be capable of analysing and interpreting the resultant data from the ECD, and to flush the buffer reservoir following each ECD analysis. Further to this, it would be desirable to further reduce the channel length which in turn would results in a smaller device. The use of smaller channels would make the generation of larger electric-fields possible at lower voltages.

7.2.3. Further Applications and Additional Work

The separation enhancement methods enable a reduction in channel length and therefore are important for the development of portable and in-situ devices for a large range of applications. A number of potential applications were discussed in Section 2.1.1. The focus has been on producing a planar device which lends itself to mass fabrication and therefore potentially a cheap sensing platform. Low cost systems capable of CE analysis could provide detailed information about numerous environments, and are of interest for a wide range of applications. In Section 2.2 other applications concerned with the detection of metal ions (such as those of interest to this project) were discussed. One example application was water quality monitoring; with little or no modification, the system discussed here could be used

for the monitoring of water quality. If the cost of the whole system can be kept low, then it becomes feasible to create a network of sensors which incorporate CE analysis. This would greatly improve the applicability of a powerful analysis technique. An advantage of the separation enhancement methods described is that they avoid the requirement of complicated chemistry, therefore making them applicable to a wide range of applications.

Since the amount of sample dispersion is directly related to the induced difference in zeta-potential it would be useful to develop a set of standard buffer solutions which could be used to set the EOF value. This value should be set to minimise the maximum variation required to execute the separation enhancement schemes. This would reduce the amount of sample dispersion which in turn would decrease analysis time or further reduce device size. Having a range of buffering solutions would make the device capable of analysing a greater range of samples, improving its applicability.

7.2.4. Conclusion

This thesis has produced new work in the field of ionic separation, and although a final complete system was not attainable within the time of the project, valuable new results have been demonstrated, showing the way forward to a novel and practical microfluidic separation system.

The enhanced separation techniques described offer an alternative solution to solve the issues of attaining high resolution CE separation in a small channel length, and the investigation of the effects of a controlling electrode on one wall only are a practical and pragmatic development allowing simplified planar systems to make use of the techniques. The modelling of both EDLs and the associated zeta-potential in 2D fields contribute to knowledge in this area and allows limits on the performance of the device to be established, allowing future developments to be progressed with some confidence. The results inform on the creation of a device appropriate for the proposed application.

Appendix A

Conference and Workshop Attendance

Year	Name of conference or workshop	Location
2008	Attended the 14th Postgraduate Conference in the Materials, Bioengineering and nCATS Research Groups	Southampton, UK
2009	Attended Eurosensors XXIII conference	Lausanne, Switzerland
2009	Presented at the 15th Postgraduate Conference in the Materials, Bioengineering and nCATS Research Groups	Southampton, UK
2010	Presented at the 5th Asia-Pacific Conference on Transducers and Micro-nano Technology (APCOT 2010)	Perth, Western Australia
2010	Presented at the 13th International Meeting on Chemical Sensors (IMCS-13)	Perth, Western Australia
2010	Presented at the 51st Corrosion Science Symposium	Southampton, UK
2011	Presented at the Marine Energy Systems workshop	Southampton, UK
2011	Presented at Joint Academic Research Programme for Defence	Wiltshire, UK
2011	Presented at the 15th International Symposium on Field- and Flow-based Separations (FFF 2011)	San Francisco, USA
2011	Attended the 17th Postgraduate Conference in the Materials, Bioengineering and nCATS Research Groups	Southampton, UK
2012	Presented at Eurosensors XXVI	Kraków, Poland

Appendix B

Publications

Here is a list of all the publications which the author has been involved with, to date:

Peer-reviewed:

G. V. Merrett, A. S. Weddell, A. P. Lewis, N. R. Harris, B. M. Al-Hashimi and N. M. White – "An Empirical Energy Model for Supercapacitor Powered Wireless Sensor Nodes", *17th International IEEE Conference on Computer Communications and Networks,* Virgin Islands, USA (2008)

A. P. Lewis, A. Cranny, N. G. Green, M. Nie, J. A. Wharton, R. J. K. Wood, K. R. Stokes and N. R. Harris – "Novel Fabrication Method for Rapid Creation of Channels using PDMS for Microfluidic Networks on Planar Substrates", *5th Asia-Pacific Conference on Transducers and Micro-nano Technology (APCOT 2010),* University of Perth, Western Australia (2010)

A. Cranny, N. Harris, A. Lewis, M. Nie, J. Wharton, R. Wood, and K. Stokes – "Screen-printed platinum electrodes for the detection of cupric and ferric ions in high chloride backgrounds", *5th Asia-Pacific Conference on Transducers and Micro-nano Technology (APCOT 2010),* University of Perth, Western Australia (2010)

A. Cranny, N. Harris, A. Lewis, M. Nie, J. Wharton, R. Wood, and K. Stokes – "Lifetime performance characteristics of screen-printed potentiometric Ag/AgCl chloride sensors", *5th Asia-Pacific Conference on Transducers and Micro-nano Technology (APCOT 2010),* University of Perth, Western Australia (2010)

A. P. Lewis, A. Cranny, N. G. Green, M. Nie, J. A. Wharton, R. J. K. Wood, K. R. Stokes and N. R. Harris – "Improving Separation Resolution of Capillary Electrophoresis to Aid Corrosion Monitoring by Dynamic Control of the EOF", *13th International Meeting on Chemical Sensors (IMCS-13)*, University of Perth, Western Australia (2010)

A. Cranny, N. Harris, A. Lewis, M. Nie, J. Wharton, R. Wood, and K. Stokes – "Screen-printed platinum electrodes for measuring crevice corrosion: Nickel aluminium bronze as an example", *13th International Meeting on Chemical Sensors (IMCS-13)*, University of Perth, Western Australia (2010)

A. P. Lewis, A. Cranny, N. G. Green, N. R. Harris, K. R. Stokes, J. A. Wharton, and R. J. K. Wood – "A Closed-loop, Non-linear, Miniaturised Capillary Electrophoresis System Enabled by Control of Electroosmotic Flow", *15th International Symposium on Field- and Flow-based Separations*, San Francisco, USA (2011)

A. P. Lewis, A. Cranny, N. R. Harris, N. G. Green, J. A. Wharton, R. J. K. Wood and K. R. Stokes – "Modelling the operational limits of a separation enhancement method for capillary electrophoresis: a designer's tool", Procedia Engineering 47 694-697 – 26th European Conference on Solid-State Transducers (*Eurosensors XXVI)* (2012)

A. P. Lewis, A. Cranny, N. R. Harris, N. G. Green, J. A. Wharton, R. J. K. Wood and K. R. Stokes – "Review on the Development of Truly Portable and In-situ Capillary Electrophoresis Systems" – Measurement Science and Technology, 24, 4 (2013)

A. P. Lewis, A. Cranny, N. R. Harris, N. G. Green, J. A. Wharton, R. J. K. Wood and K. R. Stokes – "Modelling Methods for Improving Separation in Capillary- and Planar-based Capillary Electrophoresis Systems" – *Submitted to: Materials – Special Issue Corrosion Monitoring and Control* (2013)

Other:

A. P. Lewis, A. Cranny, N. R. Harris, M. Nie, J. A. Wharton, R. J. K. Wood and K. R. Stokes – "An Investigation into Separation Enhancement Methods for Miniaturised Planar Capillary Electrophoresis Devices", *15th Postgraduate Conference in the Materials, Bioengineering and nCATS Research Groups*, Southampton, UK (2009)

A. Cranny, N. Harris, A. Lewis, S. Neodo, M. Nie, K. Stokes, J. Wharton and R. Wood – "Microfluidic Devices for Structural Health Monitoring", *Marine Energy Systems Workshop Day*, Southampton, UK (2011)

A. Cranny, N. Harris, A. Lewis, S. Neodo, M. Nie, K. Stokes, J. Wharton and R. Wood – "Microfluidic Devices for Structural Health Monitoring", *Joint Academic Research Program for Defence*, Wiltshire, UK (2011)

Appendix C

COMSOL Multiphysics Modules

For the FEM analysis COMSOL Multiphysics versions 4.1 and then later 4.2a were used. This appendix contains some brief notes on the modules and settings that were used for the computation.

Modelling the EDL

To calculate the potential distribution across the insulation layer, the EDL and in the buffer solution, the *Electrostatics* module was used to solve Poisson's equation. The element sizes of the mesh for the entire geometry had the following parameters:

Maximum element size: $1x10^{-5}$ m

Maximum element size: $2x10^{-8}$ m

Around the region of the EDL in the solution the mesh was heavily refined.

Where the Gouy-Chapman model was used for the EDL, it could be directly entered into the space charge density of the EDL region. If the Nernst-Planck equations were used to describe the EDL, then a separate module, the *Transport of Diluted Species module* was required to calculate the change in concentration due to ionic transport in the EDL.

Modelling the Ionic Transport in the Microfluidic Device

For modelling the fluid behaviour subjected to an electric-field, three modules were required:

Electrostatics: to describe the electric-field in the solution.

Laminar Flow: to describe the EOF.

Transport of Diluted Species: to describe the diffusion and movement of charged species.

With the channel length being significantly greater than the channel width, it was difficult to generate a suitable mesh. The mesh needed to be small enough to accurately model variations across the channel width. With such small elements, this meant that a large number of them would be required to describe the full channel length. With the use of mapped meshes, in which the distribution of elements along the geometry could be specified, it was possible to simulate the whole channel. For some of the work described in this thesis however, a shortened channel length, (or segment of the channel) was used to reduce the required number of elements and therefore the computing time.

Appendix D

LabView Program

The LabView program described here was used to monitor the circuitry of both CCDs and to control the HVPSs connected to the microfluidic channel and the ZPM electrode. For convenience different aspects have been separated, however it should be noted that in practice they were all run within a single while-loop.

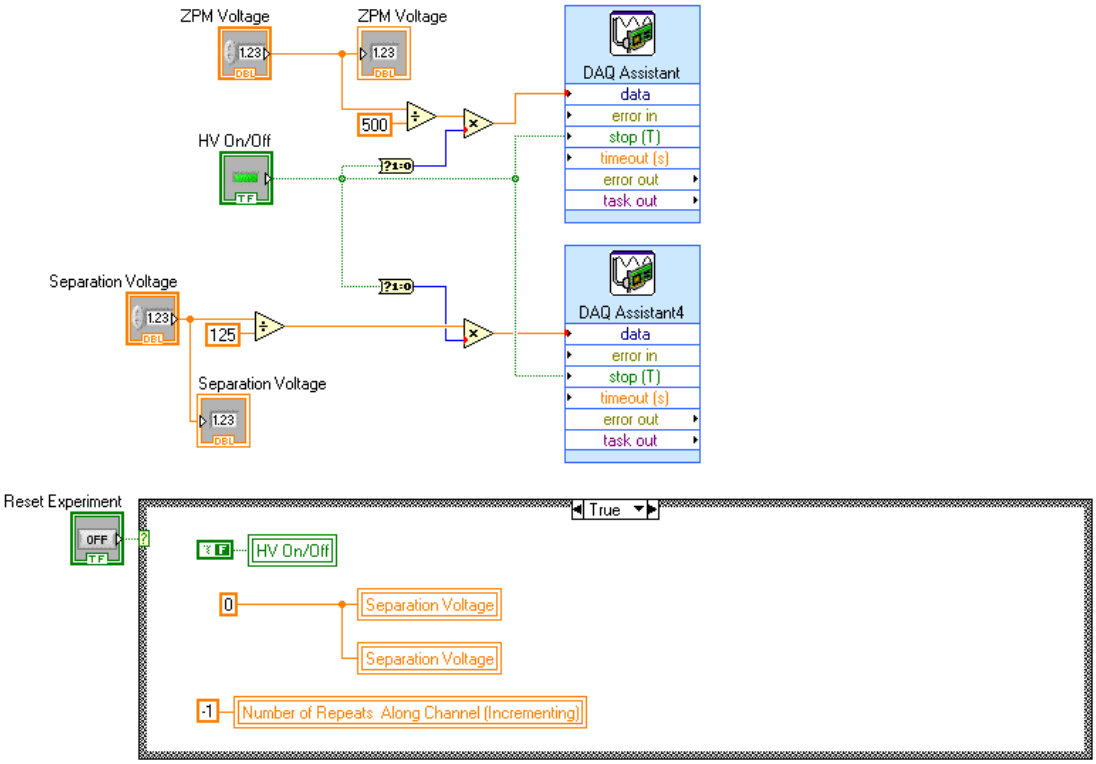

Figure 135: LabView program created to control the HVPSs connected to the microfluidic channel and ZPM.

A simplified flow chart showing the processing of the signals from the detection system is shown in Figure 136; an image of the LabView program developed to achieve this is given in Figure 137.

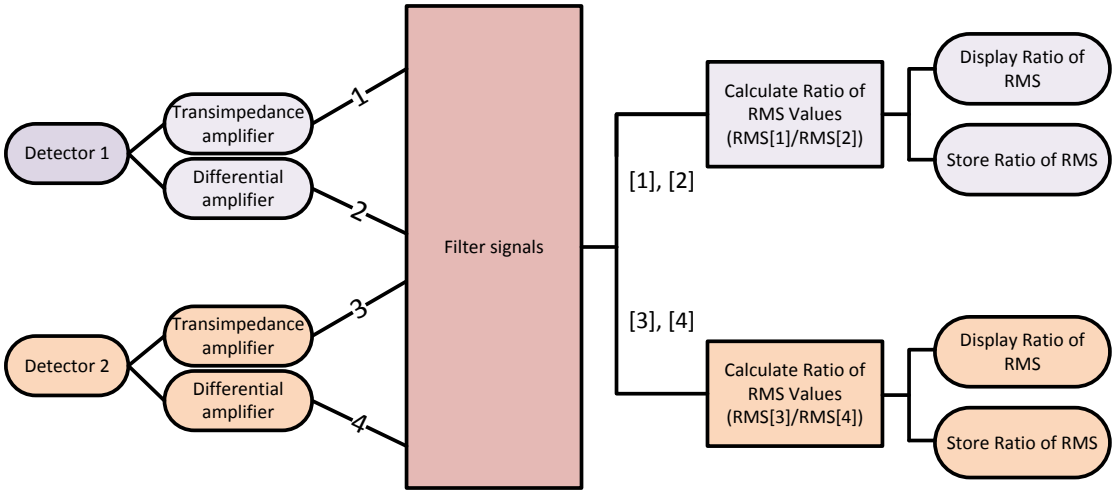

Figure 136: Flow chart showing processing of signals from detection systems.

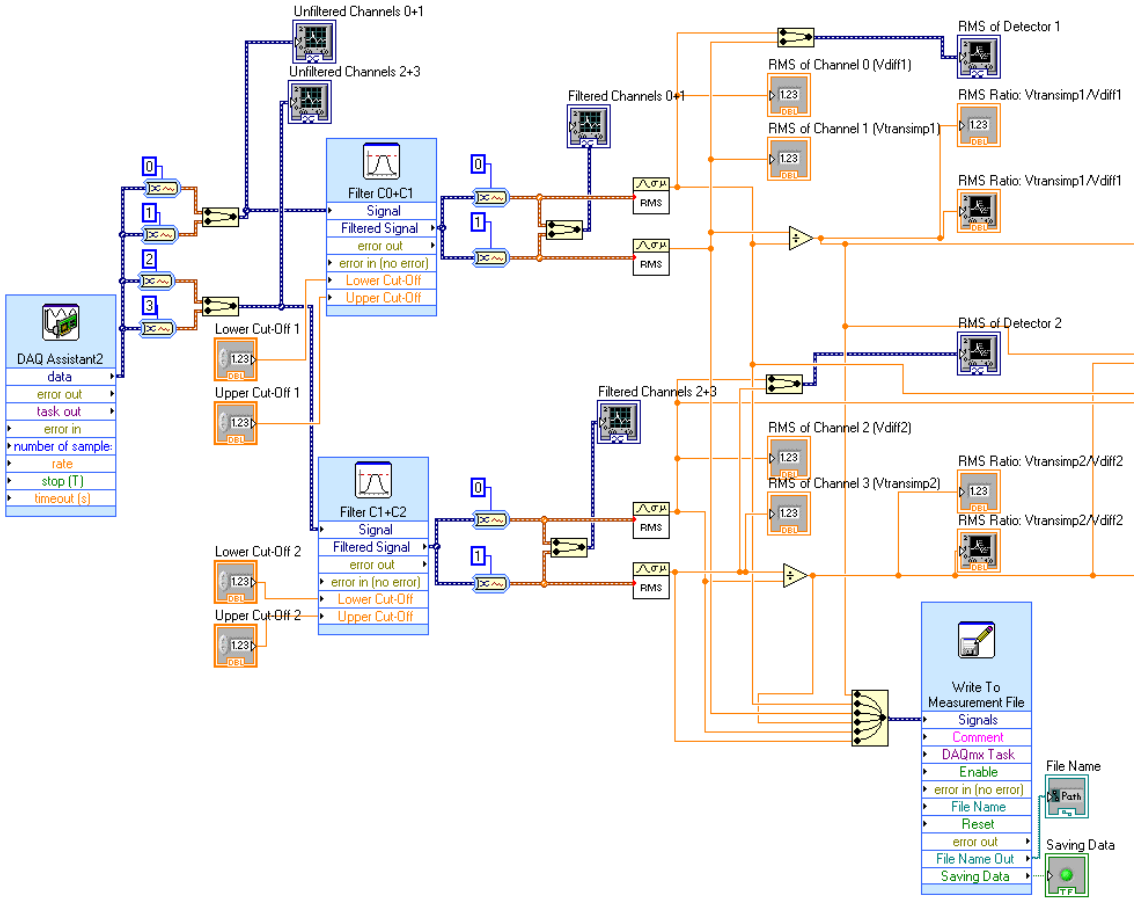

Figure 137: Image showing the LabView program designed to acquire, filter, measure and record the signals from the circuitry of the CCDs.

A flow chart for the control system for the autonomous control system for the switching separation enhancement method as described in Section 2.4.3 is shown in Figure 138.

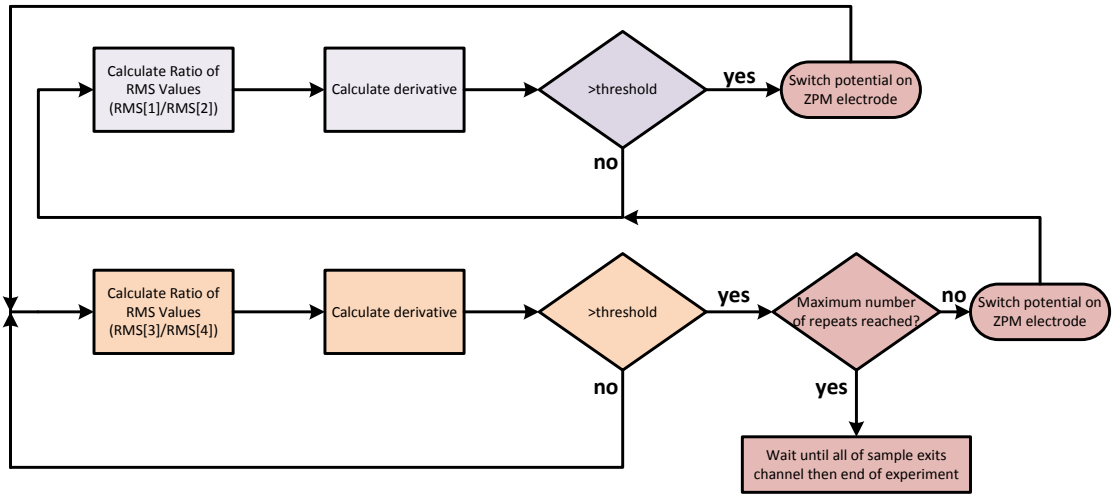

Figure 138: Flow chart describing autonomous control system for switching separation enhancement method.

The LabView implementation of this control system is shown in Figure 139

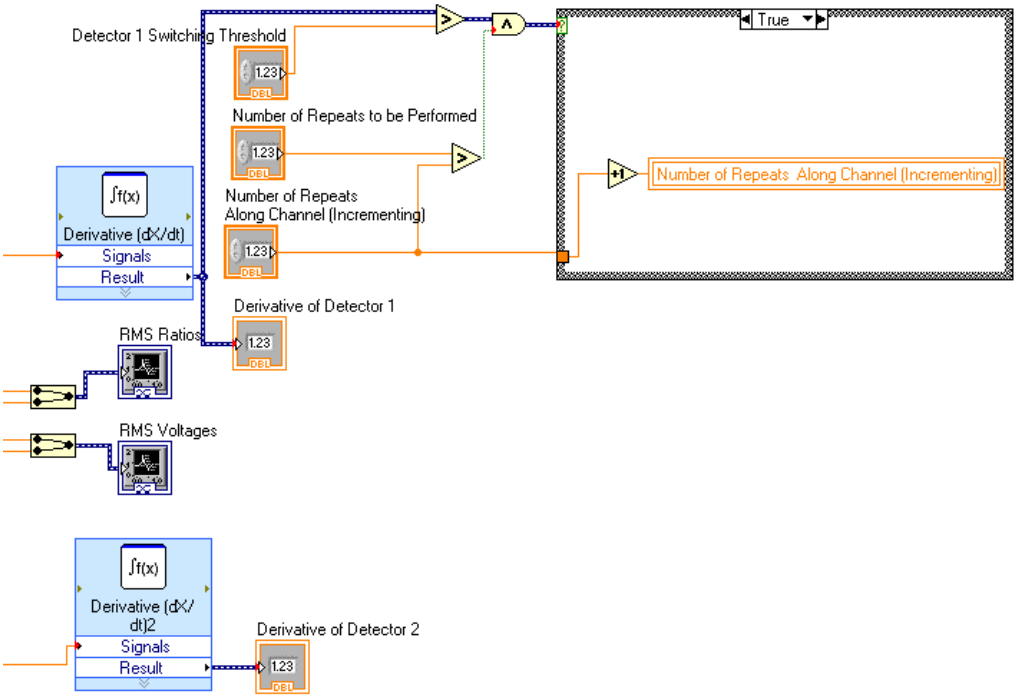

Figure 139: Proposed LabView program to enable the autonomous control for the switching separation enhancement method for the miniaturised CE system. Signal lines follow from Figure 137.

Appendix E

Novel Fabrication Method

The method can be split into two sections, the first of which uses physically removable channel formers, and the second which uses sacrificial materials.

The first method works by using a thin metal wire as the former of the channel; it is placed on the heads of two nylon bolts and surrounded with PDMS in an enclosure such as a plastic Petri dish. As well as supporting the wire above the base of the Petri dish, thus allowing the PDMS to completely surround the wire, resulting in a sealed channel, the primary purpose of the nylon bolts is to form reservoirs at either end of the channel. The PDMS is cured on a hot plate at 80 °C for 90 minutes; the use of a plastic Petri dish limited the maximum curing temperature. Once the PDMS was cured it could be easily released from the Petri dish by prising away at the edges using a little force. The nylon bolts could be removed which gives access to the underlying channel forming wire. Pulling the wire with a gentle force removed it, resulting in a complete, sealed channel, the diameter of which is approximately equal to the diameter of the wire.

Figure 140 shows two photographs of channels created by this method. In the top of Figure 140 an enclosed straight channel with a diameter of 600 μm, is shown. A channel diameter of 600 μm is considered relatively large for some researchers in the microfluidic community and so the next aim was to fabricate channels with smaller diameters. One issue that was encountered during experimentation with thinner wires was that they were more prone to breaking during removal. Our experiments with the wires showed success at making channels with diameters down to 180 μm. In the bottom picture of Figure 140 are two channels created using wires with diameters of 180 μm. Here the intention was to get a

channel to intersect another simply by overlapping the wires and pressing them together where they overlap so that no PDMS would flow at that point. As can be seen in the photograph at the bottom of Figure 140 red dye is flowed through the channels to show that this method enabled us to get the channels to connect. It is difficult to control the size of the connection made but it tends to be only a small area where the wires are in contact. For larger intersecting points a junction can be placed between the channel forming wires. Placing a junction former in PDMS is not an issue, however removing it after curing the PDMS can be. The junction former can be the same as the reservoir formers. Channels can be easily joined together by placing a junction former over the channel ends then covering in PDMS. After curing the PDMS the junction former can be removed in the same way that the reservoir formers are removed.

For initial tests to demonstrate the concept, caramel strands (a water soluble material) were used, this proved to be an effective material. Granulated white sugar was placed in a beaker and heated on a hotplate to 250 °C until it caramelised and then long strands were drawn. To draw the caramel strands a spatula was dipped into the beaker and a small amount of the liquid caramel removed and placed onto a non-stick surface. The spatula was then pulled slowly from the caramel which caused a strand to be drawn. Experimentation revealed that drawing longer strands resulted in the creation of more uniform strands of narrower dimensions. It was also discovered that pulling the strand at a constant speed helped to achieve more uniform strands. The drawn strands were placed on a non-stick surface where

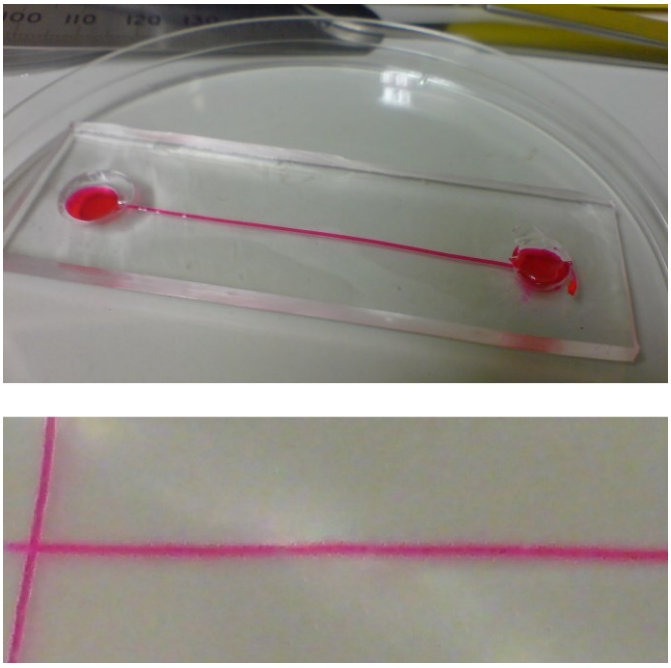

Figure 140: Photographs of microfluidic channels created by removal of wires from PDMS. Top: 600 µm diameter channel. Bottom: 180 µm diameter channel.

they could be measured and cut to the right length. After selecting, checking and modifying the strands they were moved onto a pre-cured layer of PDMS along with other structures required to produce features such as reservoirs at the ends of the channel. PDMS was then poured into the Petri dish to cover the channel and reservoir formers.

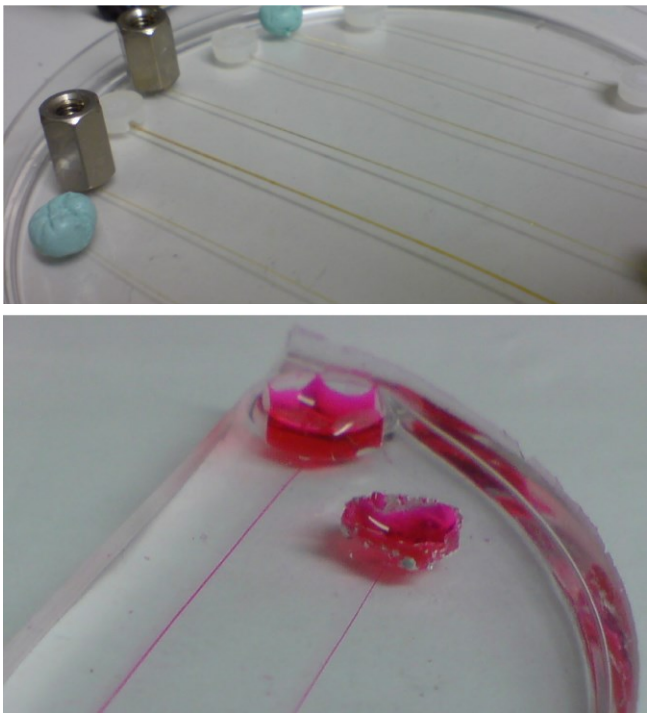

Figure 141: Top: PDMS with reservoir formers removed. Bottom: Final device with dye showing all channels are sealed and successfully connected to junctions/reservoirs.

The caramel strands are used much in the same way as the metal wires. After curing the PDMS, the end structures were carefully removed and the PDMS was peeled out of the Petri dish and placed in a beaker of deionised water and left until all the caramel dissolved. The process takes less than 24 hours; refreshing the bulk deionised water and agitating the beaker accelerates this process. Using an ultrasonic cleaner, the caramel could be dissolved in less than 10 minutes. In the top photograph of Figure 141 the caramel strands can be clearly seen in the PDMS with reservoir formers on the channel ends. Once all the caramel was dissolved the microfluidic channel is ready to be used. The hexagonal shaped reservoirs were formed due to the use of a metal hexagonal nut as the reservoir former. The sacrificial channel formers were explored primarily to achieve smaller channel dimensions. Using caramel as the sacrificial material from which strands were drawn enabled the fabrication of a microfluidic channel with a diameter of 16 μm. A photograph of this channel can be seen in the bottom of Figure 141.

This novel fabrication method enables the rapid development of microfluidic channels and structures using only basic laboratory tools and materials. In the first method casting around wires has been demonstrated to be low cost, practical and fast, enabling the fabrication of microfluidic channel networks with diameters down to 180 μm. Results from our second method which uses sacrificial caramel strands illustrates the usefulness of the principle of sacrificial layers for the development of microfluidic channels. By careful selection of the caramel strands it was shown that the method is capable of creating microfluidic channels down to 16 μm diameters. Neither of the methods described are complicated nor require specialist equipment which makes the technique suitable to a wide variety of researchers at low cost. The method is well suited for the development of a microfluidic platform for preliminary testing and prototyping reasons.

Appendix F

Recipe for Bonding PDMS to SU-8

PDMS is routinely bonded to glass wafers using an oxygen plasma. To bond PDMS to a glass wafer which has been insulated with SU-8 requires pre-treatment of the SU-8. The full bonding process is described here. This recipe was kindly provided by Dr Sam Birtwell. The steps are as follows:

1. Immerse wafer with SU-8 layer in 0.2 M APTES (amino-propyl-triethoxysilane) in EtOH for 12 hours at room temperature. Note: the SU-8 may swell slightly.
2. Rinse the wafer with EtOH then with DI water.
3. Immerse the wafer in DI water for 5 min.
4. Blow-dry the wafer with nitrogen and bake in an oven at 120 ˚C for 10 min.
5. Expose both the SU-8 and PDMS pieces to oxygen plasma with RF power of 50 W for 30 seconds.
6. Immediately bring both layers into contact then heat to 80 ˚C for 5 minutes.

References

[1] E. Bardal and J. M. Drugli, *Corrosion Detection and Diagnosis, in Materials Science and Engineering, [Ed. Rees D. Rawlings], in Encyclopedia of Life Support Systems (EOLSS)*: Eolss Publishers, Oxford, UK, 2004.

[2] J. A. Wharton and K. R. Stokes, "The influence of nickel–aluminium bronze microstructure and crevice solution on the initiation of crevice corrosion," *Electrochimica Acta,* vol. 53, pp. 2463-2473, 2008.

[3] E. Mattsson, *Basic Corrosion Technology for Scientists and Engineers*, Second ed.: The Institute of Materials, 1996.

[4] Randy K. Kent and S. Evans. Metallurgical and Microbial Aspects of Microbiologically Influenced Corrosion (MIC). *Forensic Engineering and Laboratories*. http://www.mde.com/publications/MDE_MIC_LR.pdf Last accessed: 22-09-12

[5] G. F. Kennell, R. W. Evitts, and K. L. Heppner, "A critical crevice solution and IR drop crevice corrosion model," *Corrosion Science,* vol. 50, pp. 1716-1725, 2008.

[6] E. A. Culpan and G. Rose, "Corrosion Behaviour of Cast Nickel Aluminium Bronze in Sea Water," *British Corrosion Journal,* vol. 14, pp. 160-166, 1979.

[7] J. A. Wharton and K. R. Stokes, "Analysis of nickel–aluminium bronze crevice solution chemistry using capillary electrophoresis," *Electrochemistry Communications,* vol. 9, pp. 1035-1040, 2007.

[8] M. Nie, J. A. Wharton, A. W. Cranny, R. J. K. Wood, N. H. Harris, and K. R. Stokes, "Crevice corrosion solution analysis by capillary electrophoresis with contactless conductivity detection," in *60th Annual Meeting of the International Society of Electrochemistry*, Beijing, China, 2009.

[9] M. Nie, A. W. Cranny, J. A. Wharton, N. H. Harris, R. J. K. Wood, and K. R. Stokes, "Crevice Solution Chemistries Evolution of Nickel-Aluminium Bronze in 3.5% NaCl Solution," in *8th Spring Meeting of the International Society of Electrochemistry*, Ohio, USA, 2010.

[10] A. Cranny, N. Harris, A. Lewis, M. Nie, J. Wharton, R. Wood, and K. Stokes, "Screen-printed platinum electrodes for the detection of cupric and ferric ions in high chloride backgrounds," presented at the 5th Asia-Pacific Conference on Transducers and Micro-nano Technology (APCOT), University of Perth, Western Australia, 2010.

[11] M. Nie, A. Cranny, J. A. Wharton, N. Harris, R. J. K. Wood, and K. R. Stokes, "Crevice corrosion solution analysis by capillary electrophoresis using a contactless conductivity detector," *Proceedings of the 49th Corrosion Science Symposium,* 2008.

[12] M. Nie, J. A. Wharton, A. W. Cranny, R. J. K. Wood, N. H. Harris, and K. R. Stokes, "Crevice corrosion solution analysis by capillary electrophoresis using a contactless conductivity detector," in *EuroCorr 2008*, Edinburgh, UK, 2008.

[13] A. Cranny, N. R. Harris, N. Mengyan, J. A. Wharton, R. J. K. Wood, and K. R. Stokes, "Sensors for Corrosion Detection: Measurement of Copper Ions in 3.5%

Sodium Chloride Using Screen-Printed Platinum Electrodes," *Sensors Journal, IEEE,* vol. 12, pp. 2091-2099, 2012.

[14] D. R. Crapper, S. S. Krishnan, and A. J. Dalton, "Brain Aluminum Distribution in Alzheimer's Disease and Experimental Neurofibrillary Degeneration," *Science,* vol. 180, pp. 511-513, May 4, 1973 1973.

[15] D. Perl and A. Brody, "Alzheimer's disease: X-ray spectrometric evidence of aluminum accumulation in neurofibrillary tangle-bearing neurons," *Science,* vol. 208, pp. 297-299, April 18, 1980 1980.

[16] T. Han, X. Feng, B. Tong, J. Shi, L. Chen, J. Zhi, and Y. Dong, "A novel "turn-on" fluorescent chemosensor for the selective detection of Al3+ based on aggregation-induced emission," *Chemical Communications,* vol. 48, pp. 416-418, 2012.

[17] Y.-H. Chan, J. Chen, Q. Liu, S. E. Wark, D. H. Son, and J. D. Batteas, "Ultrasensitive Copper(II) Detection Using Plasmon-Enhanced and Photo-Brightened Luminescence of CdSe Quantum Dots," *Analytical Chemistry,* vol. 82, pp. 3671-3678, 2010/05/01 2010.

[18] R. Løvstad, "A kinetic study on the distribution of Cu(II)-ions between albumin and transferrin," *Biometals,* vol. 17, pp. 111-113, 2004/04/01 2004.

[19] G. Multhaup, A. Schlicksupp, L. Hesse, D. Beher, T. Ruppert, C. L. Masters, and K. Beyreuther, "The Amyloid Precursor Protein of Alzheimer's Disease in the Reduction of Copper(II) to Copper(I)," *Science,* vol. 271, pp. 1406-1409, March 8, 1996 1996.

[20] X. Ma, Z. Tan, G. Wei, D. Wei, and Y. Du, "Solvent controlled sugar-rhodamine fluorescence sensor for Cu2+ detection," *Analyst,* vol. 137, pp. 1436-1439, 2012.

[21] P. Kubáň, P. Kubáň, and V. Kubáň, "Speciation of chromium (III) and chromium (VI) by capillary electrophoresis with contactless conductometric detection and dual opposite end injection," *Electrophoresis,* vol. 24, pp. 1397-1403, 2003.

[22] M. Urbanek, N. Delaunay, R. Michel, A. Varenne, and P. Gareil, "Analysis of sub-ppb levels of Fe(II), Co(II), and Ni(II) by electrokinetic supercharging preconcentration, CZE separation, and in-capillary derivatization," *Electrophoresis,* vol. 28, pp. 3767-3776, 2007.

[23] Y. C. Chan, M. Carles, N. J. Sucher, M. Wong, and Y. Zohar, "Design and fabrication of an integrated microsystem for microcapillary electrophoresis," *Journal of Micromechanics and Microengineering,* vol. 13, p. 914, 2003.

[24] Y. Jeong, S. Kim, K. Chun, J. Chang, and D. S. Chung, "Methodology for miniaturized CE and insulation on a silicon substrate," *Lab on a Chip,* vol. 1, pp. 143-7, 2001.

[25] S. L. S. Freire and A. R. Wheeler, "Proteome-on-a-chip: Mirage, or on the horizon?," *Lab on a Chip,* vol. 6, pp. 1415-1423, 2006.

[26] E. C. Rickard, R. J. Bopp, D. J. Skanchy, K. L. Chetwyn, B. Pahlen, and J. F. Stobaugh, "Role of capillary electrophoresis methods in the drug development process," *Chirality,* vol. 8, pp. 108-121, 1996.

[27] B. S. Sekhon, "An overview of capillary electrophoresis: Pharmaceutical, biopharmaceutical and biotechnology applications," *Indian Journal of Pharmaceutical Education and Research,* vol. 2, pp. 2-36, 2011.

[28] P. Vanýsek, *Ionic Conductivity and Diffusion at Infinite Dilution*, CRC Handbook of Chemistry and Physics 88th ed., 2007.

[29] M. Z. Bazant, K. Thornton, and A. Ajdari, "Diffuse-charge dynamics in electrochemical systems," *Physical Review E,* vol. 70, p. 021506, 2004.

[30] H. Bruus, *Theoretical Microfluidics*. Oxford: Oxford University Press, 2008.

[31] A. Manz, C. S. S Effenhauser, N. Burggraf, D. J. Harrison, K. Seiler, and K. Fluri, "Electroosmotic pumping and electrophoretic separations for miniaturized chemical analysis systems," *Journal of Micromechanics and Microengineers,* p. 257, 1994.

[32] M. X. Zhou and J. P. Foley, "Quantitative Theory of Electroosmotic Flow in Fused-Silica Capillaries Using an Extended Site-Dissociation−Site-Binding Model," *Analytical Chemistry,* vol. 78, pp. 1849-1858, 2006/03/01 2006.
[33] D. R. Baker, *Capillary Electrophoresis*: Wiley-Interscience, 1995.
[34] H.-F. Huang and C.-L. Lai, "Enhancement of mass transport and separation of species by oscillatory electroosmotic flows," *Proceedings of the Royal Society A: Mathematical, Physical and Engineering Science,* vol. 462, pp. 2017-2038, July 8, 2006 2006.
[35] H. Ban, B. Lin, and Z. Song, "Effect of electrical double layer on electric conductivity and pressure drop in a pressure-driven microchannel flow," *Biomicrofluidics,* vol. 4, pp. 014104-13, 2010.
[36] A. Sze, D. Erickson, L. Ren, and D. Li, "Zeta-potential measurement using the Smoluchowski equation and the slope of the current-time relationship in electroosmotic flow," *Journal of Colloid and Interface Science,* vol. 261, pp. 402-410, 2003.
[37] J. Ding, T. Barlow, A. Dipple, and P. Vouros, "Separation and identification of positively charged and neutral nucleoside adducts by capillary electrochromatography-microelectrospray mass spectrometry," *Journal of the American Society for Mass Spectrometry,* vol. 9, pp. 823-829, 1998.
[38] S. K. Vajandar, X. Dongyan, S. Jiashu, D. A. Markov, W. H. Hofmeister, and L. Deyu, "Field-Effect Control of Electroosmotic Pumping Using Porous Silicon - Silicon Nitride Membranes," *Journal of Microelectromechanical Systems,* vol. 18, pp. 1173-1183, 2009.
[39] E. K. Zholkovskij, A. E. Yaroshchuk, J. H. Masliyah, and J. D. Ribas, "Broadening of neutral solute band in electroosmotic flow through submicron channel with longitudinal non-uniformity of zeta potential," *Colloids and Surfaces a-Physicochemical and Engineering Aspects,* vol. 354, pp. 338-346, Feb 2010.
[40] E. K. Zholkovskij and J. H. Masliyah, "Influence of cross-section geometry on band broadening in plug-flow microchannels," *Chemical Engineering Science,* vol. 61, pp. 4155-4164, 2006.
[41] E. J. Van Der Wouden, T. Heuser, D. C. Hermes, R. E. Oosterbroek, J. G. E. Gardeniers, and A. Van Den Berg, "Field-effect control of electro-osmotic flow in microfluidic networks," *Colloids and Surfaces A: Physicochemical and Engineering Aspects,* vol. 267, pp. 110-116, 2005.
[42] W. Schüetzner and E. Kenndler, "Electrophoresis in synthetic organic polymer capillaries: variation of electroosmotic velocity and .zeta. potential with pH and solvent composition," *Analytical Chemistry,* vol. 64, pp. 1991-1995, 1992.
[43] E. A. S. Doherty, R. J. Meagher, M. N. Albarghouthi, and A. E. Barron, "Microchannel wall coatings for protein separations by capillary and chip electrophoresis," *Electrophoresis,* vol. 24, pp. 34-54, 2003.
[44] M. A. Hayes, I. Kheterpal, and A. G. Ewing, "Effects of buffer pH on electroosmotic flow control by an applied radial voltage for capillary zone electrophoresis," *Analytical Chemistry,* vol. 65, pp. 27-31, 1993/01/01 1993.
[45] D. C. Hermes, T. Heuser, E. J. Wouden van der, J. G. E. Gardeniers, and A. Berg van den, "Fabrication of microfluidic networks with integrated electrodes," *Microsystem Technologies,* vol. 12, pp. 436-440, 2006.
[46] M. A. Hayes and A. G. Ewing, "Electroosmotic flow control and monitoring with an applied radial voltage for capillary zone electrophoresis," *Analytical Chemistry,* vol. 64, pp. 512-516, 1992/03/01 1992.
[47] M. A. Hayes, I. Kheterpal, and A. G. Ewing, "Electroosmotic flow control and surface conductance in capillary zone electrophoresis," *Analytical Chemistry,* vol. 65, pp. 2010-2013, 1993/08/01 1993.

[48] N. A. Polson and M. A. Hayes, "Electroosmotic Flow Control of Fluids on a Capillary Electrophoresis Microdevice Using an Applied External Voltage," *Analytical Chemistry,* vol. 72, pp. 1088-1092, 2000.

[49] J. S. Buch, P. C. Wang, D. L. DeVoe, and C. S. Lee, "Field-effect flow control in a polydimethylsiloxane-based microfluidic system," *Electrophoresis,* vol. 22, pp. 3902-3907, Oct 2001.

[50] C.-Y. Lee, G.-B. Lee, L.-M. Fu, K.-H. Lee, and R.-J. Yang, "Electrokinetically driven active micro-mixers utilizing zeta potential variation induced by field effect," *Journal of Micromechanics and Microengineering,* vol. 14, p. 1390, 2004.

[51] N. J. Sniadecki, C. S. Lee, M. Beamesderfer, and D. L. DeVoe, "Field-effect flow control in polymer microchannel networks," *12th International Conference on Solid-State Sensors, Actuators and Microsystems,* pp. 682-5 vol.1|2 vol.(xl+xxxix+1938), 2003.

[52] N. J. Sniadecki, C. S. Lee, P. Sivanesan, and D. L. DeVoe, "Induced Pressure Pumping in Polymer Microchannels via Field-Effect Flow Control," *Analytical Chemistry,* vol. 76, pp. 1942-1947, 2004.

[53] B. J. Kirby and E. F. Hasselbrink, "Zeta potential of microfluidic substrates: 1. Theory, experimental techniques, and effects on separations," *Electrophoresis,* vol. 25, pp. 187-202, 2004.

[54] B. J. Kirby and E. F. Hasselbrink, "Zeta potential of microfluidic substrates: 2. Data for polymers," *Electrophoresis,* vol. 25, pp. 203-213, 2004.

[55] A. P. Lewis, A. Cranny, N. R. Harris, N. G. Green, J. A. Wharton, R. J. K. Wood, and K. R. Stokes, "Modelling the Operational Limits of a Separation Enhancement Method for Capillary Electrophoresis: a Designer's Tool," *Procedia Engineering,* vol. 47, pp. 694-697, 2012.

[56] C. T. Wu, T. L. Huang, C. S. Lee, and C. J. Miller, "Dispersion studies of capillary electrophoresis with direct control of the electroosmosis," *Analytical Chemistry,* vol. 65, pp. 568-571, Mar 1993.

[57] A. Varenne and S. Descroix, "Recent strategies to improve resolution in capillary electrophoresis--A review," *Analytica Chimica Acta,* vol. 628, pp. 9-23, 2008.

[58] A. P. Lewis, A. Cranny, N. G. Green, N. R. Harris, K. R. Stokes, J. A. Wharton, and R. J. K. Wood, "A Closed-loop, Non-linear, Miniaturised Capillary Electrophoresis System Enabled by Control of Electroosmotic Flow," presented at the 15th International Symposium on Field- and Flow-based Separations, San Francisco, 2011.

[59] A. J. Bard and L. R. Faulkner, *Electrochemical methods: fundamentals and applications*: Wiley, 1980.

[60] P. Vanýsek, *Electrochemical series*, CRC Handbook of Chemistry and Physics 88th ed., 2007.

[61] B. Mills. *Standard Electrode Potentials*. http://www.benjamin-mills.com/chemistry/ecells.htm Last accessed 22-09-12

[62] C. R. Nave. (2012). *HyperPhysics: Standard Electrode Potentials in Aqueous Solution at 25°C*. http://hyperphysics.phy-astr.gsu.edu/hbase/tables/electpot.html Last accessed 22-09-12

[63] S. Neodo, D. Carugo, J. A. Wharton, and K. R. Stokes, "Electrochemical behaviour of nickel–aluminium bronze in chloride media: Influence of pH and benzotriazole," *Journal of Electroanalytical Chemistry,* vol. 695, pp. 38-46, 2013.

[64] S. Neodo, M. Nie, J. A. Wharton, and K. R. Stokes, "Nickel-ion detection on a boron-doped diamond electrode in acidic media," *Electrochimica Acta,* vol. 88, pp. 718-724, 2013.

[65] C. M. A. Brett and A. M. O. Brett, *Electrochemistry: principles, methods, and applications*: Oxford University Press, 1993.

[66] A. P. Lewis, A. Cranny, N. R. Harris, N. G. Green, J. A. Wharton, R. J. K. Wood, and K. R. Stokes, "Review on the development of truly portable and in-situ capillary electrophoresis systems," *Measurement Science and Technology,* vol. 24, p. 042001, 2013.

[67] L. Bousse, C. Cohen, T. Nikiforov, A. Chow, A. R. Kopf-Sill, R. Dubrow, and J. W. Parce, "Electrokinetically controlled microfluidic analysis systems," *Annual Review of Biophysics and Biomolecular Structure,* vol. 29, pp. 155-181, 2000.

[68] J. Lichtenberg, N. F. de Rooij, and E. Verpoorte, "A microchip electrophoresis system with integrated in-plane electrodes for contactless conductivity detection," *Electrophoresis,* vol. 23, pp. 3769-3780, 2002.

[69] M. Ryvolova, J. Preisler, D. Brabazon, and M. Macka, "Portable capillary-based (non-chip) capillary electrophoresis," *Trac-Trends in Analytical Chemistry,* vol. 29, pp. 339-353, Apr 2010.

[70] G. V. Kaigala, V. N. Hoang, and C. J. Backhouse, "Electrically controlled microvalves to integrate microchip polymerase chain reaction and capillary electrophoresis," *Lab on a Chip,* vol. 8, pp. 1071-1078, 2008.

[71] X. Xu, S. Zhang, H. Chen, and J. Kong, "Integration of electrochemistry in micro-total analysis systems for biochemical assays: Recent developments," *Talanta,* vol. 80, pp. 8-18, 2009.

[72] K. A. Mahabadi, I. Rodriguez, L. Hong, P. C. Hauser, and N. F. de Rooij, "Restrictive dual capacitively coupled contactless conductivity detection for microchip electrophoresis," *Procedia Chemistry,* vol. 1, pp. 1351-1354, 2009.

[73] A. Shastry and R. Lal, "ChipCE: A silicon microsystem for migration, separation and detection of DNA," in *IEEE The Sixteenth Annual International Conference on Micro Electro Mechanical Systems*, Kyoto, 2003, pp. 427-430.

[74] R. S. Martin, K. L. Ratzlaff, B. H. Huynh, and S. M. Lunte, "In-Channel Electrochemical Detection for Microchip Capillary Electrophoresis Using an Electrically Isolated Potentiostat," *Analytical Chemistry,* vol. 74, pp. 1136-1143, 2002.

[75] C. Berg, D. C. Valdez, P. Bergeron, M. F. Mora, C. D. Garcia, and A. Ayon, "Lab-on-a-robot: Integrated microchip CE, power supply, electrochemical detector, wireless unit, and mobile platform," *Electrophoresis,* vol. 29, pp. 4914-4921, 2008.

[76] M. Benhabib, T. N. Chiesl, A. M. Stockton, J. R. Scherer, and R. A. Mathies, "Multichannel Capillary Electrophoresis Microdevice and Instrumentation for in Situ Planetary Analysis of Organic Molecules and Biomarkers," *Analytical Chemistry,* vol. 82, pp. 2372-2379, Mar 2010.

[77] D. Janasek, J. Franzke, and A. Manz, "Scaling and the design of miniaturized chemical-analysis systems," *Nature,* vol. 442, pp. 374-380, Jul 27 2006.

[78] R. Weinberger, *Practical capillary electrophoresis*: Academic Press, 2000.

[79] C. J. Evenhuis, R. M. Guijt, M. Macka, P. J. Marriott, and P. R. Haddad, "Variation of zeta-potential with temperature in fused-silica capillaries used for capillary electrophoresis," *Electrophoresis,* vol. 27, pp. 672-676, 2006.

[80] G. Y. Tang, C. Yang, C. J. Chai, and H. Q. Gong, "Modeling of Electroosmotic Flow and Capillary Electrophoresis with the Joule Heating Effect: The Nernst−Planck Equation versus the Boltzmann Distribution," *Langmuir,* vol. 19, pp. 10975-10984, 2003/12/01 2003.

[81] A. Oki, Y. Takamura, Y. Ito, and Y. Horiike, "pH Change of buffer solution in a microcapillary chip and its suppression," *Electrophoresis,* vol. 23, pp. 2860-2864, 2002.

[82] L. Szekely and R. Freitag, "Study of the electroosmotic flow as a means to propel the mobile phase in capillary electrochromatography in view of further miniaturization of capillary electrochromatography systems," *Electrophoresis,* vol. 26, pp. 1928-1939, 2005.

[83] H. Song, Y. Wang, and K. Pant, "System-level simulation of liquid filling in microfluidic chips," *Biomicrofluidics,* vol. 5, pp. 024107-16, 2011.
[84] D. B. Weibel, A. C. Siegel, A. Lee, A. H. George, and G. M. Whitesides, "Pumping fluids in microfluidic systems using the elastic deformation of poly(dimethylsiloxane)," *Lab on a Chip,* vol. 7, pp. 1832-1836, 2007.
[85] J. Monahan, A. A. Gewirth, and R. G. Nuzzo, "A method for filling complex polymeric microfluidic devices and arrays," *Analytical Chemistry,* vol. 73, pp. 3193-3197, Jul 2001.
[86] D. J. Jackson, J. F. Naber, T. J. Roussel Jr, M. M. Crain, K. M. Walsh, R. S. Keynton, and R. P. Baldwin, "Portable high-voltage power supply and electrochemical detection circuits for microchip capillary electrophoresis," *Analytical Chemistry,* vol. 75, pp. 3643-3649, 2003.
[87] Y. Xu, W. Wang, and S. F. Y. Li, "Simultaneous determination of low-molecular-weight organic acids and chlorinated acid herbicides in environmental water by a portable CE system with contactless conductivity detection," *Electrophoresis,* vol. 28, pp. 1530-1539, 2007.
[88] V. Dolník, "Wall coating for capillary electrophoresis on microchips," *Electrophoresis,* vol. 25, pp. 3589-3601, 2004.
[89] J. Wang, "Electrochemical Detection for Capillary Electrophoresis Microchips: A Review," *Electroanalysis,* vol. 17, pp. 1133-1140, 2005.
[90] C. Vogt and G. L. Klunder, "Separation of metal ions by capillary electrophoresis - diversity, advantages, and drawbacks of detection methods," *Journal of Analytical Chemistry,* vol. 370, pp. 316-331, 2001.
[91] Arne Tiselius - Biography. (2012). http://www.nobelprize.org/nobel_prizes/chemistry/laureates/1948/tiselius-bio.html Last accessed 22-09-12
[92] J. M. Butler. (2007). Topics and Techniques for Forensic DNA Analysis - Capillary Electrophoresis (and Microchip CE) Fundamentals. *Houston DNA Training Workshop*. http://www.cstl.nist.gov/strbase/pub_pres/1_CE_Fundamentals.pdf Last accessed: 22-09-12
[93] "Stellan Hjerten, Uppsala University," *Analyst,* vol. 128, pp. 1307-1309, 2003.
[94] Prince Technologies. (2012). *PrinCE-C 700 series instrument*. http://www.princetechnologies.eu Last accessed: 22-09-12
[95] CE Resources Pte Ltd. (2007). *CE Resources Pte Ltd. "CE-P2 Analyzer"*. http://www.ce-resources.com/ Last accessed 22-09-12
[96] J. Wang, G. Chen, M. P. Chatrathi, and M. Musameh, "Capillary Electrophoresis Microchip with a Carbon Nanotube-Modified Electrochemical Detector," *Anal. Chem.,* vol. 76, pp. 298-302, 2004.
[97] B. A. Peeni, D. B. Conkey, J. P. Barber, R. G. Kelly, M. L. Lee, A. T. Woolley, and A. R. Hawkins, "Planar thin film device for capillary electrophoresis," *The Royal Society of Chemistry - Lab on a Chip,* vol. 5, pp. 501-505, 2005.
[98] M.-M. Hsieh and H.-T. Chang, "Dynamic control for the separation of organic acids in capillary electrophoresis," *Journal of Chromatography A,* vol. 793, pp. 145-152, 1998.
[99] T. Hirokawa, Y. Takayama, A. Arai, and Z. Xu, "Study of a novel sample injection method (floating electrokinetic supercharging) for high-performance microchip electrophoresis of DNA fragments," *Electrophoresis,* vol. 29, pp. 1829-1835, 2008.
[100] S. Nováková, S. Van Dyck, A. Van Schepdael, J. Hoogmartens, and Z. Glatz, "Electrophoretically mediated microanalysis," *Journal of Chromatography,* vol. 1032, pp. 173-184, 2004.
[101] J. F. Dishinger and R. T. Kennedy, "Multiplexed detection and applications for separations on parallel microchips," *Electrophoresis,* vol. 29, pp. 3296-3305, 2008.

[102] J. Wang, G. Chen, and A. Muck, "Movable Contactless-Conductivity Detector for Microchip Capillary Electrophoresis," *Anal. Chem.,* vol. 75, pp. 4475-4479, 2003.
[103] A. Hilmi and J. H. T. Luong, "Electrochemical Detectors Prepared by Electroless Deposition for Microfabricated Electrophoresis Chips," *Analytical Chemistry,* vol. 72, pp. 4677-4682, 2000.
[104] J. Wang, M. Pumera, G. Collins, and O. Frantisek, "A chip-based capillary electrophoresis-contactless-conductivity microsystem for fast measurement of low-explosive ionic components," *The Royal Society of Chemistry - Analyst,* vol. 127, pp. 719-723, 2002.
[105] J. Wang and M. Pumera, "Dual Conductivity/Amperometric Detection System for Microchip Capillary Electrophoresis," *Anal. Chem.,* vol. 74, pp. 5919-5923, 2002.
[106] J. Wang, R. Polsky, B. Tian, and M. P. Chatrathi, "Voltammetry on Microfluidic Chip Platforms," *Analytical Chemistry,* vol. 72, pp. 5285-5289, 2000.
[107] D.-M. Tsai, H.-W. Tai, P.-R. Shih, R.-L. Chang, H. Wu, E. D. Conte, and J.-M. Zen, "Incorporation of Disposable Screen-Printed Electrodes for Use in Capillary Electrophoresis End-Column Amperometric Detection System," *Electroanalysis,* vol. 17, pp. 1991-1994, 2005.
[108] R.-H. Horng, P. Han, H.-Y. Chen, K.-W. Lin, T.-M. Tsai, and J.-M. Zen, "PMMA-based capillary electrophoresis electrochemical detection microchip fabrication," *Journal of Micromechanics and Microengineering,* p. 6, 2005.
[109] J. Caslavska, E. Gassmann, and W. Thormann, "Modification of a tunable UV-visible capillary electrophoresis detector for simultaneous absorbance and fluorescence detection: profiling of body fluids for drugs and endogenous compounds," *Journal of Chromatography A,* vol. 709, pp. 147-156, 1995.
[110] R. Wilke and S. Büttgenbach, "A micromachined capillary electrophoresis chip with fully integrated electrodes for separation and electrochemical detection," *Biosensors and Bioelectronics,* vol. 19, pp. 149-153, 2003.
[111] X. Zhu, G. Liu, Y. Xiong, Y. Guo, and Y. Tian, "Fabrication of PMMA Microchip of Capillary Electrophoresis by Optimized UV-LIGA Process," *Journal of Physics: Conference Series,* p. 875, 2006.
[112] V. Unterholzner, M. Macka, P. R. Haddad, and A. Zemann, "Simultaneous separation of inorganic anions and cations using capillary electrophoresis with a moveable contactless conductivity detector," *The Royal Society of Chemistry - Analyst,* vol. 127, pp. 715-718, 2002.
[113] W.-P. Yang, Z.-J. Zhang, and W. Deng, "Speciation of chromium by in-capillary reaction and capillary electrophoresis with chemiluminescence detection," *Journal of Chromatography A,* vol. 1014, pp. 203-214, 2003.
[114] T. Kappes, P. Schnierle, and P. C. Hauser, "Potentiometric detection of inorganic anions and cations in capillary electrophoresis with coated-wire ion-selective electrodes," *Analytica Chimica Acta,* vol. 350, pp. 141-147, 1997.
[115] E. Dabek-Zlotorzynska, E. P. C. Lai, and A. R. Timerbaev, "Capillary electrophoresis: the state-of-the-art in metal speciation studies," *Analytica Chimica Acta,* vol. 359, pp. 1-26, 1998.
[116] I. Ali, V. K. Gupta, and H. Y. Aboul-Enein, "Metal ion speciation and capillary electrophoresis: Application in the new millennium," *Electrophoresis,* vol. 26, pp. 3988-4002, 2005.
[117] R. G. Kelly, J. Yuan, C. M. Weyant, and K. S. Lewis, "Applications of capillary electrophoresis in corrosion science and engineering," *Journal of Chromatography A,* vol. 834, pp. 433-444, 1999.
[118] Z. Demianova, E. Poysa, S. Ihalainen, S. Saura, M. Shimmo, S. Franssila, and M. Baumann, "Development and application of a miniaturized gel electrophoresis device for protein analysis," *Molecular BioSystems,* vol. 4, pp. 260-265, 2008.

[119] A. Li, X. Chen, and V. M. Ugaz, "Miniaturized System for Rapid Field Inversion Gel Electrophoresis of DNA with Real-Time Whole-Gel Detection," *Analytical Chemistry,* vol. 82, pp. 1831-1837, 2010/03/01 2010.

[120] F. Raisi, P. Belgrader, D. A. Borkholder, A. E. Herr, G. J. Kintz, F. Pourhamadi, M. T. Taylor, and M. A. Northrup, "Microchip isoelectric focusing using a miniature scanning detection system," *Electrophoresis,* vol. 22, pp. 2291-2295, 2001.

[121] W. Tan, Z. H. Fan, C. X. Qiu, A. J. Ricco, and I. Gibbons, "Miniaturized capillary isoelectric focusing in plastic microfluidic devices," *Electrophoresis,* vol. 23, pp. 3638-3645, 2002.

[122] V. Dolnik and S. Liu, "Applications of capillary electrophoresis on microchip," *Journal of Separation Science,* vol. 28, pp. 1994-2009, 2005.

[123] M. Pumera, "Analysis of explosives via microchip electrophoresis and conventional capillary electrophoresis: A review," *Electrophoresis,* vol. 27, pp. 244-256, Jan 2006.

[124] S.-i. Wakida, K. Fujimoto, H. Nagai, T. Miyado, Y. Shibutani, and S. Takeda, "On-chip micellar electrokinetic chromatographic separation of phenolic chemicals in waters," *Journal of Chromatography A,* vol. 1109, pp. 179-182, 2006.

[125] M. C. Breadmore, M. Dawod, and J. P. Quirino, "Recent advances in enhancing the sensitivity of electrophoresis and electrochromatography in capillaries and microchips (2008–2010)," *Electrophoresis,* vol. 32, pp. 127-148, 2011.

[126] J. F. Borowsky, B. C. Giordano, Q. Lu, A. Terray, and G. E. Collins, "Electroosmotic Flow-Based Pump for Liquid Chromatography on a Planar Microchip," *Analytical Chemistry,* vol. 80, pp. 8287-8292, 2008/11/01 2008.

[127] Y. Ladner, G. Cretier, and K. Faure, "Electrochromatography in cyclic olefin copolymer microchips: A step towards field portable analysis," *Journal of Chromatography A,* vol. 1217, pp. 8001-8008, Dec 2010.

[128] J. E. Prest, S. J. Baldock, P. R. Fielden, N. J. Goddard, and B. J. Treves Brown, "Bidirectional isotachophoresis on a planar chip with integrated conductivity detection," *The Royal Society of Chemistry - Analyst,* vol. 127, pp. 1413-1419, 2002.

[129] J. E. Prest, M. S. Beardah, S. J. Baldock, S. P. Doyle, P. R. Fielden, N. J. Goddard, and B. J. T. Brown, "Determination of chlorine containing species in explosive residues using chip-based isotachophoresis," *Journal of Chromatography A,* vol. 1195, pp. 157-163, 2008.

[130] J. E. Prest, S. J. Baldock, P. E. Fielden, and B. J. T. Brown, "Determination of metal cations on miniaturised planar polymeric separation devices using isotachophoresis with integrated conductivity detection," *Analyst,* vol. 126, pp. 433-437, 2001.

[131] J. E. Prest, S. J. Baldock, P. R. Fielden, N. J. Goddard, and B. J. Treves Brown, "Miniaturised isotachophoretic analysis of inorganic arsenic speciation using a planar polymer chip with integrated conductivity detection," *Journal of Chromatography A,* vol. 990, pp. 325-334, 2003.

[132] T. Hirokawa, T. Ohta, K.-i. Nakamura, K. Nishimoto, and F. Nishiyama, "Bidirectional isotachophoresis separation of metal cations using EDTA sa a chelating agent," *Journal of chromatography A,* vol. 709, pp. 171-180, 1995.

[133] J. G. Santiago. (2012). *Stanford University - Stanford Microfluidics Laboratory - Juan G. Santiago - Journal Publications*. http://microfluidics.stanford.edu/Publications/Publications.html Last accessed 22-09-12

[134] G. Garcia-Schwarz and J. G. Santiago, "Integration of On-Chip Isotachophoresis and Functionalized Hydrogels for Enhanced-Sensitivity Nucleic Acid Detection," *Analytical Chemistry,* vol. 84, pp. 6366-6369, 2012/08/07 2012.

[135] M. Bercovici, G. V. Kaigala, K. E. Mach, C. M. Han, J. C. Liao, and J. G. Santiago, "Rapid Detection of Urinary Tract Infections Using Isotachophoresis and Molecular Beacons," *Analytical Chemistry,* vol. 83, pp. 4110-4117, 2011/06/01 2011.

[136] M. Bercovici, G. V. Kaigala, C. J. Backhouse, and J. G. Santiago, "Fluorescent Carrier Ampholtyes Assay for Portable Label-Free Detection of Chemical Toxins in Tap Water," *Analytical Chemistry,* vol. 82, pp. 1858-1866, 2010.

[137] Y. Utsumi, M. Ozaki, S. Tereabe, and T. Hattori, "Effects of improved microchannel structures to the separation characteristics of microchip capillary electrophoresis," in *International Microprocesses and Nanotechnology Conference*, Tokyo, Japan, 2002, pp. 176-177.

[138] D. L. Pugmire, E. A. Waddell, R. Haasch, M. J. Tarlov, and L. E. Locascio, "Surface Characterization of Laser-Ablated Polymers Used for Microfluidics," *Analytical Chemistry,* vol. 74, pp. 871-878, 2002.

[139] S. Datta, S. Ghosal, and N. A. Patankar, "Electroosmotic flow in a rectangular channel with variable wall zeta-potential: Comparison of numerical simulation with asymptotic theory," *Electrophoresis,* vol. 27, pp. 611-619, 2006.

[140] D. J. Jackson, J. F. Naber, R. P. Baldwin, K. M. Walsh, R. S. Keynton, M. M. Crain, T. J. Roussel Jr, and M. Diaconu, "Compact Battery Powered High Voltage Power Supply for Capillary Electrophoresis using Microchip Capillaries," presented at the Pittcon, 2001.

[141] V. Bathlagundu, D. Jackson, J. Naber, R. Baldwin, K. Walsh, R. Keyton, M. Crain, T. Roussel, and M. Diaconu, "A portable battery powered electrochemical detection circuit with a 1000 volt CE power supply for microchip capillaries," in *Proceedings 14th Biennial University/Government/Industry Microelectronics Symposium*, ed, 2001, pp. 197-200.

[142] R. S. Pai, T. J. Roussel, M. M. Crain, D. J. Jackson, J. A. Conklin, R. P. Baldwin, R. S. Keynton, J. F. Naber, K. M. Walsh, and I. Ieee, "Integrated electrochemical detection for lab on a chip analytical microsystems," in *Proceedings 14th Biennial University/Government/Industry Microelectronics Symposium*, ed, 2001, pp. 167-170.

[143] R. F. Renzi, J. Stamps, B. A. Horn, S. Ferko, V. A. VanderNoot, J. A. A. West, R. Crocker, B. Wiedenman, D. Yee, and J. A. Fruetel, "Hand-Held Microanalytical Instrument for Chip-Based Electrophoretic Separations of Proteins," *Analytical Chemistry,* vol. 77, pp. 435-441, 2005/01/01 2005.

[144] D. Lindner, "Profile: The μChemLab^{TM} project: micro total analysis system R&D at Sandia National Laboratories," *Lab on a Chip,* vol. 1, pp. 15N-20N, 2001.

[145] H. F. Zhang, X. W. Liu, W. Wang, X. L. Wang, and L. Tian, "Field-portable Capillary Electrophoresis Instrument with Conductivity Detection," *Journal of Physics: Conference Series,* vol. 48, p. 725, 2006.

[146] M. Day and B. S. Lee, "Understanding piezoelectric transformers in CCFL backlight applications," *Analog Applications Journal,* pp. 18-23, 2002.

[147] H. Becker, H. Mühlberger, W. Hoffmann, T. Clemens, R. Klemm, and C. Gärtner, "Portable CE system with contactless conductivity detection in an injection molded polymer chip for on-site food analysis," *Proc. SPIE,* vol. 6886, p. 68860C, 2008.

[148] H. Mühlberger, H. Wonhee, A. E. Guber, V. Saile, and W. Hoffmann, "Polymer lab-on-a-chip system with electrical detection," *IEEE Sensors Journal,* vol. 8, pp. 572-9, 2008.

[149] A. Fernández-la-Villa, D. F. Pozo-Ayuso, and M. Castano-Alvarez, "New analytical portable instrument for microchip electrophoresis with electrochemical detection," *Electrophoresis,* vol. 31, pp. 2641-2649, Aug 2010.

[150] T. Kappes and P. C. Hauser, "Portable capillary electrophoresis instrument with potentiometric detection," *Analytical Communications,* vol. 35, pp. 325-329, 1998.

[151] T. Kappes, B. Galliker, M. A. Schwarz, and P. C. Hauser, "Portable capillary electrophoresis instrument with amperometric, potentiometric and conductometric detection," *TrAC Trends in Analytical Chemistry,* vol. 20, pp. 133-139, 2001.

[152] T. Kappes, P. Schnierle, and P. C. Hauser, "Field-portable capillary electrophoresis instrument with potentiometric and amperometric detection," *Analytica Chimica Acta,* vol. 393, pp. 77-82, 1999.
[153] T. Kappes and P. C. Hauser, "Simplified amperometric detector for capillary electrophoresis," *The Royal Society of Chemistry - Analyst,* vol. 124, pp. 1035-1039, 1999.
[154] G. C. Gerhardt, R. M. Cassidy, and A. S. Baranski, "Square-Wave Voltammetry Detection for Capillary Electrophoresis," *Analytical Chemistry,* vol. 70, pp. 2167-2173, 1998/05/01 1998.
[155] G. C. Gerhardt, "Square-Wave Voltammetry Detection for Capillary Electrophoresis," PhD, Department of Chemistry, University of Saskatchewan, 1999.
[156] Spellman High Voltage Electronics Corporation. (2012). *Spellman High Voltage Electronics Corporation*. www.spellmanhv.com Last accessed 22-09-12
[157] P. Kubáň, P. Kubáň, P. C. Hauser, and V. Kubáň, "A flow injection-capillary electrophoresis system with high-voltage contactless conductivity detection for automated dual opposite end injection," *Electrophoresis,* vol. 25, pp. 35-42, 2004.
[158] P. Kubáň, H. T. A. Nguyen, M. Macka, P. R. Haddad, and P. C. Hauser, "New Fully Portable Instrument for the Versatile Determination of Cations and Anions by Capillary Electrophoresis with Contactless Conductivity Detection," *Electroanalysis,* vol. 19, pp. 2059-2065, 2007.
[159] A. Seiman, J. Martin, M. Vaher, and M. Kaljurand, "A portable capillary electropherograph equipped with a cross-sampler and a contactless-conductivity detector for the detection of the degradation products of chemical warfare agents in soil extracts," *Electrophoresis,* vol. 30, pp. 507-514, 2009.
[160] P. Kubáň, A. Seiman, N. Makarõtševa, M. Vaher, and M. Kaljurand, "In situ determination of nerve agents in various matrices by portable capillary electropherograph with contactless conductivity detection," *Journal of Chromatography A,* vol. 1218, pp. 2618-2625, 2011.
[161] L. Wang and C. Fu, "Miniaturized Capillary Electrophoresis System with Contactless Conductivity Detection and Flow Injection Sample Introduction," *Instrumentation Science & Technology,* vol. 32, pp. 303-309, 2004/12/27 2004.
[162] EMCO High Voltage Corporation. (2012). http://www.emcohighvoltage.com Last accessed 22-09-12
[163] J. L. Pittman, C. S. Henry, and S. D. Gilman, "Experimental Studies of Electroosmotic Flow Dynamics in Microfabricated Devices during Current Monitoring Experiments," *Analytical Chemistry,* vol. 75, pp. 361-370, 2003.
[164] J. A. Luckey and L. M. Smith, "Optimization of electric field strength for DNA sequencing in capillary gel electrophoresis," *Analytical Chemistry,* vol. 65, pp. 2841-2850, 1993/10/01 1993.
[165] L. Jiang, X. Jiang, Y. Lu, Z. Dai, M. Xie, J. Qin, and B. Lin, "Development of a universal serial bus-powered mini-high-voltage power supply for microchip electrophoresis," *Electrophoresis,* vol. 28, pp. 1259-1264, 2007.
[166] I. Buchmann. (2013). *Battery University*. http://batteryuniversity.com/ May 2013
[167] J. E. Prest, S. J. Baldock, N. Bektaş, P. R. Fielden, and B. J. Treves Brown, "Single electrode conductivity detection for electrophoretic separation systems," *Journal of Chromatography A,* vol. 836, pp. 59-65, 1999.
[168] C. D. Garcia, Y. Liu, P. Anderson, and C. S. Henry, "Versatile 3-channel high-voltage power supply for microchip capillary electrophoresis," *Lab on a Chip,* vol. 3, pp. 324-328, 2003.
[169] D. Erickson, D. Sinton, and D. Li, "A miniaturized high-voltage integrated power supply for portable microfluidic applications," *Lab on a Chip,* vol. 4, pp. 87-90, 2004.

[170] D. Erickson and D. Q. Li, "Integrated microfluidic devices," *Analytica Chimica Acta,* vol. 507, pp. 11-26, Apr 1 2004.
[171] M. Behnam, G. V. Kaigala, M. Khorasani, S. Martel, D. G. Elliott, and C. J. Backhouse, "Integrated circuit-based instrumentation for microchip capillary electrophoresis," *Iet Nanobiotechnology,* vol. 4, pp. 91-101, Sep 2010.
[172] M. Behnam, G. V. Kaigala, M. Khorasani, P. Marshall, C. J. Backhouse, and D. G. Elliott, "An integrated CMOS high voltage supply for lab-on-a-chip systems," *Lab on a Chip,* vol. 8, pp. 1524-1529, 2008.
[173] R. M. Guijt, C. J. Evenhuis, M. Macka, and P. R. Haddad, "Conductivity detection for conventional and miniaturised capillary electrophoresis systems," *Electrophoresis,* vol. 25, pp. 4032-4057, 2004.
[174] Z.-F. He, J.-L. Zhang, Y.-H. Liu, Y.-T. Zhang, and Y. Zhang, "Characteristics of a symmetrical Cockcroft-Walton power supply of 50 Hz 1.2 MV/50 mA," *Review of Scientific Instruments,* vol. 82, pp. 055116-7, 2011.
[175] O. Abutbul, A. Gherlitz, Y. Berkovich, and A. Ioinovici, "Step-up switching-mode converter with high voltage gain using a switched-capacitor circuit," *Circuits and Systems I: Fundamental Theory and Applications, IEEE Transactions on,* vol. 50, pp. 1098-1102, 2003.
[176] L. Dalessandro, F. da Silveira Cavalcante, and J. W. Kolar, "Self-Capacitance of High-Voltage Transformers," *IEEE Transactions on Power Electronics,* vol. 22, pp. 2081-2092, 2007.
[177] M. Nymand and M. A. E. Andersen, "High-Efficiency Isolated Boost DC-DC Converter for High-Power Low-Voltage Fuel-Cell Applications," *IEEE Transactions on Industrial Electronics,* vol. 57, pp. 505-514, 2010.
[178] P. Kubáň, A. Seiman, and M. Kaljurand, "Improving precision of manual hydrodynamic injection in capillary electrophoresis with contactless conductivity detection," *Journal of Chromatography A,* vol. 1218, pp. 1273-1280, 2011.
[179] M. Gong, K. R. Wehmeyer, A. M. Stalcup, P. A. Limbach, and W. R. Heineman, "Study of injection bias in a simple hydrodynamic injection in microchip CE," *Electrophoresis,* vol. 28, pp. 1564-1571, 2007.
[180] Bartels Mikrotechnik GmbH. http://www.bartels-mikrotechnik.de Last accessed: 22-09-12
[181] R. R. Lamonte and D. McNally. (2001). Cyclic Olefin Copolymers. *Advanced Materials & Processes*. http://www.elite-plastic.com.tw/COC-1.pdf Last accessed: 22-09-12
[182] K. Horiuchi and P. Dutta, "Electrokinetic flow control in microfluidic chips using a field-effect transistor," *Lab on a Chip,* vol. 6, p. 714, 2006.
[183] S. Diaham, S. Zelmat, M. L. Locatelli, S. Dinculescu, M. Decup, and T. Lebey, "Dielectric breakdown of polyimide films: Area, thickness and temperature dependence," *Dielectrics and Electrical Insulation, IEEE Transactions on,* vol. 17, pp. 18-27, 2010.
[184] J. Melai, C. Salm, S. Smits, J. Visschers, and J. Schmitz, "The Electrical Conduction and Dielectric Strength of SU-8," *Journal of Micromechanics and Microengineering,* vol. 19, 2009.
[185] M. Bhatnagar and B. J. Baliga, "Comparison of 6H-SiC, 3C-SiC, and Si for power devices," *Electron Devices, IEEE Transactions on,* vol. 40, pp. 645-655, 1993.
[186] D. Mangalaraj, M. Radhakrishnan, and C. Balasubramanian, "Electrical conduction and breakdown properties of silicon nitride films," *Journal of Materials Science,* vol. 17, pp. 1474-1478, 1982.
[187] E. J. Van Der Wouden, D. C. Hermes, J. G. Gardeniers, and A. Van Den Berg, "Directional flow induced by synchronized longitudinal and zeta-potential controlling AC-electrical fields.," *Lab on a Chip,* vol. 6, pp. 1300-1305, 2006.

[188] R. B. M. Schasfoort, S. Schlautmann, J. Hendrikse, and A. van den Berg, "Field-Effect Flow Control for Microfabricated Fluidic Networks," *Science,* vol. 286, pp. 942-945, October 1999.
[189] N. K. Hartley and M. A. Hayes, "Examination of Theoretical Models in External Voltage Control of Capillary Electrophoresis," *Analytical Chemistry,* vol. 74, pp. 1249-1255, 2002.
[190] C. S. Lee, W. C. Blanchard, and C. T. Wu, "Direct control of the electroosmosis in capillary zone electrophoresis by using an external electric field," *Analytical Chemistry,* vol. 62, pp. 1550-1552, 1990.
[191] C. T. Wu, T. Lopes, B. Patel, and C. S. Lee, "Effect of direct control of electroosmosis on peptide and protein separations in capillary electrophoresis," *Analytical Chemistry,* vol. 64, pp. 886-891, 1992.
[192] C. T. Culbertson and J. W. Jorgenson, "Flow Counterbalanced Capillary Electrophoresis," *Analytical Chemistry,* vol. 66, pp. 955-962, 1994.
[193] C. T. Culbertson and J. W. Jorgenson, "Increasing the resolving power of capillary electrophoresis through electroosmotic flow control using radial fields," *Journal of Microcolumn Separations,* vol. 11, pp. 167-174, 1999.
[194] A. E. Herr, J. I. Molho, J. G. Santiago, M. G. Mungal, T. W. Kenny, and M. G. Garguilo, "Electroosmotic Capillary Flow with Nonuniform Zeta Potential," *Analytical Chemistry,* vol. 72, pp. 1053-1057, 2000.
[195] A. A. Saha, S. K. Mitra, and X. Li, "Electroosmotic effect on flows in a serpentine microchannel with varying zeta potential," *Journal of Power Sources,* vol. 164, pp. 154-165, 2007.
[196] C.-Y. Lee, C.-H. Lin, and L.-M. Fu, "Band spreading control in electrophoresis microchips by localized zeta-potential variation using field-effect," *Analyst,* vol. 129, pp. 931-937, 2004.
[197] D. Erickson, "Towards numerical prototyping of labs-on-chip: modeling for integrated microfluidic devices," *Microfluidics and Nanofluidics,* vol. 1, pp. 301-318, Oct 2005.
[198] V. S. Bagotsky, *Fundamentals of Electrochemistry Second Edition*: John Wiley & Sons Inc., 2006.
[199] H. L. F. von Helmholtz, "Ueber einige Gesetze der Vertheilung elektrischer Ströme in körperlichen Leitern mit Anwendung auf die thierisch-elektrischen Versuche," *Proggendorff's Annals,* vol. 89, pp. 211-233, 353-377, 1853.
[200] H. L. F. von Helmholtz, "Some laws concerning the distribution of electric currents in volume conductors with applications to experiments on animal electricity," *Proceedings of the IEEE,* vol. 92, pp. 868-870, 2004.
[201] D. A. Walker, B. Kowalczyk, M. O. de la Cruz, and B. A. Grzybowski, "Electrostatics at the nanoscale," *Nanoscale,* vol. 3, pp. 1316-1344, 2011.
[202] K. S. Birdi, *Introduction to Electrical Interfacial Phenomena*: CRC Press Taylor and Francis Group, 2010.
[203] B. E. Conway. (2003). *Electrochemical Capacitors - Their Nature, Function, and Applications*. http://electrochem.cwru.edu/encycl/art-c03-elchem-cap.htm Last accessed: 22-09-12
[204] L. G. Gouy, "Sur la constitution de la charge électrique à la surface d'un électrolyte," *Comptes Rendus Hebdomadaires des Séances de L'Académie des Sciences,* pp. 654-657, 1909.
[205] L. G. Gouy, "Sur la constitution de la charge électrique à la surface d'un électrolyte " *Journal de Physique Théorique et Appliquée,* vol. 9, pp. 457-468, 1910.
[206] D. L. Chapman, "A Contribution to the Theory of Electrocapillarity " *The London, Edinburgh, and Dublin Philosophical Magazine and Journal of Science,* vol. 25, pp. 475-481, 1913.

[207] P. Pham, M. Howorth, A. Planat-Chrétien, and S. Tardu, "Numerical Simulation of the Electrical Double Layer Based on the Poisson-Boltzmann Models for AC Electroosmosis Flows," in *Comsol Users Conference*, Grenoble, 2007.
[208] M. S. Kilic, M. Z. Bazant, and A. Ajdari, "Steric effects in the dynamics of electrolytes at large applied voltages. I. Double-layer charging," *Physical Review E,* vol. 75, p. 021502, 2007.
[209] D. Hlushkou, "Numerical simulation of fluid flow and mass transport in (electro) chromatographic systems," Ph.D, Otto-von-Guericke-Universität Magdeburg, 2004.
[210] D. C. Grahame, "The Electrical Double Layer and the Theory of Electrocapillarity," *Chemical Reviews,* vol. 41, pp. 441-501, 1947.
[211] J. O. M. Bockris, M. A. V. Devanathan, and K. Müller, "On the Structure of Charged Interfaces," *Proceedings of the Royal Society of London. Series A, Mathematical and Physical Sciences,* vol. 274, pp. 55-79, 1963.
[212] Z. F. Wang, Y. X. Wu, and K. Puttachat, "Electroosmosis flow (EOF) mobility measurement in polymer micro channels," SIMTech technical reports 2009.
[213] S. A. Socolofsky and G. H. Jirka, *Environmental Fluid Mechanics 1: Mixing and Transport Processes in the Environment - 5th Edition*: Coastal and Ocean Engineering Division, Texas A&M University, 2005.
[214] L. W. Nagel and D. O. Pederson, "SPICE (Simulation Program with Integrated Circuit Emphasis)," EECS Department, University of California, Berkeley UCB/ERL M382, 1973.
[215] S. Conradi, C. Vogt, H. Wittrisch, G. Knobloch, and G. Werner, "Capillary electrophoretic separation of metal ions using complex forming equilibria of different stabilities," *Journal of Chromatography A,* vol. 745, pp. 103-109, 1996.
[216] J. E. Prest, S. J. Baldock, P. R. Fielden, N. J. Goddard, K. Kalimeri, B. J. Treves Brown, and M. Zgraggen, "Use of miniaturised isotachophoresis on a planar polymer chip to analyse transition metal ions in solutions from metal processing plants," *Journal of Chromatography A,* vol. 1047, pp. 289-298, 2004.
[217] A. Manz, N. Graber, and H. M. Widmer, "Miniaturized total chemical analysis systems: A novel concept for chemical sensing," *Sensors and Actuators B: Chemical,* vol. 1, pp. 244-248, 1990.
[218] N. A. Lacher, K. E. Garrison, R. S. Martin, and S. M. Lunte, "Microchip capillary electrophoresis/ electrochemistry," *Electrophoresis,* vol. 22, pp. 2526-2536, 2001.
[219] E. Norkus, G. Grincienė, T. Vuorinen, and R. Vaitkus, "Cu(II) Ion Complexation by Excess of β-cyclodextrin in Aqueous Alkaline Solutions," *Journal of inclusion phenomena and macrocyclic chemistry,* vol. 48, pp. 147-150, 2004/04/01 2004.
[220] N. Avcibasi, Y. Posokhov, K. Ocakoglu, C. Varlikli, M. Kus, G. Turkmen, M. K. Gumus, F. T. Tugcu, E. Aydemir, and S. Gumus, "Spectrophotometric Determination of Cu2+ with Quinolinyl Derivative in Organic and Aqueous Solutions," *Asian Journal of Chemistry,* vol. 19, pp. 1930-1942, 2007.
[221] C. E. Säbel, J. M. Neureuther, and S. Siemann, "A spectrophotometric method for the determination of zinc, copper, and cobalt ions in metalloproteins using Zincon," *Analytical Biochemistry,* vol. 397, pp. 218-226, 2010.
[222] J. H. Kim, K. T. Lau, C. Fay, and D. Diamond, "Development of optical sensing system for detection of Fe ions using conductive polymer actuator based microfluidic pump," in *Sensors, 2008 IEEE*, 2008, pp. 1155-1158.
[223] E. H. El-Mossalamy and A. A. Ibrahim, "Molecular charge transfer complexes of metal ions thiazolylazo compounds with iodine," *Pigment & Resin Technology,* vol. 33, pp. 32-38, 2004.
[224] S. H. Kim, H. S. Choi, J. Kim, S. J. Lee, D. T. Quang, and J. S. Kim, "Novel Optical/Electrochemical Selective 1,2,3-Triazole Ring-Appended Chemosensor for the Al3+ Ion," *Organic Letters,* vol. 12, pp. 560-563, 2010/02/05 2009.

[225] M. A. Schwarz, B. Galliker, K. Fluri, T. Kappes, and P. C. Hauser, "A two-electrode configuration for simplified amperometric detection in a microfabricated electrophoretic separation device," *The Royal Society of Chemistry - Analyst,* vol. 1266, pp. 147-151, 2001.
[226] H. Dong, C.-M. Li, Y.-F. Zhang, X.-D. Cao, and Y. Gan, "Screen-printed microfluidic device for electrochemical immunoassay," *The Royal Society of Chemistry - Lab on a Chip,* vol. 7, pp. 1752-1758, 2007.
[227] Y. Wu, J.-M. Lin, R. Su, F. Qu, and Z. Cai, "An end-channel amperometric detector for microchip capillary electrophoresis," *Talanta,* vol. 64, pp. 338-344, 2004.
[228] K.-W. Lin, Y.-K. Huang, H.-L. Su, and Y.-Z. Hsieh, "In-channel simplified decoupler with renewable electrochemical detection for microchip capillary electrophoresis," *Analytica Chimica Acta,* vol. 619, pp. 115-121, 2008.
[229] W. K. T. Coltro, J. A. F. da Silva, and E. Carrilho, "Fabrication and integration of planar electrodes for contactless conductivity detection on polyester-toner electrophoresis microchips," *Electrophoresis,* vol. 29, pp. 2260-2265, 2008.
[230] Y. Liu, J. A. Vickers, and C. S. Henry, "Simple and Sensitive Electrode Design for Microchip Electrophoresis/Electrochemistry," *Analytical Chemistry,* vol. 76, pp. 1513-1517, 2004.
[231] R. A. Wallingford and A. G. Ewing, "Capillary zone electrophoresis with electrochemical detection," *Analytical Chemistry,* vol. 59, pp. 1762-1766, 1987.
[232] F. Laugere, G. W. Lubking, J. Bastemeijer, and M. J. Vellekoop, "Design of an electronic interface for capacitively coupled four-electrode conductivity detection in capillary electrophoresis microchip," *Sensors and Actuators B: Chemical,* vol. 83, pp. 104-108, 2002.
[233] MicroChem Corp. (2012). *SU-8 Negative Epoxy Series Resists*. http://www.microchem.com/Prod-SU8_KMPR.htm Last accessed: 22-09-12
[234] T. Pérez-Ruiz, C. Martínez-Lozano, A. Sanz, and E. Bravo, "Separation of Fluorescein Dyes by Capillary Electrophoresis Using β-Cyclodextrin," *Chromatographia,* vol. 48, pp. 263-267, 1998.
[235] H. Becker and A. Manz, "Miniaturised chemical analysis systems-materials and bonding," London, UK, 1997, pp. 9-1.
[236] M. Pumera, A. Merkoçi, and S. Alegret, "New materials for electrochemical sensing VII. Microfluidic chip platforms," *TrAC Trends in Analytical Chemistry,* vol. 25, pp. 219-235, 2006.
[237] E. Verpoorte and N. F. de Rooij, "Microfluidics meets MEMS," *Proceedings of the IEEE,* vol. 91, pp. 930-953, 2003.
[238] S. D. Senturia, *Microsystem Design*: Springer, 2000.
[239] N. Maluf and K. Williams, *An Introduction to Microelectromechanical Systems Engineering*: Artech House, Incorporated, 2004.
[240] A. Berthold, F. Laugere, H. Schellevis, C. R. de Boer, M. Laros, R. M. Guijt, P. M. Sarro, and M. J. Vellekoop, "Fabrication of a glass-implemented microcapillary electrophoresis device with integrated contactless conductivity detection," *Electrophoresis,* vol. 23, pp. 3511-19, 2002.
[241] A. Berthold, L. Nicola, P. M. Sarro, and M. J. Vellekoop, "Glass-to-glass anodic bonding with standard IC technology thin films as intermediate layers," *Sensors and Actuators A: Physical,* vol. 82, pp. 224-228, 2000.
[242] P. Nunes, P. Ohlsson, O. Ordeig, and J. Kutter, "Cyclic olefin polymers: emerging materials for lab-on-a-chip applications," *Microfluidics and Nanofluidics,* vol. 9, pp. 145-161, 2010.
[243] J. H. Koschwanez, R. H. Carlson, and D. R. Meldrum, "Thin PDMS Films Using Long Spin Times or Tert-Butyl Alcohol as a Solvent," *PLoS ONE,* vol. 4, p. e4572, 2009.

[244] Dow Corning. (2010). *Dow Corning 184 Silicon Elastomer Datasheet*. http://www.dowcorning.com
[245] W. K. T. Coltro, S. M. Lunte, and E. Carrilho, "Comparison of the analytical performance of electrophoresis microchannels fabricated in PDMS, glass, and polyester-toner," *Electrophoresis,* vol. 29, pp. 4928-4937, 2008.
[246] Micralyne Inc. (2000-2013). *Micralyne Inc. Website*. http://www.micralyne.com/
[247] R. S. Martin, A. J. Gawron, S. M. Lunte, and C. S. Henry, "Dual-Electrode Electrochemical Detection for Poly(dimethylsiloxane)-Fabricated Capillary Electrophoresis Microchips," *Analytical Chemistry,* vol. 72, pp. 3196-3202, 2000/07/01 2000.
[248] A. Ros, W. Hellmich, T. Duong, and D. Anselmetti, "Towards single molecule analysis in PDMS microdevices: from the detection of ultra low dye concentrations to single DNA molecule studies," *Journal of Biotechnology,* vol. 112, pp. 65-72, 2004.
[249] D. C. Duffy, J. C. McDonald, O. J. A. Schueller, and G. M. Whitesides, "Rapid Prototyping of Microfluidic Systems in Poly(dimethylsiloxane)," *Analytical Chemistry,* vol. 70, pp. 4974-4984, 1998.
[250] W. M. Choi and O. O. Park, "A soft-imprint technique for direct fabrication of submicron scale patterns using a surface-modified PDMS mold," *Microelectronic Engineering,* vol. 70, pp. 131-136, 2003.
[251] E. Sollier, C. Murray, P. Maoddi, and D. Di Carlo, "Rapid prototyping polymers for microfluidic devices and high pressure injections," *Lab on a Chip,* vol. 11, pp. 3752-3765, 2011.
[252] J. C. McDonald, D. C. Duffy, J. R. Anderson, D. T. Chiu, H. Wu, O. J. A. Schueller, and G. M. Whitesides, "Fabrication of microfluidic systems in poly(dimethylsiloxane)," *Electrophoresis,* vol. 21, pp. 27-40, 2000.
[253] G. Ocvirk, M. Munroe, T. Tang, R. Oleschuk, K. Westra, and D. J. Harrison, "Electrokinetic control of fluid flow in native poly(dimethylsiloxane) capillary electrophoresis devices," *Electrophoresis,* vol. 21, pp. 107-115, 2000.
[254] C. S. Effenhauser, G. J. M. Bruin, A. Paulus, and M. Ehrat, "Integrated Capillary Electrophoresis on Flexible Silicone Microdevices: Analysis of DNA Restriction Fragments and Detection of Single DNA Molecules on Microchips," *Analytical Chemistry,* vol. 69, pp. 3451-3457, 1997.
[255] A. Khan. (2006). *Lithography*. http://www.southalabama.edu/engineering/ece/faculty/akhan/Courses/EE539-Fall06/Lecture-slides/lithography.pdf
[256] F. Ru and J. F. Richard, "Influence of processing conditions on the thermal and mechanical properties of SU8 negative photoresist coatings," *Journal of Micromechanics and Microengineering,* vol. 13, p. 80, 2003.
[257] R. M. McCormick, R. J. Nelson, M. G. Alonso-Amigo, D. J. Benvegnu, and H. H. Hooper, "Microchannel Electrophoretic Separations of DNA in Injection-Molded Plastic Substrates," *Analytical Chemistry,* vol. 69, pp. 2626-2630, 1997.
[258] N. Harris, A. Keating, and M. Hill, "Sub-Wavelength Ultrasonic Lipid Manipulation Utilising Embossed Plastic Channels," presented at the 5th Asia-Pacific Conference on Transducers and Micro-nano Technology (APCOT), Perth, Western Australia, 2010.
[259] A. M. G. Campaña, W. Baeyens, H. Y. Aboul-Enein, and X. R. Zhang, "Miniaturization of capillary electrophoresis systems using micromachining techniques," *Journal of Microcolumn Separations,* vol. 10, pp. 339-355, 1998.
[260] H. Seidel, L. Csepregi, A. Heuberger, and H. Baumgärtel, "Anisotropic Etching of Crystalline Silicon in Alkaline Solutions: I . Orientation Dependence and Behavior of Passivation Layers," *Journal of The Electrochemical Society,* vol. 137, pp. 3612-3626, November 1, 1990 1990.

[261] N. Harris, A. Keating, and M. Hill, "A Lateral Mode Flow-through PMMA Ultrasonic Separator," presented at the 5th Asia-Pacific Conference on Transducers and Micro-nano Technology (APCOT), Perth, Western Australia, 2010.
[262] S. H. Ng, R. T. Tjeung, and Z. Wang, "Formation of Embedded Microchannels by a Solvent Displacement Bonding Technique," in *9th Electronics Packaging Technology Conference (EPTC 2007)*, 2007, pp. 211-214.
[263] W. Ehrfeld and U. Ehrfeld, "Progress and profit through microtechnologies: commercial applications of MEMS/MOEMS," pp. 1-10, 2001.
[264] J. Wang, G. Chen, M. P. Chatrathi, M. Wang, R. Rinehart, and A. Muck, "Screen-Printed Contactless Conductivity Detector for Microchip Capillary Electrophoresis," *Electroanalysis,* vol. 20, pp. 2416-2421, 2008.
[265] S. Schlautmann, H. Wensink, R. Schasfoort, M. Elwenspoek, and A. v. d. Berg, "Powder-blasting technology as an alternative tool for microfabrication of capillary electrophoresis chips with integrated conductivity sensors," *Journal of Micromechanics and Microengineering,* p. 386, 2001.
[266] R. M. Guijt, E. Baltussen, G. van der Steen, R. B. M. Schasfoort, S. Schlautmann, H. A. H. Billiet, J. Frank, G. W. K. van Dedem, and A. van den Berg, "New approaches for fabrication of microfluidic capillary electrophoresis devices with on-chip conductivity detection," *Electrophoresis,* vol. 22, pp. 235-241, 2001.
[267] A. P. Lewis, A. Cranny, N. G. Green, M. Nie, J. A. Wharton, R. J. K. Wood, K. R. Stokes, and N. R. Harris, "Novel fabrication method for rapid creation of channels using PDMS for microfluidic networks on planar substrates," presented at the 5th Asia-Pacific Conference on Transducers and Micro-Nano Technology (APCOT), Perth, Western , Australia, 2010.
[268] A. P. Lewis, M. P. Down, C. Chianrabutra, L. Jiang, S. M. Spearing, and J. W. McBride, "The Effect on Switching Lifetime of Chromium Adhesion Layers in Gold-Coated Electrical Contacts under Cold and Hot Switching Conditions," presented at the 59th IEEE Holm Conference on Electrical Contacts, Newport, RI, 2013.
[269] Prince Technologies. (2012). *Prince Technologies "PrinCE-650 Instrument"*. http://www.princetechnologies.eu Last accessed 22-09-12
[270] S. A. Soper, S. M. Ford, S. Qi, R. L. McCarley, K. Kelly, and M. C. Murphy, "Peer Reviewed: Polymeric Microelectromechanical Systems," *Analytical Chemistry,* vol. 72, pp. 642 A-651 A, 2000.
[271] Aquarius Plastics Ltd. (2009). *Aquarius Plastics Ltd. Website*. http://www.aquariusplastics.co.uk/
[272] S. M. Ford, B. Kar, S. McWhorter, J. Davies, S. A. Soper, M. Klopf, G. Calderon, and V. Saile, "Microcapillary electrophoresis devices fabricated using polymeric substrates and X-ray lithography," *Journal of Microcolumn Separations,* vol. 10, pp. 413-422, 1998.
[273] Katco. (2008). *Katco Website*. www.katco.eu
[274] *Bartels Mikrotechnik GmbH - mp6-OEM Controller*. http://www.bartels-mikrotechnik.de/index.php/mp6-OEM.html (Accessed September 2010)
[275] S. J. Baldock, P. R. Fielden, N. J. Goddard, H. R. Kretschmer, J. E. Prest, and B. J. T. Brown, "A versatile sample injection system for miniaturised isotachophoresis devices," *Microelectronic Engineering,* vol. 85, pp. 1440-1442, 2008.
[276] Applied Kilovolts Ltd. (2012). *HP Series Data Sheet*. http://www.appliedkilovolts.com/pdfs/HPSeries.pdf
[277] Applied Kilovolts Ltd. (2012). *HPZ Series Data Sheet*. http://www.appliedkilovolts.com/pdfs/HPZSeries.pdf
[278] A. P. Lewis, A. Cranny, N. G. Green, M. Nie, J. A. Wharton, R. J. K. Wood, K. R. Stokes, and N. R. Harris, "Improving separation resolution of capillary electrophoresis to aid corrosion monitoring by dynamic control of the EOF," in *13th*

International Meeting on Chemical Sensors (IMCS-13), Perth, Western Australia, 2010.
[279] S. Wolfram. (2002). *A New Kind of Science*.
[280] R. F. Voss, "1/f (Flicker) Noise: A Brief Review," in *33rd Annual Symposium on Frequency Control. 1979*, 1979, pp. 40-46.
[281] A. Gover, A. Nause, E. Dyunin, and M. Fedurin, "Beating the shot-noise limit," *Nature Physics,* vol. 8, pp. 877-880, 2012.
[282] J. Lesurf. (2005). *Sources of Noise - Johnson and Shot Noise*. http://www.st-andrews.ac.uk/~www_pa/Scots_Guide/iandm/part3/page1.html September 2013
[283] P. R. Clayton, "On the Superposition of Inductive and Capacitive Coupling in Crosstalk-Prediction Models," *Electromagnetic Compatibility, IEEE Transactions on,* vol. EMC-24, pp. 335-343, 1982.
[284] D. C. Smith. (2005). *Inductive and Capacitive Coupling - Induced Current Characteristics*. http://www.emcesd.com/tt2005/tt040205.htm
[285] A. Rich, "Shilding and Guarding," *Analog Dialogue,* vol. 17, 1983.
[286] M.-s. Gupta, "Noise in avalanche transit-time devices," *Proceedings of the IEEE,* vol. 59, pp. 1674-1687, 1971.
[287] G. Vasilescu, *Electronic Noise and Interfering Signals - Principles and Applications*: Springer, 2005.
[288] *Hanna Instruments Ltd. - Pocket Conductivity Testers 2010*. http://www.hannainst.co.uk/ Last accessed 22-09-12
[289] A. Cranny, N. Harris, A. Lewis, S. Neodo, M. Nie, K. Stokes, J. Wharton, and R. Wood, "Microfluidic Devices for Structural Health Monitoring," presented at the Marine Energy Systems Workshop Day, 2011.
[290] A. Cranny, N. Harris, A. Lewis, S. Neodo, M. Nie, K. Stokes, J. Wharton, and R. Wood, "Microfluidic Devices for Structural Health Monitoring and Integrity," presented at the Joint Academic Research Program for Defence, 2011.
[291] M. J. Donachie, *Titanium: A Technical Guide*: ASM International, 2000.
[292] K. W. Vogt, P. A. Kohl, W. B. Carter, R. A. Bell, and L. A. Bottomley, "Characterization of thin titanium oxide adhesion layers on gold: resistivity, morphology, and composition," *Surface Science,* vol. 301, pp. 203-213, 1994.
[293] C. W. Tan and J. Miao, "Optimization of sputtered Cr/Au thin film for diaphragm-based MEMS applications," *Thin Solid Films,* vol. 517, pp. 4921-4925, 2009.
[294] T. Sikanen, S. Tuomikoski, R. A. Ketola, R. Kostiainen, S. Franssila, and T. Kotiaho, "Characterization of SU-8 for electrokinetic microfluidic applications," *Lab on a Chip,* vol. 5, pp. 888-896, 2005.
[295] M. Castaño-Álvarez, M. T. Fernández-Abedul, A. Costa-García, M. Agirregabiria, L. J. Fernández, J. M. Ruano-López, and B. Barredo-Presa, "Fabrication of SU-8 based microchip electrophoresis with integrated electrochemical detection for neurotransmitters," *Talanta,* vol. 80, pp. 24-30, 2009.
[296] J. Ou, T. Glawdel, C. L. Ren, and J. Pawliszyn, "Fabrication of a hybrid PDMS/SU-8/quartz microfluidic chip for enhancing UV absorption whole-channel imaging detection sensitivity and application for isoelectric focusing of proteins," *Lab on a Chip,* vol. 9, pp. 1926-1932, 2009.
[297] M.-H. Wu, H. Cai, X. Xu, J. G. Urban, Z.-F. Cui, and Z. Cui, "A SU-8/PDMS Hybrid Microfluidic Device with Integrated Optical Fibers for Online Monitoring of Lactate," *Biomedical Microdevices,* vol. 7, pp. 323-329, 2005/12/01 2005.
[298] V. Kumar and N. N. Sharma, "SU-8 as Hydrophobic and Dielectric Thin Film in Electrowetting-on-Dielectric Based Microfluidics Device," *Journal of Nanotechnology,* vol. 2012, p. 6, 2012.
[299] B. Raj, M. Dhindsa, N. R. Smith, R. Laughlin, and J. Heikenfeld, "Ion and Liquid Dependent Dielectric Failure in Electrowetting Systems," *Langmuir,* vol. 25, pp. 12387-12392, 2009/10/20 2009.

[300] F. Mugele and J. C. Baret, "Electrowetting: from basics to applications," *Journal of Physics: Condensed Matter,* vol. 17, pp. 705-74, 2005.
[301] J. Yota, "Effects of Deposition Method of PECVD Silicon Nitride as MIM Capacitor Dielectric for GaAs HBT Technology," *ECS Transactions,* vol. 35, pp. 229-240, April 25, 2011 2011.
[302] W. A. P. Claassen, W. G. J. N. Valkenburg, M. F. C. Willemsen, and W. M. v. d. Wijgert, "Influence of Deposition Temperature, Gas Pressure, Gas Phase Composition, and RF Frequency on Composition and Mechanical Stress of Plasma Silicon Nitride Layers," *Journal of The Electrochemical Society,* vol. 132, pp. 893-898, April 1, 1985 1985.
[303] M. J. Helix, K. V. Vaidyanathan, B. G. Streetman, H. B. Dietrich, and P. K. Chatterjee, "R.F. plasma deposition of silicon nitride layers," *Thin Solid Films,* vol. 55, pp. 143-148, 1978.
[304] C. H. Mastrangelo, Y.-C. Tai, and R. S. Muller, "Thermophysical properties of low-residual stress, Silicon-rich, LPCVD silicon nitride films," *Sensors and Actuators A: Physical,* vol. 23, pp. 856-860, 1990.
[305] D. A. P. Bulla and N. I. Morimoto, "Deposition of thick TEOS PECVD silicon oxide layers for integrated optical waveguide applications," *Thin Solid Films,* vol. 334, pp. 60-64, 1998.